Online Prediction of the Post-Disturbance Frequency Behaviour of a Power System

A thesis submitted to the University of Manchester for the degree of

Doctor of Philosophy

in the Faculty of Engineering and Physical Sciences

2013

Peter Richard Wall

School of Electrical and Electronic Engineering

Table of Contents

Word Count: 63,738

List of Figures

List of Tables

List of Abbreviations

AGC	Automatic Generation Control
AGR	Advanced Gas Cooled Reactor
AMI	Advanced Metering Infrastructure
AUFLS	Adaptive Under Frequency Load Shedding
BSV	Bounded Support Vector
CCGT	Combined Cycle Gas Turbine
CCS	Carbon Capture and Storage Technology
CHP	Combined Heat and Power
CIGRE	International Council on Large Electric Systems
CSC	Current Source Converter
CSUM	Consecutive Sum
CT	Current Transformer
DC	Data Concentrator
DFIG	Doubly Fed Induction Generator
DG	Distributed Generation
DRC	Demand Response Control
EMS	Energy Management System
EU	European Union
EV	Electric Vehicle
FNET	Wide Area Frequency Monitoring Network
GB	Great Britain
GPS	Global Positioning System
HEV	Hybrid Electric Vehicle
HVDC	High Voltage Direct Current
IEEE	Institute of Electrical and Electronics Engineers
IET	Institute of Engineering and Technology
IGBT	Insulated Gate Bipolar Transistor
IPSO	Improved Particle Swarm Optimisation
IQR	Inter Quartile Range
KKT	Karush-Kuhn-Tucker
LB	Lower Bound
LCPD	Large Combustible Plant Directive

MG	Motor Generator
NERC	North American Electricity Reliability Corporation
NGC	National Grid Company
OCGT	Open Cycle Gas Turbine
OFGEM	Office For Gas and Electricity Markets
OLTC	On Load Tap Changer
OpTel	Operational Telecoms
PHEV	Plug in Hybrid Electric Vehicle
PMSM	Permanent Magnet Synchronous Machine
PMU	Phasor Measurement Unit
PNRA	Power Networks Research Academy
PSS	Power System Stabilizer
PV	Photo Voltaic
SCADA	Supervisory Control And Data Acquisition
SFR	Simplified Frequency Response
SIPS	System Integrity Protection Scheme
SMES	Super Conducting Magnetic Energy Storage
SMT	Synchronous Measurement Technology
SPS	Special Protection Scheme
SV	Support Vector
SVM	Support Vector Machine
TCSC	Thyristor Controlled Series Compensation
UB	Upper Bound
UFLS	Under Frequency Load Shedding
USV	Unbounded Support Vector
VPP	Virtual Power Plant
VSC	Voltage Source Converter
VT	Voltage Transformer
WAMPAC	Wide Area Monitoring Protection And Control

Abstract

The University of Manchester
Faculty of Engineering and Physical Sciences
Peter Richard Wall
Doctor of Philosophy
Online Prediction of the Post-Disturbance Frequency Behaviour of a Power System
28/02/2013

The radical changes that are currently occurring in the nature of power systems means that in the future it may no longer be possible to guarantee security of supply using offline security assessment and planning. The increased uncertainty, particularly the reduction and variation in system inertia that will be faced in the future must be overcome through the use of adaptive online solutions for ensuring system security. The introduction of synchronised measurement technology means that the wide area real time measurements that are necessary to implement these online actions are now available.

The objective of the research presented in this thesis was to create methods for predicting the post-disturbance frequency behaviour of a power system with the intent of contributing to the development of real time adaptive corrective control for future power systems. Such a prediction method would generate an online prediction based on wide area measurements of frequency and active power that are recorded within the period of approximately one second after a disturbance to the active power balance of the system. Predictions would allow frequency control to respond more quickly and efficiently as it would no longer be necessary to wait for the system frequency behaviour to violate pre-determined thresholds.

The research presented in this thesis includes the creation of an online method for the simultaneous detection of the time at which a disturbance occurred in a power system, or area of a power system, and the estimation of the inertia of that system, or area. An existing prediction method based on approximate models has been redesigned to eliminate its dependence on offline information. Furthermore, the thesis presents the novel application of pattern classification theory to frequency prediction and a five class example of pattern classification is implemented.

Declaration

No portion of the work referred to in the thesis has been submitted in support of an application for another degree or qualification of this or any other university or other institute of learning.

Copyright Statement

Acknowledgements

I would like to take this opportunity to thank the IET and National Grid for funding my PhD through the PNRA scheme and also to offer my thanks to Professor Vladimir Terzija for securing this funding and for supervising my PhD research.

Furthermore, I would like to thank all of my colleagues and friends who have helped me during my time at the University of Manchester either in the form of encouragement, assistance or just by being somebody to talk to.

Finally, I have always found my family to be a great source of encouragement and support. Without them, my life would surely have been much the poorer and I would never have enjoyed the opportunities that have led to this thesis. Therefore, I would like to take this opportunity to say that my thoughts and love are always with them wherever they may be.

1 Introduction

This chapter seeks to introduce the basic objectives, background and motivation of this research as well as its specific goals and contributions. The primary objective of the research is described in Section 1.1 and a brief description of the motivation and background for this research is given in Section 1.2. The main goals of the research are listed in Section 1.3 and the contributions made by the research are described in Section 1.4. Finally, the content of the other thesis chapters is summarised in Section 1.5.

1.1 Objective

The objective of the research presented in this thesis was to create methods for predicting the post-disturbance frequency behaviour of a power system. After a disturbance occurs in the system, the prediction of the post-disturbance frequency behaviour should contain sufficient information to inform operators, or a closed loop controller, if the post-disturbance frequency deviation will be a threat to system security and to allow adaptive control actions to be designed to counter any threat posed by a frequency deviation. The prediction method would generate a prediction online, based on wide area measurements of frequency and active power that are recorded within the period of approximately one second after a disturbance to the active power balance of the system. The intent of this research is to contribute to the development of real time adaptive corrective control for future power systems as prediction of the post-disturbance frequency behaviour would be a valuable resource for improving frequency control and situational awareness during a disturbance.

The focus of this work was on predicting the initial frequency behaviour of the system. This was because it was determined that this was the most important behaviour to be aware of when considering protection and control actions. The first swing of the oscillatory frequency deviation that occurs after a disturbance to the active power balance is usually the largest and as such it is the greatest threat to system security. The proposed predictions could take the form of predicting the maximum deviation from

the nominal frequency, the violation of a certain frequency threshold, or the time the frequency will violate this threshold for.

An example of the generic execution of the frequency prediction process is given in Figure 1-1. This shows that the general process for predicting the post disturbance frequency behaviour of a power system, based on the initial post-disturbance frequency trajectory, consists of four elements. The first element is the detection of a disturbance to the active power balance in the system and estimation of the time at which this disturbance is reflected in the frequency data recorded. The second element is the estimation of the values of the model parameters that the prediction method will use, this is necessary due to the increased levels of uncertainty that will be encountered in future power systems. The third element involves performing the prediction and distributing it to the relevant applications or operators that will take action based on the prediction, e.g. initiate Under Frequency Load Shedding (UFLS), in the fourth element of the process.

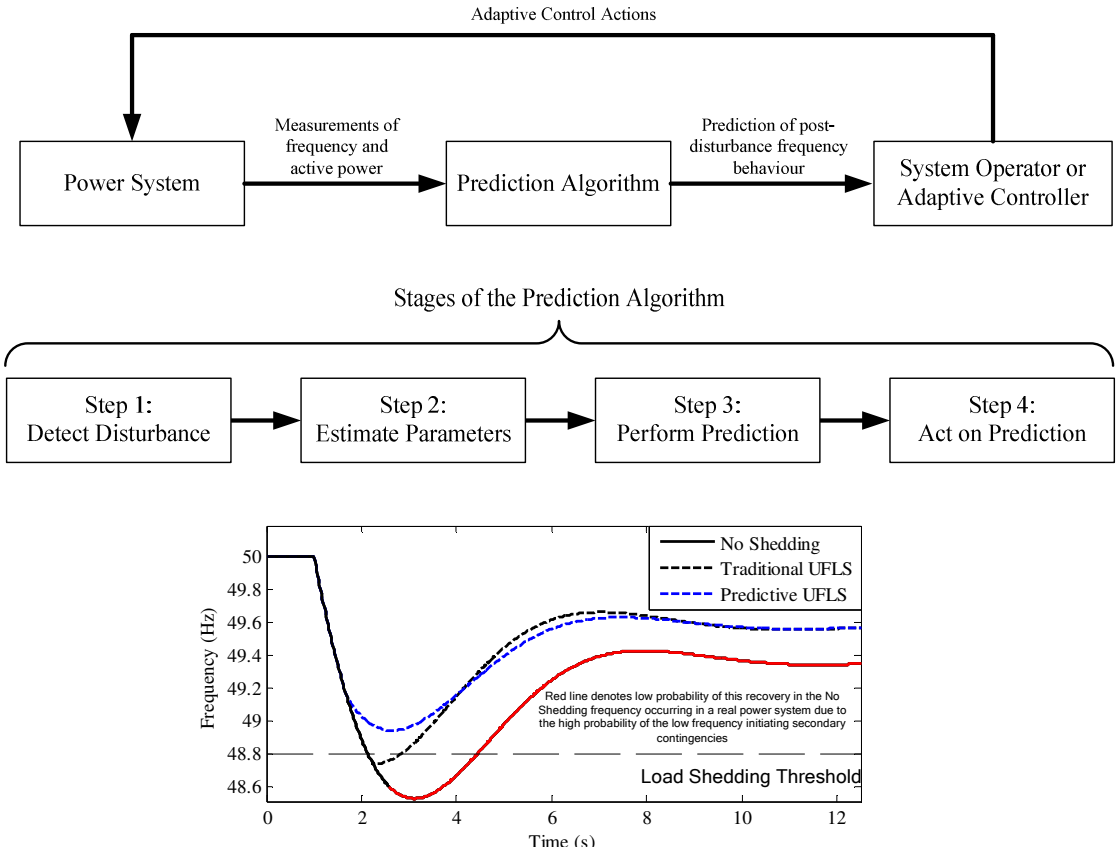

Figure 1-1 – Depiction of the main stages of the generic execution of a frequency prediction algorithm and the possible benefits it offers, simulated example using the Simplified Frequency Response (SFR) model proposed in [1]. Shedding the same amount of load but earlier, based on a prediction, allows the frequency deviation to be limited. The prediction algorithm must be capable of detecting a disturbance, estimating the relevant system parameters and then generating an accurate and reliable prediction that may be acted upon.

Figure 1-1 compares the frequency traces for the prediction supported and traditional response for a simple example, which is detailed in Chapter 8, note that the same amount of load reduction was used in both cases but it was possible to implement the prediction supported action sooner as the traditional response is forced to wait for the threshold to actually be violated. This simple example demonstrates the potential for prediction based actions to arrest dangerous declines in frequency earlier than traditional actions. In practical implementations the ability to arrest the frequency decline earlier would be a significant advantage for system operators, as the longer the system is exposed to a large frequency deviation the more likely it is that the frequency deviation will trigger secondary contingencies or even a cascade of failures. Therefore, to maximise the benefit offered by prediction supported actions it is important to minimise the time taken to execute the four stages of the prediction process.

The primary advantage of using predictions of the post disturbance frequency to design control actions is that it would allow actions to be taken earlier than in the existing frequency control paradigm, also the use of wide area measurements will allow the actions taken to be based on the true system state, and not that anticipated at the planning stage.

1.2 Background and Motivation

Traditionally power systems have been planned and operated based on offline security assessments. However, as power systems become increasingly complex the potential risk of blackouts increases and the creation of methods for the online security assessment of a power system has become an area of great interest in an attempt to combat this threat [2] [3]. The introduction of wide area measurement technologies means that the data necessary to perform these online assessments has become increasingly available to system operators [4] [5].

Methods have been proposed that assess the voltage stability and rotor angle stability using tools such as pattern classification [6], decision trees [7] and the calculation of security indices [8]. Methods have also been proposed for assessing frequency stability [9] [10]. Much of this research [11] [12] [13] has focused upon the prediction of the

post-disturbance frequency behaviour. This thesis seeks to offer a contribution to this body of research with a focus on the prediction of the transient frequency response of a power system after a large disturbance.

1.2.1 Frequency Stability

Frequency stability is defined as: "the ability of a power system to maintain steady frequency following a severe system upset resulting in a significant imbalance between generation and load" by a joint IEEE/CIGRE working group in [14]. It is the role of frequency control to guarantee the frequency stability of a power system and the measures employed by frequency control are discussed in detail in Chapter 2.

Guaranteeing frequency stability is a necessity because the frequency of a power system is a key measure of the health of that power system, as it reflects the active power balance in the system; that is, the instantaneous imbalance between the generation of, and demand for active power in the system. Therefore, any event that disturbs this active power balance will cause the frequency to deviate from nominal. Examples of such disturbances include the loss, or deloading, of a generator and sudden increases or decreases in the load demand.

The performance of many power system elements is dependent on the frequency of the power with which they are supplied [15]. For example, turbine blades experience cumulative damage when forced to operate during frequency deviations of more than 2.5 Hz from the nominal frequency and any auxiliaries driven by motors, e.g. the coolant pumps of a nuclear power plant, will slow down as the frequency falls, potentially compromising their operation. Therefore, a large deviation from nominal can cause the behaviour of many system elements to vary dramatically from their normal modelled behaviour and can lead to cascading failures that will further stress the power system, aggravate the frequency deviation and eventually lead to a blackout [16].

In future power systems adaptive corrective control will be a necessity as the increasing levels of uncertainty that will be encountered in the future may severely compromise the traditional deterministic control [17].

1.2.2 Power System Developments

The increased levels of uncertainty that threatens frequency control will arise from the introduction of new technologies and operating practices. A key motivation for these changes is the need for power systems to deliver on environmental targets and ensure optimal exploitation of assets. In the case of the UK government the key targets are a 37 % reduction in CO_2 emissions by 2030 and a 60 % reduction by 2050, based on emission levels in 1990 [18]. Achieving these targets will require power systems to move away from the traditional dependence on centralized fossil fuelled power generation. The EU's large combustion plant directive (LCPD) will lead to the closure of approximately 20 GW of generation capacity in the UK [19]; much of which is planned to be replaced by the construction of 47 GW of wind generation by 2030 [19].

In the future the load on the power system will likely increase due to the burden placed upon it by the decarbonisation of the heating and transport industries and the four million new homes that are expected in the UK by 2030 [18]. The additional stress this increased load will place on the system will likely be managed in two ways. The first of these is the use of adaptive protection and control that will allow maximum exploitation of existing assets without compromising the security of supply. The second is to significantly increase the rating of key transmission corridors by constructing new transmission assets. However, the difficulty of obtaining permission to construct these new assets on shore has resulted in plans to use undersea High Voltage Direct Current (HVDC) links. HVDC offers many advantages when considering undersea transmission so the constraints placed on on-shore construction will mean that future power systems will likely have HVDC links operating both as interconnections to neighbouring systems and in parallel with the AC system.

Whilst the changes that are occurring in power systems pose a threat to their successful operation they also offer many opportunities for the creation of new control tools, for

example synthetic inertia [20]. The threats posed and the opportunities offered by the changes that are most relevant to frequency stability and control are described in detail in Chapter 3.

1.2.3 Synchronised Measurement Technology

Like other adaptive online actions the prediction methods proposed in this thesis are only feasible if sufficient synchronised measurement technology (SMT) is available to provide accurate time stamped measurements of phasors, frequency and active power [4]. SMT is a key enabler of the wide area monitoring, protection and control (WAMPAC) systems that many power systems are seeking to create [5]. Other key components of WAMPAC that the prediction methods will depend on for their successful operation will be communication networks, which allow fast and reliable data transmission, and data storage and concentration tools, which will allow the information needed by the prediction methods to be extracted from the vast quantity of data gathered by SMT [21]. The speed of data transmission and information extraction will be a critical factor in determining the success of the prediction methods, as any prediction must be made sufficiently in advance of the predicted event occurring to allow adaptive corrective actions to be designed and implemented. SMT, WAMPAC and frequency measurement algorithms are discussed in Chapter 4.

1.3 Goals

From the outset of this research the main goal was the creation of a method that could accurately predict the post disturbance frequency behaviour of a power system. Achieving this main goal can be broken down into the following sub-goals:

- Create a method for estimating the time at which a disturbance occurs.
- Create a method for estimating the inertia of a power system, the inertia has significant influence on the frequency behaviour of a power system in the initial period after a disturbance and as such is a focus of this research.
- Investigate reduced order models of the power system frequency response that can be used for creating predictions.

- Investigate machine learning techniques that could be used to create predictions.
- Investigate the use of direct methods, e.g. Lyapunov type methods, for creating predictions.
- Validate the methods created using simulated power system models in PowerFactory® [22] and MATLAB® [23] as well as measurements taken from real power systems.
- Demonstrate the benefit of using adaptive corrective control actions that are supported by frequency predictions.

1.4 Contribution

The research presented in this thesis was focused on the creation of online post-disturbance frequency prediction methods that could serve to support occasional and emergency frequency control actions. The main contributions of this research can be separated into four parts:

1. Definition of generic requirements.
2. Creation of an on-line method of identifying the time of a disturbance and predicting the system inertia at that time.
3. Creation of an on-line means of predicting the nadir of the post-disturbance frequency response.
4. Creation of a frequency prediction method using pattern classifier techniques.

These are described as follows.

1. A definition of the generic requirements of a method for predicting the post-disturbance frequency behaviour of a power system (Chapter 5) that was based on a review of the existing frequency control and the anticipated developments in power systems and synchronised measurement technology. The key elements of this definition are that a prediction method is required to:
   - Operate quickly, in a matter of seconds, if it is to support the fast actions demanded from occasional and emergency frequency control.

- Be both secure and dependable as any failure in frequency control will compromise frequency stability and consequently the stability of the power system.
- Be capable of performing the online estimation of any model parameter values that are required by the prediction method to overcome the increased level of uncertainty that is anticipated in future power systems.
- Seek to minimise the time taken to create a prediction as the primary benefit of frequency prediction is that it allows control actions to be implemented before the predicted deviation occurs, so any delay in the performing the prediction will reduce the benefit offered by the prediction.

2. Creation of an online method for the simultaneous detection of the time at which a disturbance occurred in a power system, or area of a power system, and the estimation of the inertia of that system, or area (Chapters 6 and 7). This method uses the swing equation and a comparison of the residue between a set of sliding filter windows; the key benefits of this online method are:
   - The exploitation of the availability of synchronised measurements will allow it to replace the traditional offline and post-mortem methods for estimating system inertia.
   - The inertia is a key parameter in determining the initial system frequency response to a disturbance and as such its online estimation is a necessity if the potential benefits of post-disturbance frequency prediction are to be realised.
   - Simultaneously estimating the inertia and the time of disturbance means that the method is not dependent on any outside applications for a time of disturbance estimate and this estimate can also be used to support other applications; e.g. the estimation of any other parameters required by a prediction method.

3. An online method that uses measurements of the initial (0.5 seconds) frequency and active power response to determine the parameter values of an approximate model of the frequency response and thereby predict the nadir of the post-disturbance frequency response. This is achieved by solving this model for the

condition of a zero first derivative with respect to time (Chapter 8). This research was based on an existing prediction method and the improvements made during the course of this research are:

- An online parameter estimation method that eliminates the dependence of the original method on the offline testing of every generator in the system.
- The proposal of two alternate methods for using these predictions to design adaptive load shedding strategies.
    i. The first method initiated fixed load shedding based on a prediction and in the example case allowed a 15.5 % reduction in the minimum frequency.
    ii. The second method determined the minimum amount of load shedding that would ensure frequency stability and in the example case allowed a reduction of approximately 40 % in the amount of load shed.

4. Creation of a frequency prediction method using pattern classifier techniques (Chapter 9). This method defined the future frequency behaviour of the system in terms of five class labels (extreme under frequency, below statutory limit, within statutory limits, above statutory limit and extreme over frequency) using the initial post-disturbance frequency and active power behaviour and a polynomial regression classifier. The primary benefit of this approach to frequency prediction is that the supervised learning process that is used to train the classifier will implicitly represent the variation in the system; reducing the need for online parameter estimation when compared to an approximate model based approach.

1.5 Outline of the Thesis

Chapter 2 – A Summary of the Existing Frequency Control in Power Systems

This chapter describes the frequency control mechanisms that are in use in contemporary power systems and the motivation behind them. Understanding the operation of this control, as well as past successes and failures, was critical to defining

the requirements that frequency predictions must satisfy if they are to be capable of supporting frequency control in the future.

Chapter 3 – Power System Developments

Many of the developments that are occurring in the power systems will directly influence the implementation and success of frequency control. This chapter describes the developments that will have the most influence on frequency control and highlights both the potential threats and opportunities.

Chapter 4 – Synchronised Measurement Technology

The advent of WAMPAC and SMT are the enabling factor that will allow the practical implementation of online tools such as frequency prediction. This chapter describes the support that will be available to frequency prediction in future power systems. Issues discussed include the communication and data processing delays involved, and the quality of synchrophasor and frequency measurement algorithms.

Chapter 5 – Defining Frequency Prediction

This chapter contains a detailed discussion of what exactly frequency prediction entails in the context of this thesis and the constraints under which it must operate. The scope of this definition includes the purpose of frequency prediction, the form that any frequency prediction will take and candidate methods for achieving frequency prediction.

Chapter 6 – Estimating the Inertia of a Power System

The inertia heavily influences the frequency response of a power system immediately after a disturbance. Therefore, understanding the inertia and creating a method for the estimation of inertia online formed a key part of this research. This chapter introduces the challenge of estimating inertia and presents a novel method created during this research that allows the accurate and reliable online estimation of the inertia.

Chapter 7 – Simultaneous Estimation of the Inertia and Time of Disturbance

The novel inertia estimation method presented in Chapter 6 depends upon receiving an estimate of the time of disturbance from an external source. This is an unfortunate weakness as the accurate estimation of this time of disturbance can prove difficult in practical applications. This chapter presents a novel method that combines the inertia

estimation method with a residue based approach for estimating the time of disturbance. Therefore, this novel method allows the simultaneous estimation of both the inertia and the time of disturbance.

Chapter 8 – Post-Disturbance Frequency Prediction using Approximate Models

This chapter details the attempts made to achieve frequency prediction using a method based on solving an approximate model of the system frequency response. An existing method is adapted and its dependence on offline information is eliminated. This method is tested and its relative success is discussed. Furthermore, an online method for using frequency predictions to design adaptive under frequency load shedding actions is proposed.

Chapter 9 – Frequency Prediction using Pattern Classification Theory

This chapter introduces the basic concepts behind pattern classification theory and its potential as a prediction tool. The possibility of using a polynomial kernel classifier, support vector machine (SVM), and neural network for performing frequency prediction is studied. The training, validation and testing of a classifier is presented and the potential application of these methods to a practical system is considered.

Chapter 10 – Summary

This chapter summarises the research presented in this thesis and its contribution. In addition, some possible opportunities for the further development of this research are proposed.

1.6 References

[1] Anderson, P.M.; Mirheydar, M.; , "A low-order system frequency response model," *Power Systems, IEEE Transactions on* , vol.5, no.3, pp.720-729, Aug 1990

[2] Morison, K.; Lei Wang; Kundur, P.; , "Power system security assessment," Power and Energy Magazine, IEEE , vol.2, no.5, pp. 30- 39, Sept.-Oct. 2004

[3] Bertsch, J.; Kaba, M.; Quaintance, W.; Rehtanz, C.; , "Enhanced reliability and other benefits with online security assessment," Developments in Power System

Protection, 2001, Seventh International Conference on (IEE) , vol., no., pp.246-249, 2001

[4] Phadke, A.G.; Thorp, J.S.; *Synchronized Phasor Measurements and their Applications*. 1 ed, ed. A.S. M.A. Pai. 2008, New York: Springer Science+Business Media.

[5] Terzija, V.; Valverde, G.; Deyu Cai; Regulski, P.; Madani, V.; Fitch, J.; Skok, S.; Begovic, M.M.; Phadke, A.; , "Wide-Area Monitoring, Protection, and Control of Future Electric Power Networks," *Proceedings of the IEEE* , vol.99, no.1, pp.80-93, Jan. 2011

[6] Rajapakse, A.; Gomez, F.; Nanayakkara, K.; Crossley, P.; Terzija, V.; , "Rotor angle instability prediction using post-disturbance voltage trajectories," Power and Energy Society General Meeting, 2010 IEEE , vol., no., pp.1, 25-29 July 2010

[7] Ruisheng Diao; Kai Sun; Vittal, V.; O'Keefe, R.J.; Richardson, M.R.; Bhatt, N.; Stradford, D.; Sarawgi, S.K.; , "Decision Tree-Based Online Voltage Security Assessment Using PMU Measurements," Power Systems, IEEE Transactions on , vol.24, no.2, pp.832-839, May 2009,

[8] Ming Ni; McCalley, J.D.; Vittal, V.; Tayyib, T.; , "Online risk-based security assessment," Power Systems, IEEE Transactions on , vol.18, no.1, pp. 258- 265, Feb 2003

[9] Hengxu Zhang; Zhiyuan Hou; Yutian Liu; , "Online Security Assessment of Power System Frequency Deviation," Power and Energy Engineering Conference (APPEEC), 2012 Asia-Pacific, vol., no., pp.1-4, 27-29 March 2012

[10] Chih-Wen Liu; Thorp, J.S.; , "New methods for computing power system dynamic response for real-time transient stability prediction," Circuits and Systems I: Fundamental Theory and Applications, IEEE Transactions on , vol.47, no.3, pp.324-337, Mar 2000

[11] Mirzazad-Barijough, S.; Mashhuri, M.; Ranjbar, A.M., "A predictive approach to control frequency instabilities in a wide area system," Power Systems Conference and Exposition, 2009. PSCE '09. IEEE/PES , vol., no., pp.1-6, 15-18 March 2009

[12] Larsson, M.; Rehtanz, C.; , "Predictive frequency stability control based on wide-area phasor measurements," Power Engineering Society Summer Meeting, 2002 IEEE , vol.1, no., pp.233-238 vol.1, 25-25 July 2002

[13] Egido, I.; Fernandez-Bernal, F.; Centeno, P.; Rouco, L.; , "Maximum Frequency Deviation Calculation in Small Isolated Power Systems," *Power Systems, IEEE Transactions on* , vol.24, no.4, pp.1731-1738, Nov. 2009

[14] Kundur, P., et al., Definition and classification of power system stability IEEE/CIGRE joint task force on stability terms and definitions. Power Systems, IEEE Transactions on, 2004. 19(3): p. 1387-1401.

[15] Kundur, P., *Power System Stability and Control* 1994, New York: McGraw-Hill.

[16] U.S.-Canada Power System Outage Task Force "Final Report on the August 14, 2003 Blackout in the United States and Canada: Causes and Recommendations" [Online], Available: http://www.nerc.com/filez/blackout.html [Accessed: Sept 4, 2011]

[17] Strbac, G.; Jenkins, N.; Green, T.; "Future Network Technologies", *Report to DTI (UK)*. 2006.

[18] National Grid Report "UK Future Energy Scenarios", November 2011, URL: http://www.nationalgrid.com/NR/rdonlyres/86C815F5-0EAD-46B5-A580-A0A516562B3E/50819/10312_1_NG_Futureenergyscenarios_WEB1.pdf

[19] Department of Energy and Climate Change "Planning our electric future: a white paper for secure affordable and low carbon electricity", July 2011, ISBN: 9780101809924,
URL:https://www.gov.uk/government/uploads/system/uploads/attachment_data/file/48129/2176-emr-white-paper.pdf

[20] Morren, J.; de Haan, S.W.H.; Kling, W.L.; Ferreira, J.A., "Wind turbines emulating inertia and supporting primary frequency control," Power Systems, IEEE Transactions on , vol.21, no.1, pp. 433- 434, Feb. 2006

[21] Chakrabarti, S.; Kyriakides, E.; Tianshu B.; Cai, D.; Terzija, V.; , "Measurements get together," *Power and Energy Magazine, IEEE* , vol.7, no.1, pp.41-49, January-February 2009

[22] DIgSILENT, "DIgSILENT PowerFactory," V 14.0523.1 ed Gomaringen, Germany: DIgSILENT GmbH, 2011.

[23] Mathworks, "MATLAB," 7.10.0.499 (R2010a) ed Natick, Massachusetts, U.S.A., 2011.

2 A Summary of the Existing Frequency Control in Power Systems

This chapter provides a detailed description of the motivation for frequency control and its implementation in modern power systems. Section 2.1 discusses the importance of developing an understanding of frequency control before attempting to create prediction algorithms to support it. The importance of the role played by frequency control in modern power systems is discussed in Section 2.2, whilst Section 2.3 describes the practical implementation of frequency control. Finally, Section 2.4 describes the success enjoyed by frequency control in the current operating environment and Section 2.5 summarises the elements of this chapter that are most relevant to the task of researching novel post-disturbance frequency prediction algorithms.

2.1 Chapter Introduction

It was important to develop a thorough knowledge of the existing frequency control environment in power systems before attempting the creation of prediction methods. This knowledge is necessary to allow an understanding of the challenges faced by frequency control. This understanding could then be used to inform the design of the prediction methods in terms of the most useful forms of prediction, the time available to make the prediction and the accuracy requirements that should be imposed.

2.2 Frequency Control

Power systems have three main forms of stability: voltage stability, rotor angle stability and frequency stability [1]. Frequency control is responsible for helping to ensure frequency stability, which is defined as: "the ability of a power system to maintain steady frequency following a severe system upset resulting in a significant imbalance between generation and load" by a joint IEEE/CIGRE working group in [1]. The role that frequency control plays in ensuring the frequency stability of a power

system means that providing satisfactory frequency control is one of the key tasks of a system operator.

2.2.1 Scope of Frequency Control

Frequency control is responsible for balancing the second by second changes in load and generation that occur in a power system and ensuring that the frequency is approximately nominal throughout the day. This task is accomplished using continuous frequency control services. Furthermore, frequency control is responsible for limiting the frequency deviation that occurs after a large disturbance to the power balance in the system, e.g. the loss of a generator, as well as then returning the frequency to the nominal value within the required time. This task is accomplished using occasional frequency control services. The contrast between these two types of frequency deviation can be seen in Figure 2-1.

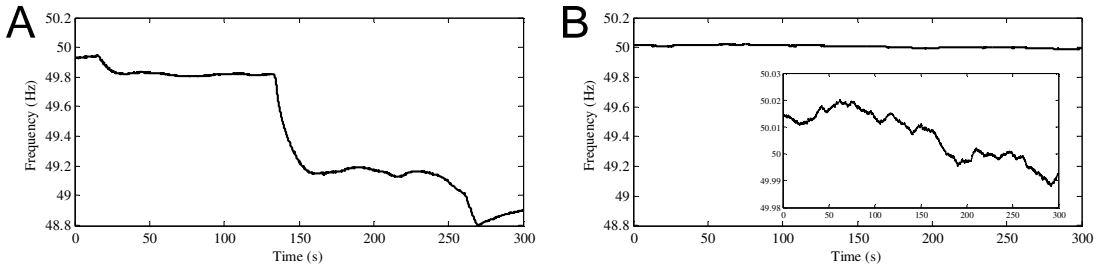

Figure 2-1 – The frequency response of a system during a sequence of large disturbances, A, and during normal operation, B, are compared on the same scales to display the significant variation. Furthermore, B contains an inset on a more useful scale that depicts the nature of the second by second variations in frequency.

The separation between occasional and continuous services is depicted in Figure 2-2. It is not the task of frequency control to balance the larger variations in load that occur in the system on the time scale of hours. These larger changes are accommodated by varying the dispatch of the system through market based power balancing mechanisms such as bilateral trades and spot markets.

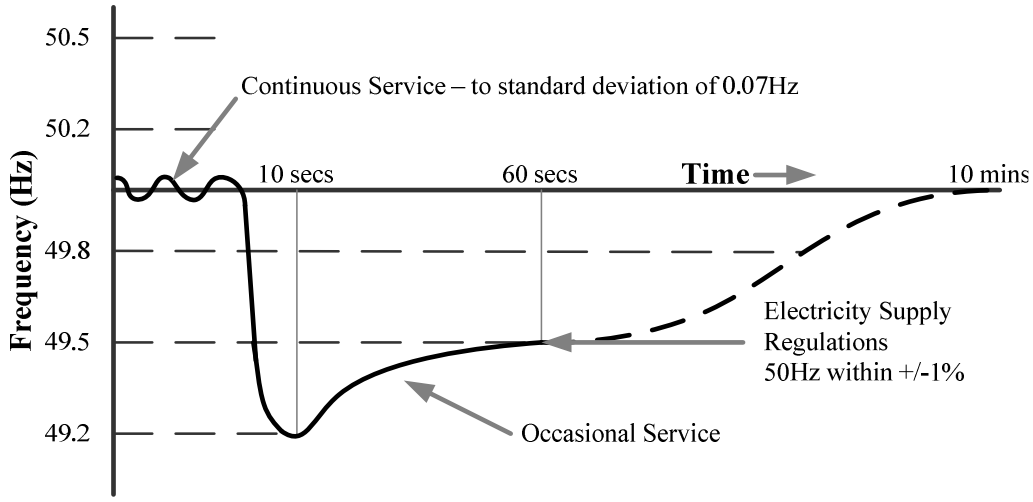

Figure 2-2 – Frequency control is responsible for accommodating the small second by second variations in load using continuous services and any large unexpected disturbances to the power balance, e.g. the loss of a generator, using occasional services. Figure taken from [2].

2.2.2 Technical Motivation for Frequency Control

Power systems are complex systems that are vulnerable to a wide array of disturbances. The relationship between frequency and the active power balance, namely that an excess of active power generation cause the frequency to rise whilst a deficit of active power will cause the frequency to fall, means that disturbances to the active power balance will be of most concern for frequency control. Examples of these disturbances include the loss of a power station, load centre, interconnection or HVDC link [3].

Power systems are designed to operate at near nominal frequency. Many elements of the power system will begin to experience non-standard operation or suffer lasting damage if forced to operate at a frequency that is too far above or below the nominal. This improper operation at off-nominal frequency gives rise to the threat of frequency instability and as such is the origin of the need for frequency control in power systems.

The following are some examples of the improper operation associated with frequency deviations from nominal. Turbine blades experience permanent and cumulative damage due to resonant vibrations [4] when forced to operate at a frequency of more than 2.5 Hz below nominal. The auxiliary elements of a power plant, e.g. coolant feed pumps, will be externally fed during normal operation and as such their proper

operation is dependent on system frequency [4]. When generators are forced to operate at speeds above nominal the main valve will be closed which can stress the boiler after a prolonged period and lead to unstable conditions such as flame instability [3].

Due to the sensitivity of system operation to the system frequency it is possible for frequency deviations to initiate a major disturbance, e.g. the tripping of a generator due to low frequency, or allow the effects of a disturbance to propagate through the system and stress system elements that are remote from the original disturbance, e.g. the cascading loss of multiple generators as the frequency continues to fall as each generator is lost [4].

The cascading loss of generators due to low frequency is the greatest threat posed by poor frequency control [1]; as the consequence of losing a generator due to low frequency is a further fall in frequency and an increased risk of other generators being disconnected from the system to protect them. Without drastic corrective steps, such as controlled islanding [5] and extensive load shedding, this cycle of generator tripping will cause the system to reach a condition in which it is inadequate and from which a blackout is inevitable. This cascading loss of generation will usually be initiated by the loss of an older steam turbine unit, the operation of which is less robust against frequency deviations than more modern generator designs [4].

The threat of the cascading loss of generation is the reason that low frequency conditions are considered to be more serious than high frequency conditions in a power system [3], as in the worst case of the loss of a generator due to high frequency the loss of generation will help to correct the imbalance rather than exacerbate it.

Blackouts are the greatest threat faced by power systems [1]. They involve the complete loss of supply to entire sections of the power system; the political, social and economic consequences of which can be severe. Blackouts rarely occur due to adherence to the N-1 operating principle and when they do they are usually caused by a sequence of unanticipated and/or low probability events [4]. Due to the severity of the consequences of a blackout a great deal of time and effort is expended by system operators and planners in an attempt to anticipate and then mitigate the most likely causes of a blackout in any system. However, the low probability nature of the sequence of events that initiate a blackout makes this task incredibly challenging.

Frequency instability has played a role in a number of recent blackouts [6] [7] [8] and can pose a problem in both densely meshed and lightly meshed power systems [4] as the source of frequency instability is the balance between and distribution of the active power generation and load. However, the threat of frequency instability is greater in isolated systems as they have access to fewer external generation resources through tie-lines [9]. During a large disturbance the frequency in a large system will vary across the system because it can take between one and three seconds for the frequency disturbance to traverse the power system [3]. This increases the challenge of frequency control as different parts of the system may be experiencing different frequency conditions.

2.2.3 Commercial Motivation for Frequency Control

The liberalisation of electricity markets made electricity a commodity. Therefore, any electricity supplied must meet certain standards in terms of quality [10]. These standards are imposed because in almost all power systems the transmission aspect is a monopoly; and therefore, customers cannot choose to be supplied with electricity of higher quality, or lower cost that has been carried by a different transmission system. Standards, enforced by a regulatory body, are therefore used to ensure that the electricity supplied by the transmission system will be satisfactory to the user [11].

Power quality is measured in a variety of ways, one of which is frequency [10]. The quality of the electricity supplied is determined, in terms of frequency, by considering the number, duration and magnitude of fluctuations from the nominal system frequency [11]. This means that in addition to meeting the technical requirements there are commercial requirements imposed upon frequency control [12]. Meeting these requirements takes the form of the operator ensuring that the cost of any frequency control service is justified by the benefit it offers [13].

It is important to note that frequency control existed before the liberalisation of the power industry and the commercial demands this entailed simply added new considerations for planners and operators when implementing frequency control.

2.2.4 Core Tasks of Frequency Control

Given the sensitivity of a wide array of system elements to the system frequency and the threat of frequency instability triggering blackouts, either through the propagation of disturbed system conditions or cascading loss of generation the primary tasks of frequency control can be summarised as follows [1]:

- Hold the system frequency within the defined limits during both normal operation and after a disturbance.
- Prevent a cascading loss of generation assets.
- Protect generation and transmission plant from frequency deviations.
- Ensure commercial competitiveness of all services procured.

Any protection and control actions implemented as part of a frequency control strategy must be reliable as frequency control must satisfy the N-1 design criterion applied to the power system [4].

2.2.5 An Example of Frequency Control Practices: National Grid

Frequency control practices differ significantly between the various transmission system operators in the world. This section describes the frequency limits that are applied in the National Grid.

The National Grid Company (NGC) is responsible for the operation of the transmission system in England and Wales and this activity is regulated by the Office of the Gas and Electricity Markets (OFGEM). National Grid's primary control has three components [11]: Primary Response, Secondary Response and High Frequency Response. The bulk of the primary response must be available within ten seconds, the secondary response must be available within thirty seconds and sustained for up to thirty minutes whilst the high frequency response must be available within ten seconds and then sustained indefinitely. The details of what each of these response stages involves is described in the next section but it is important to recognise here the short time frames in which frequency control is expected to operate.

National Grid's frequency control practices are laid down in The Grid Code [11] they define the duties of, were applicable, the following parties: large power stations with registered capacity of more than 50 MW, network operators, DC converter stations, providers of ancillary services and any externally interconnected system operators.

A diagram depicting the main control thresholds and operational limits in terms of the absolute frequency magnitude that are used by National Grid can be seen in Figure 2-3 and this highlights the narrow range that the power system frequency must be kept within.

Frequency control services are treated as a commodity and therefore the value of any service that is offered by a generator must be defined. The methods used to define the frequency services offered include [14]: benchmarking of the actual service provided by a unit through online monitoring and assessment, measuring the dynamic response of service, and testing of units to identify the service that can be expected from them and the frequency region in which this service can be delivered.

The sources of reserve and other frequency services used are [14]: partially-loaded steam plants, pumped storage plants, partially-loaded gas turbines both open cycle and combined cycle gas turbines, interconnections with external systems, and loads with frequency activated relays. Loads with frequency activated relays constitute the systems ability to perform Under Frequency Load Shedding (UFLS) and these relays use the absolute magnitude of frequency to trigger their operation.

Minimum frequency response provisions for new build generation units have been imposed to try and ensure that as the system develops the available frequency response services continue to be sufficient. These require: frequency response capability of 10 % and a minimum de load capability of 65 %. Where both percentages are given in terms of the generators rated capacity.

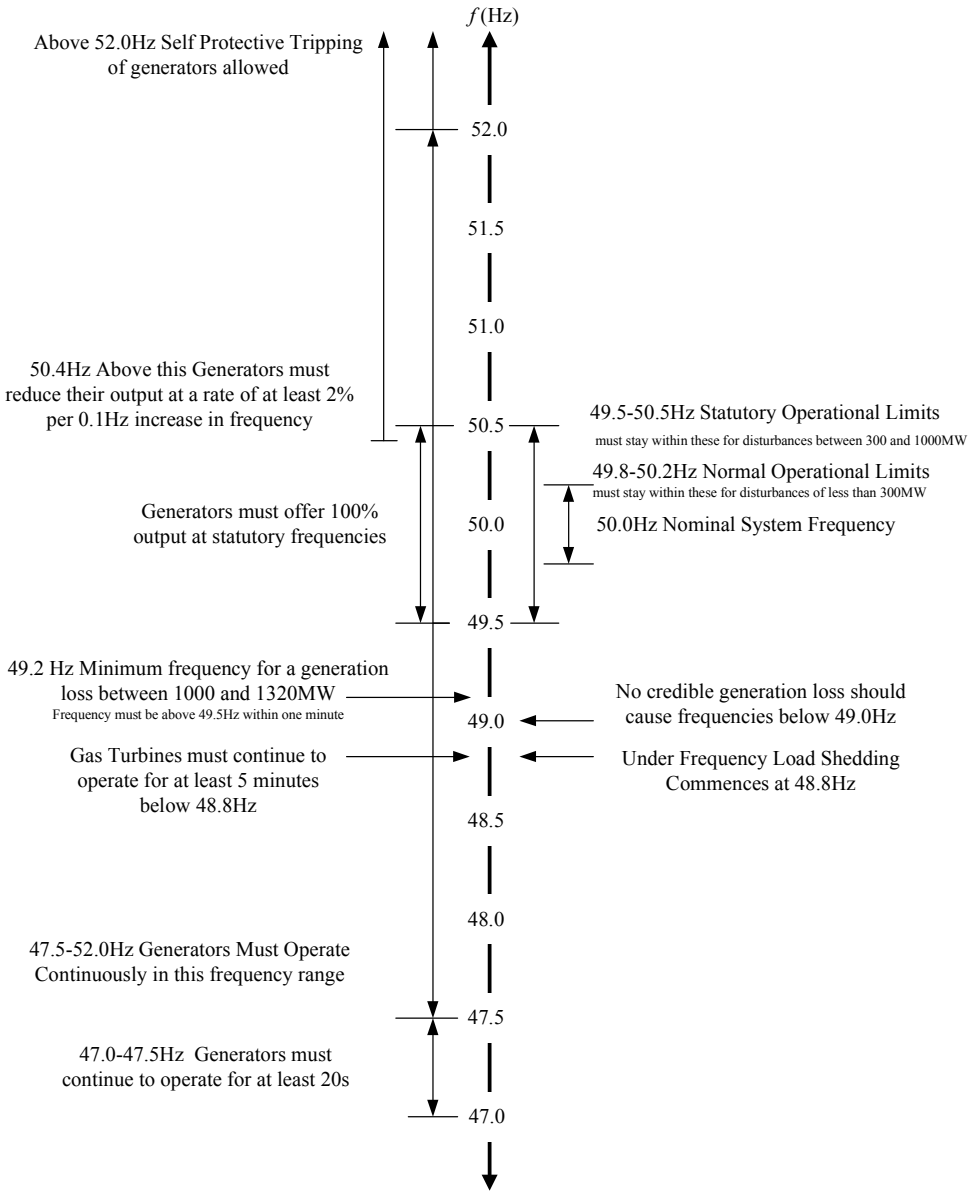

Figure 2-3 – The main frequency thresholds and operating limits defined as part of National Grid's frequency control practices. Figure based on information from the Grid Code [11].

2.3 Elements of Existing Frequency Control

The frequency control services that are available to a transmission system operator are separated into different levels of control [9] [12]. These levels of control include: fast actions that only have a local influence on frequency, slower actions that allow the frequency across the entire system to be managed and emergency actions that can be called upon as a last resort to limit the size and duration of any large frequency excursions that develop.

2.3.1 Primary Control

Primary control is provided by the governor of a generator and is expected to be available within a few seconds. It is based upon the relationship that causes a change in the electrical loading, and therefore electrical torque, of a generator to translate into a change in the rotor speed of that generator. This change in rotor speed will change the electrical frequency of the power produced by the generator.

Control of this change in electrical frequency can be achieved by comparing the measured rotor speed to a reference speed to identify any deviation. This change in speed signal can then be used to calculate the adjustment to the primary energy input of the generator that will be necessary to correct the power imbalance at the generator terminals and limit the speed deviation this imbalance has caused. A block diagram of this process can be seen in Figure 2-4.

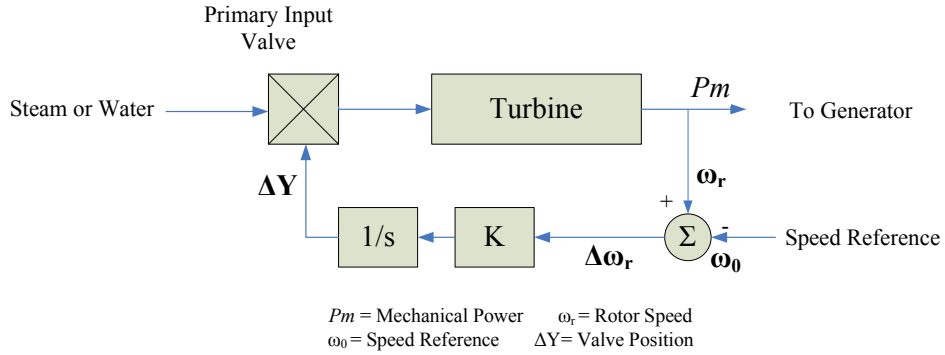

Figure 2-4 – A block diagram of a simple governor controller that implements primary control, figure based on one from [12].

In order to allow multiple generators to operate in parallel they must operate at the same frequency or the generators would drive against one another, in an attempt to force the system frequency to their frequency set point [12]. It is possible to operate units in parallel by applying another input signal to the governor, in the form of a speed droop. This droop, ρ, is defined as the change in frequency, Δf , normalised to the nominal frequency, f_n, divided by the change in power output, ΔP, normalised to a given power base, P_n. The inverse of the droop is R and it is referred to as the stiffness of the generator.

$$\frac{\Delta f}{f_n} \Big/ \frac{\Delta P}{P_n} = \rho \quad \text{[p.u.]} \tag{2-1}$$

The use of speed droop allows units with different characteristics to move to the same new frequency by dividing the change in load between the units in such a way as to cause the same speed change in each unit [12]. This means that units which have a smaller speed droop will pick up more load, and vice versa.

The speed droop characteristic of a generator is implemented through a feedback loop in the generator control system. This takes the form of the previous change in primary energy input being used to reduce the change in speed signal seen by the governor. In a simplified block diagram this is represented by dividing the change in primary power signal by the value of the generator speed droop and subtracting this from the calculated speed imbalance, as seen in Figure 2-5.

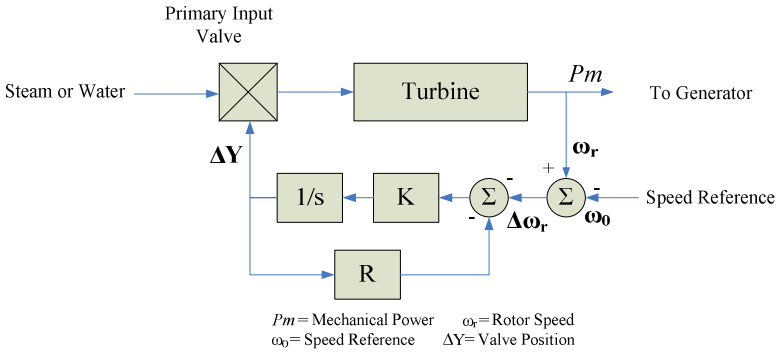

Figure 2-5 – Block diagram of a simple governor controller for a generator with the addition of a speed droop feedback, with stiffness R, that allows dissimilar generators to operate in parallel, figure based on one from [12].

The aggregation of the response of multiple units gives a stiffer speed droop characteristic, case (A) in Figure 2-6, and for large systems with many generators the characteristic will be very close to horizontal [12].

However, this aggregation does create the danger of a large change occurring in the speed droop characteristic of a system when moving between the responses of different units, case (B) in Figure 2-6. This may occur if the change in power would cause the dispatch of a unit to exceed its maximum output. This would mean that the droop characteristic of this unit would become unavailable and the characteristic of a different, potentially less stiff, unit would be relied upon [12].

System loads are also sensitive to a change in frequency. However, the response of the system generation to any such change is far more significant [12]. This can be seen when comparing the typical stiffness of loads, K_L, and of generators, K_T, given in [12] . These are $K_L = 0.5 \rightarrow 3, \quad K_T \approx 20$.

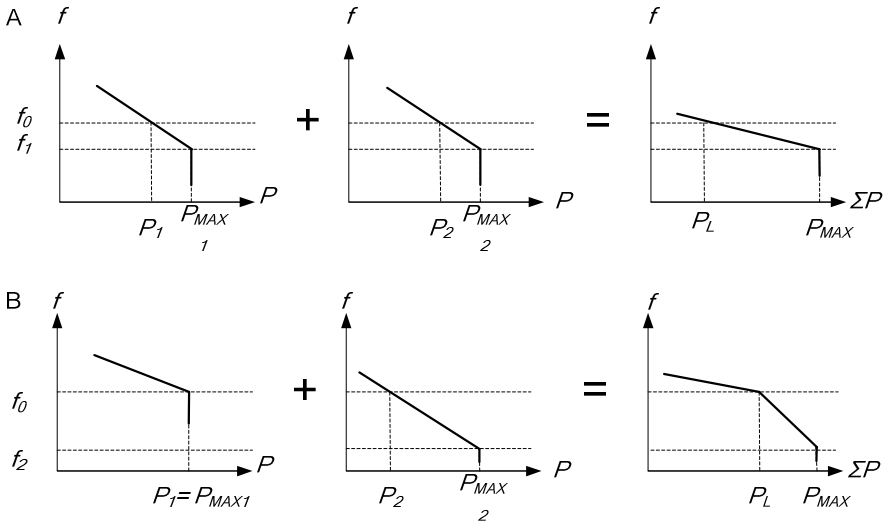

Figure 2-6 – Speed droop allows dissimilar generators to operate in parallel here two generators are shown with P_1 and P_2 marking the dispatch of generator 1 and 2 respectively. The aggregation of the speed droop of several generators provides a stiffer system speed droop characteristic (A). However, there is a risk of discontinuities in the droop characteristic when the response of a generator is exhausted (B). Figure based on one from [12].

Most units have a dead band around the nominal system frequency included in their droop characteristic [12]. This prevents the machine from having to respond to particularly small changes in frequency. Responding to these changes would cause the fuel input to the machine to be subjected to a large number of rapid adjustments with no real benefit to the system. This would expose the machines control systems, valves

etc, to premature ageing and would most likely increase the cost of frequency control provision without providing any benefit. The size of the dead band implemented determines when the machine begins to influence the frequency response of the system. A dead band with width of ~10 mHz means that the machine will participate in primary frequency control, whilst a dead band with width of ~200 mHz means that it will instead offer additional reserve in the event of a large disturbance [12].

The fact that this control action takes place purely within the generators means that it is a fast acting form of control with a highly localised effect. Despite this localised effect the fast acting nature of primary control means that it is an essential part of the system's ability to keep the system frequency close to the nominal and minimise the initial frequency deviation after a disturbance [14].

2.3.2 Secondary Control

The purpose of secondary control actions is to restore the system frequency to the nominal set point and ensure that any tie-line flows in the system are at their contracted level. This action is necessary because the primary control achieved through the introduction of a speed droop can only act to limit the deviation and not to correct it.

This secondary control is achieved by moving the load reference set point of some, or all, of the system generators to allow an increase, or decrease, in the power generated thus allowing the frequency to be returned to the nominal value.

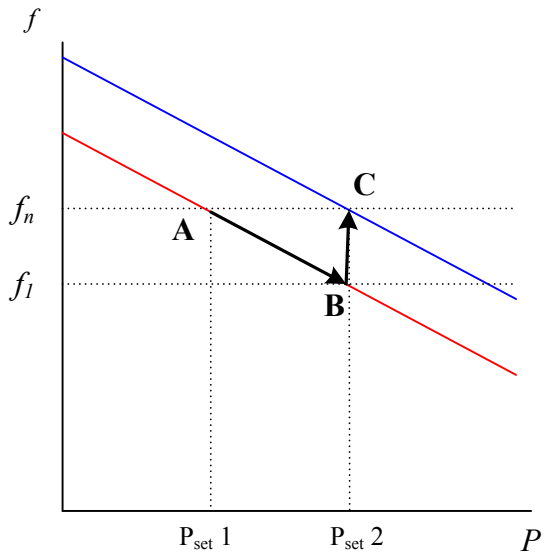

Figure 2-7 – After a change in load the primary control allows the frequency to fall from its nominal value at position A to f_1 at position B along the red characteristic. The secondary control then moves the power output set point, P_{set}, of the generator from position 1 to 2 so the blue characteristic is used to return the frequency to its nominal value, f_n, at position C, based on a figure from [12].

Moving the set point in this way is achieved by subtracting a load reference set point variable from the speed change feedback loop in Figure 2-5 to give the new controller block diagram depicted in Figure 2-8. This additional feedback causes the controller to see an apparent speed deviation that is larger than the one there actually is. The response to this apparent deviation allows the speed of the generator to be returned to nominal whilst generating more power, compare points A and C in Figure 2-7.

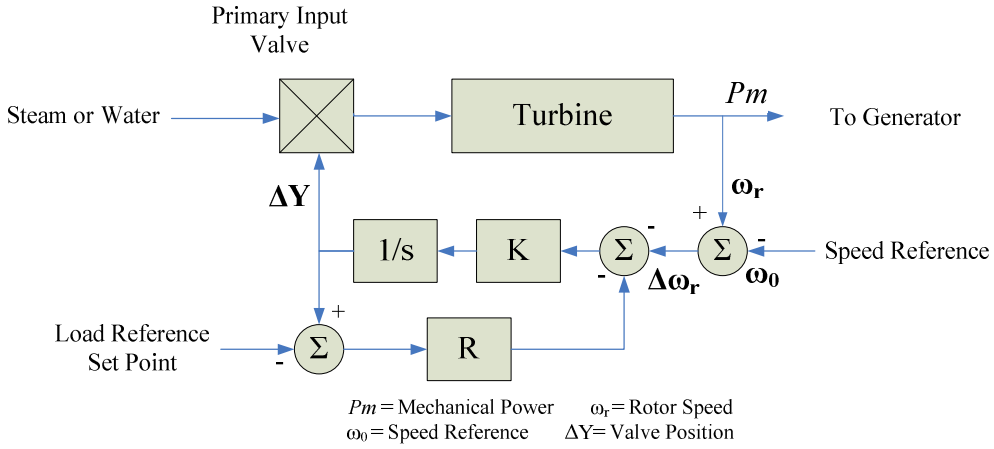

Figure 2-8 – Block diagram of a simple governor controller for a generator with the addition of a feedback loop that allows the load set point to be moved. This controller can therefore supply secondary control, figure based on one from [12].

A movement of the droop characteristic in this way for one unit will move the droop characteristic of the entire system, due to the effect of aggregation. This means that not

all units must be a part of this secondary control for it to have the desired impact. Therefore, it tends to be medium sized units that are responsible for applying secondary control actions [9] [12] because they have good flexibility, capacity and efficiency. These properties mean that medium sized units can offer reserve for the desired control action more cost effectively than smaller units whilst also allowing larger base load units to continue to operate at their optimum output.

The discussion above assumes that the individual generating units themselves will control the load set point adjustments. Only in the case of an isolated power system will this be true as in larger interconnected systems, with multiple control areas connected via tie-lines, it is necessary to calculate the set point adjustments centrally. This is because if each local unit were allowed to respond independently imbalances in some areas may not be resolved and tie-line flow limits may be violated.

Centralised control overcomes this problem because it can identify the location of a disturbance, based upon information from units spread around the system. Access to this knowledge allows the central control to automatically calculate set point changes for each unit that will remove their local imbalances and preserve any tie-line flow limits. This control approach is known as automatic generation control (AGC) and the time frame for these actions is between ten seconds and fifteen minutes after the initial disturbance [12].

2.3.3 Tertiary Control

Tertiary control acts after the system frequency has been returned to, or very near to, the nominal value. Tertiary control is different to primary and secondary control because it does not deal directly with controlling the frequency. Instead the main task of tertiary control is to ensure that the resources tasked with providing primary and secondary control are sufficient to deliver the necessary control actions, as defined in the relevant regulations, when they are called upon.

Ensuring that these control actions are available may require generators to be re-dispatched if the control actions taken previously have exhausted the capability of those units, or others, to provide the necessary control actions. This change in the

dispatch of generators is also used to ensure that both the load and the necessary frequency control services are provided in the most economic way possible; whilst maintaining the desired level of system security.

The actions available to tertiary control include: adjusting the set point of a generator and turning on, or off, fast starting generation units. Fast starting is usually defined as a generator capable of generating rated power within fifteen minutes of being turned on [12]. These actions can be taken either manually or automatically depending on the system operator practices.

When planning control actions it is important to consider the availability of plant capacity in the form of de-loaded units as well as spinning and standing reserve that will be able to provide the necessary capacity for any desired control action. It can sometimes be cost effective to partially de-load a medium sized unit, to provide reserve, rather than starting an additional generator.

It is also important to bear in mind during tertiary control that due to the local nature of most control actions it is not just the MVA capacity of reserve that is important. Rather, the physical location of reserve on the network is also a parameter in determining its value, as a small amount of reserve in a key strategic location may offer more benefit than a larger reserve elsewhere [12].

2.3.4 Under Frequency Load shedding

Under frequency load shedding (UFLS) is a widely used [3] [15] [16] last resort [12] [17] against large low frequency events that may cause cascading outages and even the disconnection of parts of a system.

This means that unlike the other forms of frequency control discussed above UFLS is an emergency service and is therefore only responsible for ensuring that frequency stability is preserved after severe contingencies have occurred. UFLS is not responsible for accommodating the small fluctuations in load that the other frequency control services discussed above deal with.

UFLS operates by automatically disconnecting load if the local frequency behaviour violates certain thresholds and is usually executed in stages rather than all at once. The thresholds that define when a load shedding stage will be executed can be based on many factors, including: the absolute value of the frequency, the absolute value of the derivative of frequency, the time spent below a certain frequency, the value of the derivative of frequency relative to the absolute frequency, or a combination of the above. Some load shedding schemes also consider the voltage magnitude in the system or the status of key feeders [16]. UFLS schemes that use these sorts of additional inputs are usually referred to as Adaptive Under-Frequency Load Shedding (AUFLS).

Load shedding is usually executed in stages [9] with each defined portion of load being shed as its thresholds are exceeded. The earlier stages of load shedding usually shed low value loads or loads that have agreed to be used for this purpose in return for some form of benefit. The variation in the frequency across larger power systems during a disturbance means that the location of any shedding will be a factor in determining its success in arresting the frequency decline.

The loads shed during this process are separated into two categories; these are firm load and probabilistic load. Firm load has a dependable load profile and therefore the actual reduction in load when firm load is shed is reliable. Probabilistic load does not have a dependable load profile and therefore a large number of these loads are grouped together. This aggregation ensures a good (above 90 %) [12] chance of the desired amount of load actually being shed when the instruction is given. This grouping allows probabilistic loads to serve as a useful part of under frequency load shedding

When discussing load shedding it is important to bear in mind that over shedding is a potential hazard as it can cause the frequency to become too high. Another issue related to load shedding is that whilst the shedding itself is automated the load reconnection tends to be manual [17].

2.3.5 System Integrity Protection Schemes (SIPS)

The N-1 design criterion has led to power systems being remarkably secure in their operation. However, the vital role that the transmission system plays in a modern

economy means that operators continue to strive to improve the security of their system. It has been recognised that the success of applying the N-1 criterion has resulted in the cause of most blackouts being a combination of multiple contingencies [6] [7] [8]. When a specific set of contingencies are identified as being particularly likely, or a severe threat to a system, System Integrity Protection Schemes (SIPS) are designed to protect the system from this specific set of contingencies [3] and Figure 2-9 depicts their general structure. These schemes were initially referred to as Special Protection Schemes (SPS); however, as their use became increasingly wide spread and common place they were redefined as SIPS. The use of SIPS is now a world wide practice [4] and an ever increasing number of these schemes are being designed and implemented. SIPS form part of the growing trend in power systems toward the integration of protection and control functions [4].

A SIPS can be summarised as a set of pre-determined actions that are designed based on offline system studies and are implemented after a very precise set of conditions have been detected in the system [3]. For a scheme to be classed as a SIPS the actions implemented must go beyond simply isolating the faulted elements.

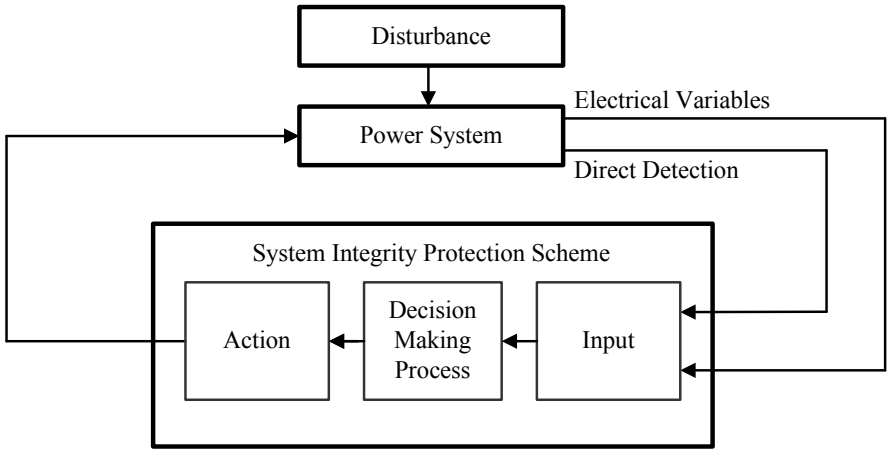

Figure 2-9 – This is the general structure of a system integrity protection scheme. After a disturbance inputs are taken from the power system in the form of measurements, status flags etc and pre-defined actions are implemented if the necessary decision making criteria are met. This figure is taken from [3].

Many SIPS are armed by one condition and then the pre-determined actions are triggered by a second condition. For example, a SIPS may be armed by the loss of one transmission line in an area. It will then be triggered when a second line is lost in the area and a pre-determined generator is disconnected to prevent the remaining lines in

the area from being overloaded, this action would serve to prevent the cascade tripping of the lines due to sequential overloading.

SIPS can be separated into two general types, response based and event based. Response based SIPS are armed based on the measured system response, e.g. violation of a frequency threshold, and can respond to any contingency that causes the necessary change in the system response [4]. Event based SIPS are armed by a certain combination of events, e.g. the loss of a transmission line. This means that response based SIPS are more adaptive but event based SIPS will respond more quickly as they do not need to wait for a measurable response of the system to occur [4].

Response based SIPS can respond to a wide range of contingencies, which allows them to have a more powerful influence on the system. However, this also means that the design of a response based SIPS is far more complex than the design of an event based SIPS, as far more possible operating scenarios must be considered. This can prove an issue as the complexity of any SIPS should be minimised wherever possible, as they must satisfy the dual requirements of any protection system, security and dependability [3]. These requirements are both a necessity as if the SIPS fails to operate, i.e. it is not dependable, the system will be left exposed to a severe set of contingencies and if the SIPS operates spuriously, i.e. it is not secure, then the SIPS may itself initiate a severe set of contingencies due to the extensive authority they are given over key system elements such as generators and transmission lines.

It is important to note that whilst devices like Thyristor Controlled Series Compensation (TCSC) and Power System Stabilisers (PSS) provide dynamic control they are transmission devices and are not SIPS in general. However, if a scheme were designed that adjusted their control mode to help counter a contingency this would constitute a SIPS action [4].

A SIPS can be designed to aid frequency control of a power system during extreme conditions and can be a cost effective solution for preventing system breakdown [3]. A primary advantage of a SIPS is that, unlike equipment protection, they can be designed to ensure system integrity and adequacy [3]. In the context of frequency control a SIPS is used to increase the system security for extreme contingencies. However, in other

contexts a SIPS can be used to increase the utilisation of an asset, e.g. a transmission line, whilst maintaining a fixed security margin [3].

The actions available to a SIPS that is dedicated to improving frequency control are diverse in nature and some are more extreme than others but all of them deal with adjusting the active power balance in the system.

The actions that are currently available for containing a decline in frequency include:

- Increase in generation from fast starting units such as gas turbines and hydro units where available.
- Increased active power generation from fast start hydro units by switching them from compensator mode to generation mode.
- Under frequency load shedding.
- The blocking of on-load tap changers (OLTC).
- Tripping tie lines to areas with low frequency to prevent the spread of disturbed system conditions.

The actions that are currently available for containing a rise in frequency include:

- Generator runback.
- Generator rejection.
- Early disconnection of hydro units due to their greater sensitivity to overspeed.
- Braking resistors.

The actions that are currently available for containing either a rise or a fall in frequency include:

- Fast changes in the power flow on HVDC links.
- Controlled separation of the power system, i.e. Controlled Islanding

Each action has its own benefits and consequences and in general the more powerful the effect of the action on the frequency the greater the risk involved. For example, separating an area of the system with low frequency by opening transmission lines is a powerful action but an inherently high risk one, due to the difficulty involved in selecting the best lines to open and the near certainty of undesirable secondary effects after opening loaded transmission lines [4].

Generator rejection is an action that is commonly used as part of a SIPS [4]. This action reduces the system frequency by reducing the quantity of generation. The preference is to use hydro units as they are more resilient against the consequences of sudden disconnection than thermal units. These consequences include extreme over speeds, thermal stress and shock induced fatigue of the shaft. If hydro units are unavailable, and the rejection of the available thermal units is particularly undesirable fast valving of thermal units can be used to achieve a similar effect. Fast valving involves rapidly opening and closing the primary valve to reduce the power in the prime mover; this action requires a high degree of technical coordination and may stress the valves and primary fuel systems [3]. Fast valving is not possible for hydro units as water cannot be compressed as much as gas leading to the water hammer effect placing intolerable pressure on the valve.

The introduction of HVDC links into transmission systems has the potential to afford a powerful new tool for controlling both over and under frequency conditions. The high degree of controllability inherent to the active power flow on an HVDC link allows rapid changes to the power flow to be used to counter active power imbalances and a response time of two seconds has been achieved in pilot projects in Norway [3]. However, most HVDC links will serve as connections between asynchronous systems operated by different bodies. Therefore, implementing this action will require agreements between both parties and consideration of the risk of propagating the frequency disturbance between the two systems [3].

2.4 The Performance of Existing Frequency Control

The existing preventative frequency control has allowed very few reportable frequency excursions to occur, e.g. one reportable frequency excursion occurred in the power system of Great Britain between 2005 and 2010 [18]. However, despite the limited occurrence of large frequency excursions, they have contributed to the occurrence of several recent wide area blackouts. For example, frequency conditions were normal prior to the 2003 blackout in the United States and Canada but the initial frequency swings that occurred played a significant role in allowing the initial disturbance to propagate through the system [6].

The success of existing preventative control measures is dependent on the consistent nature of existing power systems, i.e. the variables of existing system models are relatively reliable. Developments in the nature of power systems, discussed in detail in Chapter 3, will erode this consistency, potentially compromising the success of the existing preventative control [19].

2.5 Chapter Summary

This chapter has introduced the system frequency as a measure of the active power balance in the system. The concept of frequency stability in power systems is defined as the requirement to ensure that the system frequency remains within the given security limits during both normal operation and emergency conditions [1]. Frequency stability is ensured using two mechanisms: power balancing and frequency control.

Power balancing uses a variety of mechanisms such as bilateral trades, agreed up to several years in advance, and spot markets to ensure that sufficient generation assets will be available to satisfy the forecasted load during the planning period, usually a half hour period. The time frame in which power balancing is executed means that it is not specifically relevant to achieving frequency prediction.

In contrast frequency control is responsible for ensuring that the generation can accommodate the constant changes in load that occur during this planning period as well as any large disturbances to the power balance, such as the loss of a generator, without compromising frequency stability. Therefore, the operation of frequency control is of central importance to understanding the operating environment in which any prediction method must exist.

The frequency deviations from the constant changes in load are accommodated using continuous services whilst those arising from large disturbances are accommodated using occasional services. In general, frequency control services can be separated as follows. Fast acting local services that limit the initial frequency decline, primary response. Slower system wide actions that return the frequency to nominal, secondary

response, and a tertiary response that involves operators restoring the necessary levels of primary and secondary response resource over the course of several minutes.

The fast acting nature of primary response, full response is required within ten seconds by NGC, indicates the short time frame in which frequency control operates. The constraints of this time frame mean that if frequency prediction is to be of any use to system operators or control schemes then they must be performed and communicated within a period of only a few seconds.

Failure to provide satisfactory frequency control through the provision of sufficient ancillary services will leave a system vulnerable to the cascading loss of generators and blackouts. Therefore, it is vital that any element of frequency control satisfies the dual requirements of security and dependability. As such these requirements must be considered when developing any frequency prediction tool.

System Integrity Protection Schemes are introduced in this section as they can play a key role in ensuring that the system will be capable of preserving frequency stability during exceptional circumstances. Frequency predictions may prove to be a valuable input for a novel SIPS.

2.6 References

[1] Kundur, P., et al., Definition and classification of power system stability IEEE/CIGRE joint task force on stability terms and definitions. Power Systems, IEEE Transactions on, 2004. 19(3): p. 1387-1401.

[2] Hung, W.; , "Transmission System Requirements and Ancillary Services Provision," *Power Generation Control, 2007 IET Seminar on* , vol., no., pp.37-53, 6-6 Dec. 2007

[3] CIGRE Report on 'System Protection schemes in Power Networks', Task Force 38.02.19 June 2001

[4] CIGRE Task Force C2.02.24, "Defense Plan Against Extreme Contingencies", April 2007

[5] Lei Ding; Gonzalez-Longatt, F.M.; Wall, P.; Terzija, V.; , "Two-Step Spectral Clustering Controlled Islanding Algorithm," *Power Systems, IEEE Transactions on* , vol.28, no.1, pp.75-84, Feb. 2013

[6] U.S.-Canada Power System Outage Task Force "Final Report on the August 14, 2003 Blackout in the United States and Canada: Causes and Recommendations" [Online], Available: http://www.nerc.com/filez/blackout.html [Accessed: Sept 4, 2011]

[7] Bakshi, A.S., "Report of the enquiry committee on grid disturbance in Northern region 30th July 2012 and in Northern, Eastern and North-Eastern region 31st July 2012", 16th August 2012. http://www.powermin.nic.in/pdf/GRID_ENQ_REP_16_8_12.pdf

[8] Andersson, G.; Donalek, P.; Farmer, R.; Hatziargyriou, N.; Kamwa, I.; Kundur, P.; Martins, N.; Paserba, J.; Pourbeik, P.; Sanchez-Gasca, J.; Schulz, R.; Stankovic, A.; Taylor, C.; Vittal, V.; , "Causes of the 2003 major grid blackouts in North America and Europe, and recommended means to improve system dynamic performance," *Power Systems, IEEE Transactions on* , vol.20, no.4, pp. 1922- 1928, Nov. 2005

[9] Kundur, P., *Power System Stability and Control* 1994, New York: McGraw-Hill.

[10] Rebours, Y.G., et al., A Survey of Frequency and Voltage Control Ancillary Services – Part II: Economic Features. Power Systems, IEEE Transactions on, 2007. 22(1): p. 358-366.

[11] Transmission, N.G.E., The Grid Code. 2010, National Grid Electricity Transmissions.

[12] Machowski, J.; Bialek, J.; W.; Bumby, J., Power System Dynamics: Stability and Control. 2008: John Wiley & Sons.

[13] Carlton, J. Current mechanisms for procurement and payment of power reserve services. in IEE Colloquium on Economic Provision Of A Frequency Responsive Power Reserve Service (98/190). 1998.

[14] Wood, G.F.; Hung, W.W., Generating plant frequency control services. in Frequency Control Capability of Generating Plant, IEE Colloquium on. 1995.

[15] Terzija, V.V.; Koglin H.J., Adaptive underfrequency load shedding integrated with a frequency estimation numerical algorithm. Generation, Transmission and Distribution, IEE Proceedings-, 2002. 149(6): p. 713-718.

[16] El Azab, R.M.; Eldin, E.H.S.; Sallam, M.M., Adaptive Under Frequency Load Shedding using PMU. in Industrial Informatics, 2009. INDIN 2009. 7th IEEE International Conference on. 2009.

[17] ARRUDA, G.C., Special protection schemes for load shedding: practices used by CHESF, in Study Committee B5 Colloquium. 2009: Jeju Island, Korea.

[18] National Grid "Report to the gas and electricity markets authority, National Electricity Transmission System Performance Report 2009 – 2010", 2010. [Online], Available:http://www.nationalgrid.com/uk/Electricity?Info/performance/ [Accessed:Sept 4, 2011]

[19] Strbac, G; Jenkins, N.; Green, T., "Future Network Technologies", *Report to DTI (UK)*. 2006.

3 Power System Developments

The radical changes that power systems are undergoing will pose a threat to the success of frequency control. This is one of the major motivations for this research as frequency prediction could be a valuable tool for supporting frequency control in this more hostile operating environment. This chapter describes the developments that will occur in future power systems that are the most relevant to the delivery of satisfactory frequency control and the motivation for these developments is described in Section 3.1. The developments that are discussed in this chapter are large scale renewable generation (Section 3.2), HVDC (Section 3.3), distributed generation (Section 3.4), demand response control (Section 3.5) and energy storage (Section 3.6). The focus of this chapter is upon the influence of power system developments on frequency control and prediction and these are discussed in detail for the specific developments in each section and a summary of their combined effect is given in Section 3.7.

3.1 Chapter Introduction

The proposed frequency prediction tools are intended to support frequency control in the more uncertain future power system. Therefore, it was necessary to understand how the future power system will be different from the existing power system and how these differences will influence frequency control.

Many of the changes that are occurring in power systems are driven by the need to meet the environmental goals laid down by governments. In the case of the UK government the key targets are a 37 % reduction in CO_2 emissions by 2030 and a 60 % reduction by 2050, based on emission levels in 1990 [1]. In addition abiding by the EU's large combustion plant directive (LCPD) will require the closure of many existing carbon intensive generation technologies, such as coal plants and open cycle gas turbine generation (OCGT) that are not modified to satisfy the new requirements, this could result in the loss of approximately 20 GW of capacity in the UK [2]. Much of the generation deficit created by this action will be met by a dramatic increase in the quantity of renewable generation in the system, much of which will be involve the

construction of 47 GW of wind generation in the UK by 2030. New gas and coal generation will also be constructed; this will consist of modern Combined Cycle Gas Turbines (CCGT) and coal plants that are equipped with carbon capture and storage technologies (CCS). In addition to the life extensions of existing Advanced Gas-cooled Reactors (AGR) a new generation of nuclear power plants will be commissioned. These third generation reactors will have ratings of up to 1600 MW, which is in excess of the current maximum single contingency, or reference incident, of most systems. In the UK this reference incident is currently only 1320 MW.

These changes to the generation portfolio of power systems will be occurring at a time when the demand on the system is expected to increase significantly. This increase will occur due to the burden of delivering the decarbonisation of the heating and transport sectors falling firmly on the power system [1]. Their will also be an increasing number of homes in the UK, approximately 4 million more by 2030 [1].

3.2 Large Scale Renewable Generation

3.2.1 Background

If the environmental targets that are being imposed on the operation of power systems are to be met then large scale, more than 50 MW, renewable generation must become common place in the future power system. Wind generation, either on or off shore, is currently the primary scalable renewable generation technology that is commercially available [3]. The current dominance of wind power in the large scale renewable generation market can be seen in the UK targets for installing a total of 26 GW (9 GW onshore and 17 GW offshore) of wind generation by 2020 and 47 GW (10 GW onshore and 37 GW offshore) of wind generation by 2030 [2].

The intermittency from environmental factors that characterise most renewable generation technologies is the most striking difference between them and traditional synchronous generation units. The effect of this intermittency can be described using the concept of capacity credit, which is defined as the quantity of traditional

synchronous generation that can be securely displaced by the intermittent source in terms of the rating of the intermittent source. The capacity credit of UK wind will be between 20 % and 30 %, although it should be noted the capacity credit will fall as the penetration level increases [4]. The low capacity credit of intermittent generation makes it difficult for renewable generation to directly replace the existing generation assets without adjustment to operating practices, e.g. frequency control.

3.2.2 Wind Turbine Generation

The ever increasing role that wind generation is expected to play in power systems is characterised by the fact that wind turbines are now expected to ride through a fault and contribute to system security rather than simply trip [5]. Furthermore, it is now seen as inappropriate to follow the practice of modelling wind generation as either a negative load or by using an equivalent synchronous machine model [6].

Wind turbine generation can be supplied by either fixed speed or variable speed units. Early wind turbines used fixed speed wind turbine designs, like squirrel cage induction generators and wound rotor induction generators. These designs suffer from poor energy extraction and require support from capacitor banks as they offer no reactive power control. However, their rugged nature and the lack of slip rings means that fixed speed turbines can play a role in some situations.

The weaknesses of fixed speed units meant that it was the development of variable speed units that was a key driver for the introduction of plans for large scale offshore wind farms. The two forms of variable wind speed turbine are Doubly Fed Induction Generators (DFIGs) and Permanent Magnet Synchronous Machines (PMSMs); both of these technologies make extensive use of power electronic converters.

A DFIG feeds power directly to the system and uses a power electronic converter to supply current to the rotor winding of the induction generator. The speed of the machine is then controlled by varying the frequency of this current. The stator of a DFIG can provide reactive power support to the system but the power extraction is sub optimal and there are maintenance issue due to the use of a gear box.

A PMSM feeds power to the power system through a power electronic converter that controls the frequency of the output power. This allows the PMSM to offer maximum power extraction at a wider range of speeds than a DFIG without depending on a gearbox or slip rings, both of which pose issues in terms of maintenance. Furthermore, this operation allows separate control of active and reactive power and as such a PMSM will offer a wider range of control options to the power system.

DFIGs are currently the preferred technology for large wind farms and a key advantage they possess over PMSMs is that the converter used in a DFIG is rated at only 20 % to 30 % of the DFIG rating whilst the converter used in a PMSM is rated at 100 % of the rating of the PMSM. This represents a significant difference in the cost of each technology at this time [7].

It should be noted that wound rotor induction generators can achieve some limited speed variation, up to 10 %, by using a direct current chopper over an external resistor. However, this is a poor substitute for the operational range offered by DFIG and PMSM based wind turbines.

3.2.3 Influence on Frequency Control

The main impact that the introduction of increasing levels of intermittent large scale renewable generation will have on frequency control is the displacement of traditional synchronous generation services without offering equivalent technical performance.

This displacement will reduce the system inertia and the availability of traditional primary response, allowing faster and deeper drops in frequency in response to a given loss of generation. Without a change in operating practices this will mean that frequency control will have less time in which to contain a frequency deviation and fewer resources with which to do so [7] [8]. Furthermore, intermittency increases the level of uncertainty in the system and makes the scheduling of the remaining traditional assets more difficult [4].

The threat that high penetration levels of intermittent generation poses to the system is currently countered by granting life extensions to existing nuclear and gas units and by enforcing limits on the level of intermittent generation that is allowed to generate at any one time, e.g. the 50 % limit imposed by operators of the network on the island of Ireland [8]. However, this will not be feasible in the future and new operating practices must be developed to exploit the potential of large scale renewable generation to support the system.

Despite these threats to frequency control the introduction of variable speed wind turbines also offers an attractive new tool for frequency control due to their ability to rapidly change their power output, when the necessary wind resource is available. This property introduces two considerations for frequency control. The first of these is that during normal operation large wind farms will need to limit the ramp rate of their output change to prevent spikes in the system frequency [9]. The second consideration is the possibility of introducing supplementary controllers that allow the wind turbine to rapidly increase its output during a frequency decline, allowing it to act as a source of synthetic inertia [7] [8].

This synthetic inertia is created by increasing the torque set point of the generator based on a measured fall in frequency. This increase in torque output is achieved by decreasing the rotor speed, which means that the synthetic inertia is a finite resource as there is a limit on how much the rotor speed can be decreased [7]. Furthermore, after the synthetic inertia is provided the output of the wind turbine must be reduced below its pre-disturbance value to reaccelerate the rotor [7]. To ensure optimum performance the adjustment of the torque set point should be supported by an adjustment to the pitch angle control of the wind turbine [7]. This involves preventing an increase in the pitch angle during the provision of synthetic inertia and where possible reducing the pitch angle in order to ensure that the mechanical power captured by the turbine blades is not reduced when synthetic inertia is being supplied.

The deployment of primary response and reserves by intermittent generation will mean that the availability of these services will no longer be intrinsically linked to the load demand as it is now. This is because in the existing system more generation units, i.e. traditional sources of reserve and primary response, are deployed as the load increases

whereas wind generation is dependent on the wind profile, the peaks of which do not necessarily coincide with the load peaks.

3.3 High Voltage Direct Current (HVDC) Transmission

3.3.1 Background

HVDC has become a technology of increasing relevance to modern power systems. The developments in the fields of power electronic converters means that it has become possible to cost effectively step direct current voltages up and down, a key prerequisite of a viable transmission system. HVDC will serve two roles in power systems: linking asynchronous systems and operating in parallel with a synchronous system.

The primary reason for the preference for HVDC in these roles is that the converters electrically isolate the neighbouring systems. Furthermore, the capacitive charging currents inherent to HVAC overhead lines make them less cost effective than HVDC at distances of above 70 to 100 km [10]. This advantage of HVDC links over HVAC links is particularly relevant when considering undersea cables due to the expense of installing offshore platforms for compensation of HVAC cables. This makes HVDC a logical choice for the connection of offshore wind farms to the transmission system.

The challenge of securing permission to construct new onshore lines, regardless of the voltage type used, has meant that system planners have been forced to construct new transmission lines offshore. This has led to plans to introduce undersea HVDC lines in parallel with the existing HVAC if the operator wishes to deliver a large increase in the capacity of a transmission corridor. Whilst other technologies can allow the capacity of a corridor to be increased by extending security limits, for example series compensation [11], the construction of a new link offers the opportunity for a much a larger increase in capacity by increasing the thermal limit of the corridor.

Unfortunately, some issues exist with the deployment of HVDC. The first of these is that the commercial solutions currently on offer in the market differ radically based on supplier. Therefore, when planning the development of HVDC networks, considerations regarding the integration of assets purchased now with assets purchased in the future are a significant concern that could impair confidence in the cost effectiveness of any deployment of HVDC [10]. Another issue related to the deployment of HVDC on a large scale is uncertainty regarding the availability of manufacturing facilities and skilled labour, e.g. offshore cable layers. These shortages could lead to significant delays in the delivery of projects or significant uncertainty in the cost of any project as shortages can lead to dramatic price inflation [10].

3.3.2 Technologies

Existing HVDC solutions can primarily be separated by the converter technology used. The two different types are current source converters (CSC) and voltage source converters (VSC). CSC is the more mature technology and has been in use since 1954 and there are now almost one hundred CSC HVDC links in use around the world with ratings of between 100 MW and 720 MW [10].

CSC links require strong AC networks at both terminals to ensure proper commutation of the thyristors. Where strong is defined as the network having a short circuit capacity that is twice the rating of the link. Therefore, CSC HVDC is unlikely to offer cost effective solutions for connecting offshore wind farms due to the need to install compensation at the wind farm side of the link to ensure the system is strong enough to allow the thyristors to commutate [10].

VSC was first demonstrated in 1997 and uses self commutating Integrated Gate Bipolar Transistors (IGBT). The self commutating nature of IGBTs means that VSC links do not require strong AC networks at both ends like a CSC link does. VSC links produce fewer harmonics than CSC but more importantly, from the perspective of frequency control, a VSC link allows separate control of active and reactive power.

3.3.3 Influence on Frequency Control

HVDC links offer no natural response to a frequency deviation or support for frequency control. This will mean that the inclusion of HVDC links into a system, either in parallel or as an interconnection, will reduce the system inertia and damping [12]. In the case of an interconnection this will be because the power supplied by the HVDC link will displace generation in the system that would have supplied inertia and frequency control services. In the case of offshore wind farms that are connected over HVDC links this will occur as the link will decouple the inertia and damping of the wind farm from the system. If this issue is left unresolved it will allow faster and deeper frequency deviations to occur after any given disturbance. This will force frequency control to contain a larger deviation in less time and with fewer resources.

However, HVDC links depend heavily on power electronics and it is possible to exploit the highly controllable nature of these power electronics to achieve new frequency control services. The proper control of the HVDC links offers an opportunity for rapid changes to the power injection at the connection point that can serve as a source of high quality frequency control services. Due to the potential for a high speed of response that is independent from the system frequency this could be particularly useful during emergency conditions [13]. HVDC links in Norway have been used to provide active power support with a time delay of two seconds [13]. The development of HVDC control schemes is a challenging task, particularly for the sort of supplementary control that this form of frequency support would require, so this support would need to be considered on a case by case basis at this time [14].

3.4 Distributed Generation

3.4.1 Background

Distributed generation (DG) will play a role in future power systems by allowing small, independent and dispersed generators to participate in power system markets [13]. This DG will be provided using a variety of energy sources, including wind, hydro, oil, diesel, gas, biomass, solar, tidal and marine.

The UK energy review [2] highlighted that one of the key elements of achieving a low carbon future would be opening access to the market for small, independent providers of low carbon generation. This distributed generation will usually be connected to the distribution system and under the existing connection policy and operating practices is not required to contribute to frequency control. In the future the level of DG installed in the UK system will be significant; 2.1 GW of embedded wind will be installed by 2012 and this will increase to 3.1 GW by 2030 as part of a total of 19 GW of distributed capacity that is expected by 2030 [1].

Operational experience exists with DG as nations like Denmark, Spain and the Netherlands have penetration levels of approximately 40 %, 20 % and 20 % respectively [15]. Furthermore a proliferation of DG is expected in the USA due to increasing retail prices and deferral of investment in transmission assets [16].

A key benefit of DG is management of transmission network congestion. This will allow a reduction of investment in expensive transmission reinforcement schemes as well as the operational benefits of DG but market mechanisms will need to be updated to reflect this [16].

3.4.2 Technologies

DG has many different designs for even a single energy source and there is a multitude of possible energy sources, including wind, hydro, oil, diesel, gas, biomass, solar, tidal

and marine. DG can be synchronous (small gas/hydro turbines), asynchronous (induction machine based wind) or converter interfaced (direct current sources like Photo Voltaic (PV) panels and batteries). Furthermore, in the case of many Combined Heat and Power (CHP) plants their operation will be optimised for the generation of heat and electrical power is treated as a useful by product [17].

The discussion of the individual characteristics of each of these energy sources and generation designs goes far beyond the scope of this thesis. However, their existence does not. The presence of such a multitude of DG technologies will mean the characterisation of the impact of DG on frequency control will prove difficult; as will the standardisation and regulation of DG. These tasks will become increasingly challenging as the proliferation of DG continues and the ratings of the installed DG begins to increase [17].

The challenge of understanding the disparate DG technologies will be mitigated some what as the low individual ratings of each DG unit will mean that when called upon to act as part of a system control scheme a number of different DG resources will be aggregated to provide sufficient resource.

3.4.3 Influence on Frequency Control

A dependence on distributed generation, rather than the current preference for large centralised generating units, will make the provision of frequency control more problematic in future power systems due to the unknown contribution and operational characteristics of the many technologies [13]. The uncertainty regarding the nature of the DG in the system will make the quality and availability of the frequency control tools that are available to the operator increasingly unclear.

DG can offer frequency responsive reserve and due to its dispersed nature it will increase the geographical availability of reserve [17]. Thus, DG could offer primary response in parts of the system in which it has previously never been economically feasible to implement it [17]. With sufficient support from new communication networks the aggregation of DG could be used to create frequency control tools for

both primary and secondary response. However, how cost effective these tools would be is currently unclear.

The contribution of DG to the provision of ancillary services would require extensive communication and control infrastructures to be installed. Furthermore, it may prove difficult for operators to quantify the level of service offered to a sufficient degree of certainty for these new services to be used as part of a secure frequency control solution.

3.5 Demand Response Control

3.5.1 Background

The burden of decarbonising carbon intensive sectors, such as heating and transport, will fall on the power system. This may cause the electrical load to double by 2050, despite the anticipated improvements in efficiency and consumer awareness of consumption [2].

Road based transport makes up 22 % of UK emissions, 79 % of which is from cars, so decarbonisation of transport is a priority if emission reduction targets are to be met [2]. Therefore, the focus of this decarbonisation is on domestic and light industrial vehicles, also heavy goods vehicles are too heavy for cost effective use of existing electrical motors. The vehicles that will replace existing vehicles will consist of Electric Vehicles (EV), which use only a battery powered electrical motor, Hybrid Electric Vehicles (HEV), which use an electrical motor and internal combustion engine in parallel, and Plug in Hybrid Electric Vehicles (PHEV), which are similar to HEV except their batteries can be charged using the power system. EVs and PHEVs will be the focus for power systems as they will depend on the power system for charging, which may place a severe burden on distribution networks.

Domestic heating represents 50 % of UK energy consumption, much of which is gas fuelled heating [18]. As such, decarbonisation of this sector of the economy will be of

critical importance if emission targets are to be met. This decarbonisation will primarily consist of replacing domestic gas and resistive electrical heating with heat pumps and centralised Combined Heat and Power (CHP) generators.

Whilst it is expected that up to 8 million heat pumps will be installed in the UK, the increase in load due to these heat pumps will be compensated for by a decrease in resistive heating, which is wasteful [1]. Therefore, the challenge for power systems that will arise from the decarbonisation of heating is the larger variation of heating loads (500 GWh to 3000 GWh per day) when compared to existing electrical loads (690 GWh to 1110 GWh) [1]. If actions are not taken to accommodate this variation the difference between the peaks and troughs of the daily load profile could increase dramatically, this would cause the loading factors of generators to fall and with that their efficiency will also fall.

This increase in the total load and the variation of the load when combined with the increased levels of uncertainty in the future system, which will arise primarily due to intermittency of generation, will mean that the traditional approach of passive load and active generation will no longer be tenable. Therefore, the load must begin to play a role in balancing supply and demand if system security is to be ensured in a cost effective way. Energy loads (e.g. heating) and the distributed storage made available by EVs and PHEVs offer the best opportunities to do this as they can defer power consumption to a later time and create a flatter load profile [1]. This manipulation of the power system load is referred to as Demand Response Control (DRC).

3.5.2 Implementing Demand Response Control

The core concept behind Demand Response Control (DRC) is that loads change their demand from normal practices in real time to help improve system performance and security. In general, these changes will be made throughout the day as a part of normal operation to create a flatter load profile, although it will also be possible for these load changes to serve as occasional frequency control services during a disturbance [19].

The loads that are most suitable for use in DRC are those that naturally contain some form of energy storage be it thermal, as in the case of heating, or electrical, as in the case of EVs and PHEVs. These energy loads are most suitable for DRC as they can defer power consumption to later time without necessarily compromising their performance. It is important to recognize that DRC does not reduce the amount of electrical energy consumed by a load; instead it manages the time at which the load draws power so that it best suits system operation.

It has been identified that 63 % of domestic load would be suitable for use in DRC schemes. These are energy based loads that can have their short term power consumption deferred and include hot water (25 %), heating (23 %) and refrigeration (10 %) [19]. Furthermore, NERC reported in [20] that a 5 % to 8 % deferment of peak load could save $15 billion annually. So the possible benefits of DRC are clear.

To realize the financial and operational benefits DRC will require extensive support in the form of new market arrangements that recognise the benefit offered by DRC [21]. Furthermore, the link that exists in many power systems between utility income and price may need to be restructured to ensure that system operators are given the proper incentives [21].

However, the most pressing requirement for the practical implementation of DRC in a power system is a communication and control infrastructure that connects each of the DRC enabled loads and the body that is responsible for managing DRC. This communication and control infrastructure is referred to as advanced metering infrastructure (AMI).

3.5.3 Influence on Frequency Control

DRC will allow a flatter load profile that can be directly influenced by the operator through incentives or time of use pricing. This will allow more generators to operate at their baseline, the operating point at which they are most efficient, without compromising frequency control provision [20]. A flatter load profile will make

implementing frequency control easier as the uncontrolled changes in load that must be contained by continuous services will be smaller and less frequent.

EV and PHEV can be used to achieve fast changes in power flow by reversing charging into discharging. However, such a service would require extensive contractual backing to manage customer issues such as battery lifetime and vehicle availability [21].

The increased competition in the ancillary services market created by AMI enabled DRC would likely reduce the cost of the provision of frequency control. DRC that is based on the aggregation of multiple, geographically dispersed, loads could allow the creation of frequency control actions that are specifically tailored for the system operating conditions [21].

DRC could allow the replacement of the existing discrete steps of load shedding, used as an emergency action during extreme system conditions, with specifically tailored changes in load. This would be particularly advantageous as discrete steps in load pose the risk of causing spikes in the system frequency that may themselves stress the system and trigger secondary contingencies. Furthermore, DRC is less intrusive on the customers as it defers load to a later time instead of disconnecting it entirely.

If most loads in the system were enabled by AMI to act as part of DRC then the system would be approaching a condition in which it truly satisfied one of the requirements of effective frequency control actions, specifically the requirement that the available frequency control actions be distributed evenly across the system [22].

3.6 Energy Storage

3.6.1 Background

One of the greatest challenges of operating a power system is that electrical energy cannot be directly stored. Therefore, in order to maintain the active power balance and

preserve frequency security the generation and demand in the system must be balanced on a second-by-second basis. In the future power system this balancing will become increasingly complex due to issues such as generator intermittency. It may be possible to use energy storage to shift power generated during off-peak times to peak times and help accommodate this [14].

In general, this power shifting could be implemented in one of two ways. The first is that an owner of energy storage buys off peak power and then stores it for sale at peak times. The second option is that the storage owner is also an owner of intermittent generation and stores any excess power generated at off peak times for sale at peak times. This option is particularly attractive for the owners of intermittent generators that would otherwise have to simply curtail the generation of this excess power; for example, the spilling of wind.

This would allow financial gain, as the stored energy could be sold at the higher peak time price or used to bid on to the ancillary services market. This provision of ancillary services would allow energy storage to also offer technical benefits, as the off-peak intermittent generation would contribute to system security during peak times, instead of simply being curtailed.

3.6.2 Technologies

Whilst electricity cannot be directly stored, it can be converted into another form of energy and then stored for conversion back to electrical power at a later time. The challenge of energy storage for power systems is finding a process that can efficiently convert the electrical energy into some other medium, which can store the energy with minimal leakage for a period of up to several hours, and then release it on demand [23] The storage medium is usually the defining feature of an energy storage system and can be chemical, mechanical or electrical potential.

The main energy storage technologies that are ready for deployment in power systems are pumped hydro, advanced batteries (Lithium Ion, Nickel Cadmium and Sodium Sulphur), flow cells, flywheels and superconducting magnetic energy storage (SMES)

[23]. Some of the advantages and disadvantages of these technologies are summarised in Table 3-1.

Table 3-1 – Advantages and Disadvantages of Energy Storage Technologies that can Support Frequency Control [24]

Technology	Advantages	Disadvantages
Pumped Storage	– High energy and power ratings – Low cost per MW	– High capital costs – Specific site requirements
Advanced Batteries	– High energy and power densities – High efficiency	– High production costs
Flow Cells	– Independent power and energy ratings – High storage capacity	– Low energy density
Flywheels	– High power	– Low energy density
SMES	– High power	– Low energy density – High Production Costs

Energy storage technologies are of varying designs and in turn possess varying energy storage capacity and power discharge ratios. Some technologies offer long discharge times at low power whilst others can fully discharge in a few seconds. The potential range of energy and power ratings offered by the technologies most likely to play a role in the provision of frequency control are summarised in Figure 3-1.

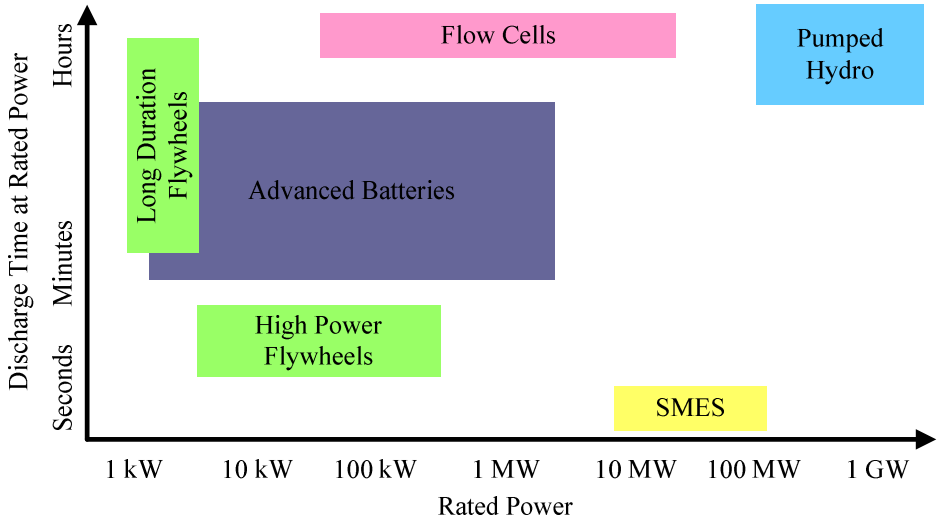

Figure 3-1– Summary of the potential rated power and rated discharge time of the energy storage technologies that may support frequency control in the future [24]

.

The aggregation of the response of different storage technologies allows the different characteristics and advantages of these storage technologies to be exploited for the creation of a flexible tool for providing support to the system. This aggregation could

allow energy storage to offer support for longer, by discharging several units in series, or at a greater rating, by discharging units in parallel. However, this aggregation will depend on the implementation of a new communication and control infrastructure.

3.6.3 Influence on Frequency Control

Storage can be used to compensate for the need to provide additional balancing and security services when a high penetration of intermittent generation is present in a power system. Improving the flexibility of these intermittent generation technologies will allow greater penetration levels to be realised without compromising frequency control provision [25]. From the perspective of frequency control this will be of great benefit as it will allow intermittent generation to compete more effectively in the ancillary services market. This improved competition will reduce the cost of frequency control provision and give access to control resources in a more diverse range of geographical locations.

If sufficient levels of energy storage were to bid on to the market for the provision of generation reserves then the system operator could act to replace spinning reserve with standing reserve. This is possible as the energy storage would provide the fast response services, usually associated with spinning reserve, and as the storage becomes depleted the standing reserve will be coming online and will be capable of replacing the contribution of the energy storage and also contribute to secondary frequency control actions, if necessary. Therefore, as spinning reserve is currently provided by fossil fuel units, this would have the benefit of reducing the fuel costs, and CO_2 emissions, related to providing frequency control services without sacrificing the quality of the primary response.

3.7 Chapter Summary

This chapter has summarised the key developments in power systems that will influence the provision of frequency control. Many of these changes pose a threat to

the provision of frequency control and studies in the USA have identified that the frequency response characteristics of their major interconnected systems are in decline, this trend will likely be observed in other mature systems that are undergoing changes to play their part in delivering a low carbon future [5].

The displacement of traditional synchronous generation by intermittent renewable generation and the increased level of power flow over HVDC links will reduce the system inertia and limit access to traditional primary response. This means the natural, or inertial, part of the frequency response will become increasingly weak and characterised by large, fast swings in frequency due to low inertia. Therefore, the proposed frequency prediction algorithms will have even less time in which to operate than they would in the existing power system.

The displacement of traditional generation by new generation technologies will not only reduce inertia. It will also result in system inertia becoming highly variable, due to the variation in the characteristics of the generation that is displacing the traditional generation at any one time. Frequency predictions could serve as a valuable tool in this context as they could offer an early warning of the large frequency deviations that could occur unexpectedly for a small disturbance in low inertia systems.

Whilst, it is true that many of the developments in power systems will threaten the existing frequency control, they will also offer opportunities for the creation of new frequency control tools. An example of this would be the opportunity to use distributed generation and demand response control, enabled using advanced metering infrastructure (AMI), to create primary frequency control resources in vulnerable parts of the system [20].

It is likely that the new challenges introduced by these developments can be overcome by the proper deployment of the new tools they themselves enable. Furthermore, many of these developments could complement one another to improve system operation. For example, the impact of the intermittent nature of renewable generation could be compensated for by using DRC and energy storage to shift the load peaks to times of peak wind.

It is likely that this combination of threats and opportunities will result in the frequency control of future power systems being of similar nature to the existing frequency control of power systems. This can be expected due to the successful nature of existing frequency control and the difficulties inherent in radically overhauling any key component of a system as complex as a modern transmission system.

The differences that will exist in the future will include the presence of more flexible tools for frequency control, which will be a necessity for allowing frequency control to accommodate the varied inertia and reduced availability of traditional response. However, the flexible nature of these tools will mean that many of them, like synthetic inertia, will be designed to mimic the existing frequency control services. Therefore, one of the conclusions of this chapter is that if the proposed frequency prediction algorithms can serve to support the existing frequency control services then they should equally be able to support frequency control in the future power system.

Finally, many of the new frequency control tools that will exist in the future power system are more adaptive in nature than the existing frequency control. Therefore, frequency predictions could be of great use when adaptively determining the necessary level of response. However, like many of these new frequency control tools, frequency prediction will require access to a new communication and control infrastructure to enable the necessary measurements and data collection. In the case of frequency prediction this enabling infrastructure is wide area monitoring protection and control and it is introduced in the next chapter.

3.8 References

[1] National Grid Report "UK Future Energy Scenarios", November 2011, URL: http://www.nationalgrid.com/NR/rdonlyres/86C815F5-0EAD-46B5-A580-A0A516562B3E/50819/10312_1_NG_Futureenergyscenarios_WEB1.pdf

[2] Department of Energy and Climate Change "Planning our electric future: a white paper for secure affordable and low carbon electricity", July 2011 URL:https://www.gov.uk/government/uploads/system/uploads/attachment_data/file/48129/2176-emr-white-paper.pdf

[3] Shakoor, A.A.; Strbac, G.; Allan, R., "Quantifying Risk of Interruptions and Evaluating Generation System Adequacy with Wind Generation," *Probabilistic Methods Applied to Power Systems, 2006. PMAPS 2006. International Conference on* , vol., no., pp.1-7, 11-15 June 2006

[4] UKERC Report, “The costs and impacts of intermittency: An Assessment of the Evidence on the costs and impacts of intermittent generation on the British electricity network.”, 2006, URL:http://www.ukerc.ac.uk/Downloads/PDF/06/0604Intermittency/0604IntermittencyReport.pdf

[5] Zavadil, R.; Miller, N.; Ellis, A.; Muljadi, E.; Pourbeik, P.; Saylors, S.; Nelson, R.; Irwin, G.; Sahni, M.S.; Muthumuni, D.; , "Models for Change," *Power and Energy Magazine, IEEE* , vol.9, no.6, pp.86-96, Nov.-Dec. 2011

[6] Moreno, R.; Konstantinidis, C.V.; Pudjianto, D.; Strbac, G., "The new transmission arrangements in the UK," *Power & Energy Society General Meeting, 2009. PES '09. IEEE* , vol., no., pp.1-7, 26-30 July 2009

[7] Vittal, V. Ayyanar, R. “Grid Integration and Dynamic Impact of Wind Energy”, Springer, 2013

[8] Tuohy, A.; Denny, E.; Meibom, P.; Barth, R.; O'Malley, M.; , "Operating the Irish power system with increased levels of wind power," *Power and Energy Society General Meeting - Conversion and Delivery of Electrical Energy in the 21st Century, 2008 IEEE* , vol., no., pp.1-4, 20-24 July 2008

[9] Shun-Hsien Huang; Maggio, D.; McIntyre, K.; Betanabhatla, V.; Dumas, J.; Adams, J., "Impact of wind generation on system operations in the deregulated environment: ERCOT experience," *Power & Energy Society General Meeting, 2009. PES '09. IEEE* , vol., no., pp.1-8, 26-30 July 2009

[10] ENTSOE-E, “Offshore Transmission Technologies Report”, 2011, URL: https://www.entsoe.eu/publications/system-development-reports/north-seas-grid-development/

[11] Hor, C.; Finn, J.; Thumm, G.; Mortimer, S., "Introducing series compensation in the UK transmission network," *AC and DC Power Transmission, 2010. ACDC. 9th IET International Conference on* , vol., no., pp.1-5, 19-21 Oct. 2010

[12] National Grid, “Operating the Electricity Transmission Networks in 2020”, 2011, URL: http://www.nationalgrid.com/NR/rdonlyres/DF928C19-9210-4629-AB78-BBAA7AD8B89D/47178/Operatingin2020_finalversion0806_final.pdf

[13] CIGRE Working Group 38.02.19, “ Special Protection Schemes in Power Systems” 2001

[14] Doherty, R.; Mullane, A.; Nolan, G.; Burke, D.J.; Bryson, A.; O'Malley, M.; , "An Assessment of the Impact of Wind Generation on System Frequency Control," *Power Systems, IEEE Transactions on* , vol.25, no.1, pp.452-460, Feb. 2010

[15] Djapic, P.; Ramsay, C.; Pudjianto, D.; Strbac, G.; Mutale, J.; Jenkins, N.; Allan, R.; , "Taking an active approach," *Power and Energy Magazine, IEEE* , vol.5, no.4, pp.68-77, July-Aug. 2007

[16] Novosel, D., “Final Report: Phasor Measurement Application Study” prepared for CIEE by KEMA, 2007, URL: http://uc-ciee.org/downloads/PMTA_Final_Report.pdf

[17] Econnect Consulting report to the department of trade and industry “*Accommodating Distributed Generation”* May 2006 http://www.berr.gov.uk/files/file31648.pdf

[18] Mancarella, P.; Chin Kim Gan; Strbac, G., "Evaluation of the impact of electric heat pumps and distributed CHP on LV networks," *PowerTech, 2011 IEEE Trondheim* , vol., no., pp.1-7, 19-23 June 2011

[19] Black, J.W.; Ilic, M.; , "Demand-based frequency control for distributed generation," *Power Engineering Society Summer Meeting, 2002 IEEE* , vol.1, no., pp.427-432 vol.1, 25-25 July 2002

[20] FERC report, “Assessment of Demand Response and Advanced Metering”, 2006, URL: http://www.ferc.gov/legal/staff-reports/demand-response.pdf

[21] Strbac, G.; Farmer, E.D.; Cory, B.J.; , "Framework for the incorporation of demand-side in a competitive electricity market," *Generation, Transmission and Distribution, IEE Proceedings-* , vol.143, no.3, pp.232-237, May 1996

[22] Kundur, P., et al., “Definition and classification of power system stability IEEE/CIGRE joint task force on stability terms and definitions”. Power Systems, IEEE Transactions on, 2004. 19(3): p. 1387-1401

[23] Baxter, R. “Energy Storage: A non-technical guide”, PenWell Books, 2007

[24] Electricity Storage Association, URL: http://www.electricitystorage.org/about/welcome

[25] Black, M.; Silva, V.; Strbac, G.; , "The role of storage in integrating wind energy," *Future Power Systems, 2005 International Conference on* , vol., no., pp.6 pp.-6, 18-18 Nov. 2005

4 Synchronised Measurement Technology

The unprecedented access to system measurements that is offered by synchronised measurement technology (SMT) will be the key enabler for the practical implementation of any online frequency prediction algorithm created in this research. This chapter introduce the core concept of SMT in Section 4.1 and the enabling principle of phasor measurements in Section 4.2. The key elements of the wide area monitoring protection and control (WAMPAC) system that will facilitate the communication and processing of the data on which prediction algorithms will depend are described in Section 4.3. Section 4.4 summarises the key properties of SMT and WAMPAC that must be considered when developing post-disturbance frequency prediction algorithms.

4.1 Chapter Introduction

A key development in the future of power systems will be the increasing deployment of synchronised measurement technology (SMT) as part of attempts to realise Wide Area Monitoring, Protection and Control (WAMPAC). This is a key enabler for online applications like the frequency prediction methods proposed here. Without the accurate, time stamped measurements that SMT makes available once per cycle it would be impossible to consider, let alone perform, the online parameter estimation and prediction that is proposed here. WAMPAC is also a necessity for these predictions, as without the communication and data concentration capabilities it offers the necessary data could never be collected and coordinated for use by the prediction method within the time necessary. In general, the level of access these technologies can offer power system operators to the system state has the potential to revolutionise the way that power systems are operated. A valuable demonstration of the potential for wide area measurements is the wide area frequency monitoring network (FNET) [1]. FNET measures the frequency at approximately 50 locations in the USA [1] and communicates this data to a central server over the internet and has been used to demonstrate new visualisation and fault location methods.

4.2 Synchronised Measurements and Phasors

The core concept of SMT is that each power system measurement has both a location and a time attached to it so that they can be combined into a single set of measurements that represent the entire system. The approach proposed in [2] for achieving this began the development of SMT [3].

Time stamped phasors from multiple locations represent a new age of situational awareness for operators. However, this development is of relevance to frequency prediction as the concept of phasors was the motivator for the development of the SMT and WAMPAC system that will enable accurate time stamped measurements of frequency and active power to be made available to a frequency prediction algorithm.

The following is a brief introduction to the concept of phasors. A continuous sinusoidal signal can be defined as follows.

$$x(t) = X_m \cos(\omega t + \phi) \tag{4-1}$$

This can be converted into a phasor X, depicted in Figure 4.1, of the following form.

$$X = \left(X_m / \sqrt{2} \right) e^{j\phi} \tag{4-2}$$

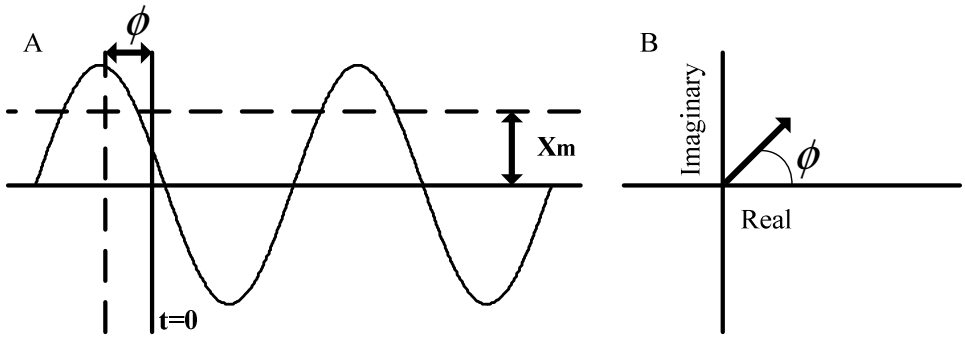

Figure 4-1 – A simple sinusoid (A) and its corresponding phasor representation (B), this concept forms the fundamental basis of existing wide area measurements in a power system. Note that the phase angle is dependent on the reference time used. Figure taken from [3].

In practical power system applications the phasor is calculated using samples of the continuous signal. So a more useful form of the phasor definition given 4.2 would be that given in 4.3.

$$X = \frac{\sqrt{2}}{N} \sum_{k=1}^{N} x_k e^{-j2k\pi/N} \tag{4-3}$$

This definition for a sampled signal assumes that N samples are taken per cycle of the sinusoid and x_k is the k^{th} sample of the signal.

Furthermore, in a real power system applications a phasor representing the positive sequence of the system would be of far more use than a phasor representing each of the phases. The positive sequence phasor can be calculated from the three phase phasors (X_a, X_b and X_c) using 4.4.

$$X_1 = \frac{1}{3}(X_a + \alpha X_b + \alpha^2 X_c) \tag{4-4}$$

where α is a 120° phase shift.

Accurately time stamped phasors defined in this way and taken from multiple locations can be collected at a single location and directly compared. This direct comparison of measurements from remote locations in real time and with a reporting rate of once per cycle offers a remarkable improvement in situational awareness and is the key benefit of time stamped measurements. This benefit is equally applicable to frequency and active power as it is to phasors.

The phase angle of a phasor is usually given relative to the time stamp applied to it and not a reference phasor, as would be usual with traditional power system phasors. This difference must be taken into consideration if SMT phasors and traditional phasors are to be used alongside one another [3].

It should be noted that the concept of phasors can only be applied directly to a pure constant sinusoid [3]. This poses a challenge as the voltage and current waveforms in a

power system will be distorted by a variety of factors and the system itself will never actually be in steady state. This challenge has been overcome using a variety of techniques, e.g. filtering, in existing applications of phasor measurements [3].

At the same time that [2] identified the potential of SMT and phasors, the global positioning system (GPS) was being deployed by the US Department of Defence [3]. Accurate timing is a critical element of GPS and as such the one pulse per second signal it generates seemed a logical choice for the source of the time stamps that are necessary for SMT. GPS currently consists of 30 satellites in patterns that ensure at least 6 satellites are visible from any location on earth at any moment in time [3]. GPS is not unique as a source of accurate time stamps. Any accurate and cost effective replacement would serve the same purpose but at this time cheap and robust GPS receivers are so prevalent that it still seems like the logical choice in most circumstances.

4.3 Wide Area Monitoring Protection and Control

Wide Area Monitoring Protection and Control systems are being deployed in existing power systems to collect, distribute and process the vast quantities of data made available by SMT. They are a powerful tool for gaining access to real time synchronised power system measurements, e.g. frequency and active power, and as such will be a key enabler for frequency prediction.

In a simple case of WAMPAC, as shown in Figure 4-2, Phasor Measurement Units (PMUs) will use signals from voltage and current transformers to calculate the phasor representation of these sinusoidal signals. These phasors have a common time stamp applied to them using the one pulse per second transmitted as part of the Global Positioning System (GPS). The communication infrastructure then allows these time stamped phasor measurements to be transmitted from the remote locations were they are made to a central Data Concentrator (DC). This DC would then align the time stamped phasors received from every PMU and transmit them to the applications that need them.

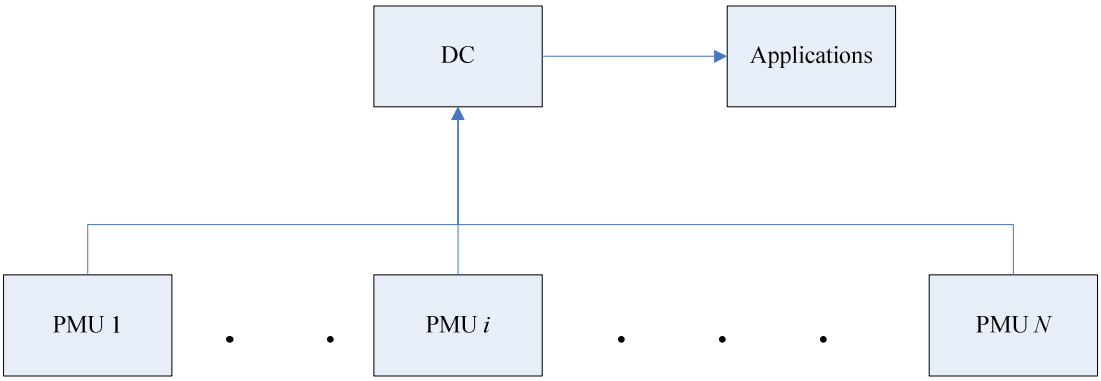

Figure 4-2– An example of a simple, single level, SMT architecture with all *N* PMUs supported by a single DC that forms a coherent data record and passes it to every application.

In reality the simple structure shown in Figure 4-2 would be of limited use, because every application would be forced to wait for the arrival of every phasor before it could act even if it did not need every phasor. In practice, the architecture of a WAMPAC system would have several levels of DCs as shown in Figure 4-3.

A multi level hierarchy, of the type shown in Figure 4-3, is preferable to a single DC architecture because it allows a compromise to be made between the scope of the data available to an application and the time that it takes to collect that data. The higher levels of the hierarchy have access to global data, but endure longer delays, whilst the lower levels only have access to local information, but receive it with minimal delay. Therefore, in multi-level WAMPAC architectures it is possible to match applications to the correct level based on the scope of data necessary and the level of delay that is acceptable. For example, this leads to protection applications appearing at lower levels whilst monitoring applications will appear at higher levels. It is not necessary to connect applications at every point of the hierarchy, note DC 3 in Figure 4-3.

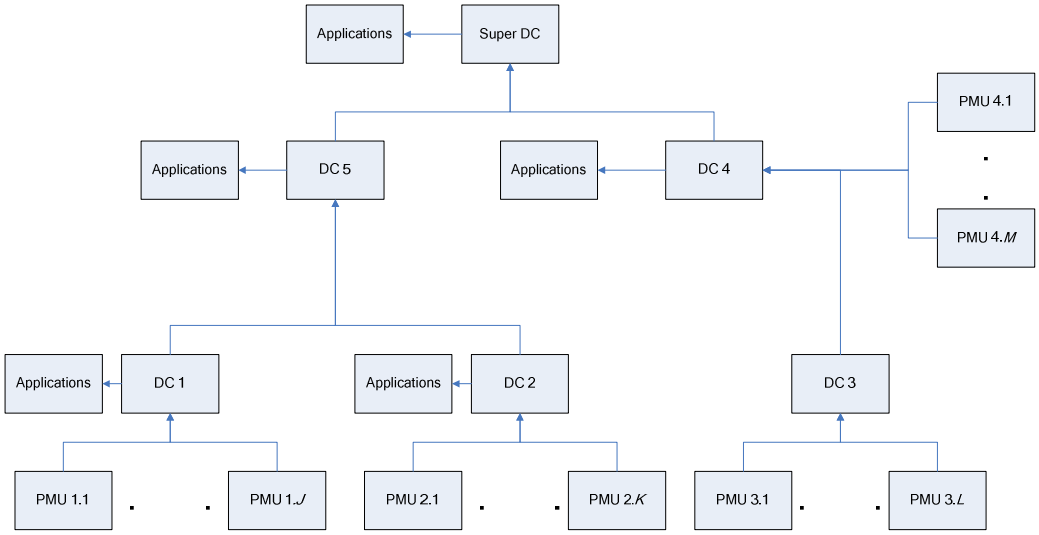

Figure 4-3 – An example of a SMT architecture that has a hierarchy of DCs that allow data to be used by applications at the suitable levels of scope and therefore delay. The variable *J*, *K*, *L* and *M* represent the number of PMUs supported by each DC.

From these architectures it is clear that the basic elements of any WAMPAC system are PMUs for data acquisition and DCs and communication links for data collection and distribution. The properties of these elements will now be discussed with a focus on the sources of errors and delays, as these are the factors that will impact most significantly on the requirements highlighted in Chapter 2 that frequency prediction be fast, secure and dependable.

4.3.1 Phasor Measurement Units

The role of Phasor Measurement Units (PMUs) in a WAMPAC system is producing the time stamped voltage and current phasors and time stamped measurements of frequency and active power. As such they are an important consideration in the development of a frequency prediction algorithm as the accuracy of the PMU will directly impact on the accuracy of the frequency prediction.

PMUs are the most accurate time synchronised measurement device currently available [4]. A PMU produces time stamped measurements by transforming the signals produced by voltage transformers (VTs) and current transformers (CTs). The basic structure of a PMU can be seen in Figure 4-4.

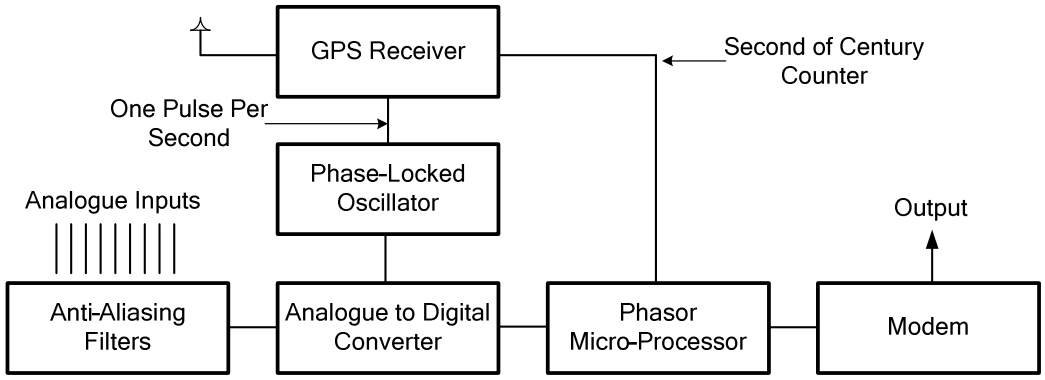

Figure 4-4 – The PMU is the most accurate synchronised measurement device and is therefore a key SMT technology. As SMT needs synchronised measurements, Filters prevent aliasing by satisfying the Nyquist criterion. This figure is taken from [3].

The one pulse-per-second signal, generated by GPS, is divided by a phase-locked oscillator into *N* pulses per second, where *N* is the number of samples to be taken of the analogue inputs per second. The algorithms used to calculate the positive sequence phasors, frequency and active power are executed by a microprocessor. The transducers that generate the analogue signals are a limiting factor in the accuracy of the existing measurement tools. In particular, instrument transformers introduce magnitude and phase errors into PMU measurements [5] [6].

The micro-processor in a phasor measurement unit can execute algorithms that allow it to perform a number of operations on the input data beyond the measurement of phase; these include the calculation of the active power and frequency measurements that will be a necessity for frequency prediction. A number of such algorithms have been proposed in the literature [7] [8] [9] and have been implemented in practical PMUs [10] [11].

The nature of modern power systems as competitive markets, the size of a WAMPAC system and the necessity of avoiding common mode or type failures means that it will be necessary to operate PMUs in parallel with PMUs and DCs from different manufactures. Therefore, to ensure that operators can make purchasing decision with confidence and that WAMPAC will be a success the development of suitable standards is a necessity. At this time the IEEE C37.118 ‘synchrophasor’ standard [12] defines what is required of the operation of a synchronised measurement device and serves to replace the older IEEE c1344 standard.

In general, recursive techniques for phasor calculation are more efficient than non-recursive techniques [13]. Recursive techniques also offer the advantage of producing a fixed phasor for a constant sinusoid, as apposed to the rotating phasor a non-recursive technique would produce [2].

PMUs can be separated into two types, these are: stand alone and integrated. Integrated PMUs are integrated into an existing device and use its voltage transformer (VT), current transformer (CT) and connections to the system whilst stand alone PMUs are independent of other devices [14].

Integrated PMUs cost less and are included in the current synchrophasor standard [12] so they should be capable of operating alongside other types of integrated and stand alone PMUs that meet this standard. However, their may be issues because the original purpose of the VT and CT of the relay may not have the same level of accuracy as those used in a stand alone PMU or other integrated PMUs. In addition, upgrades and alterations may need to be made to the relay when installing the PMU functionality. Due to the case by case nature of this sort of work integrated PMUs of the same type may not necessarily have the same response [14]. Stand alone PMUs are independent of other hardware and should therefore have the same response as all other stand alone PMUs of their specific type. The use of a dedicated metering VT and CT is costly but ensures a high level of accuracy [14].

4.3.2 Data Concentrators

The primary function of a DC is to receive data from PMUs and DCs that are lower in the data hierarchy, perform some form of bad data rejection and then align this data into a coherent record that can be used. The coherent data record can then be transmitted to applications or other DCs. In some cases the DC will possess the capacity to store the coherent data records that it has produced [3]. Some DCs may also have some PMU management capability through which they can be used to send control signals to remote PMUs.

A DC can be implemented through the use of a dedicated hardware solution or it can be implemented using a software solution that runs on a standard server. The hardware type of DC offers a better option for receiving the data transmitted by PMUs whilst the software type of DC offers a superior user interface and data storage capabilities [14].

4.3.3 Communication

An integral element of any WAMPAC system is the communication links that allow the local measurements made by the PMUs to be communicated to other levels of the hierarchy. This communication is a necessity of WAMPAC but it does increase the delay before the data will be available at higher levels of the hierarchy and as such increases the delay before a frequency prediction could be made and the necessary actions taken.

The sources of the delays inherent to communication can be separated into three types [5]. The first type are fixed delays, arising from sources such as transducers, filtering, signal processing, data concentrators and multiplexing, that are usually of the order of 75 μs. The second type of delay is the propagation delay of the link, this is dependent on the medium of the link and the physical distance the link traverses. Typical values for the propagation delay for a power system are given in [5] and range from 25 μs to 200 μs, for fibre optics and satellite communication respectively. The third type of delay is the data transmission delay, which can be calculated by dividing the quantity of the data transmitted by the data rate it is transmitted at. Therefore, this delay is heavily dependent on the data rate supported by the link and for the transmission of a typical 3500 bit PMU frame [5] can range from a negligible delay for fibre optic links up to a 110 μs delay for 33.6 Kbps telephone link [5]. Furthermore, communication links will be exposed to a fourth source of delays due to random delays or jitter [15].

Traditional communication in power systems is based on dedicated operational telecommunication (OpTel) services that offer resilient exchange of certain circuit data as well as measurement and coordination information between adjacent substations [5]. These communication links already form a critical part of modern power system infrastructure [6] and the data records for important assets can be accessed using non-

OpTel dial-up services [4]. These dedicated links allow the high level of communication availability that is necessary for the protection and control of a power system. An average communication availability of 99.95 % is suggested as necessary to support a power system application in [5].

The communication network that will support a WAMPAC system will be dramatically different to this traditional OpTel network. This will be driven by the dramatic difference in the scale of data that will be generated by SMT compared to the data generated for the existing Supervisory Control and Data Acquisition (SCADA) and Energy Management System (EMS). SCADA and EMS use one sample every few seconds whilst most SMT applications expect one sample every cycle [3].

The high cost of any dedicated communication channel means that some form of long term vision will be necessary when considering their development. A variety of possible communication channel options exist, including: telephone lines, power line carriers, microwave and fibre optics. Fibre optics appears to be the current technology of choice [3]. However, some systems in current operation use internet based communications [1]. Ethernet, and other non-deterministic communication systems, could play a role in delivering the communication network for a WAMPAC system. However, they should have their performance carefully examined due to the likelihood of maintenance and uncontrollable downtime [5].

4.4 Chapter Summary

SMT and WAMPAC are major emerging technologies in power systems that will allow accurate time stamped measurements, made by PMUs at remote locations, to be communicated to both centralised and decentralised decision makers.

The unprecedented level of system awareness offered by WAMPAC will enable a new generation of real time protection and control algorithms [4]. In particular, the ability of WAMPAC to collect wide area measurements of frequency and active power at a single location is a critical factor in making the concept of online post-disturbance frequency prediction that is proposed in this thesis feasible.

The IEEE C37.118 ‘synchrophasor’ standard [12] defines the accuracy requirements for the output of PMUs. These requirements allow a clear understanding of the error levels that will be present in the frequency and active power measurements that the frequency prediction algorithms proposed in this thesis will depend upon.

The PMUs, DCs and communication networks that make up the cornerstones of a WAMPAC system can be combined in any number of architectures. However, the multi level WAMPAC architectures that are proposed for large power systems would be of particular benefit to frequency prediction. This is because the variation in frequency across the system during a disturbance will likely make it necessary to perform frequency predictions for multiple areas of a power system, rather than for the entire system. In this context the prediction algorithm could be deployed at a DC in a lower level of the hierarchy, which received measurements from the area the prediction is to be performed for. This would reduce the communication delays and risks of unavailability by shortening the hierarchy the algorithm is exposed to.

The need for high levels of both security and dependability in power system protection and control means that power system operators impose stringent requirements on their communication networks in terms of latency, security and reliability. The stringent requirements imposed upon these communication networks [5] means that they will be able to support the requirements for frequency prediction.

When considering a practical implementation of frequency prediction it would still be advisable to minimize any communication delays by ensuring that the data requested from the WAMPAC system is necessary, particularly in the case of the data with the largest, and therefore constraining, delay. This is advisable as the greatest benefit of frequency prediction is that it allows operators to act before a large frequency deviation develops and as such limits the risk that this deviation will initiate secondary disturbances. Therefore, the faster the prediction is made the faster that it can be acted upon and the greater the benefit of the prediction will be.

4.5 References

[1] Zhian Zhong; Chunchun Xu; Billian, B.J.; Li Zhang; Tsai, S.J.S.; Conners, R.W.; Centeno, V.A.; Phadke, A.G.; Yilu Liu; , "Power system frequency monitoring network (FNET) implementation," Power Systems, IEEE Transactions on , vol.20, no.4, pp. 1914- 1921, Nov. 2005

[2] Phadke, A. G.; Thorp, J.S.; Adamiak, M.G., "A new measurement technique for tracking voltage phasors, local system frequency, and rate of change of frequency", IEEE Transactions on PAS. vol. 102, no. 5, pp 1025–1038, May 1983.

[3] Phadke, A. G.; Thorp, J.S., Synchronized Phasor Measurements and their Applications. 1 ed, ed. A.S. M.A. Pai. 2008, New York: Springer Science+Business Media.

[4] Terzija, V., et al., Wide-Area Monitoring, Protection, and Control of Future Electric Power Networks. Proceedings of the IEEE. PP(99): p. 1-14.

[5] Novosel, D., "Final Report: Phasor Measurement Application Study" prepared for CIEE by KEMA, 2007, URL: http://uc-ciee.org/downloads/PMTA_Final_Report.pdf

[6] CIGRE Task Force C2.02.34, "Defense Plan Against Extreme Contingencies", April 2007

[7] Kezunovic, M.; Spasojevic, P.; Perunicic, B.; , "New digital signal processing algorithms for frequency deviation measurement," Power Delivery, IEEE Transactions on , vol.7, no.3, pp.1563-1573, Jul 1992

[8] Terzija, V.; Djuric, M.; Kovacevic, B.; , "A new self-tuning algorithm for the frequency estimation of distorted signals," Power Delivery, IEEE Transactions on , vol.10, no.4, pp.1779-1785, Oct 1995

[9] Lobos, T.; Rezmer, J.; , "Real-time determination of power system frequency," Instrumentation and Measurement, IEEE Transactions on , vol.46, no.4, pp.877-881, Aug 1997

[10] Arbiter Systems, Model 1133A Power Sentinel Data Sheet,www.arbiter.com.

[11] Alstom Grid, MiCOM Alstom P847, http://www.alstom.com/grid/products-and-services/substation-automation-system/protection-relays/MiCOM-Alstom-P847

[12] IEEE Standard for Synchrophasors for Power Systems. IEEE Std C37.118-2005 (Revision of IEEE Std 1344-1995), 2006: p. 0_1-57.

[13] Phadke, A.G. and Thorp, J.S., “History and Applications of Phasor Measurements”. in Power Systems Conference and Exposition, 2006. PSCE '06. 2006 IEEE PES. 2006.

[14] Sykes, J., et al. Synchrophasors: A primer and practical applications. in Power Systems Conference: Advanced Metering, Protection, Control, Communication, and Distributed Resources, 2007. PSC 2007. 2007.

[15] Eissa, M.M.; Masoud, M.E.; Elanwar, M.M.M.; , "A Novel Back Up Wide Area Protection Technique for Power Transmission Grids Using Phasor Measurement Unit," Power Delivery, IEEE Transactions on , vol.25, no.1, pp.270-278, Jan. 2010

5 Defining Frequency Prediction

This chapter provides a detailed definition of what an online post-disturbance frequency prediction algorithm entails. Section 5.1 discusses the importance of this definition to the research and how it was based on the information contained in Chapters 2, 3 and 4. The definition can be broken down into different elements, each of which is discussed in a separate section. The core requirements of frequency prediction and its role in both existing and future power systems are defined in Section 5.2. Whilst the forms of prediction that will help serve this purpose are defined in Section 5.3 and the possible methods for achieving these forms of prediction are described in Section 5.4. Finally, the ways in which this definition influenced the course of this research are discussed in Sections 5.5.

5.1 Chapter Introduction

A definition of the purpose of an online post-disturbance frequency prediction algorithm and the constraints imposed upon it was necessary because it was important to ensure that any prediction method considered would be capable of generating frequency predictions that would be useful to system controllers. This definition was based on the nature of the existing frequency control (Chapter 2) and the developments in power systems (Chapters 3 and 4) and it is assumed that any prediction method will use wide area measurements of frequency and active power to generate accurate predictions for the system operators or closed loop controllers following the simple generic structure depicted in Figure 5-1.

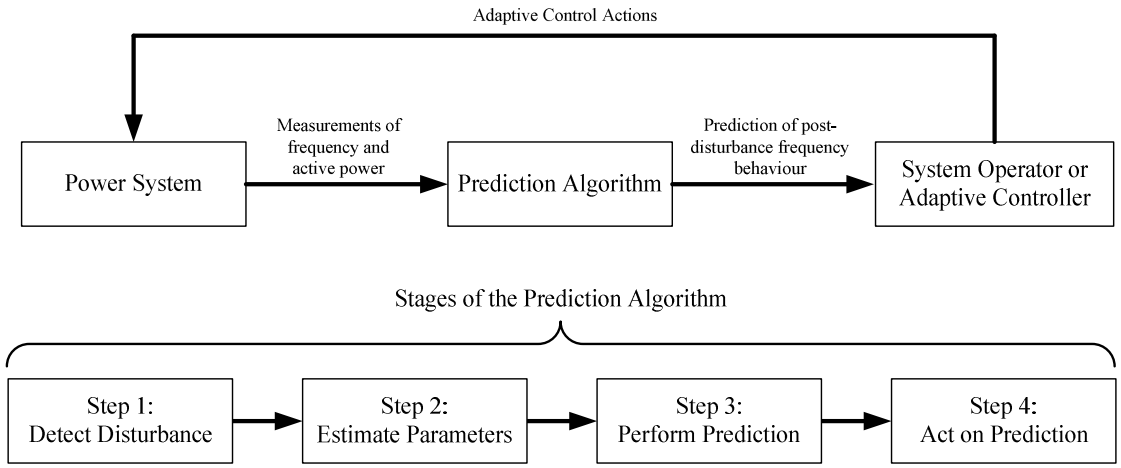

Figure 5-1 – Overview of the role of a prediction algorithm and the four stages of a post-disturbance frequency prediction algorithm.

The possible forms of the frequency predictions include the prediction of specific values, for example the time and magnitude of the nadir of the frequency response, and the prediction of the violation of certain thresholds. The form of prediction desired will heavily influence the nature of the prediction method considered, and vice versa.

5.2 The Purpose of Frequency Prediction

The core purpose of frequency prediction is to help improve the quality of frequency control in power systems. Considering this, in combination with the success of the existing deterministic frequency control in power systems, it seems likely that the most promising application of frequency predictions will be in supporting this existing frequency control.

The primary advantage that frequency predictions offer to the existing emergency frequency control is that they allow occasional frequency control services to be implemented sooner. This is possible because the existing approach to emergency frequency control involves responding to a frequency deviation violating a specific pre-determined threshold and then attempting to correct it using deterministically designed control actions. In contrast a prediction based approach for emergency frequency control could respond to a prediction of the threshold being violated and

then design adaptive control actions, based on this prediction and online parameter estimation, that will limit the deviation to within the given security limits. This is beneficial as in the context of frequency control the sooner that actions are taken the more effective they are. Furthermore, acting sooner allows the control actions to be implemented before the deviation has become too large and reduces the risk of extreme frequency deviations initiating secondary disturbances [1] [2].

Despite the success of frequency control in existing power systems it will require support of some kind in the future as many of the changes that are occurring in power systems will be a threat to this success, particularly the displacement of traditional synchronous generation by intermittent energy resources. Therefore, the existing frequency control must become more adaptive as any failures in frequency control would give rise to an increase in the probability of blackouts [1] [2]. Fortunately, many of the changes in power systems will also offer opportunities for new frequency control tools, such as synthetic inertia, that could be used in combination with frequency prediction to create a more adaptive form of frequency control that can overcome the challenges posed by future power systems without sacrificing the success of the existing control.

5.2.1 The Requirements Imposed upon Online Post-Disturbance Frequency Prediction Algorithms

The general requirements imposed during this research on frequency prediction algorithms were based on the background described in the previous chapters of this thesis. Chapters 2, 3 and 4 reviewed three areas that are vital to the development of a frequency prediction algorithm. These are the existing frequency control practices, power system developments and synchronised measurement technology.

The review of existing frequency control in Chapter 2 revealed that failing to ensure satisfactory frequency control could leave systems vulnerable to cascading generator outages and blackouts. Therefore, a frequency prediction algorithm must be both secure and dependable and as such a high degree of accuracy should be expected from any prediction algorithm. Furthermore, the high speed of operation demanded of

frequency control means that any prediction algorithm must itself operate quickly if it is to be useful.

The discussion of power system developments in Chapter 3 highlighted that the frequency behaviour of future power systems will be increasingly uncertain. Therefore, prediction algorithms should be capable of performing online estimation of any system parameters which they require and that this estimation must be performed quickly and with only limited system measurements due to the high speed of operation of frequency control.

The review of SMT and WAMPAC in Chapter 4 revealed that whilst these technologies offer unprecedented access to system measurements in real time it would be unrealistic to expect complete observability of the system and instant access to these measurements. Therefore, the prediction algorithms created during this research must consider the communication, data processing and other delays that will be inherent to a WAMPAC system and seek to limit the scope of the data required by the algorithm to minimise these delays.

5.2.2 Role of Prediction Support in Existing Systems

The existing prediction methods [3][4][5], and those proposed in this thesis, are only capable of estimating system parameters and producing predictions after recording the initial frequency response of the system to a disturbance. The stiff nature of existing power systems, particularly large interconnected power systems, means that many disturbances do not cause the system to experience frequency deviations of sufficient size to perform accurate predictions.

As system planning and operation is governed by the *N-1* criterion, this means that the support offered by frequency prediction to a stiff system should focus upon the risk that a second disturbance would pose frequency stability. This support could take the form of predictions being used to alert system operators to a vulnerable system state, adaptively adjust the settings of emergency frequency control elements, or to arm

response based System Integrity Protection Schemes (SIPS) that are designed to contain any extreme deviations that would occur from a secondary disturbance.

5.2.3 Role of Prediction Support in Future Power Systems

In the future, the inertia of power systems will fall as traditional large synchronous generation is displaced by small intermittent generation and more power is delivered over converters. This loss of inertia will cause systems to become less stiff and experience larger and faster frequency deviations after a disturbance. This loss of inertia will be combined with a reduction in the number of generators that offer traditional primary response services. The combination of these two factors will make the system more vulnerable to unacceptably large frequency deviations after a single contingency unless increasing quantities of traditional spinning and standing reserve are dispatched, and paid for, by the system operator.

However, this loss of inertia will also increase the number of disturbances in the system for which a prediction could be made. In this low inertia operating environment frequency predictions could be used to design adaptive actions that provide efficient occasional frequency control services by exploiting the availability of demand response control, energy storage and synthetic inertia in future power systems. This would be in addition to the supporting role played by predictions in a stiff system and the availability of this prediction based support would serve to reduce the need for dispatching increasing quantities of traditional reserves by combining these new tools into a fast acting form of primary response.

Ensuring the accuracy of a frequency prediction algorithm will be of the up most importance. This is because the adaptive control actions that are designed based on a frequency prediction will be specifically tailored to that prediction to ensure that frequency stability is preserved in the most efficient way possible. Therefore, any error in the prediction would be included in the design of the control actions. This would lead to either insufficient actions or excessive actions being taken, depending on the nature of the error in the prediction. As such it would be wise to ensure that some form of redundant automatic emergency frequency control still exists in the low inertia

scenario as any failure in frequency control could lead to a blackout. The most logical candidate for providing this redundancy would be the existing load shedding relays with adjusted settings to reflect their new role.

5.3 The Different Forms of Frequency Prediction

The specific nature of the support available from frequency predictions will depend heavily upon the nature of the predictions themselves. This section describes the different forms of predictions that were identified as part of this research and also describes the forms of support they could provide.

5.3.1 Specific Frequency Values

The main example of the prediction of specific frequency values that is considered in this thesis is the prediction of the nadir, or maximum deviation from nominal, of the frequency response as proposed in [5]. This frequency value could also be combined with a prediction of the time at which the nadir will occur.

The prediction of specific frequency values would allow the support offered to be tailored precisely to the frequency deviation that is occurring. This would allow efficient actions to be designed online that would also take into account the prevailing system conditions estimated during the prediction process. Therefore, this form of prediction lends itself to the concept of prediction supported frequency control for low inertia systems described in section 5.2. In addition, it is worth noting that these predictions could equally be used to support the concept proposed for supporting frequency control in stiff systems.

Finally, whilst a method for predicting the steady state post-disturbance frequency is presented in [4], performing a prediction of this nature is not considered in this thesis because the focus here is upon supporting emergency frequency control and steady state predictions would serve only to support secondary and tertiary control.

5.3.2 Threshold Violation Flags

Threshold violation flags represent predictions of whether the frequency deviation will violate certain thresholds. These thresholds would be set by the user and Figure 5-2 shows an example based on the frequency response requirements set out in the grid code followed by NGC [6].

A set of N thresholds can be seen to separate the range of possible frequency responses into N+1 separate zones, like those marked in Figure 5-2. Where a lower zone number denotes a greater threat and the subscripts o and u are used to denote over and under nominal, respectively.

Thresholds can also be set for the duration of any violation, see the vertical thresholds set for an arbitrary time t_{th} in Figure 5-2. This would be useful as a sustained deviation of a given magnitude can be a threat to system stability when a transitory deviation of that magnitude may not be.

These predictions contain less information than the predictions of specific frequency values, as the threshold violation flags do not provide any information about exactly when the threshold will be violated or by how much, except that the deviation will not violate the next threshold. These predictions could still be used to allow frequency control to respond before the deviation occurs or to arm a SIPS, as discussed in Section 5.2.

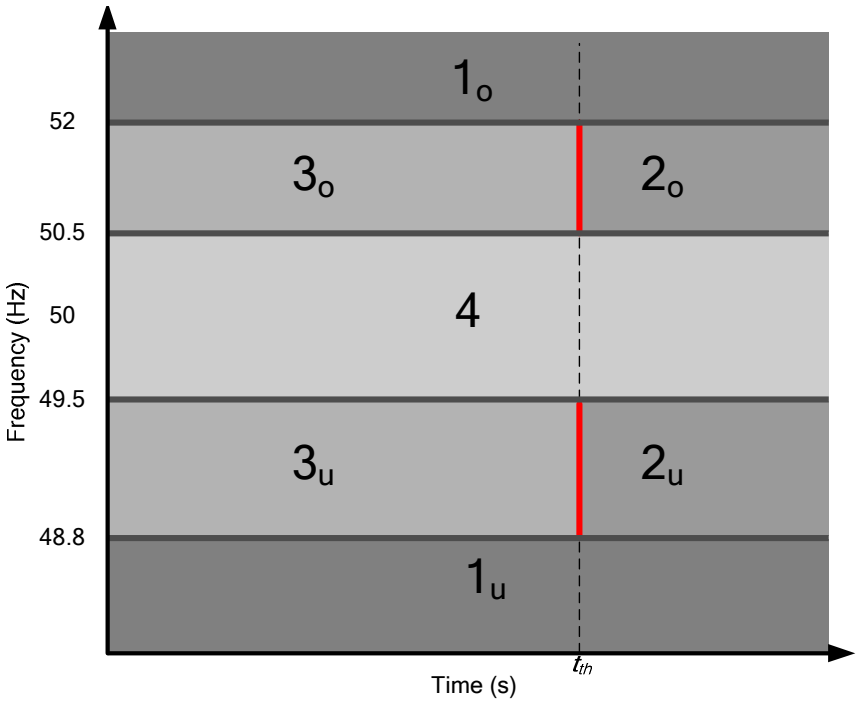

Figure 5-2– Threshold based predictions of the post disturbance frequency response would indicate which of the numbered zones the frequency will enter. A lower zone number denotes a greater threat and the subscripts o and u are used to denote over and under nominal, respectively. Thresholds can also be set for the duration of any violation, see the red thresholds set for an arbitrary time t_{th}.

5.4 Possible Methods for Achieving Frequency Prediction

In the same fashion that the nature of the predictions available will determine the form of support that the predictions can offer, the method used to create the prediction will determine the nature of the prediction. Any prediction method must generate predictions that are accurate and reliable. Furthermore, the time necessary to execute the method must be minimised as far as is reasonable as the primary benefit of using frequency predictions to support frequency control is that it allows control actions to be deployed more quickly and potentially before an extreme deviation has even occurred.

During a disturbance the frequency at different locations in a large system will cease to be the same. This will mean that a prediction method might need to be applied to specific areas in a system and not the system as a whole. Therefore, these methods must support this requirement and when applying any of these methods in practice a sound methodology must be used to define the areas in which the methods are applied.

Methods used as part of designing schemes for the controlled islanding of a power system would offer a basis for the development of these methods [7].

5.4.1 Frequency Prediction using Approximate Models of the System Frequency Response

Creating a prediction method based on approximate models of the system frequency response would first consist of defining a suitable approximate model for the system frequency response. When defining this approximate model it would be vital to balance the accuracy of representation of the frequency response against the time required to perform the online estimation of the parameter values of the model. Due to the complexity of developing suitable approximate models and the time available for performing the prediction this would need to be done offline.

It is necessary to perform online parameter estimation of the values of the model parameters due to the increasing uncertainty that will exist in future power systems. This uncertainty will cause many of the parameter values to vary significantly with time and as such any frequency prediction that is based on assumed knowledge or offline estimates of these parameters values would not accurately represent the true system frequency response.

Having defined the approximate model offline, when a disturbance in the system was detected it would then be necessary to perform online parameter estimation to determine suitable parameter values for every parameter of the approximate model. This populated model could then be solved for specific conditions such as a derivative of zero to find the frequency nadir.

Approximate model based prediction would generate specific frequency value predictions and as such could be used to support frequency control in any number of ways. The key challenges of achieving prediction based on approximate models will be defining a suitable approximate model and then creating methods for performing the necessary online parameter estimation. The model selection must balance the accuracy with which it represents the system frequency response against the number of

parameters that must be estimated and the observability of these parameters in the data available.

5.4.2 Pattern Classification

Pattern classification is a form of supervised machine learning that can be used to assign a class to a member of a population, or pattern. This class membership will define certain properties of this pattern that will not have been immediately apparent. This assignment is made by evaluating a discriminant function that is trained using past examples of the classification problem in question. A detailed introduction to pattern classification theory is given in Chapter 9.

This theory can be applied to frequency prediction to create threshold violation flags. A number of different pattern classifiers exist in the literature that use polynomial regression [9] [10], multi-layer neural networks [9] [10] [11] and support vector machines [12] [13]. The proper training of the classifier will pose a challenge due to the complexity of power systems and the wide array of possible contingencies.

5.4.3 Direct Methods

Direct methods that use a Lyapunov type energy function are used in power systems to determine rotor angle stability through the equal area criterion [14]. However, the definition of frequency stability is the ability of the system to ensure that the system frequency is kept within the defined security limits [15]. Therefore, frequency stability does not have a form of classical instability like that seen in rotor angle or *P-V* nose curves. Therefore, unlike in other applications of direct methods for determining power system stability there is no natural definition of a Lyapunov type energy function that would be useful for determining frequency stability. The application of a direct method would thus require the construction of an energy function with artificial limit cycles, which would likely become rather arbitrary and awkward in nature. This issue meant

that direct methods were not pursued as a possible avenue for the form of frequency prediction considered in this research.

5.5 Chapter Summary

This chapter has attempted to define the core concept of frequency prediction and its role in supporting frequency control in power systems. Two possible forms of support exist depending on the nature of the power system in question. For the stiff systems in operation today frequency predictions could serve a valuable role by providing an indication of the vulnerability of the system in the immediate aftermath of a disturbance and allowing system operators to manually respond or to automatically arm SIPS that are intended to protect the system from extreme frequency deviations. This would help the system to be more resilient against any secondary disturbances that may occur and help reduce the risk of blackouts, as adherence to the *N*-1 criterion means that most blackouts occur because of a sequence of events rather than one single contingency. As power systems evolve in the future the loss of inertia and traditional primary response will make the system more vulnerable to large frequency deviations from a single contingency. However, the introduction of demand response control, energy storage and synthetic inertia could be combined with frequency predictions to design adaptive control actions that preserve frequency stability and compensate for the loss of inertia and primary response.

There are two general forms of frequency prediction that are proposed in this research: specific value prediction and threshold violation flags. Table 5-1 presents three possible methods for achieving frequency prediction, the form of prediction they offer and the key challenge in implementing them. Direct methods are not considered further in this thesis due to the problem of inserting artificial limit cycles when defining the necessary Lyapunov type energy function.

Specific value predictions, such as predictions of the frequency nadir, must be generated using approximate model based prediction and provide the ability to design highly tailored adaptive actions but entail a high degree of complexity in terms of

balancing the accuracy of the approximate model against the feasibility of performing the online parameter estimation in the time available.

Threshold violation flags involve predicting whether the frequency will violate certain user defined thresholds. These predictions will be best achieved by creating a pattern classifier that determines the thresholds that will be violated based on past behaviour of the system through supervised learning. These predictions will provide less information than specific value predictions but if the classifier is properly trained the inherent variability of the system will be included in the classifier naturally, rather than through a complex model selection process.

Table 5-1 – Possible Methods for Achieving Frequency Prediction

Method	Form of Prediction	Challenge
Approximate Models of the System Frequency Response	Specific value	Defining a suitable approximate model
Pattern Classification	Threshold violation flags	Designing a properly trained classifier
Direct	Threshold violation flags	Defining a suitable Lyapunov type energy function

5.6 References

[1] Andersson, G.; Donalek, P.; Farmer, R.; Hatziargyriou, N.; Kamwa, I.; Kundur, P.; Martins, N.; Paserba, J.; Pourbeik, P.; Sanchez-Gasca, J.; Schulz, R.; Stankovic, A.; Taylor, C.; Vittal, V.; , "Causes of the 2003 major grid blackouts in North America and Europe, and recommended means to improve system dynamic performance," Power Systems, IEEE Transactions on , vol.20, no.4, pp. 1922- 1928, Nov. 2005

[2] Sforna, M.; Delfanti, M.; , "Overview of the events and causes of the 2003 Italian blackout," Power Systems Conference and Exposition, 2006. PSCE '06. 2006 IEEE PES , vol., no., pp.301-308, Oct. 29 2006-Nov. 1 2006

[3] Mirzazad-Barijough, S.; Mashhuri, M.; Ranjbar, A.M.; , "A predictive approach to control frequency instabilities in a wide area system," Power Systems

Conference and Exposition, 2009. PSCE '09. IEEE/PES , vol., no., pp.1-6, 15-18 March 2009,

[4] Larsson, M.; Rehtanz, C.; , "Predictive frequency stability control based on wide-area phasor measurements," Power Engineering Society Summer Meeting, 2002 IEEE , vol.1, no., pp.233-238 vol.1, 25-25 July 2002,

[5] Egido, I.; Fernandez-Bernal, F.; Centeno, P.; Rouco, L.; , "Maximum Frequency Deviation Calculation in Small Isolated Power Systems," Power Systems, IEEE Transactions on , vol.24, no.4, pp.1731-1738, Nov. 2009

[6] Transmission, N.G.E., The Grid Code. 2010, National Grid Electricity Transmissions.

[7] Lei Ding; Gonzalez-Longatt, F.M.; Wall, P.; Terzija, V.; , "Two-Step Spectral Clustering Controlled Islanding Algorithm," Power Systems, IEEE Transactions on , vol.28, no.1, pp.75-84, Feb. 2013

[8] Eissa, M.M.; Masoud, M.E.; Elanwar, M.M.M.; , "A Novel Back Up Wide Area Protection Technique for Power Transmission Grids Using Phasor Measurement Unit," Power Delivery, IEEE Transactions on , vol.25, no.1, pp.270-278, Jan. 2010

[9] Schurmann, J. “Pattern Classification: A Unified View of Statistical and Neural Approaches.”, Wiley and Sons, 1996

[10] Michie, D., Spegelhalter, D.J., Taylor, C.C., “Machine Learning, Neural and Statistical Classification.”, Ellis Horwood, 1994

[11] James, M. “Classification Algorithms”, Collins, 1985

[12] Campbell, C., Yin, Y., “Learning with Support Vector Machines”, Morgan and Claypool, 2011

[13] Shigeo, A. “Support Vector Machines for Pattern Classification”, Springer, 2005

[14] Kundur, P., Power System Stability and Control 1994, New York: McGraw-Hill.

[15] Kundur, P., et al., Definition and classification of power system stability IEEE/CIGRE joint task force on stability terms and definitions. Power Systems, IEEE Transactions on, 2004. 19(3): p. 1387-1401.

6 Estimating the Inertia of a Power System

This chapter describes the creation of a novel algorithm for the accurate and reliable estimation of system inertia based on wide area measurements of frequency and active power. The system inertia is one of the key parameters that must be estimated as part of frequency prediction; the importance of inertia and the necessity to estimate it are discussed in Section 6.1. Section 6.2 defines the mathematical concept of inertia and Section 6.3 introduces the swing equation based method for its estimation. Section 6.4 describes the research performed into validating this method. The relative success of this algorithm is discussed in Section 6.5 as are possible improvements.

6.1 Chapter Introduction

The inertia of a system is a critical factor in determining the frequency behaviour after a disturbance to the active power balance of that system [1]. Many of the changes that are occurring in power systems will cause the inertia of a system to begin to vary radically across the system, both spatially and temporally, when compared to the reliable nature of this key system parameter in contemporary power systems.

The consequences of a reduction in inertia can be seen in Figure 6-1. For a 0.075 p.u. increase in load a 10 % reduction in the inertia constant used in the SFR model, described in [1] and Chapter 8, leads to a 0.0514 Hz/s (10 %) increase in the initial derivative of frequency and a 0.01 Hz (2.5 %) larger maximum deviation that occurs 0.14 seconds (7.3 %) earlier. All percentage changes are given in terms of the properties of the deviation that occurs for the original inertia constant of 4.0 seconds on a MVA base of 100 MVA.

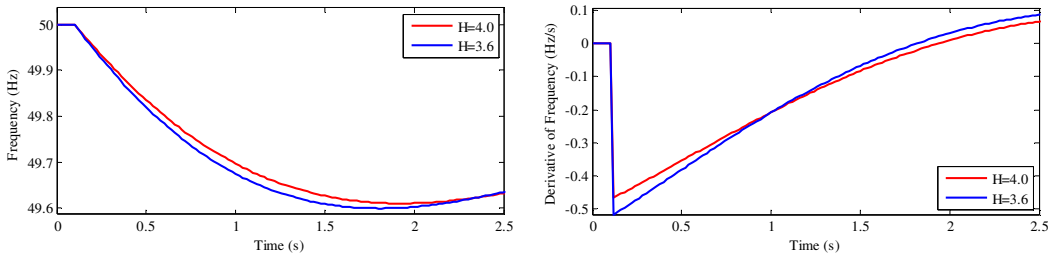

Figure 6-1 – A reduction in system inertia leads to a faster deeper frequency swing after a given disturbance.

Particular examples of the changes that will begin to undermine the consistency of system inertia are wind generation, HVDC and the deployment of an increasing number of loads connected over power electronic converters. Wind turbines provide inherently less inertia per MW than synchronous machines [3] and DFIG units have their inertia decoupled from the power system by power electronic converters [4]. This decoupling of inertia is also an issue for the large industrial loads that are now being connected over power electronic converters, as these loads tend to consist mostly of large induction motors that contribute inertia to the system. The introduction of HVDC in parallel with the system and as interconnections between neighbouring systems will mean that an increasing quantity of the power flow in a system will have no natural inertial response [5]. These technologies also offer opportunities to temporarily create a synthetic inertial response by using controllers which will help protect the system from operating with dangerously low levels of inertia but such actions will also contribute to the level of uncertainty about the inertia available to a future power system. This uncertainty will mean that accurate online estimation of the inertia of a system will be a key element of any prediction method.

Any method developed to produce online estimates of the inertia that is available during a disturbance must consider three criteria for its successful operation. The first criterion is accuracy; any estimate made must be accurate so that the decisions made based on it will be the correct decisions. The second criterion is reliability; the estimates made must be reliable so that they can be depended upon by decision makers. The third criterion is execution time; the shorter the execution time of the algorithm the greater the benefit of prediction algorithms will be.

6.2 Defining the Inertia Constant

The inertia is a measure of the rotational energy, E, stored in a rotating mass and is defined as follows

$$E = \frac{1}{2} J \omega_m^2 \quad [MVAs] \tag{6-1}$$

where J is the moment of inertia of the rotating mass (kgm^2) and ω_m is the rotational speed of the rotating mass (rad/s). When calculating the inertia of a machine that consists of multiple rotating masses that are connected to one another it is necessary to consider the moment of inertia for all of the connected masses to accurately calculate the inertia of the complete machine.

By this definition it can be seen that the rotational energy varies with the rotational speed. It is more convenient to convert this variable definition of energy with an inertia constant, or H constant [6], as defined in (6-2). This definition is based on the assumption that the speed of the machines connected to a power system will usually be approximately equal to the synchronous speed of that system ω_{sm}. Furthermore, this definition of H is normalised using a power base, S_b. This normalisation of H means that it now defines the time for which the energy stored within the rotating mass could supply the power equal to S_b.

$$H = \frac{1}{2} \frac{J \omega_{sm}^2}{S_b} \quad [s] \tag{6-2}$$

The H constant of a machine is usually normalised using the rating of the machine. Therefore, before the H constants of different machines can be combined into an equivalent H constant for the system, a base transformation must be applied so that they all appear on the new system base.

The most common examples of rotating masses in a power system are the prime movers and shafts of generators and motors; these are collectively referred to as machines in the remainder of this chapter. Therefore, the H constant of a power system can be defined as the sum of the H constants of the M motors and N generators that are

directly connected, i.e. not connected over power electronic converters or a HVDC link, to the system. When the necessary base conversion to the power system base, $S_{b,sys}$, is included the system H constant, H_{sys}, can be calculated using (6-3).

$$H_{sys} = \sum_{n=1}^{N} \frac{1}{2} \frac{J_n \omega_{sm,n}^2}{S_{b,sys}} S_{b,n} + \sum_{m=1}^{M} \frac{1}{2} \frac{J_m \omega_{sm,m}^2}{S_{b,sys}} S_{b,m} \quad [s] \tag{6-3}$$

The novel method presented in this chapter can estimate the H constant of an entire system or sub-system to serve as an input to the prediction methods. However, much of the work presented deals with estimating the inertia of a single generator. This is because the H constant of a generator is a known name plate parameter and as such these single generator estimates can be used to validate the method. This is in contrast to the H constant of a system, the exact value of which has a high degree of uncertainty included in it due to the inclusion of loads in the definition and the unknown properties and connection status of distributed generation.

6.3 Estimating H using the Swing Equation

From the definition in Section 6.2 it has been established that the H constant of a machine is an accurate measure of the stored energy within the rotating mass of a machine. It is the behaviour of this stored energy during a disturbance that causes the inertia to be of critical importance when attempting to understand and predict the initial frequency behaviour of a system. When an imbalance occurs in the torques applied over the air gap of a machine this stored energy will act in an attempt to correct the imbalance. This action consists of releasing energy, and decelerating, if there is an excess of electromagnetic torque (for example after a loss of generation in the system) or absorbing energy, and accelerating, if there is an excess of mechanical torque (for example after a loss of load in the system or when the generator becomes islanded from the system). This relationship between the air gap torques and the machine speed are defined using the swing equation (6-4) and are the origin of the frequency deviation that occurs immediately after a disturbance to the active power balance of a system.

6.3.1 Deriving a Suitable form of the Swing Equation

This section details the derivation of a suitable discrete form of the swing equation that can be used to perform the online estimation of the H constant based on wide area measurements of frequency and active power. The swing equation defines the oscillations in the shaft speed that will occur if the shaft is exposed to an unbalanced torque. The basic form of this swing equation is given in (6-4), the mechanical damping of the shaft is assumed to be negligible in this context [6].

$$J\Delta\frac{d\omega_m}{dt} = T_m - T_e \quad \text{[Nm]} \tag{6-4}$$

where J is the moment of inertia T_m and T_e are the mechanical and electromagnetic air gap torques, respectively. Furthermore, Δ is included here because this equation expresses the relationship between a torque imbalance and a change in the derivative of the mechanical speed not the absolute value of derivative of the mechanical speed.

However, it is customary to use (6-5), which expresses the swing equation in terms of electrical frequency and active power, when applying the swing equation in power systems. The derivation of (6-5) from (6-4) is given in Appendix A and further discussion of the swing equation and this derivation can be found in [5] and [6].

$$2H\Delta\frac{df}{dt} = P_m - P_e = \Delta P \quad \text{[p.u.]} \tag{6-5}$$

where f is the per unit frequency, P_m and P_e are the per unit mechanical power and electrical load applied to the shaft, respectively, and ΔP is the power imbalance at the measurement location.

The inclusion of mechanical power in (6-5) is inconvenient as it not possible to directly measure the mechanical power from the electrical side of the system. This can be overcome by recognising that the variation of the mechanical power will be much slower than the variation of the electrical power because it is governed by mechanisms

with larger time constants, e.g. boiler dynamics. This means that when the estimation process is supported by measurements with sufficient reporting rate, e.g. the one per cycle reporting rates offered by modern PMUs [7], then the mechanical power immediately after the disturbance can be assumed to be equal to the electrical power prior to the disturbance. If the reporting rate of the measurements results in a delay of Δt between each set of measurements then (6-5) can be expressed without the mechanical power term in a discrete form:

$$2H\Delta\frac{df(t)}{dt} \approx P_e(t-\Delta t) - P_e(t) \approx \Delta P(t) \quad \text{[p.u.]} \tag{6-6}$$

This approximation is valid provided that the measurements used are recorded immediately after the disturbance. It is important to recognise the significance of the inclusion of Δ prior to the derivative of frequency term in (6-6). This is included as it denotes the fact the H constant determines the relationship between a change in power and a change in the derivative of frequency. This relationship arises because of the rotational reference frame that is used during the derivation of the swing equation, see Appendix A. In a practical power system the derivative of frequency will never truly be zero due to the constant changes in load and generation that occur. Therefore, when estimating H it is vital that only the change in the derivative of frequency is considered, i.e. any pre-existing value of the derivative of frequency is accommodated in the expression used for estimating H. This can be achieved by modifying (6-6) to form (6-7)

$$\tilde{H} = \frac{1}{2}\frac{P_e(t-\Delta t) - P_e(t)}{\frac{df(t)}{dt} - \frac{df(t-\Delta t)}{dt}} \quad \text{[s]} \tag{6-7}$$

where $\tilde{H}$ is a close approximation of H and (6-7) forms the basis of the H estimation research presented in this chapter.

The novel estimation process presented in this chapter is based on this discretised approximate swing equation (6-7). Therefore, measurement data representing the response of the generator to a disturbance in the active power balance in the system is necessary to produce an estimate. Here this data consists of measurements of the active

power flow and the rate of change of frequency for a generator. These measurements should be recorded during a disturbance in the system. Data of this nature will become increasingly available because of the growing deployment of synchronized measurement technology in power systems [7].

6.3.2 Existing *H* Estimation Methods

This chapter deals with the online estimation of the *H* constant using the swing equation. Existing work that describes the estimation of inertia using the swing equation is limited to the application of the swing equation during post-mortem analysis [8] [9]. Other methods that deal with the estimation of the *H* constant involve the fitting of a model to data recorded during a disturbance to the system [10]. Estimating the *H* constant using methods of this nature is not suitable for supporting frequency prediction due to the challenges posed by the time available prior to the events being predicted and the observability of parameters during this period; this is discussed in detail in Chapter 8.

The existing work that describes the estimation of *H* did not have the benefit of access to SMT and WAMPAC. This meant that the method had to be implemented offline during post-mortem analysis, as the lack of accurate time stamps meant the data had to be aligned properly before use. Furthermore, in this previous work only measurements of frequency were available. The lack of active power measurements meant that the known size of the disturbance (P_d) was used to serve as the power imbalance, so (6-7) is replaced with the following expression:

$$2H \frac{df(t_{td})}{dt} = P_d \quad \text{[p.u.]} \tag{6-8}$$

where t_d denotes the time at which the disturbance was deemed to have begun to influence the frequency response.

The use of only a single measurement of the derivative of frequency leaves this process vulnerable to noise, particularly as the derivative process serves as a noise

amplifier, as any error in the derivative of frequency value will be directly included in the H estimate. For the purposes of the discussion presented in this chapter this approach is referred to as the single value method.

Due to the lack of active power measurements, the single value method assumes a known disturbance size (P_d) to serve as an approximation of the power imbalance. It is important to recognise that in a real power system estimates made using (6-8) will differ somewhat from estimates based on (6-7) and active power measurements, like those proposed here. These differences occur because not all of the active power imbalance created by the disturbance will appear across the air gaps of the machines in the system, instead some of this imbalance will be accommodated by the other elements of the system e.g. voltage and frequency dependent non-rotating loads. This will mean that H estimates made using P_d will include this response and as such they will usually be larger than H estimates based on active power measurements. This inclusion of the response of other system elements into the estimate will mean that the H estimate may vary significantly with the type and location of the disturbance, whereas estimates based on active power measurements will not.

6.3.3 Estimating *H* using Filter Windows

The previous work devoted to estimating the H constant using the swing equation was performed offline. Therefore, it was possible to study the frequency response and select a suitable derivative of frequency value for the given size of disturbance and thus estimate H using (6-8) in a single value approach. However, some issues did exist with erroneous estimates that had to be discarded [9]. These issues would be unacceptable if the H estimate generated was expected to support an online frequency prediction method. In the context of online estimation, the two main problems in the single value method are: detecting the presence of an erroneous estimate to avoid erroneous predictions and, if the erroneous estimate is properly indentified, the consequent failure of the prediction method to generate a prediction. The obvious way to overcome this vulnerability in the single value method is to adopt an approach in which multiple measurements of active power and frequency from both before and after the time of disturbance are used to estimate the inertia. The method proposed here for implementing this is to estimate the pre disturbance and post disturbance active

power and derivative of frequency based on simple windowing filters placed either side of the disturbance time.

6.3.3.1 Defining the Windowed *H* Estimation Process

A windowing process should allow the *H* estimation process to be more robust against noise, and can be described using Figure 6-2. The single values used previously in (6-7) are now replaced by the output of these smoothing filters, so the *H* estimate is calculated using the following expression:

$$H = \frac{1}{2}\frac{P_1 - P_2}{R_2 - R_1} \quad \text{[s]} \tag{6-9}$$

The outputs of the smoothing filters are estimates of the pre disturbance and post disturbance active power and derivative of frequency, and in the case of rectangular windows these are calculated according to (6-10).

$$P_1 = \frac{\sum_{i=t_0-M_1}^{t_0} P(i)}{A_1} \qquad P_2 = \frac{\sum_{i=t_0+W}^{t_0+W+M_2} P(i)}{A_2}$$

$$R_1 = \frac{\sum_{i=t_0-M_3}^{t_0} \frac{df}{dt}(i)}{A_3} \qquad R_2 = \frac{\sum_{i=t_0+W}^{t_0+W+M_4} \frac{df}{dt}(i)}{A_4} \tag{6-10}$$

where *W* is the width of any pre-filtering that was applied to the data. Such pre-filtering is unnecessary but it is important to demonstrate that this approach can be applied in its presence. The window widths of A_1, A_2, A_3 and A_4 could be set to different values. However, for simplicity they are all set to the same value for research presented in this thesis.

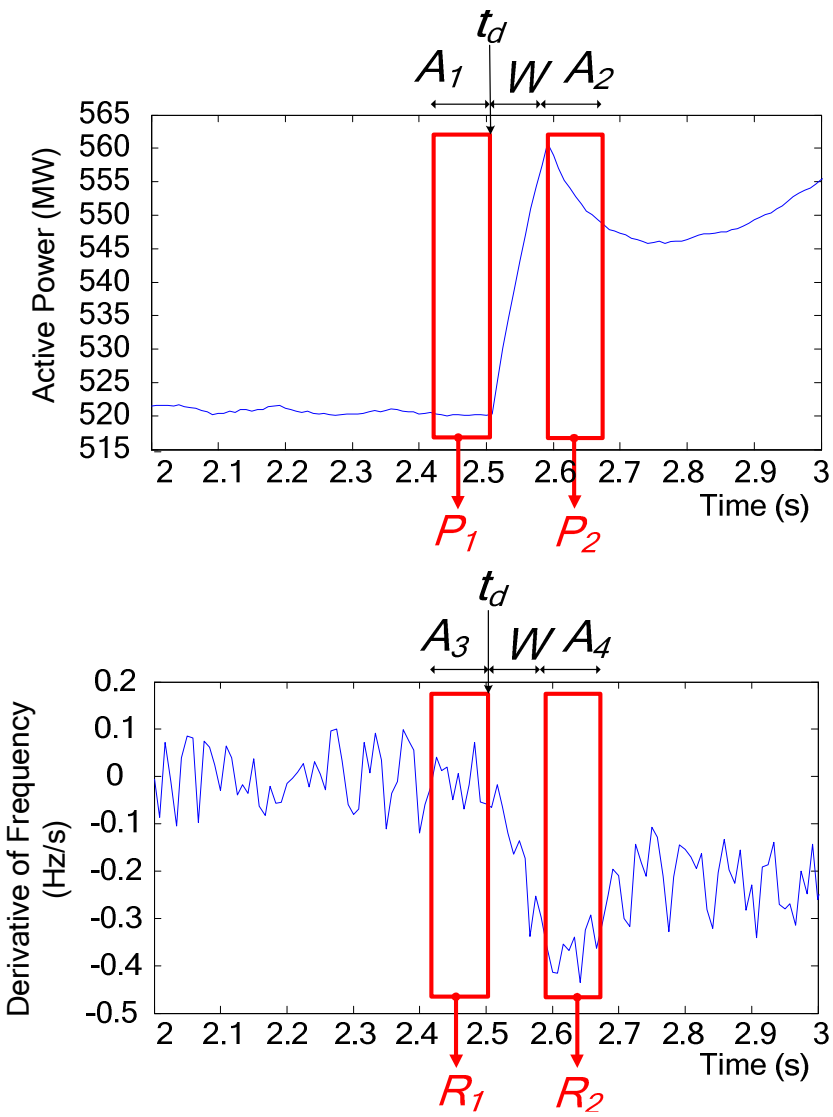

Figure 6-2 – Sampling windows can be used to overcome the issue of the noise present in both the measurements of power and frequency. These measurements are taken from a PowerFactory® [14] model of the IEEE 39 bus test system. The separation between the windows, marked W, is to accommodate the filter extending the transient step from infinitely small to the width of the filter. A_1, A_2, A_3 and A_4 are the widths of the four data windows, t_d is the time of the disturbance, and R_1, R_2, P_1 and P_2 denote the output of the data windows.

The output of the data windows will not be a perfectly accurate reflection of the swing equation relationship, as measurements from times other than t_d are used, and as such they will introduce some error into the calculation. When applying this method to a specific system the error introduced by the windows will need to be balanced against the improved resilience against noise that these filter windows offer. The combination of the assumptions made in forming (6-7) with this extension of the swing equation relationship beyond the period for which they are traditionally assumed to be valid means that it is important to carefully investigate the behaviour of the windowed H estimation method and ensure that it is valid, such an investigation is presented in Section 6.5.

The key steps in applying this windowed estimation method, where all window widths have a value of A and a pre- filter with width W is used can be summarised as follows.

1. A disturbance occurs in the system.
2. Time of disturbance (t_d) received from an external application.
3. Store the previous A measurements of df/dt and P.
4. Wait for an additional W+A measurements to be made of df/dt and P.
5. Filter the W+2A measurements of df/dt and P.
6. Apply the data windows to the active power and derivative of frequency data, centred on t_d.
7. Calculate the inertia of the generator using (6-9).

This method can be used to estimate the H constant of a system or single generator, depending on the nature of the measurements used. Estimating the inertia of a single generator is a useful approach to follow for validating the method as the true value of the H constant is known and as such the accuracy of the estimate made can be assessed.

6.4 Validating the Windowed H Estimation Process

It is important to develop a thorough understanding of the strengths and weaknesses of the windowed H estimation process because of the proposed online application of this method in support of frequency prediction. The first stage of this validation of the windowed H estimation process was a comparison of its noise free behaviour with that of the single value method to demonstrate the change in accuracy as the windows vary in width. In addition to this simple comparison, DIgSILENT™ PowerFactory® [14] simulations of the IEEE 39 bus test system are used to explore the response of the method to different disturbances. The testing presented in this section deals with the estimation of the H constant of an individual generator, so a true H value exists for comparison, using frequency and active power measured at the generator point of connection. Later examples deal with the estimation of H for a system.

6.4.1 Noise Free Demonstration of Windowed *H* Estimation

This section offers a simple demonstration of the windowed H estimation process and compares it to the single value method. Figure 6-2 depicts noise free derivative of frequency and active power traces for a disturbance of -0.2 p.u. simulated using the SFR model proposed in [1]. The window based estimation process was then applied to this data for a range of *A* values, the results of which are presented in Table 6-1. For comparison, the result of applying the single value estimation method to this example is presented in Table 6-2.

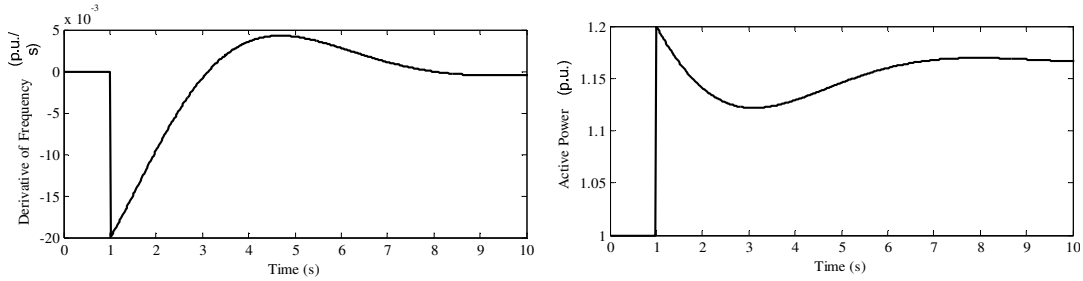

Figure 6-3 – Traces of the derivative of frequency and active power (Electrical) for an increase in electrical load of 0.2 p.u..

Table 6-1 – Estimates of Inertia for a noise free example and varied A values

A	R1 (p.u.)	R2 (p.u.)	P1 (p.u.)	P2 (p.u.)	Hest (s)	Error (%)
10	0	-0.0190	1	1.1930	5.07	-1.48
20	0	-0.0180	1	1.1858	5.16	-3.26
30	0	-0.0169	1	1.1791	5.29	-5.77
40	0	-0.0159	1	1.1730	5.45	-9.09
50	0	-0.0148	1	1.1675	5.66	-13.28

Table 6-2 – Single value method estimate of Inertia for a noise free example

df/dt (p.u.)	ΔP (p.u.)	Hest (s)	Htrue (s)	Error (%)
- 0.0199	-0.2000	5.02	5	-0.48

A comparison of the estimation results in Table 6-1 and Table 6-2 demonstrates that the accuracy of the window based method for this noise free example is slightly poorer than that of the single value method and the accuracy falls as the window size is increased. This decline in accuracy, the characteristic of which is depicted in Figure 6-4, is to be expected as the assumptions on which the modified swing equation is based are only valid immediately after the disturbance. However the accuracy of the

window based method is acceptable and it is likely that the lower accuracy of the window based method in the best case scenario will be compensated for by improved resilience against noise, as seen in the examples in the next section when *A* is equal to 1.

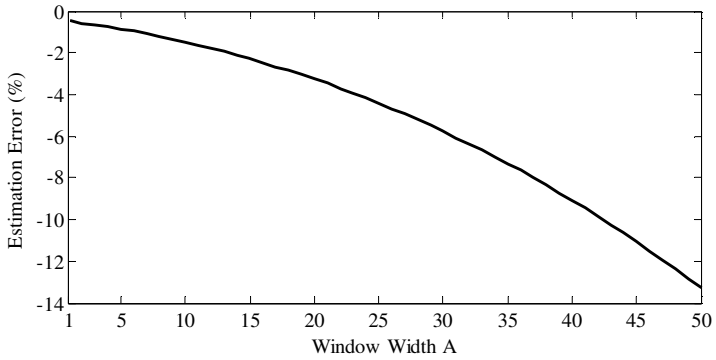

Figure 6-4– The relationship between window width and inertia estimation error for a noise free case

6.4.2 Applying Windowed *H* Estimation to Simulations of the IEEE 39 Bus Test System

The windowed *H* estimation process is now tested using simulations of the IEEE 39-bus test system, shown in Figure 6-5 and details of which can be found in [13] and Appendix D, using DIgSILENT™ PowerFactory® [14]. These simulations were performed to demonstrate the performance of the estimation process and the improved resilience against noise that it offers. The results presented here were produced using a MATLAB® [15] script of the estimation method.

The purpose of this testing was to demonstrate the validity of the method when exposed to the more complex dynamics of a more complete power system model. Furthermore, these tests served to assess the resilience of the method against noise. To ensure that that noise used in each set of tests was the same, noise values were generated randomly in MATLAB® [15] and stored. One thousand, five second noise signals, for both frequency and power, were simulated for each generator. For the purpose of this discussion a set of these noise signals, i.e. the five second frequency and power noise signals for each of the ten generators, is referred to as a noise profile. These one thousand noise profiles are used in all of the cases presented to allow a

statistical analysis of the proposed methods behaviour in the presence of noise. To investigate the effect of the window width on the estimation procedure window widths of 1, 2, 3, 4, … and 54, in terms of samples, were considered.

The simulated data presented in this section used a sampling frequency of 120 Hz. The simulations were executed for five seconds and the relevant disturbance occurs at 2.5 seconds. In all of the cases presented here noise was added to the simulated signals for both frequency and power. White noise was added to the per unit derivative of frequency signal with a magnitude of ±0.005 p.u./s and to the per unit power signal with a magnitude of ±0.05 p.u.. This noise level is higher than those seen for current PMUs [16] and this higher level was selected to accommodate other sources of noise that may exist between the measurement point and where the method is executed. The filtering applied to this data consisted of a simple moving window filter with a width of 10 data points, i.e. 0.0833 seconds. Examples of the active power and derivative of frequency data gathered from these simulations are given in Figure 6-6.

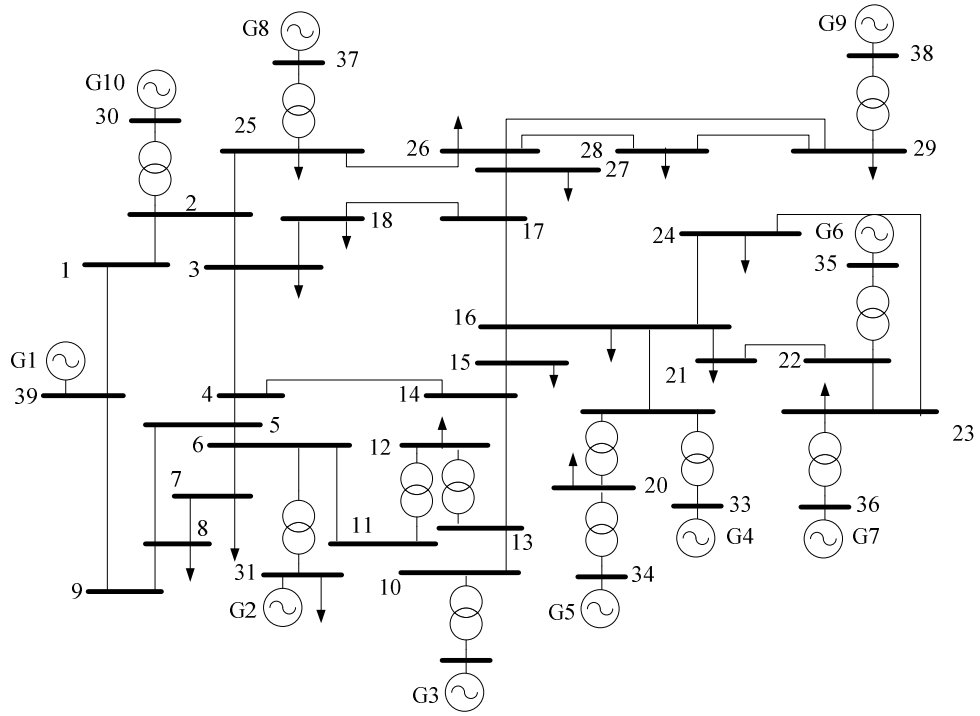

Figure 6-5 – Simulations of the IEEE 39 Bus Test System have been used to validate the *H* estimation method and investigate its behaviour.

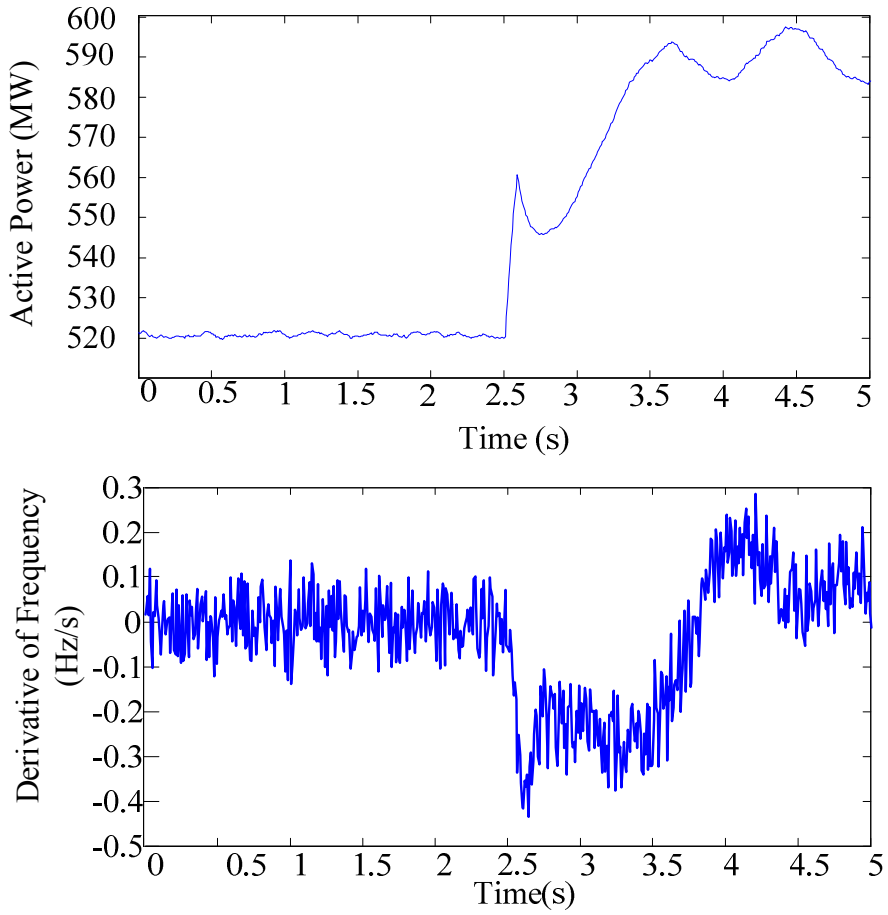

Figure 6-6 –Traces of the active power and derivative of frequency data gathered from the Simulations of the IEEE 39 Bus Test System. These examples are taken from Generator 2 for the outage of Generator 6 (a 520.68 MW disturbance).

6.4.2.1 Testing Windowed *H* Estimation for Generator Outages

The data presented in this section was produced as follows. The disconnection of each of the ten generators in the IEEE 39-bus system was simulated and the frequency and active power measured at the connection point of the generators still connected to the system was then stored for each of these ten cases. Then for each of these ten cases the windowed H estimation method was applied for the range of window widths considered and in the presence of each of the one thousand noise profiles and the error in this estimate was calculated. The end result of this process is a data set that represents the error in nine thousand estimates of the H constant of each generator of the IEEE 39 bus system for each of the window widths considered.

This data set was analyzed using the median, inter-quartile range (IQR) and absolute range of all nine thousand errors for each window width. These measures were used as the mean and standard deviation of the errors concealed the presence of a number of extreme outliers in the data set. The median and IQR of the errors for each window width are shown in Figure 6-7. These results show that the estimation method performs very well for window widths of between approximately 10 and 40 points. The median and inter quartile range of the errors for this set of points are shown in detail in the inset of Figure 6-7. Selecting the 'best' window width from this range is a challenge of balancing the superior median error seen for the lower values in the range against the superior inter quartile range seen for the higher values in the range. In this case a window width of 30 points appears to offer the best balance with a median error of 1.68 % and an inter quartile range of 13.5 %.

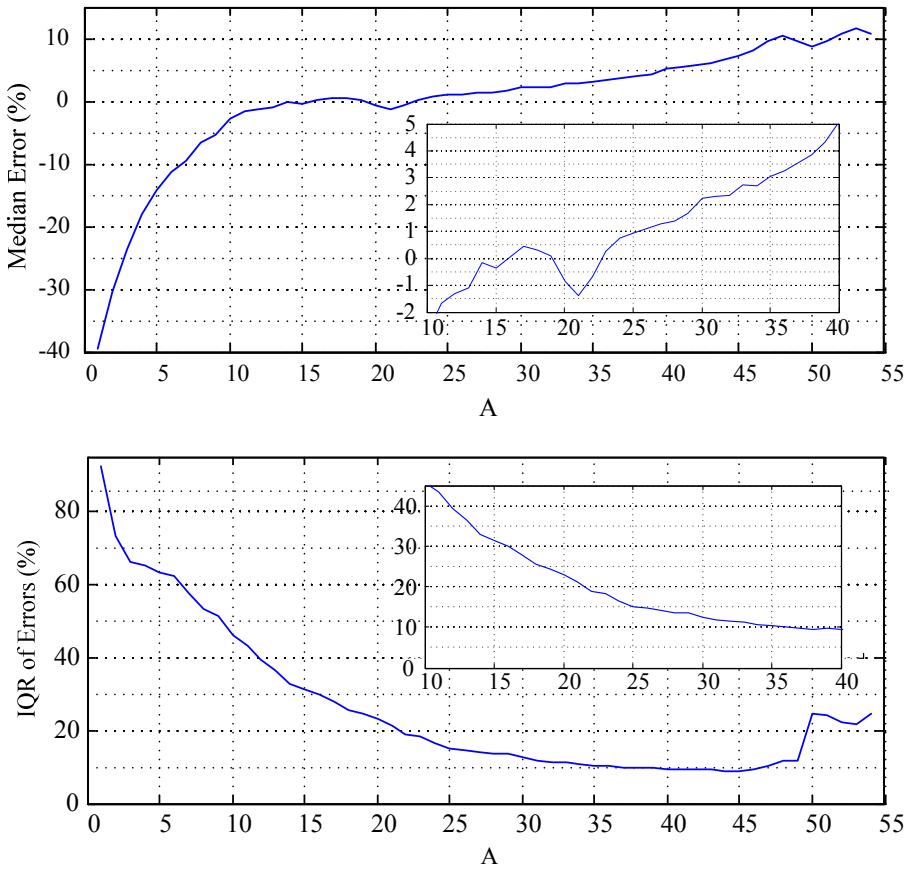

Figure 6-7 – Median and IQR of error for a range of window widths, the insets show a focused view for the results for window widths between 10 and 40 points.

For window widths less than 15, the noise rejection offered by the data windows is insufficient and this leads to very large errors. Conversely, for window widths above 45 the swing equation relationship begins to decay rapidly and the median and inter quartile range of the errors increases rapidly.

Presented in Figure 6-8 is a comparison of the absolute (100 %) range of the errors with the 99 % and 90 % range of the errors. (Note that here the 90 % range refers to the difference between the 5th percentile and the 95th percentile.) This comparison shows that the absolute range of the errors is highly variable with only a small period of consistent behaviour between approximately 30 and 40. In contrast the behaviour of the 99 % range is similar to that of the inter quartile range.

This extreme variation exists because a few extreme outliers dominate the size of the 100 % range. This can be seen in the relationship between the three ranges presented in Figure 6-8. The difference between the 99 % range and the 100 % range is at least an order of magnitude greater than the difference between the 99 % and 90 % range. This indicates that outer 1 % of data causes a vastly larger increase in the range than the next 9 %.

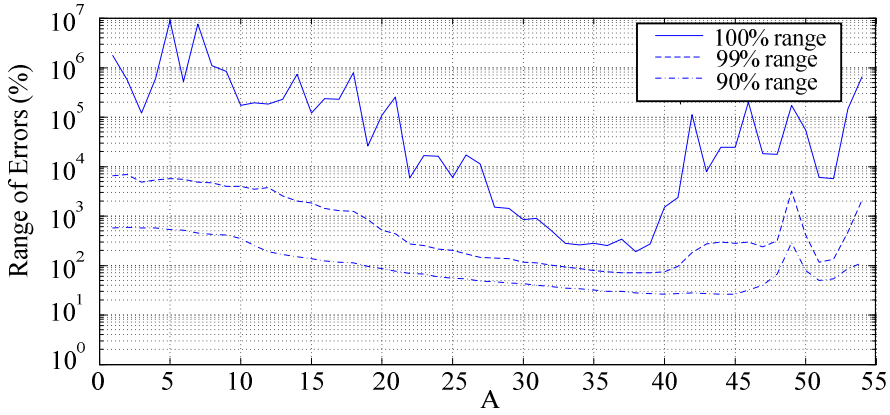

Figure 6-8 – The 100 %, 99 % and 90 % range of the errors for the range of window widths. This data is plotted with a logarithmic scale on the y-axis due to the extreme differences between their respective values.

Noticeable in Figure 6-8 is the increase in the range of the errors as the window size increases beyond approximately 40. This behaviour, similar to that seen in Figure 6-7, is an indication of the decay of the degree to which the measurements being used actually reflect the swing equation relationship. The extreme outliers that cause this behaviour could be dealt with by using an improved function for the data window, e.g. some form of recursive mean calculation that eliminates points based on their deviation from the mean.

A comparison of the estimation results for the outage of generator G9 and G10 is included here as the outage of G9 was one of the largest generator outages, whilst the outage of G10 was the smallest, so it was felt this comparison would offer some useful insights.

A comparison of the median error for the range of window sizes is presented in Figure 6-9. This comparison shows that the estimation of the inertia has a smaller median error for the key window sizes between 15 and 40 for the outage of G9. This improvement occurs because the estimation method appears to be more accurate for larger disturbances. This is likely because the deviations in frequency and power that occur throughout the system are larger and more sustained, and therefore less vulnerable to noise, in the case of the larger disturbance. The comparison of the inter quartile and 90 % ranges, presented in Figure 6-10, shows that the estimates are also far more reliable for the larger disturbance, that occurs for the disconnection of G9, as *A* is reduced.

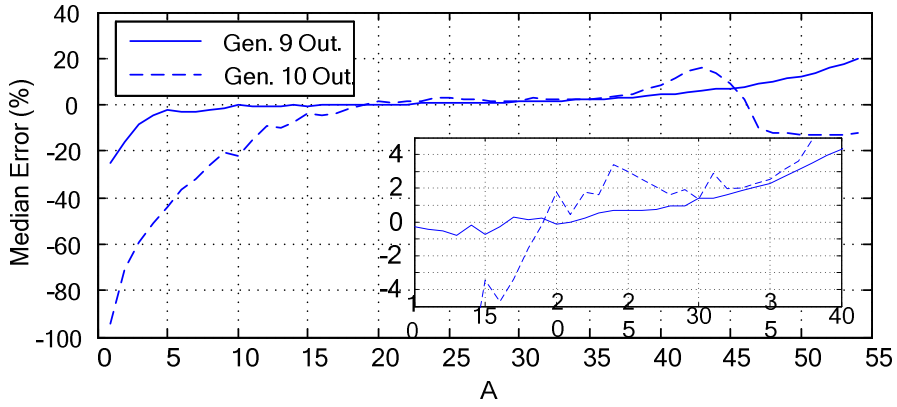

Figure 6-9 – This comparison of the median error for the estimates of inertia for the outage of G9 and G10 shows that the estimation method offers superior results for larger disturbances. The inset shows a view of the errors for A values of between 10 and 40.

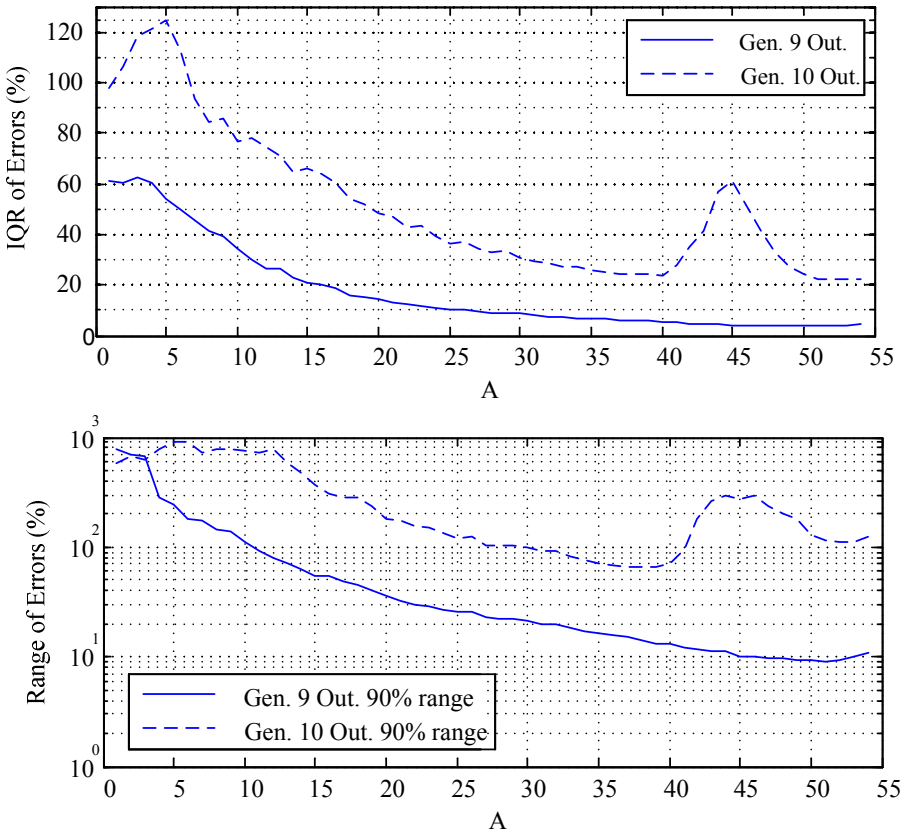

Figure 6-10– A comparison of the inter quartile range and 90 % range of errors for the outage of generator's G9 and G10.

An interesting feature in Figure 6-10 is the pronounced peaks, centred at window sizes of approximately 5 and 45, in the inter quartile range of the errors found for the outage of G10. These peaks exist because the outage of G10 initiates dynamic behaviour in the system that occurs around these points. This highlights a risk of increasing the value of *A*. This risk is that as *A* is increased the likelihood that the frequency response to events other than the original disturbance will be included in the window increases. The inclusion of this response to other events, such as inter-area oscillations or a second disturbance, would compromise the accuracy of the estimation, as the data used would no longer reflect the swing equation relationship.

6.4.2.2 Testing Windowed *H* Estimation for Bus Short Circuits

The assessment of the methods performance for data simulated for a short circuit was performed using the same process described in section 6.4.2.1. Therefore, instead of ten data sets like those shown in Figure 6-6, there are thirty-nine, i.e. one per bus.

Comparison of the results for the short circuit simulations and the generator outage simulations that is presented in Figure 6-11 shows that the method has similar behaviour for both disturbance types. The median and inter quartile range of the errors seen is somewhat smaller for the short circuit cases. These differences appear to be consistent with those seen for the comparison of the two generator outages, shown in Figure 6-9 and Figure 6-10, and are likely due to the same reasons because the bus short circuits tended to cause a larger power imbalance than the generator outages.

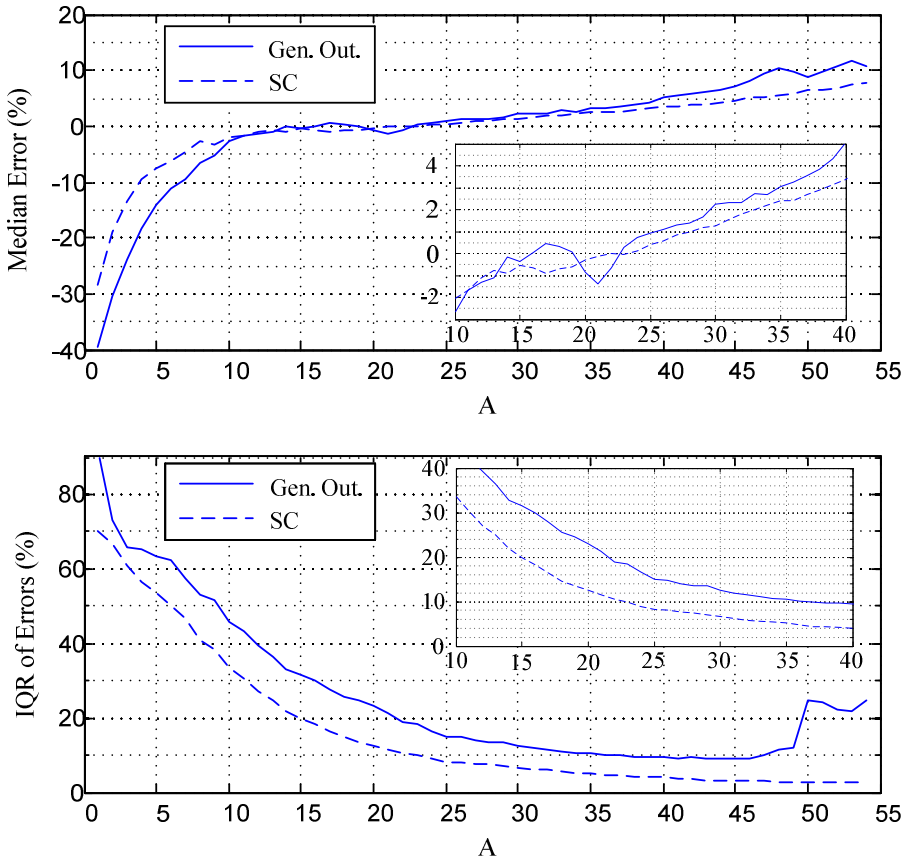

Figure 6-11 – Comparison of the Median and inter quartile range of the error seen for estimates made during Generator Outage and Short Circuit Disturbances.

A comparison of the 90 % range for the two separate disturbance types, Figure 6-12, demonstrates the same improved reliability for a larger disturbance. Finally, the data presented in Figure 6-13 shows that the estimates made based on the short circuit disturbances are vulnerable to the same extreme outliers that are seen in the generator outage case, shown in Figure 6-9.

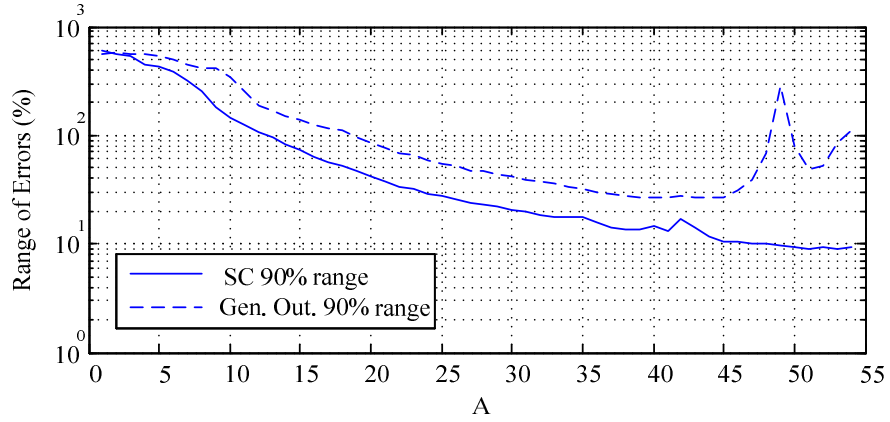

Figure 6-12– Comparison of the 90% range of the errors for estimates made during Generator Outage and Short Circuit Disturbances.

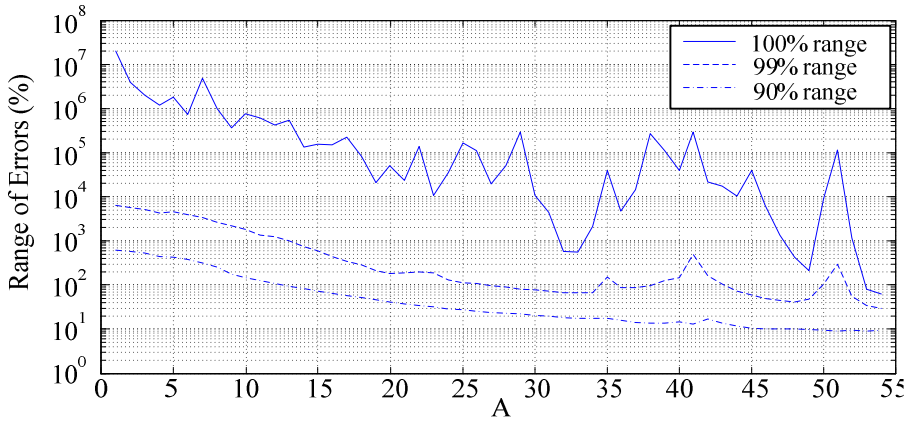

Figure 6-13 – 100 %, 99 % and 90 % range data for estimates made during short circuit disturbances. This data is plotted with a logarithmic scale on the y-axis due to the extreme differences between their respective values.

6.4.3 The Impact of using an Incorrect Disturbance Time

The dependence of the windowed *H* estimation method upon a known disturbance time is a threat to the opportunity of implementing it online. This is because it is unreasonable to expect access to perfect data regarding the time of the disturbance. To address this potential weakness the simulations performed in section 6.4.2.1 are repeated here using window widths of 30 and 40. However, instead of using the true disturbance time, which is 2.5 seconds, the data presented in the following sub-sections was created using disturbance times ranging from 2.2 seconds to 2.8 seconds. This was done to investigate the behaviour of the method when an inaccurate disturbance time is used. The results of this process are shown in Figure 6-14.

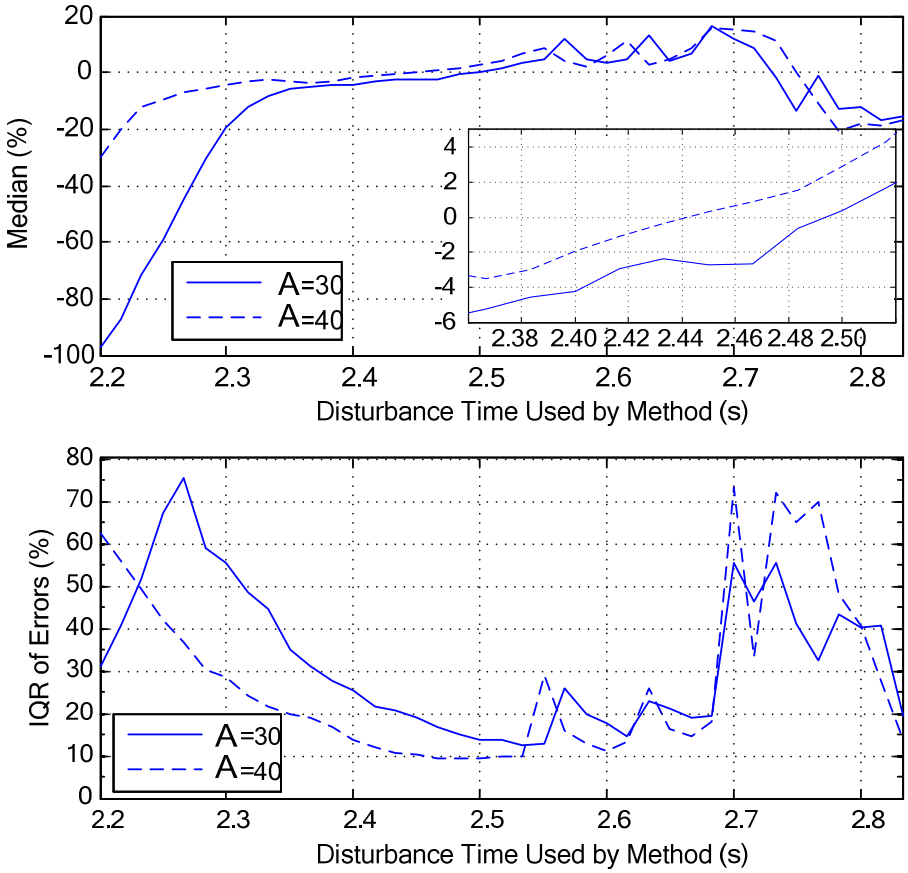

Figure 6-14 – Behaviour of the estimation method for the window widths of 30 and 40 when the time of disturbance used is that plotted on the x-axis and not the true time of disturbance of 2.5 seconds.

This figure shows that when the disturbance time used is less than the true disturbance time (2.5 seconds) the method can produce useful results. In fact, the results for the window width of 40 samples for disturbance times as early as 2.4 seconds are almost equivalent to those seen when the true disturbance time is used.

In general, the behaviour of the longer window width, 40 samples, is superior to that of the shorter window, 30 samples. This is because, as the longer window uses more data points, it is more capable of tolerating erroneous points. However, the performance of the method decays more rapidly when the disturbance time used is greater than the true disturbance time (2.5 seconds). This is because the value calculated for the pre-disturbance derivative of frequency and active power includes values for the post disturbance behaviour, thus compromising the performance of the estimation method. This issue cannot be completely overcome; however, it could be alleviated somewhat by using recursive mean calculations, like those proposed to deal with extreme outliers in subsection 6.4.2. This may allow the estimation method to produce accurate results, like those seen for disturbance times of less than 2.5 seconds, for disturbance times

that are greater than 2.5 seconds. Furthermore, in light of the sustained good performance of the method for disturbance times of 0.1 seconds below the true disturbance some form of guard time could be implemented to limit the risk of the disturbance time used being greater than the true disturbance time.

Finally, the low value of the inter quartile range for the window width of 30 points, which occurs for an assumed disturbance time of approximately 2.2 seconds, is misleading, and occurs for the same reason as the median error of approximately -100 % seen. The reason behind this is that because the assumed disturbance time is so far from the true disturbance time the post-disturbance data windows do not actually 'see' the disturbed system. Therefore, the inertia estimate returned is purely based on the noise in the system, and is thus approximately zero.

6.5 Chapter Summary

This chapter has demonstrated the implementation of a method that allows the accurate and reliable online estimation of system inertia based on WAMPAC enabled measurements of frequency and active power. With proper selection of the width of the data windows this method is capable of offering a very good level of accuracy. With a window width of 30 samples the estimates performed using varying noise profiles and simulated data of generator outage disturbances in the IEEE 39-bus test system produced results with a median error of 1.68 % and an inter quartile range of 13.5 %. Similarly, the estimates performed for short circuit disturbances in the system produced results with a median error of 1.53 % and an inter quartile range of 6.6 %. The method is capable of producing results that are approximately equivalent to these even if the disturbance time used by the method is not accurate. Accurate and reliable estimates of inertia will form a key part of any frequency prediction algorithm.

The selection of A is a key element of implementing this novel method for estimating the inertia constant. When selecting A it is important to balance the improved robustness against noise that larger A values offer against the increased risk of including other system dynamics or secondary contingencies in the filter windows. Pre-filtering of width W is used in the examples presented in this chapter to

demonstrate that the novel estimation method operates properly when applied to filtered data. This demonstration was necessary as in practical power system applications the wide area measurements supplied to the method will likely have undergone some form of filtering. However, this pre-filtering is not necessary for the method to function properly, as demonstrated in the next chapter of the thesis.

The estimation of system inertia is sensitive to the location at which the measurements are recorded. Further research should be performed to develop a proper understanding of this sensitivity and the geographical variation in the inertial response of a system to a disturbance. With sufficient access to data recorded from a power system research of this nature could contribute to the creation of a method for generating an inertia fingerprint for a system. This fingerprint would represent the geographical and temporal variation of inertia in a system and be of benefit to system planners and operators.

The dependence of this method upon an external estimate of the time of disturbance is undesirable and the next chapter of this thesis details the creation of method that overcomes this shortcoming.

6.6 References

[1] Machowski, J.; Bialek, J.; W.; Bumby, J., Power System Dynamics: Stability and Control. 2008: John Wiley & Sons.

[2] Anderson, P.M.; Mirheydar, M.; , "A low-order system frequency response model," Power Systems, IEEE Transactions on , vol.5, no.3, pp.720-729, Aug 1990

[3] National Grid Report "UK Future Energy Scenarios", November 2011, URL: http://www.nationalgrid.com/NR/rdonlyres/86C815F5-0EAD-46B5-A580-A0A516562B3E/50819/10312_1_NG_Futureenergyscenarios_WEB1.pdf

[4] Vittal, V. Ayyanar, R. "Grid Integration and Dynamic Impact of Wind Energy", Springer, 2013

[5] Strbac, G.; Jenkins, N.; Green, T., "Future Network Technologies", Report to DTI (UK). 2006.

[6] Kundur, P., Power System Stability and Control 1994, New York: McGraw-Hill.

[7] Phadke, A. G.; and Thorp, J. S. , Synchronized phasor measurements and their applications. New York; London: Springer, 2008.

[8] Inoue, T.; Taniguchi, H.; Ikeguchi, Y. and Yoshida, K. "Estimation of power system inertia constant and capacity of spinning-reserve support generators using measured frequency transients," Power Systems, IEEE Transactions on, vol. 12, pp. 136-143, 1997.

[9] Chassin, D. P.; Huang, Z.; Donnelly, M.K.; Hassler, C.; Ramirez, E. and Ray, C., "Estimation of WECC system inertia using observed frequency transients," Power Systems, IEEE Transactions on, vol. 20, pp. 1190-1192, 2005.

[10] Littler, T.; Fox, B.; and Flynn, D., "Measurement-based estimation of wind farm inertia," in Power Tech, 2005 IEEE Russia, 2005, pp. 1-5.

[11] Mullane, A.; Bryans, G.; O'Malley, M.; , "Kinetic energy and frequency response comparison for renewable generation systems," Future Power Systems, 2005 International Conference on , vol., no., pp.6 pp.-6, 18-18 Nov. 2005

[12] Anderson, P.M.; Mirheydar, M.; , "A low-order system frequency response model," Power Systems, IEEE Transactions on , vol.5, no.3, pp.720-729, Aug 1990

[13] http://www.ee.washington.edu/research/pstca/.

[14] DIgSILENT, "DIgSILENT PowerFactory," V 14.0523.1 ed Gomaringen, Germany: DIgSILENT GmbH, 2011.

[15] Mathworks, "MATLAB," 7.10.0.499 (R2010a) ed Natick, Massachusetts, U.S.A., 2011.

[16] Arbiter Systems, Model 1133A Power Sentinel Data Sheet,www.arbiter.com.

7 Simultaneous Estimation of the Inertia and Time of Disturbance

The inertia estimation method presented in the previous chapter was shown to be accurate for a number of algorithm settings and system conditions. However, its dependence on an accurate known time of disturbance will limit its application. This chapter describes the creation of a novel algorithm that uses the continuous execution of the window based estimation algorithm to detect the time of disturbance. Section 7.1 describes the benefits of eliminating the estimation algorithms dependence on an external time of disturbance. The algorithm that allows the simultaneous estimation of the time of disturbance and inertia is described in Section 7.2. Section 7.3 gives the results of initial simulation based testing that led to a modification being made to the algorithm to improve its performance. The results of the extensive simulation based testing of this extended algorithm are also presented in this chapter. Sections 7.4 and 7.5 provide examples of the algorithms application to data collected from a laboratory based motor-generator set and the National Grid operated transmission system. Finally, Section 7.6 discusses the general performance of this algorithm and the value it offers to prediction algorithms.

7.1 Chapter Introduction

The inertia of a system heavily influences its initial frequency response to a disturbance. However, the review of power system developments in Chapter 4 highlighted that the inertia will become highly variable in future power systems and as such estimation of the inertia will be a critical element of any frequency prediction algorithm. The previous chapter introduced a window based method that uses a modified swing equation to produce accurate estimates of inertia. However, this method depended upon a time of disturbance estimate from an external application. This weakness is undesirable due to the critical importance of inertia estimation to frequency prediction. This chapter describes the research performed during the creation of a method that used the continuous execution of the window based method to simultaneously estimate both the inertia and the time of disturbance. This time of

disturbance estimate not only eliminates the weakness of the inertia estimation algorithm but will also serve as a valuable input for any other parameter estimation performed as part of the prediction algorithm.

7.2 Detection and Estimation Algorithm

The algorithm presented in this chapter is designed to determine the time of a disturbance in a power system whilst simultaneously estimating the inertia in the system at that time. This algorithm is intended to operate online with input data composed of synchronized measurements of the active power and rate of change of frequency that are updated every Δt seconds. The algorithm operates by exploiting the fact that the modified swing equation (7-1) is only valid in the period immediately after a disturbance.

$$2H\Delta\frac{df(t)}{dt} \approx P_e(t-\Delta t) - P_e(t) \approx \Delta P(t) \quad \text{[p.u.]} \tag{7-1}$$

where Δt is the interval between measurements and P_e now simply denotes the active power flow at the location at which the rate of change of frequency is measured.

The windowing method that is presented in the previous chapter is executed continuously and the output of this is used to estimate the time of disturbance and inertia of the system based on the generic process depicted in Figure 7-1. The following sections describe how this is achieved, but first the execution of the window based inertia estimation method that was introduced in the previous chapter will be described here with a greater focus on certain issues relevant to its continuous execution.

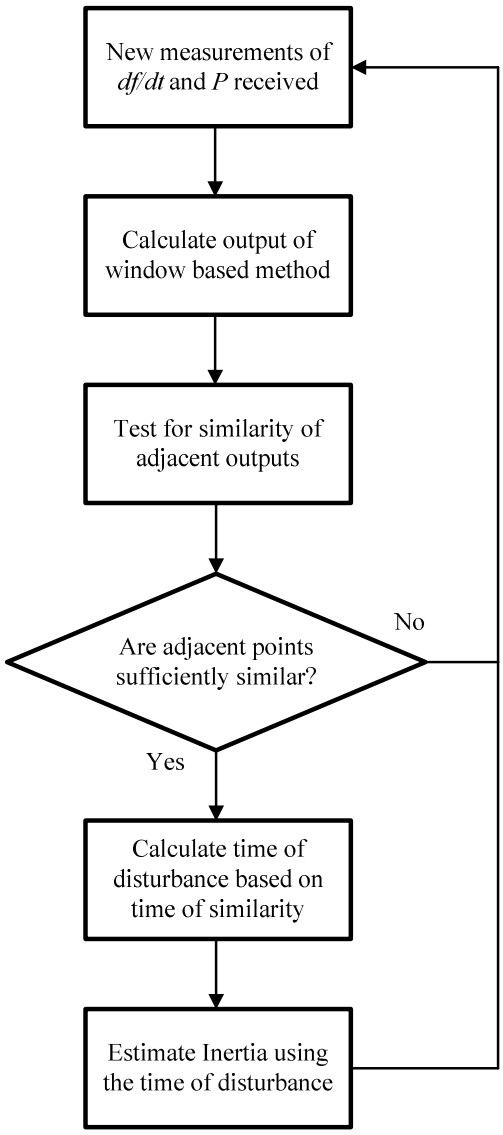

Figure 7-1 – The generic process for using the continuous execution of the window based inertia estimation method to determine the time of disturbance

7.2.1 Estimating the Inertia

At the core of this algorithm is a set of four smoothing filters that in this combined time of disturbance and inertia estimation application are applied as sliding windows in order to estimate the inertial response represented by the measured frequency and active power behaviour. The estimation process is executed each time a new set of measurements are received, here it is assumed that a set of synchronous measurements are received every Δt seconds, so the output will consist of one estimate for every time step. At this stage in the discussion it is important to be clear that only those estimates for the period of time in which a disturbance has occurred will be accurate estimates of the inertia, the rest will be erroneous.

The windows are smoothing filters so the estimation process for the time t_n, when a set of new measurements are received, will be centred at the time t_c, as depicted in Figure 7-2. Each window has a width of A data points or samples, and therefore a width of $(A-1)\Delta t$ seconds, and the separation between each pair of windows is determined by the width of any pre-filtering applied to the data, W.

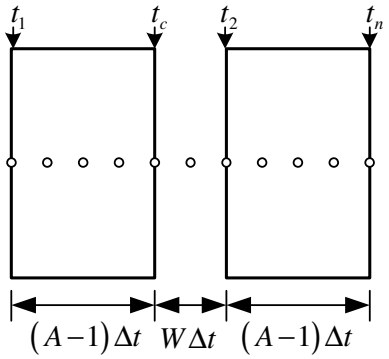

Figure 7-2– A pair of windows are used to process each set of data, in this example the black circles are data points so A=5 and W=2.

From the figure the relationship between each of the key time stamps can be determined relative to the time when the set of new measurements are received, t_n. Clearly defining these times is important as they will be used to determine the time of disturbance.

$$t_2 = t_n - (A-1)\Delta t \quad \text{[s]} \tag{7-2}$$

$$t_c = t_n - ((A-1)+W)\Delta t \quad \text{[s]} \tag{7-3}$$

$$t_1 = t_n - (2(A-1)+W)\Delta t \quad \text{[s]} \tag{7-4}$$

where these times are the start of the second window, t_2, the time at which the windows are centred, t_c, and the start of the first window, t_1, as marked in Figure 7-2. This allows the output of the windows for the time at which new measurements are received to be defined as follows, for the case where the filters take a straight mean of the data points.

$$P_1(t_n) = \frac{1}{A}\sum_{t=t_1}^{t_c} P(t) \quad \text{[p.u.]} \tag{7-5}$$

$$P_2(t_n) = \frac{1}{A}\sum_{t=t_2}^{t_n} P(t) \quad \text{[p.u.]} \tag{7-6}$$

$$R_1(t_n) = \frac{1}{A}\sum_{t=t_1}^{t_c} \dot{f}(t) \quad \text{[p.u.]} \tag{7-7}$$

$$R_2(t_n) = \frac{1}{A}\sum_{t=t_2}^{t_n} \dot{f}(t) \quad \text{[p.u.]} \tag{7-8}$$

Each of the windows provides one of the variables in the modified swing equation. The first window, R_1, provides the rate of change of frequency prior to t_c and the second window, R_2, provides the rate of change of frequency after t_c. The third and fourth windows, P_1 and P_2, provide the pre t_c and post t_c active power. This can be represented by adjusting the notation of the modified swing equation to correspond to the window definitions.

$$H = \frac{1}{2}\frac{P_1 - P_2}{R_2 - R_1} \quad \text{[s]} \tag{7-9}$$

The example data in Figure 7-3 represents the response of a synchronous generator, with inertia of 5 s, to a 0.05 p.u. step decrease in load after five seconds and was created using the simplified frequency model proposed in [1].

The noise added to the signal was white noise with magnitude of between plus and minus 0.01 p.u. and plus and minus 0.001 p.u./s for the active power and derivative of frequency, respectively. No pre-filtering was applied to this data as it is unnecessary for the successful execution of the algorithm.

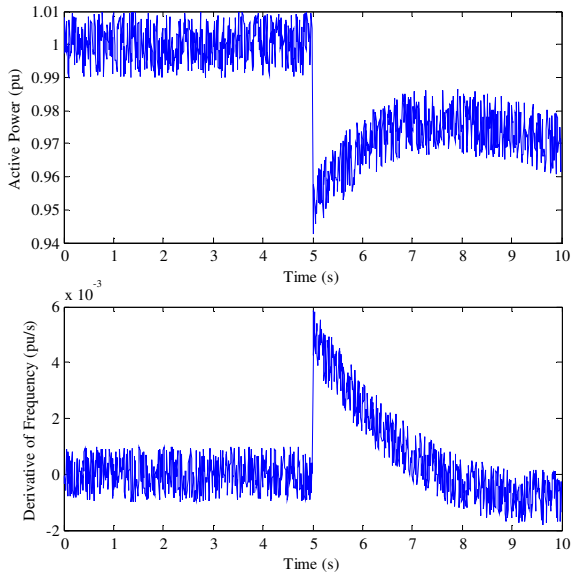

Figure 7-3 – The algorithm for the simultaneous estimation of the time of disturbance and inertia requires measurements of the active power and derivative of frequency. No pre-filtering is necessary. This example data is for a 0.05 p.u. decrease in load after five seconds for a SFR model with inertia of 5 seconds.

When the windows are applied to the example active power and rate of change of frequency signals presented in Figure 7-3 the output is the signal presented in Figure 7-4. The data presented in the figure was cropped so that it lies between the limits of zero and fifty; this was done to make the data more presentable and no meaningful information was lost.

The time axis in Figure 7-4 is given in terms of t_c, defined in Figure 7-2, that the estimate represents, thus the output appears to respond prior to the disturbance occurring, this is simply due to the smoothing nature of the process and the choice of time reference. This is done because it is the t_c for the estimate convergence that will correspond to the time of the disturbance and not t_n. The label of the y axis in Figure 7-4 is Output because only a small subset of the data presented there is actually an estimate of the inertia, specifically the data centred at the time of the disturbance, so to refer to it all as H would be misleading.

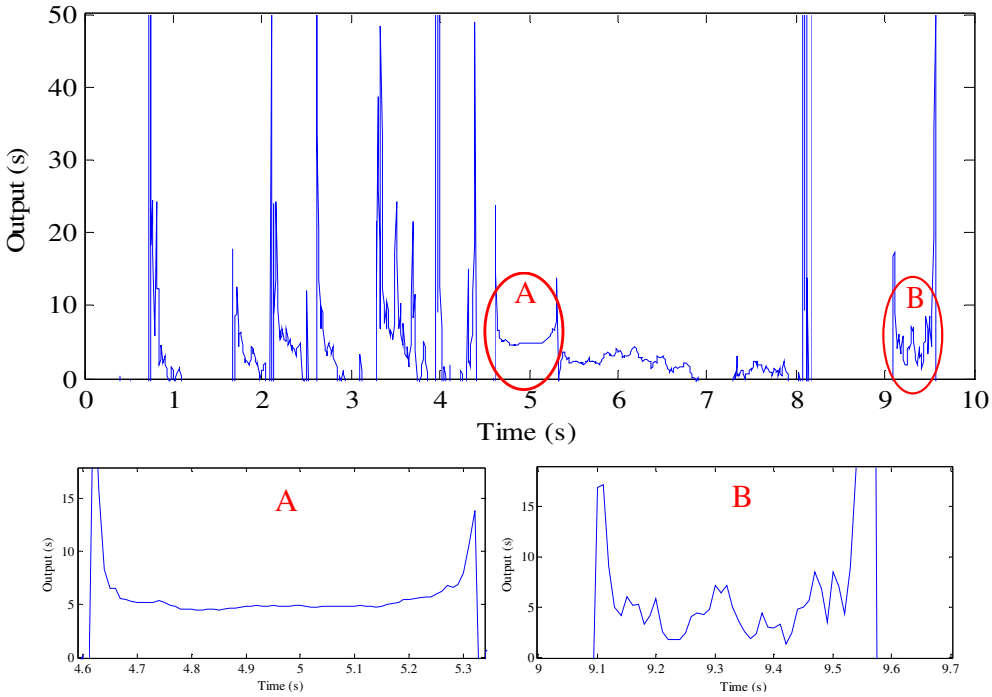

Figure 7-4 – The output of the windowing process for an example set of data created using the SFR model with a load step increase of 0.05 p.u., sub plots A and B highlight the behaviour of the output for the time of disturbance and for noise.

It can be seen that the output converges to approximately five, the true value of the inertia, during the disturbance, see subplot A of Figure 7-4. Therefore, with access to this output the challenge of estimating the time of disturbance simply becomes the challenge of detecting the convergence of the output of the swing equation to an approximately fixed value. The primary challenge in achieving this will be separating between the behaviour seen in sub plot A of Figure 7-4, during the disturbance, and sub plot B of Figure 7-4, from noise and other system behaviour. This convergence can be detected by calculating the residues between adjacent estimates using the process described in the next section. This method was preferred to others, such as variance calculations or wavelet transforms, due to its mathematical simplicity and hence the potential it offers for high speed execution.

7.2.2 Determining the Time of Disturbance

The detection process presented in this paper exploits the convergent properties of the windowing process during a disturbance, see Figure 7-4. The output of the key stages

of the detection process are summarised in Figure 7-5 and Figure 7-6 and the following discussion is a detailed description of the stages of the flow diagram in Figure 7-7.

The detection process uses the sum of the residues, r, between the current output of the windowing process, $O(t_n)$, and the N previous estimates from the windowing process to determine the degree of similarity between these estimates. This residue is calculated using (7-10) and estimates are denoted here as O to represent the fact that they are not necessarily estimates of the inertia constant H.

$$r = -NO(t_n) + \sum_{k=1}^{N} O(t_n - k\Delta t) \quad \text{[s]} \tag{7-10}$$

This comparison is performed each time a new estimate is received and a disturbance is deemed to have occurred once a certain number of consecutive new estimates are classed as being sufficiently similar to one another. In the examples in this section N is equal to three.

A set of N consecutive samples are classed as being sufficiently similar if the absolute value of the sum of the residue between them and the current sample is below a dynamic threshold value referred to as r_{MAX}. This is a dynamic threshold because it is calculated as the product of the current estimate and a user defined value tr. The advantage of using this dynamic threshold is that it allows the measure of similarity to vary with the level noise in the measurements that are being used. Furthermore, this method for setting the threshold is independent of the true inertia of the system and thus the estimation method can be applied to a system with variable and uncertain inertia; a key requirement if the method is to support the proposed frequency prediction methods.

Each time a set of consecutive samples satisfy this dynamic threshold the consecutive sum (*CSUM*) is incremented by one, if any set of consecutive samples fails to satisfy the dynamic threshold then *CSUM* is reset to zero. *CSUM* is also reset to zero if the new estimate is less than zero or greater than a user defined limit H_{MAX}; this is included to avoid the needless processing of excessive quantities of data and particularly large value estimates and has no effect on the estimation performance of the algorithm. In the examples here the value of H_{MAX} is 50, for a system where the true inertia is 5.

A disturbance is deemed to have occurred if *CSUM* exceeds *A*, the behaviour of *CSUM* for the example case is depicted in Figure 7-5. The time of the disturbance t_d can then be estimated based on the t_n at which *CSUM* was equal to *A* by simply making adjustments for the delays introduced by each stage.

$$t_d = t_n - \left(W + \left(A - 1\right) + A\right)\Delta t \quad \text{[s]} \tag{7-11}$$

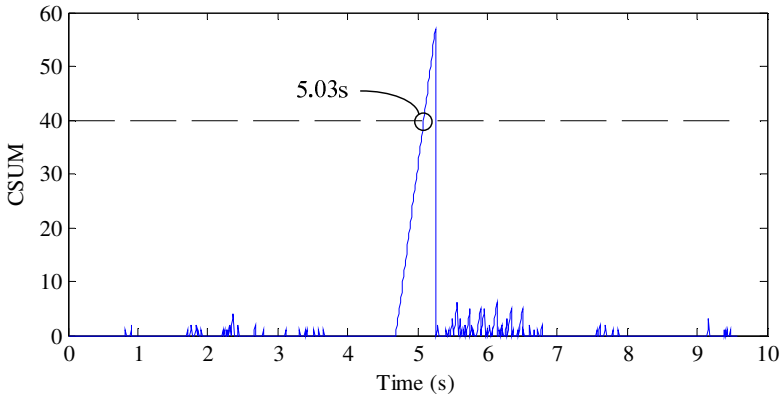

Figure 7-5 – *CSUM* is used to determine the presence of a disturbance and it can be seen here that it only approaches the detection threshold for the disturbance. This figure was generated using an *A* value of 40 and a *tr* value of 0.25

Having detected a disturbance and estimated the time of its occurrence the inertia can be estimated based on the *H* values either side of t_d. The selection of which H values to use is can be defined in any number of ways but the preferred method here was to use the *A*/4 values either side of t_d. Figure 7-6 shows the result of this targeting process for the example case. A truncated mean was used as a simple way to improve the accuracy of the estimate; this involved taking the mean of only those points that lie within the inter quartile range of the selected estimates. This mean is used to improve the accuracy of the estimate and any similar method for improving the accuracy of a mean taken from a set of samples could be substituted in its place.

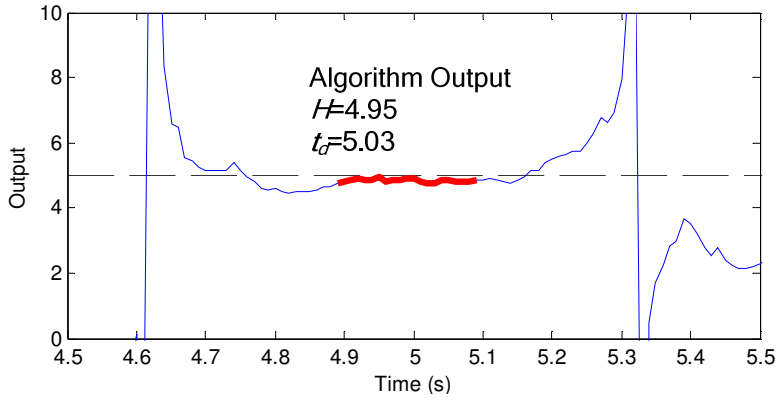

Figure 7-6 – An example of the targeting process used by the algorithm this converts the Output of the windowing algorithm (blue line) into an inertia estimate using the A/4 estimates either side of td (thick red line). This figure was generated using an *A* value of 40 and a *tr* value of 0.25

This process clearly has two key properties that are defined by the user, namely the window width *A* and the dynamic threshold ratio *tr*. The variable *tr* is used to scale the dynamic threshold and allows the convergence of the estimates to be detected. A particular advantage of this approach is that it allows the process to distinguish between sets of low residuals that occur because of convergence and those which occur because of a sequence of low/near zero estimates. This parameter should be set based primarily on the expected noise level in the measurements used. The influence of *tr* on the process is explored in detail in Section 7.3 using simulation results.

The convergent period has a width of approximately *A* so larger values of *A* offer a longer period of convergence and hence increased robustness. However this comes at the cost of an increased delay in the process, (7-11) shows that an increase of ΔA will lead to a $2\Delta A$ increase in the delay.

This process can be executed using the following steps, which are also depicted in Figure 7-7.

1. New Measurements of Rate of Change of Frequency and Active Power are received at t_n.
2. Calculate a new H value using the window based approach; this value is limited to between zero and H_{MAX} to create H_L.
3. Calculate the total residue between the new H_L value and the N previous H_L values (r).
4. Calculate the dynamic threshold (r_{MAX}) for this new H_L value.
5. Compare r with r_{MAX} and if it is less than the dynamic threshold set $flag_R$ to 1, else set it to zero.

6. For every consecutive $flag_R$ value that is 1 increment *CSUM* by 1, if $flag_R$ is ever zero or if the new *H* value is either less than or equal to zero or greater than or equal to H_{MAX} then reset *CSUM* to zero.
7. If *CSUM* is equal to *A* set $flag_D$ to 1.
8. If $flag_D$ is 1 then the time of the disturbance can then be calculated using (7-11) based on the current t_n.
9. The inertia can then be estimated using the *H* estimates centred around t_d.

A disturbance will not be deemed to have occurred for every sample time at which $flag_D$ is high. A disturbance is only deemed to have occurred the first time that $flag_D$ is high. This can be enforced by having the disturbance detected on the rising edge of $flag_D$ and not the absolute value.

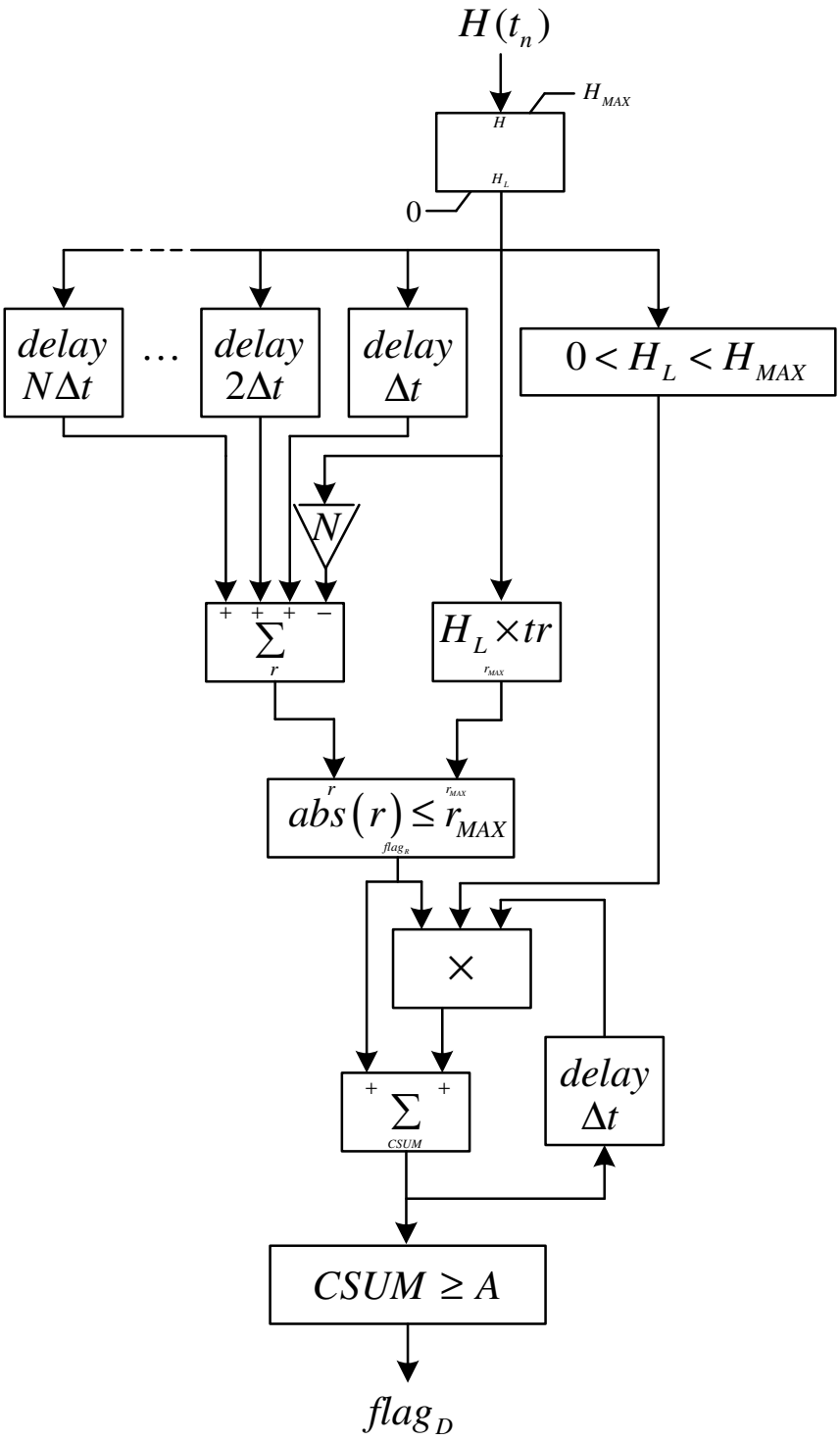

Figure 7-7 – A flow diagram showing the execution of the inertia and time of disturbance estimation algorithm. *N* is the number of adjacent residues used, *A* is the window width, *Δt* is the delay between receiving each new set of measurements, H_{MAX} is an arbitrary limit that prevents the algorithm from processing junk data, *CSUM* is the cumulative sum of sequential adjacent values that have been deemed similar to one another, *tr* is a threshold value that allows the dynamic threshold r_{max} to be calculated based on the current output of the window based method H_L.

7.3 Simulated Examples

A set of simulations were performed to investigate the behaviour of the novel algorithm proposed here for simultaneously estimating the time of disturbance and the inertia. These simulations were performed using the simplified frequency response model (SFR), proposed in [1] and detailed in Chapter 8. The inertia of the model was set to 5 seconds and the reporting rate of the frequency and active power measurements is 50 Hz. The investigation took the form of varying the parameters *A* and *tr* as well as the size of the disturbance and the noise added to the signals.

The success of the method is assessed based on four criteria:

1. Preventing the occurrence of false detections.
2. Successfully detecting that a disturbance has occurred.
3. Accurately estimating the time of the disturbance.
4. Accurately estimating the inertia.

The satisfaction of these criteria were measured using the expectation of false detections, true detections, the error in the time of disturbance estimate in seconds and the error in the inertia estimate in percent. The number of trials performed for each *A* and *tr* combination was one thousand and this was deemed sufficient to approximate the expectation of each measure as the mean of the output of each trial for each measure.

The number of consecutive estimates used to calculate the residuals (N) is set to three for all of the examples presented here. Sub-section 7.3.1 details some initial results that highlighted a flaw in the method. Sub-sections 7.3.2 and 7.3.3 outline the solution to this flaw and the results of simulations that demonstrate its success. Subsection 7.3.4 discusses the factors that influence the proper selection of the key algorithm parameters, *A* and *tr*.

7.3.1 Initial Results

These initial results for the expectation of true and false detection that are shown in Table 7-1 and Table 7-2 were generated using 1000 simulations of each *A* and *tr* combination with additive white noise of magnitude between plus and minus 0.01 p.u. for the power measurements and plus and minus 0.001 p.u./s for the derivative of frequency measurements. The measurements have a reporting rate of 100 Hz, i.e. two measurements per cycle in the 50 Hz system. The disturbance was a 0.2 p.u. step increase in active power demand after 5 seconds. No pre-filtering was applied in these simulations; this is because such pre-filtering is not necessary for the success of the algorithm and thus serves only to introduce delays. The windowing process is shown to be successful in the presence of pre-filtering in the previous chapter and [2].

The results presented in Table 7-1 and Table 7-2 demonstrate that, whilst the algorithm can successfully detect the disturbance, there are a disturbingly high number of false detections. Therefore, the time of disturbance and inertia estimates will not be discussed in this subsection, as in the presence of such a high number of false detections they are a secondary consideration for the successful development of the algorithm. Analysis of the inertia and time of disturbance estimates returned by the algorithm for simulated data is given in Subsection 7.3.3 in which the issue of false detections has been dealt with using the method proposed in Subsection 7.3.2.

Table 7-1– Expectation of True Detections
for a 0.2 p.u. increase in load for ±0.01 p.u. Power Error and ±0.001 p.u./s df/dt Error

tr\A	10	20	30	40
0.1	0.570	0.986	1	1
0.25	1	1	1	1
0.75	1	1	1	1
1.25	1	1	1	1
1.5	1	1	1	1

Table 7-2 – Expectation of False Detections
for a 0.2 p.u. increase in load for ±0.01 p.u. Power Error and ±0.001 p.u./s df/dt Error

tr\A	10	20	30	40
0.1	0	0	0	0
0.25	0	0	0.002	0.130
0.75	0.014	0.504	1.824	1.264
1.25	0.236	2.610	1.684	1.192
1.5	0.618	3.040	1.672	1.212

The high expectation of false detections exists because of the system behaviour that occurs after the disturbance, specifically due to the oscillations that occur after the first zero crossing of the derivative of frequency, the frequency nadir. This behaviour creates a second convergent period associated with the disturbance, marked in Figure 7-8. This convergence is weaker than that seen for the period of the disturbance. This can be determined by observing the fall in false detections (Table 7-2) that occurs as the window size is reduced from 20 samples to 10 samples. This occurs because the shorter window offers a lower attenuation of the noise so the damping convergence is sufficiently corrupted so that it does not always satisfy the convergence threshold. There is no corresponding fall in the true detections indicating that the damping convergence is weaker than the convergence seen for the disturbance. The fall/elimination of false detections as *tr* is reduced to 0.25 and then 0.1 also demonstrates that this damping convergence is weaker in nature than the convergence seen for the disturbance.

The fall in false detections seen as the window size is reduced from 20 to 10 is contrary to the previous trend of increasing false detection as the window size is reduced from 40 samples to 30 samples and then 20 samples. This behaviour is not driven by the signals being measured, but instead by the properties of the estimation algorithm. Due to the length of the damping convergence, relative to the window width, it is possible for the windows to detect the damping convergence multiple times. As the window width is reduced this is more likely to occur until the limit is reached at which the window size is too small relative to the noise in the signal.

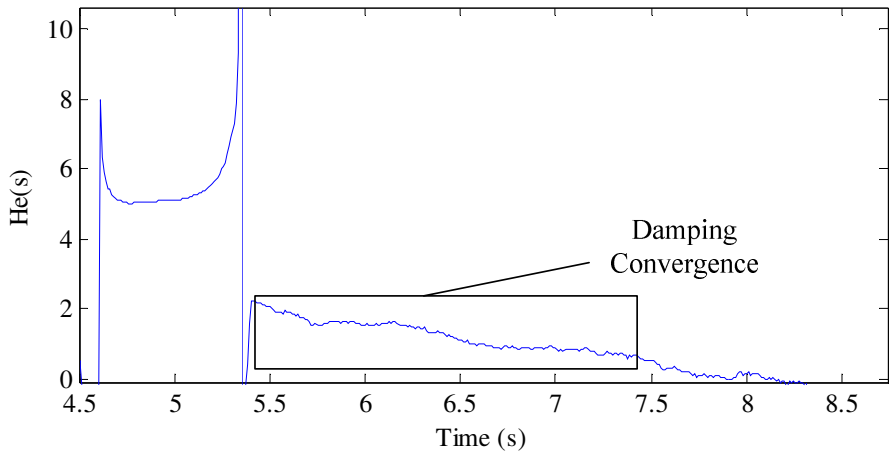

Figure 7-8 – The post disturbance oscillations create an extended period of weak convergence that can trigger the algorithm and cause false detection. *He* is marked on the y axis to distinguish it from true estimates of *H*.

This damping convergence is only consistently seen in cases where the system is subjected to a large disturbance in a low noise environment. Therefore it may not be seen in data recorded for a real power system, particularly larger systems where the inertia is higher and the relative size of the largest credible contingency is lower. However, the presence of this behaviour is still a concern. Possible solutions could include exploiting the influence of *tr* and *A* on the false detection rates. However, this is highly undesirable as these parameters are the only tools available to the user to determine the noise tolerance of the algorithm and the size of disturbance that it can reliably detect and adjusting them to accommodate the issue of damping convergence could severely undermine the performance of the algorithm. Therefore, the solution proposed here is the introduction of a set of confidence curves that can be used to determine the feasibility of any proposed detection, based on the associated inertia estimate, the implementation of these curves is described in the next Section (7.3.2) and an assessment of their performance is given in Section 7.3.3.

7.3.2 Introducing Confidence Curves

This sub section details the inclusion of a set of limits that will allow the rejection of unlikely inertia estimates that occur due to false detections, from the damping convergence or otherwise. There are two limits, an upper bound (UB) and a lower bound (LB), which together are referred to here as confidence curves and take the form depicted in Figure 7-9. Any estimate that lies outside of these curves is rejected on the

basis that it is extremely unlikely to have actually occurred, based on the definition of a likely maximum sudden change in inertia of *mv*.

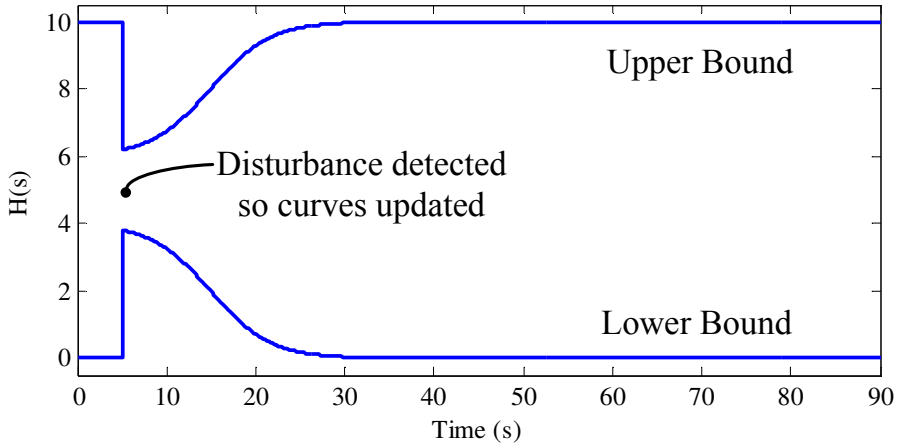

Figure 7-9 – A depiction of the shape of the proposed confidence curves for assessing the feasibility of an estimate, prior to the disturbance being detected curves are at the maximum limits due to lack of recent information

These curves are formed using the following expressions:

$$UB(t) = H_p(1+mv) + \left(UB_L - H_p(1+mv)\right)\left(1 - \frac{1}{1+\alpha e^{-(t-t_P)\beta}}\right) \quad [\text{s}] \qquad (7\text{-}12)$$

$$LB(t) = H_p(1-mv) - \left(LB_L + H_p(1-mv)\right)\left(1 - \frac{1}{1+\alpha e^{-(t-t_P)\beta}}\right) \quad [\text{s}] \qquad (7\text{-}13)$$

where

$$\beta = -\frac{\log(1/\alpha)}{0.5\alpha} \qquad (7\text{-}14)$$

and *mv* is the maximum expected sudden variation of inertia as a proportion of the current inertia, α is a constant that represents the increase in the likelihood of inertia variation over time, UB_L and LB_L are the maximum and minimum values that the inertia is expected to take, H_P is the last known inertia estimate and t_P is the time at which it was made.

The functionality of these curves can be demonstrated using a simple example in which the system experiences the cascade loss of two large generating units. The first generation loss occurs at 5 seconds and represents a 0.2 p.u. loss of generation and a

0.5 s drop in inertia. The second generation loss occurs at 6 seconds and represents a 0.2 p.u. loss of generation and a 1 s drop in inertia. The variation in the inertia that this causes is depicted in Figure 7-10. The same noise magnitudes that were used when generating the results presented in Section 7.3.1 were also applied here (0.01 p.u. for power and 0.001 p.u./s for derivative of frequency).

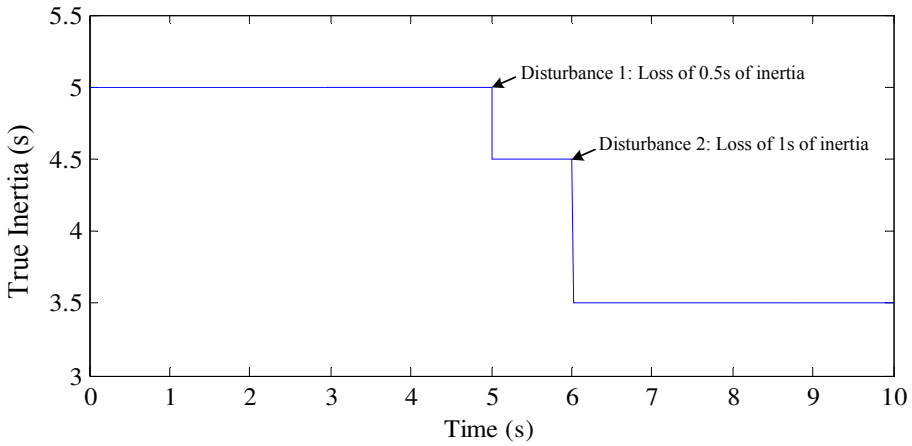

Figure 7-10 – The variation in system inertia caused by the two disturbances in the demonstration case for the confidence curves.

Applying the algorithm to the scenario presented here resulted in three event detections, the first two were accurate detections of the disturbances and the third was a false detection triggered by the damping behaviour. These detections are presented in Table 7-3 alongside the decision made based on the confidence curves. Figure 7-11 shows the evolution of the confidence curves as the events are detected. The settings for these curves are: mv=0.3, α=30, UB_L=10, LB_L=0.

Table 7-3 – Detections Made for Confidence Curves Example

Detection	$t_{d\ estimated}$ (s)	$t_{d\ true}$ (s)	$H_{estimated}$ (s)	H_{true} (s)
1 – accepted	5.04	5	4.64	4.5
2 – accepted	6.11	6	3.69	3.5
3 – rejected	6.68	–	1.75	3.5

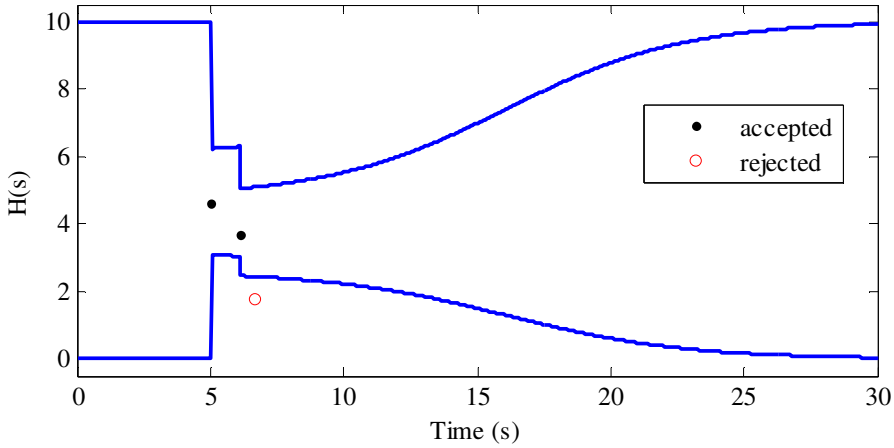

Figure 7-11 – The confidence curves evolve as the disturbances are detected, the two detections that correspond to the disturbances are accepted whilst the false detection is rejected as it lies outside of the confidence curves.

7.3.3 Results for Algorithm with Confidence Curves

The simulations performed here use the same approach as that used in Subsection 7.3.1. The SFR model is simulated with inertia of 5 s and measurements are recorded at a rate of 100 Hz. The algorithm uses three consecutive estimates to calculate the residuals (N=3) and the confidence curves presented in Subsection 7.3.2 are included in the algorithm. The settings for these curves are: mv=0.3, α=30, UB_L=10, LB_L=0.

The first scenario simulated was for a 0.2 p.u. load increase at t=5 seconds with noise of 0.01 p.u. for the power measurements and 0.001 p.u./s for the derivative of frequency, 1000 noise signals for both power and derivative of frequency were created to allow an investigation of the statistical behaviour of the algorithm. Table 7-4 and Table 7-5 present the expectation of true and false detections, whilst Table 7-6 presents the expectation of the percentage error in the inertia estimate. Table 7-7 presents the expected estimate of the time of the disturbance.

The false detections seen in Table 7-2 have been eliminated for the longer windows and significantly reduced for the shorter windows. Those false detections seen here occur because the shorter windows are still more vulnerable to detecting the damping convergence. Furthermore, whilst the expected error seen in Table 7-6 is better for smaller windows, the estimates made using smaller windows have a larger standard deviation which undermines the performance of the confidence curves. The true detection rate is practically unaffected by the introduction of the confidence curves.

Table 7-4 – Expectation of True Detections
for a 0.2 p.u. increase in load for ±0.01 p.u. Power Error and ±0.001 p.u./s df/dt Error

tr\A	10	20	30	40
0.1	0.569	0.986	1	1
0.25	1	1	1	1
0.75	1	1	1	1
1.25	1	1	1	1
1.5	1	1	1	1

Table 7-5 – Expectation of False Detections
for a 0.2 p.u. increase in load for ±0.01 p.u. Power Error and ±0.001 p.u./s df/dt Error

tr\A	10	20	30	40
0.1	0	0	0	0
0.25	0	0	0	0
0.75	0.012	0.004	0	0
1.25	0.06	0.032	0	0
1.5	0.175	0.038	0	0

Table 7-6 – Expectation of Error in Inertia Estimate (%)
for a 0.2 p.u. increase in load for ±0.01 p.u. Power Error and ±0.001 p.u./s df/dt Error

tr\A	10	20	30	40
0.1	-0.355	-1.281	-1.922	-2.303
0.25	-0.159	-0.971	-1.637	-2.089
0.75	-0.076	-0.888	-1.554	-1.998
1.25	0.061	-0.818	-1.511	-1.930
1.5	0.303	-0.783	-1.472	-1.902

Table 7-7 – Expectation of the Estimated Time of the Disturbance (s)
for a 0.2 p.u. increase in load for ±0.01 p.u. Power Error and ±0.001 p.u./s df/dt Error

tr\A	10	20	30	40
0.1	5.04	5.06	5.06	5.06
0.25	5.03	5.04	5.04	5.04
0.75	5.03	5.03	5.03	5.03
1.25	5.02	5.02	5.02	5.02
1.5	5.02	5.02	5.02	5.01

A second scenario was simulated to investigate the behaviour of the algorithm for smaller disturbances and an increased noise level. This involved a 0.05 p.u. load increase after 5 seconds with additive white noise of between plus and minus 0.05 p.u. for the power measurements and plus and minus 0.005 p.u./s for the derivative of frequency. Table 7-8 and Table 7-9 present the expectation of true and false detections, whilst Table 7-10 presents the expectation of the percentage error in the inertia estimate. Table 7-11 presents the expected estimate of the time of the disturbance. The table entries marked with a dash denote those settings which returned no estimates. The number of false detections has fallen due to the combination of the increased noise level and the smaller disturbance size limiting the damping convergence.

The accuracy of the estimates in Table 7-10 and Table 7-11 is generally good but the combination of a smaller disturbance in the presence of an increased noise level has reduced it somewhat when compared to Table 7-6 and Table 7-7. The exception to this is the shortest window width of 10 samples; whilst it was capable of accurately detecting the disturbance it could not render accurate estimates of H due to its reduced ability to accommodate the level of noise in the measurements. This is possible as whilst the smallest window converges to an erroneous value of H it does still converge. As in Table 7-6 and Table 7-7 the tendency is toward an overestimate and increasing tr limits this tendency but increasing A aggravates it.

Table 7-8 – Expectation of True Detections
for a 0.05 p.u. increase in Load for ±0.05 p.u. Power Error and ±0.005 p.u./s df/dt Error

tr\A	10	20	30	40
0.1	0	0	0	0
0.25	0	0	0	0
0.75	0.014	0.086	0.360	0.690
1.25	0.149	0.588	0.928	0.994
1.5	0.259	0.802	0.980	0.998

Table 7-9 – Expectation of False Detections
for a 0.05 p.u. increase in Load for ±0.05 p.u. Power Error and ±0.005 p.u./s df/dt Error

tr\A	10	20	30	40
0.1	0	0	0	0
0.25	0	0	0	0
0.75	0	0	0	0
1.25	0.002	0	0	0
1.5	0.012	0	0	0

Table 7-10– Expectation of Error in Inertia Estimate (%)
for a 0.05 p.u. increase in Load for ±0.05 p.u. Power Error and ±0.005 p.u./s df/dt Error

tr\A	10	20	30	40
0.1	-	-	-	-
0.25	-	-	-	-
0.75	25.168	-9.900	-6.123	-5.350
1.25	51.118	-2.123	-3.950	-3.159
1.5	53.509	-2.075	-3.558	-2.734

Table 7-11– Expectation of the Estimated Time of the Disturbance (s)
for a 0.05 p.u. increase in Load for ±0.05 p.u. Power Error and ±0.005 p.u./s df/dt Error

tr\A	10	20	30	40
0.1	-	-	-	-
0.25	-	-	-	-
0.75	5.066	5.089	5.121	5.142
1.25	5.042	5.076	5.096	5.107
1.5	5.042	5.073	5.084	5.092

7.3.4 Considerations when Selecting the Window Size (*A*) and the Dynamic Threshold Ratio (*tr*)

The results presented in Subsection 7.3.3 demonstrate several factors that must be considered when selecting *A* and *tr*. The most noticeable of these is that *tr* must be increased as the noise present in the measurements increases to ensure that the disturbance is still detected. An increase in *tr* also allows smaller disturbances to be detected by the algorithm, as these tend to be less convergent than larger disturbances.

Increasing *tr* causes fewer of the earlier estimates in the convergent period to be discarded as non-convergent so the time of disturbance estimate is more accurate. Including these earlier estimates also limits the tendency of the algorithm to overestimate *H*. However, these advantages of increasing *tr* will come at the price of an increased risk of false detections, so a balance must be struck.

The main advantage of increasing *A* is that it serves to reduce the risk of false detections and increase the likelihood of true detections, independent of the *tr* value selected. However, increasing *A* increases the degree to which *H* and the time of the disturbance will be overestimated by and introduces additional delay into the algorithm. When applying this algorithm it would be prudent to define some form of relationship between *A* and *tr* to govern their relative setting. An example of this would be increasing *A* as *tr* is increased, this would ensure that unfavourable settings, such as low *A* and high *tr*, would not be allowed.

7.4 Motor-Generator Set Test

This section describes the results of applying the algorithm to measurements received from the laboratory testing of a Motor-Generator (MG) set using load step changes. A brief description of the laboratory set up is given below and it is depicted in Figure 7-12, more details can be found in [3]. A step down transformer was used to transform the generator terminal voltage to the level required by the measurement devices. This voltage signal was recorded using a 12-bit Data Acquisition Digital System (DADS), with a sampling frequency of 1600 Hz. The frequency of this voltage was measured

using a HP 3457A Multimeter (HP) after it was passed through a low pass filter (LP) with cut off frequency of 125 Hz. The HP and DADS are both connected to the PC over an IEEE-488-Bus.

It should be noted that the rating of the MG set used during this test was 1 kW and that this is incredibly small compared to the size of a power system. Despite this, any results produced using this MG set are still useful in demonstrating the application of the novel algorithm proposed here. This is because the laws that govern the initial response of a body rotating around a fixed axis to an imbalance of torque are the same for this small MG set as they are for the generators in a power system.

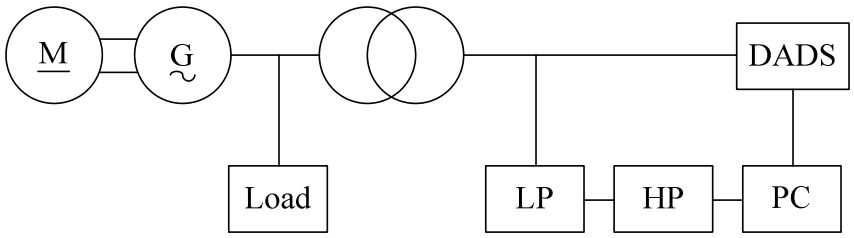

Figure 7-12 – Laboratory set up for the Motor Generator Set testing of the novel algorithm proposed in this thesis for simultaneous estimation of the time of disturbance and the inertia

Two step increases of load were performed separately, the first of these was an increase of 75 W at t=3.42 seconds and the second was an increase of 300 W at t=1.69 seconds. The active power load on the MG set and the derivative of frequency of its output are shown in Figure 7-13. The measurements were recorded at reporting frequency of 25 Hz.

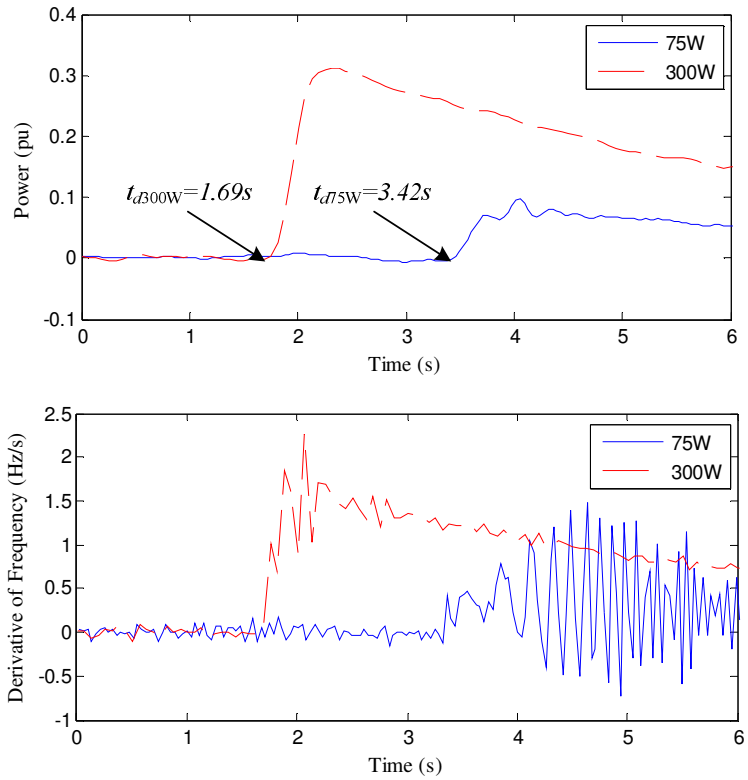

Figure 7-13 – Data recorded for two separate load changes that were applied to a motor-generator set and used to test the algorithm

The proposed algorithm was applied to these measurements using A=20 and tr=0.75. The data was pre-filtered with a width of 6 samples. The results of the algorithm are presented in Figure 7-14 and Figure 7-15, where the bold red line marks the values used to estimate H. The time of disturbance results are accurate and the inertia estimates are consistent. Furthermore, there are no false detections.

The selection of the A and tr values used here was based on the discussion given in Section 7.3.4. Comparison of these A and tr with those found to be most successful in Section 7.3.3 demonstrates that the selection of the parameter values is system specific. The parameter values selected here allowed the successful application of the algorithm to two different disturbances of very different sizes. This indicates that it should be possible to select values of A and tr that will allow the algorithm to perform acceptably for a specific system based on an understanding of the system characteristics and the noise that is usually present in the measurements

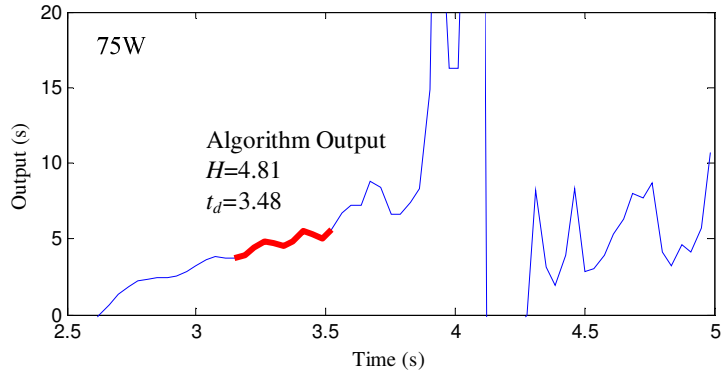

Figure 7-14 – Algorithm output for a 75W step increase in the MG set load at t=3.42 seconds using *A*=20 and *tr*=0.75

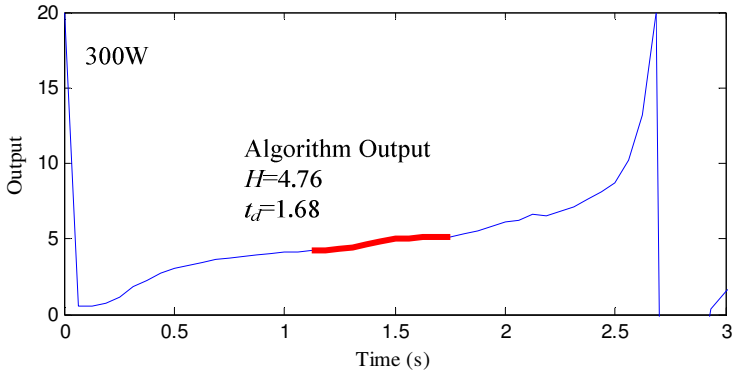

Figure 7-15 – Algorithm output for a 300W step increase in the MG set load at t=1.69 seconds using *A*=20 and *tr*=0.75

7.5 National Grid Example

This section gives the results of applying the algorithm to data recorded by the National Grid Company (NGC). On the 27th May 2008 the NGC system experienced the sequential loss of two generating units; Longannet (345 MW) and Sizewell B (1237 MW) [4]. The frequency and derivative of frequency during these disturbances are presented in Figure 7-16 and were sampled at a frequency of 25 Hz. The algorithm was applied using *A*=45 and *tr*=1.75 and the results achieved are presented in Figure 7-17 and Figure 7-18. The time of disturbance results are accurate and the inertia estimates are consistent, once again there are no false detections.

As in Section 7.4 the parameter values for *A* and *tr* used in this test were based on the discussion presented in Section 7.3.4. Comparison of these values with those successfully used in Section 7.4 and Section 7.3.3 further indicates that the algorithm settings must be customised for a specific system.

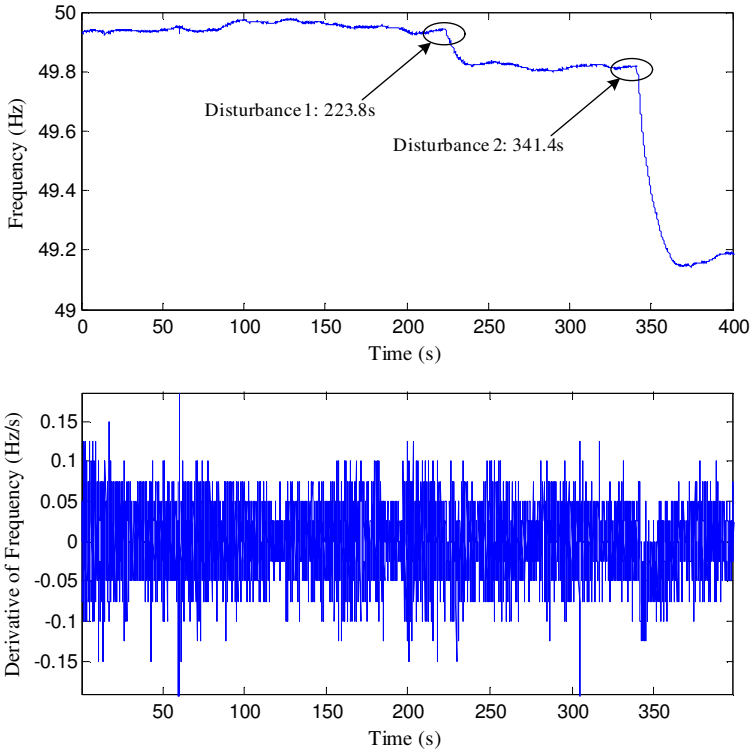

Figure 7-16 – Frequency and derivative of frequency during two sequential disturbances in the National Grid network

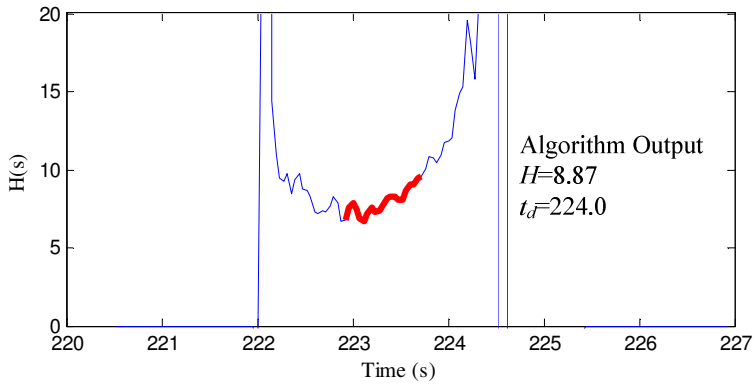

Figure 7-17 – Algorithm output for the first National Grid example, loss of Longannet (345 MW) after 223.8 seconds. The algorithm was applied using *A*=45 and *tr*=1.75.

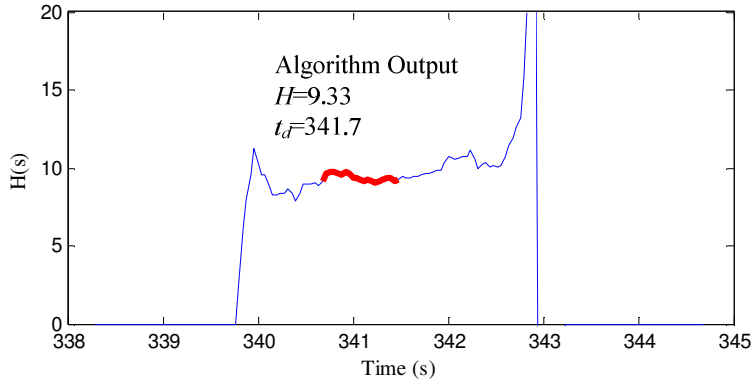

Figure 7-18– Algorithm output for the second National Grid example, loss of Sizewell B (1237 MW) after 341.4s. The algorithm was applied using *A*=45 and *tr*=1.75

7.6 Chapter Summary

This section presented a novel algorithm for simultaneously estimating the time of a disturbance and the inertia. These estimates represent the time of disturbance and inertia at the measurement location and not in the system as a whole. This is an important distinction to make in a larger system because of the possible geographical variation in the inertial response and the delay involved in disturbed frequency conditions propagating through a large system.

The algorithm uses a set of sliding windows to continuously calculate candidate inertia estimates, these candidate estimates will converge to the true inertia during a disturbance. The residues between these candidate estimates is used to detect this convergence and consequently detect the disturbance and estimate both the time at which it occurred and the inertia in the system. The results presented in this section demonstrate that the proposed algorithm can accurately estimate the time of disturbance and inertia for both small and large disturbances as well as for both simulated data and data recorded from the field. Before applying this method online it would be useful to explore the possibility of developing a recursive version of the algorithm. This would be of particular benefit as the algorithm in its current form requires a significant amount of data buffering.

The algorithm parameters (A and tr) must be selected based on experience with the system, the expected noise level and the size of disturbance that the algorithm is expected to detect. This method could be improved by introducing a control loop that automatically adjusts the algorithm parameters (most likely tr) as the noise conditions in the system change. It could also be possible to use the duration of the convergence (the time for which $flag_D$ is high) as a measure of the certainty that a disturbance has occurred. Further research could also include testing the algorithm by applying it to long periods of data that does not contain a disturbance to properly verify the likelihood of false detections. This is because any uncertainty regarding the accuracy of the detections made will severely compromise the usefulness of the application due to the potential consequences of applying unnecessary control actions to the power system.

7.7 References

[1] Anderson, P.M.; Mirheydar, M.; , "A low-order system frequency response model," Power Systems, IEEE Transactions on , vol.5, no.3, pp.720-729, Aug 1990

[2] Wall, P.; González-Longatt, F.; Terzija, V.; , "Estimation of Generator Inertia available during a disturbance", in Power and Energy Society General Meeting, 2012 IEEE.

[3] Terzija, V.V.; , "Improved recursive Newton-type algorithm for frequency and spectra estimation in power systems," *Instrumentation and Measurement, IEEE Transactions on* , vol.52, no.5, pp. 1654- 1659, Oct. 2003

[4] National Grid, "Report of the National Grid Investigation into the Frequency Deviation and Automatic Demand Disconnection that occurred on the 27th May 2008". Available http://nationalgrid.com/NR/rdonlyres/D680C70A-F73D-4484-BA54-95656534B52D/26917/PublicReportIssue1.pdf [Accessed January 24th 2013]

8 Post-Disturbance Frequency Prediction Using Approximate Models of the System Frequency Response

This chapter describes research into performing frequency prediction based on an approximate model of the frequency response the parameters of which are estimated online. Section 8.1 describes the motivation for this element of the research and introduces some of the challenges faced by it. The basic concept of performing online model based prediction is described in Section 8.2 and a brief review of existing frequency response modelling is given in Section 8.3. Section 8.4 describes the efforts made during this research to estimate the load damping of a frequency response. Section 8.5 describes a method for performing frequency prediction that uses a two parameter approximate model to represent the inertial response and a simple ramp governor. The method tested using simulations and a novel adaptive form of prediction based load shedding is proposed. Finally, Section 8.6 provides a summary of the success and contribution of this research into approximate model based frequency prediction and makes some proposals for how it could be continued.

8.1 Chapter Introduction

Frequency prediction based on approximate models fundamentally consists of defining an approximate model of the system frequency response and then solving this model for specific events, e.g. the nadir of the frequency response, or moments in time. One advantage of a model based prediction method is that it naturally lends itself to creating predictions that consist of exact values of the time and system frequency for critical points in the response, for example the frequency nadir. However, a key difference between the prediction concept considered here and that considered in the existing work [1] [2] [3] is that the prediction methods proposed here are expected to function in an uncertain system state. Therefore, the parameter values required by any model must be estimated online based on the wide area measurements available in the period between the disturbance occurring and the prediction being performed. The inertia and time of disturbance are assumed to be available in the research presented

here based on the novel methods for their estimation proposed in Chapters 6 and 7. The requirement for online parameter estimation poses a challenge as only data that can be collected and processed by the prediction algorithm sufficiently in advance of the event to be predicted can be used as part of the estimation process. This limitation on the data available will render the estimation of model parameter values a significant challenge.

The focus of this research was predicting the nadir of the frequency deviation. This is because this will likely prove the most useful information when predictions are being used to support frequency control; as the magnitude of the deviation from the nominal frequency will heavily determine the threat the deviation poses to the system. A model based method for predicting the minimum value of the system frequency response is proposed in [3] and this will form the basis for this research. Unfortunately, this method requires detailed knowledge of the system state that exists during the disturbance and as such extensive modifications will be necessary before it can satisfy the requirements imposed during this research.

8.2 Model Based Prediction Concept

The core concept behind approximate model based prediction is using wide area measurements to create an approximate model of the frequency response of a small system or an area of a large system. The model will be defined by a set of parameters the value of which must be estimated during the initial frequency response to the disturbance and obviously prior to the occurrence of the event that is to be predicted. An example of the period of data that will likely be available for performing parameter estimation is marked in Figure 8-1. Once populated with suitable parameter values the model can then be used to calculate the approximate value of the frequency response for specific times or conditions, e.g. the frequency nadir will correspond to a zero derivative condition. The execution of a generic model based prediction algorithm is depicted in Figure 8-2.

The nature of the approximate model will likely need to be defined offline as this will allow the accuracy and reliability of its approximations to be thoroughly tested.

Furthermore, it is unlikely that sufficient time will be available after the disturbance has occurred to adapt the structure of the model online in a robust fashion. The two key elements that must be defined for any approximate model based frequency prediction method are the frequency model to be used and the parameter estimation methods that will populate it with the necessary parameter values. However, these two elements are not independent as the model must be selected based on the parameter values that can be estimated.

The methods tested in this thesis are applied to a single frequency trace. When measurements from N locations are available they can be combined into a single trace that represents the system by using the concept of the frequency of the inertia centre, f_c [4].

$$f_c(t) = \frac{\sum_{i=1}^{N} f_i(t) H_i}{\sum_{j=1}^{N} H_j} \quad \text{[p.u.]} \tag{8-1}$$

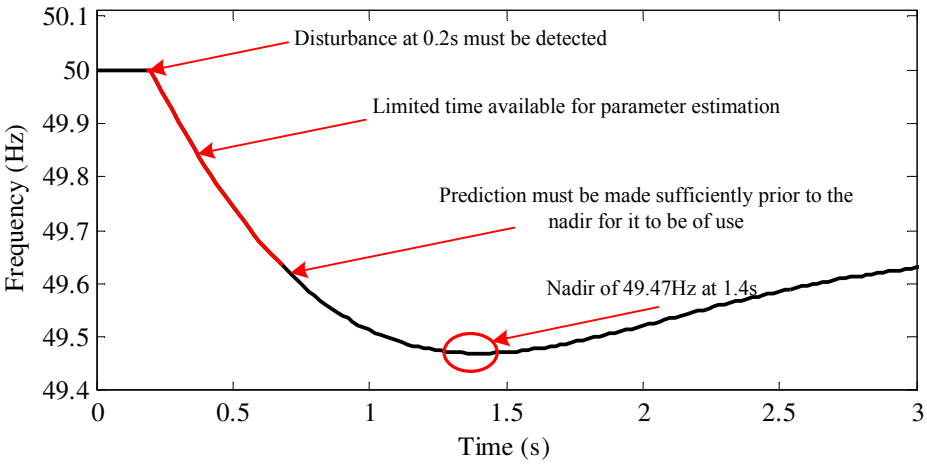

Figure 8-1 – An example of a post-disturbance frequency trace that indicates the time available for each stage of a generic model based post-disturbance frequency prediction algorithm.

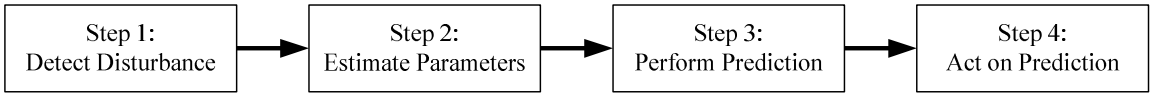

Figure 8-2 – The four stages of a generic post-disturbance frequency prediction algorithm based on an approximate model.

8.3 Modelling of the System Frequency Response

Models of frequency response are usually tailored for a specific generation technology such as a steam turbine [5][6], combined cycle unit [7], hydro power [8] or wind generation [9] and they are included as part of complete models of the technology and not just its frequency response. Therefore, the complexity of these models meant that it was inconceivable to estimate the parameter values of any of these models or a composite model based on them using only the limited data available to the prediction methods that are considered in this research.

This complexity meant that the simplified frequency response model, proposed in [4], was considered as the basis for any frequency prediction based on approximate models. This model represents the system frequency as a single equivalent frequency and assumes that the system is dominated by reheat steam turbines. The model for the response to disturbance, P_d, which is modelled as step change in the active power demand is depicted in Figure 8-3 and can be described using the following equations.

$$\Delta\omega(t) = \frac{RP_{step}}{DR + K_m}\left[1 + \alpha e^{-\varsigma\omega_n t}\sin(\omega_r t + \phi)\right] \quad [\text{p.u.}] \tag{8-2}$$

where

$$P_d(s) = \frac{P_{step}}{s} \tag{8-3}$$

$$\omega_n^2 = \frac{DR}{2HRT_R} \tag{8-4}$$

$$\varsigma = \omega_n\left(\frac{2HR + T_R\left(DR + K_m F_H\right)}{2\left(DR + K_m\right)}\right) \tag{8-5}$$

$$\alpha = \sqrt{\frac{1 - 2T_R\varsigma\omega_n + T_R^2\omega_n^2}{1 - \varsigma^2}} \tag{8-6}$$

$$\omega_r = \omega_n\sqrt{1 - \varsigma^2} \tag{8-7}$$

$$\phi = \phi_1 - \phi_2 = \tan^{-1}\left(\frac{\omega_r T_R}{1 - \varsigma\omega_n T_R}\right) - \tan^{-1}\left(\frac{\sqrt{1 - \varsigma^2}}{-\varsigma}\right) \tag{8-8}$$

where D is the load damping factor, F_H is the fraction of power generated by the high pressure turbine, H is the inertia constant, K_m is the mechanical gain, R is the governor regulation (the inverse of which is the droop) and T_R is the reheat time constant.

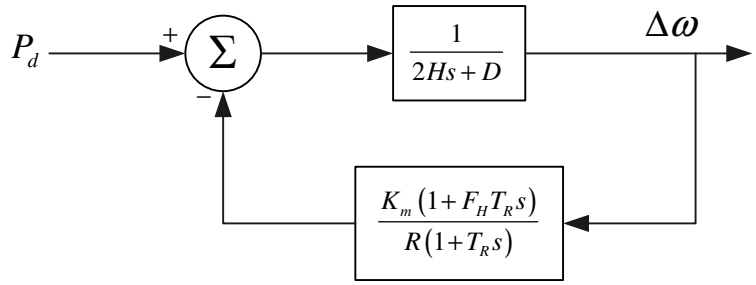

Figure 8-3 – The Simplified Frequency response model for the system frequency response to a disturbance of magnitude P_d

8.3.1 Parameter Estimation for SFR Model using Improved Particle Swarm Optimisation (IPSO)

The frequency trace in Figure 8-4 depicts the response of the SFR model to a step increase in active power demand of 0.2 p.u. at zero seconds for the parameter values given in Table 8-1. This frequency trace was used to assess the possibility of estimating the SFR model parameter values for the varying periods of data marked in the Figure 8-4.

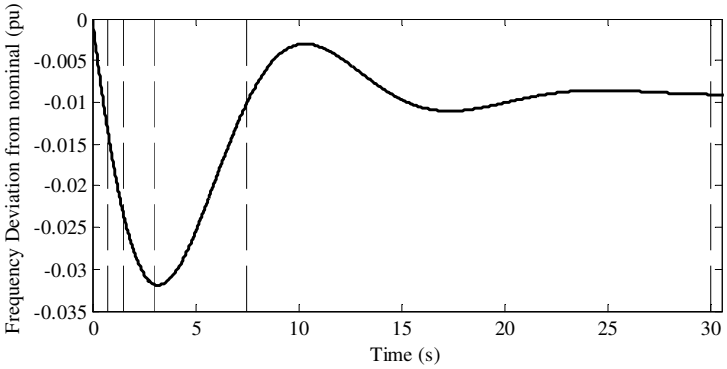

Figure 8-4 – Frequency deviation from nominal for step increase in load of 0.2 p.u. simulated using the SFR model, the dashed lines indicate the periods of data for which parameter estimation was performed (30, 7.5, 3, 1.5 and 0.75 seconds)

The data in Table 8-1 shows the result of applying a standard improved particle swarm optimisation algorithm (IPSO), described in Appendix B as well as [11] and [12], to the problem of estimating the parameters of the SFR model. IPSO is an intelligent algorithm that solves a curve fitting problem by optimising a least squares objective. IPSO was used for this estimation as it is both a powerful and flexible tool for solving optimal curve fitting based estimation problems. The IPSO algorithm fitted the model to the frequency response one hundred times for a range of time periods. The results in this table show the severe reduction in accuracy, in terms of the mean (*mu*) and

standard deviation (σ), as the time period, t, over which the curve fitting is performed is reduced.

Table 8-1– Error in IPSO Curve Fitting to SFR

	t(s)	30		7.5		3		1.5		0.75	
	True	*mu*	σ	*mu*	σ	*mu*	σ	*mu*	σ	*mu*	σ
D	1.5	1.46	0.43	1.58	0.44	1.82	0.53	2.13	1.76	2.33	1.60
F_H	0.05	0.05	0.02	0.05	0.02	0.06	0.02	0.08	0.07	0.10	0.10
H	5.00	4.92	0.17	4.80	0.19	4.77	0.09	4.68	0.08	4.53	0.10
K_m	0.95	1.13	0.42	1.30	0.53	1.19	0.37	1.35	1.37	1.59	2.68
R	0.05	0.06	0.02	0.06	0.02	0.06	0.02	0.08	0.06	0.08	0.12
T_R	9.00	9.16	0.45	11.4	3.58	11.8	3.3	17.0	11.4	17.6	17.0

It is also necessary to consider that the time available to any prediction tool developed cannot be devoted entirely to parameter estimation; as time will be needed to communicate the prediction and implement any control actions.

The results in Table 8-1 show that it is unlikely to be possible to estimate the value of all of the model parameters prior to the occurrence of the frequency nadir. Therefore, the initial focus of this attempt at frequency prediction will be the development of methods for estimating the necessary model parameters using a limited period of measured frequency data. The SFR model still represented a useful tool for this research as its simplicity allows it to be used to quickly investigate the properties of these estimation methods. Furthermore, this IPSO approach could be used to form a representative SFR model of a more complex system using offline analysis of data records that could be used for the study of that system.

8.3.2 Sensitivity Analysis of the SFR model

The importance of each parameter in determining the frequency response of the SFR model varies as a function of time and can be analysed using trajectory sensitivity analysis [13]. Trajectory sensitivity is defined as the evolution of the model's states in time with respect to the initial conditions and model parameters. Therefore, unlike steady state analysis, trajectory sensitivity analysis allows the variation in the sensitivity of the frequency response to each parameter during the transient response to be calculated.

The results in the previous section demonstrated that a full SFR model could not be fitted accurately to the data available to a prediction algorithm. Therefore, trajectory sensitivity analysis was used to understand the importance of each parameter and determine the possibility of estimating any of the individual SFR parameters during the time available to the prediction methods proposed in this thesis. The sensitivity analysis presented in Figure 8-5 was performed for the SFR model using the method proposed in [13].

The sensitivities in Figure 8-5 indicate that for approximately the first 0.3 seconds H is the most significant parameter in determining the behaviour of the SFR model. Whilst this was of benefit when estimating H in the previous chapters it means that in this context it will prove difficult to estimate other parameters during this period.

The sensitivity of the model to the other parameters peaks prior to the occurrence of the nadir of the frequency response. This suggested that if the influence of an individual parameter could be separated from the influence of the other unknown parameters then it may be possible to estimate the parameter value. However, a threat to this is that the sensitivity of the model to F_H and R is at least an order of magnitude greater than it is to the other parameters during this period so they may mask the influence of other parameters. Furthermore, a suitable approximate model must be identified that allows the separation of the influenced of each parameter.

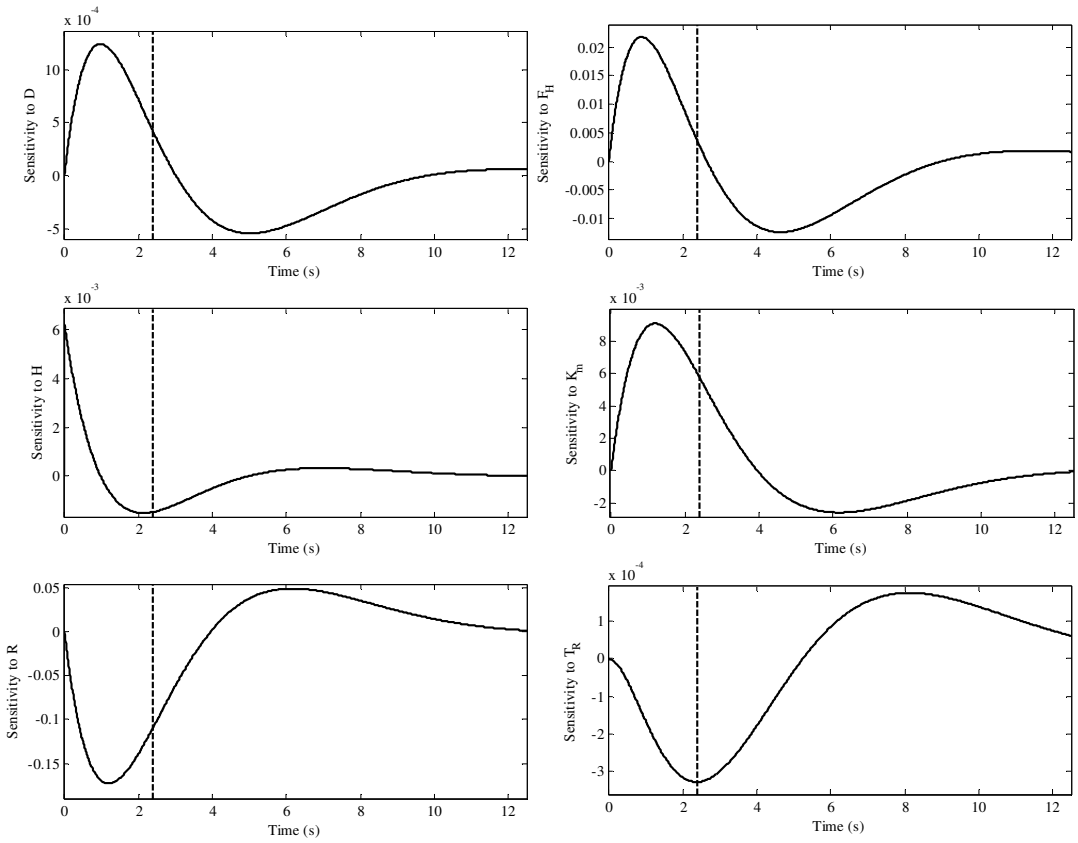

Figure 8-5 – Sensitivity Analysis for the SFR model

8.3.3 Estimating *D* using Improved Particle Swarm Optimisation

The load damping (D) determines how the electrical load varies with frequency and acts to damp any deviation. The approach for modelling this load damping that is proposed in [4] is that the load can be separated into two elements; one of which is independent of frequency and the other which varies proportionally with frequency. In this context the load damping is the constant of proportionality that governs the change in load (ΔP_L) that is seen for a given change in frequency (Δf).

Creating a method that allows the estimation of D would allow the natural response of the system, defined by H and D, to be separated from the governor response. For a real system or complex system model the value of D is unknown. Therefore, for this research into the estimation of D the SFR model is used as it has a known value of D that can be used to determine the accuracy of the estimation procedure.

The improved particle swarm optimization (IPSO) algorithm, described in Appendix B as well as [11] and [12], was used for the parameter estimation performed here. IPSO is not normally considered as a practical solution for applications that require online estimation due to its computationally intensive nature. However, the flexibility of intelligent methods like IPSO allows a thorough investigation of the possibility of estimating *D* and if successful the estimation process could be replicated with a method that is suitable for online application, e.g. a Newton type method.

The estimation of *D* was performed by fitting an approximate model of the natural frequency response of a system to a disturbance, specifically the mass load response that is depicted in Figure 8-6 and described in [13]. This mass load response model is introduced to study if it is possible to estimate D based on the initial 0.5 seconds of frequency data that is record after a disturbance to the active power balance that is represented as a step change of magnitude *Pd*.

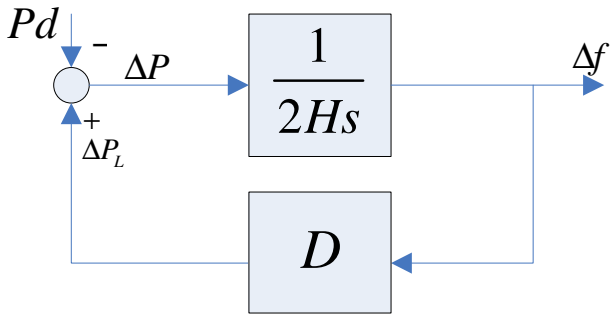

Figure 8-6 – Block diagram of the mass load response. This model is a reasonable approximation of the natural frequency response of a system

The mass load response is only a function of the inertia constant (*H*) and the load damping (*D*) of a system and can be described using the following equation.

$$\Delta f(t) = \frac{Pd}{D}\left(1 - \exp(-t\frac{D}{2H})\right) \quad [p.u.] \tag{8-9}$$

It must be recognised that the mass load response deals with per unit values of power and speed and as such a deviation in per unit speed represents an equivalent per unit deviation in frequency. This direct equivalency exists here due to the normalisation of the equations leading to the cancellation of the pole pair and unit conversion (i.e. 2π)

terms that govern the proportional relationship between speed and frequency, as detailed in Appendix A, and it should not be assumed to exist in general.

The results presented in this section are for the fitting of the mass load response to simulated data from the SFR model using the parameters given in Table 8-2 and a reporting rate of 50 Hz for the frequency measurements. The inertia constant (*H*) was estimated here, in addition to *D*, to provide a comparison for the verification of the accuracy of the estimates made by the novel online method presented in Chapters 6 and 7.

Table 8-2–SFR Parameter Values for *D* Estimation

D	F_H	$H(s)$	K_m	R	$T_R(s)$	$Pd\ (pu)$
1.50	0.05	5.00	0.95	0.05	9.00	-0.20

The mean and standard deviation of the results of executing the IPSO algorithm one hundred times are presented in Table 8-3 and Table 8-4. These results were achieved using the IPSO parameters given in Table 8-5 and indicate that the proposed *D* estimation process is not successful.

The accuracy of the *H* estimation here is slightly better than that achieved by the novel method proposed in Chapters 6 and 7. However, the error given in Table 8-4 is the mean error for one hundred executions for signals without noise and IPSO is a far more complex algorithm that is normally considered to be too computationally intensive for online implementation. Therefore, this is a positive result that further verifies the accuracy of the novel method for the estimation of inertia that is proposed in Chapters 6 and 7.

Table 8-3– IPSO Estimation Results for the load damping factor (D)

True Value (pu)	Mean Estimate (pu)	Standard Deviation (pu)	Mean Estimate Error (%)
1.5	2.71	1.64	-81%

Table 8-4 – IPSO Estimation Results for the inertia constant (*H*)

True Value (pu)	Mean Estimate (pu)	Standard Deviation (pu)	Mean Estimate Error (%)
5	5.10	0.41	-2%

Table 8-5 – IPSO Algorithm Settings

Estimation Period (s)	Number of Particles	Number of Generations	c_1	c_2	ω
0.5	50	200	2	2	0.7

This poor performance of the proposed D estimation method is likely because the mass load response was selected as an approximation due to its simplicity and not its accuracy. Therefore, the quality of the mass load response as an approximation of the system response decays rapidly. This decay occurs because the governor begins to influence the frequency response. The primary result of this decay is that when fitting the mass load response to a measured frequency trace, of sufficient length to feasibly estimate the model parameter values, the true values of H and D, H_T and D_T, do not produce the best fit. Instead, a second pair of values H_G and D_G provides a better fit to the system response. This better fit can be seen in Figure 8-7 where it is marked as a dot dash line. This renders the true values of H and D a local minimum of the problem, which will prove problematic during the estimation process as it is important that the parameter estimation method developed for this application is capable of producing estimates that are approximately H_T and D_T, and not H_G and D_G.

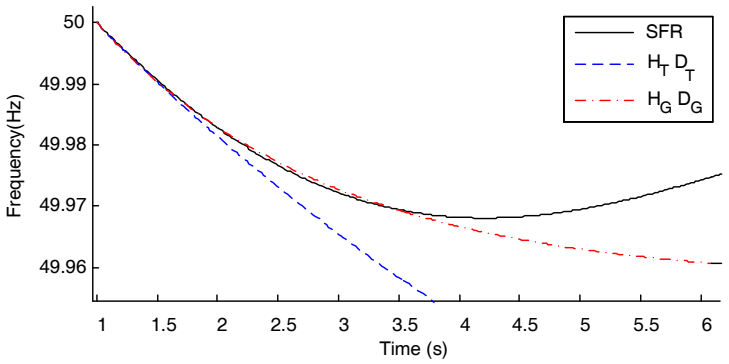

Figure 8-7 – The existence of a global minimum that is not the true model parameters, to the problem of fitting the mass load response to the measured response is an issue.

The evolution of the best particle position of the IPSO algorithm for each generation is shown in Figure 8-8. From this it is clear that the algorithm does pass through the local minima represented by the true value of D before it converges to the global minima.

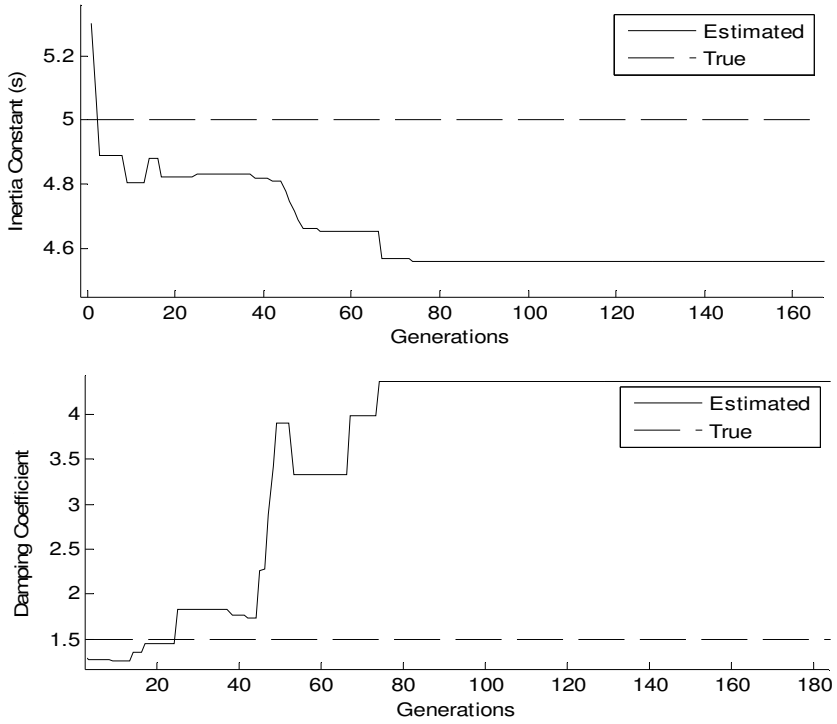

Figure 8-8 – The evolution of the *H* and *D* values held by the best global particle passes through a local minima that is close to the true values. However, it then moves toward a better solution to the problem that is further from the true values, due to the poor mass load approximation.

The possibility of extracting the local minima was considered and the following simple methodology was proposed. Instead of using the final best position of the IPSO algorithm the best position would be sampled several times during the execution and an estimate would be calculated based on these samples. This would allow the local minima to be determined provided that the algorithm passed through it. As this could not be guaranteed this approach requires multiple executions of the IPSO algorithm. Therefore, the algorithm would be execute *NI* times and the current best position should be sampled every five iterations between the generation S_B and the generation S_E. This approach was tested for the range of settings given in Table 8-6 in the hope of finding those that encourage convergence to a local minimum. For this purpose only the swarm sensitivity of the particles (c_2) was varied and the cognitive sensitivity (c_1) was fixed at 2.00 as the swarm sensitivity is a key parameter in determining the convergence of the IPSO algorithm to a local minimum.

Table 8-6– IPSO settings considered for *D* Estimation

	Minimum	Interval	Maximum
NI	1	5	31
Particles	12	6	42
c_2	0.50	0.25	2.00
S_B	24	1.00	0.10
S_E	5	5	65
ω	0.1	0.2	0.9

The five best IPSO settings for optimizing the estimation of *D* are presented in Table 8-7 and represent a significant improvement in the estimation accuracy. However, the unreliable nature of the algorithm meant that the best results all required the maximum number of IPSO executions. Unfortunately, the use of multiple iterations exploits the properties of intelligent methods and as such this approach could not be followed when using a more traditional estimation algorithm that could be applied online.

Table 8-7– Best IPSO settings for the Estimation of *D*

Rank	Particles	c_2	ω	S_B	S_E	NI	H Error (%)	D Error (%)
1	24	1.00	0.10	5	5	31	-4.25	-25.66
3	24	1.00	0.10	5	20	31	-4.29	-26.35
4	24	1.00	0.10	5	35	31	-4.30	-26.48
5	24	1.00	0.10	5	50	31	-4.30	-26.53

8.4 Governor Model Parameter Estimation

The governor action of generators acts to limit the initial frequency deviation and as such its accurate representation is a necessity for any post-disturbance frequency prediction method. However, based on the results of the previous section and the failure to accurately estimate the value of the load damping it would appear that, given the limited period of system measurements, it will not prove possible to accurately estimate the value of any specific parameter, other than inertia, as part of the prediction process. Furthermore, it is likely that the overestimation of *D* that is consistently seen in the previous section was due to the governor response acting to reduce the frequency deviation, this action will have been attributed to the load damping due to the limitations of the mass-load response model. This means that any attempts to estimate the parameters of an approximate governor model will suffer from similar issues unless the model represents both the load damping and the governor action.

8.4.1 An Existing Approximate Governor Prediction Method

An approximate governor model is proposed in [3] that represents the governor response of the system as a fixed ramp. In the equations presented here the system response is assumed to be represented by a single equivalent generator, the frequency response of which could be calculated based on more than one measurement location using the calculation of the frequency of the inertia centre (8-1). The gradient of this ramp is determined by the size of the disturbance, the inertia and a single parameter *C*. The governor response is determined by the deviation of the frequency from the nominal value and the inertia constant *H*.

$$\Delta\frac{df(t)}{dt}=\frac{\Delta P}{2H}-\frac{\Delta f(t)}{2H}C \quad \left[\frac{\text{p.u.}}{\text{s}}\right] \tag{8-10}$$

In [3] it was proposed that the deviation seen by the governor during the initial frequency decline could be approximated using the inertial response.

$$\Delta f(t)=\frac{\Delta P}{2H}t \quad [\text{p.u.}] \tag{8-11}$$

Therefore, this model allows the frequency response of the system after a disturbance to be represented using the inertial response to a disturbance of ΔP and a ramp governor based on the following equations:

$$\Delta\frac{df(t)}{dt}=\frac{\Delta P}{2H}-\frac{\Delta P}{4H^2}Ct \quad \left[\frac{\text{p.u.}}{\text{s}}\right] \tag{8-12}$$

$$\Delta f(t)=\frac{\Delta P}{2H}t-\frac{\Delta P}{8H^2}Ct^2 \quad [\text{p.u.}] \tag{8-13}$$

The value of *C* that allows (8-12) and (8-13) to accurately calculate the frequency response varies with time. Therefore, a value of *C* must be estimated that will allow the maximum frequency deviation to be predicted accurately. This value is referred to as C_{max} and a novel online method for its estimation is presented in Section 8.4.2.

Solving (8-12) to find the time at which the derivative is zero allows the time of the maximum frequency deviation, t_{max}, to be calculated in terms of C_{max}.

$$t_{max} = \frac{2H}{C_{max}} \quad [\text{s}] \tag{8-14}$$

Furthermore, substituting (8-14) into (8-13) allows the maximum frequency deviation to be calculated.

$$\Delta f_{max} = \frac{\Delta P}{2C_{max}} \quad [\text{p.u.}] \tag{8-15}$$

The frequency in Hz during this deviation, f_{dev}, can then be calculated based on the base frequency of the system, f_B, and the pre-disturbance frequency in Hz, f_d.

$$f_{dev} = f_d + f_B \Delta f_{\max} \quad [\text{Hz}] \tag{8-16}$$

This method assumes that the frequency is equal across the system and that there are no oscillations. The simplicity of this model is attractive as it reduces the burden on the prediction method in terms of parameter estimation. Chapters 6 and 7 propose a method for estimating the inertia so the only other parameter that must be estimated is C_{max}.

In [3] C_{max} was estimated based on the response of the simple model depicted in Figure 8-9. The parameter values of this model were themselves estimated during the offline testing of each generator to a step change in power.

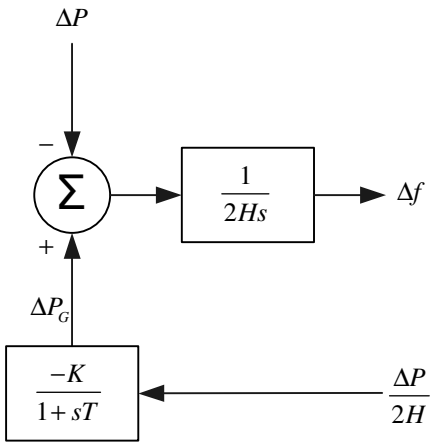

Figure 8-9 – Approximate Governor response used in [3] to estimate C_{max}

The response of this model is described by the following equation

$$\Delta P_G(t) = \frac{\Delta P}{2H} K \left(1 - \frac{T}{t} \left(1 - e^{-t/T} \right) \right) \quad \text{[p.u.]} \tag{8-17}$$

The parameters K and T can then be used to calculate C_{max} by assuming that the behaviour of the governor model at the time t_{max} can be represented using the constant C_{max}. Based on this assumption t_{max} and C_{max} can be calculated by solving the following two equations.

$$C_{max} = K \left(1 - \frac{T}{t_{max}} \left(1 - e^{-t_{max}/T} \right) \right) \quad \text{[p.u.]} \tag{8-18}$$

$$t_{max} = \frac{2H}{C_{max}} \quad \text{[s]} \tag{8-19}$$

The dependence of this method on offline testing meant that in its current form the method proposed in [3] does not satisfy the requirements defined in this thesis for an online post-disturbance frequency prediction method

Before discussing the creation of a novel method for estimating the approximate governor parameter, C_{max}, it should be noted that this governor model averts the risk of the load damping having a negative influence on the accuracy of any online estimate. This is because the action of the approximate governor and the load damping can be treated as being equivalent (8-20), where (8-20) is derived by modifying (8-10) to include the effect of load damping , if the assumption in (8-11) holds. Therefore, any online estimate of C implicitly includes the contribution of the load damping.

$$\Delta \frac{df(t)}{dt} = \frac{\Delta P}{2H} - \frac{\Delta f(t)}{2H} C - \frac{\Delta f(t)}{2H} D \quad \left[\frac{\text{p.u.}}{\text{s}} \right] \tag{8-20}$$

8.4.2 Novel Method for the online Estimation of the Approximate Governor Parameter (C_{max})

The first stage of creating a method for estimating C_{max} was developing an understanding how C varies during the frequency response of the system. This was done by calculating the value of C that would give the correct deviation of frequency for a specific time t and the corresponding measurement of $\Delta f(t)$ using the following expression, whihc can be found by rearranging (8-13) to make $C(t)$ the subject.

$$C(t) = 4H \frac{\Delta Pt - 2H\Delta f(t)}{\Delta Pt^2} \tag{8-21}$$

The variation in C depicted in Figure 8-10 suggested that the initial evolution of C could be modelled using an inverted parabola defined in terms C_{max}, t_{max} and a shaping parameter α.

$$\tilde{C}(t) = C_{max} - \alpha(t_{max} - t)^2 \tag{8-22}$$

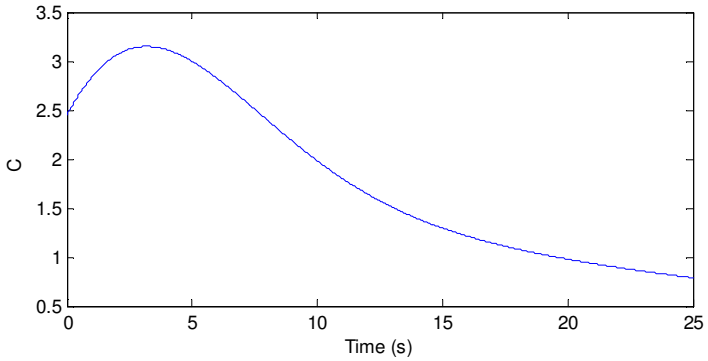

Figure 8-10 – The variation in the C value calculated using (8-21)

The values of the three variables in (8-22) could then be estimated by fitting this expression to the $C(t)$ values that are calculated for the initial period of the frequency response. This fitting could be performed using numerous methods but a simple non-linear-least squares method was used here. For this purpose the parameter vector **x** is defined as

$$\mathbf{x} = \begin{bmatrix} C_{max} \\ t_{max} \\ \alpha \end{bmatrix} \tag{8-23}$$

Following a standard Newton type algorithm allows the optimum value of this parameter vector to be found by iteratively executing the following expression until satisfactory convergence or the maximum number of iterations is reached.

$$\mathbf{x_{i+1}} = \mathbf{x_i} + \left(\mathbf{J^T J}\right)^{-1} \mathbf{J^T} \left(\mathbf{C(t)} - \tilde{\mathbf{C}}(\mathbf{x_i}, \mathbf{t}) \right) \tag{8-24}$$

where **t** is the vector of sampling times for which calculated $C(t)$ values are available and the j^{th} row of the Jacobian (**J**) can be defined as.

$$\mathbf{J}(j) = \begin{bmatrix} 1 & -2\alpha_i \left(t_{max,i} - \mathbf{t}(j)\right) & -\left(t_{max,i} - \mathbf{t}(j)\right)^2 \end{bmatrix} \tag{8-25}$$

8.4.3 Comparison of Prediction using Offline and Online Estimation of the Approximate Governor Parameter (C_{max})

A logical way to provide an initial confirmation of the accuracy of this new online method for estimating C_{max} was to compare the result of its application with that of the existing method proposed in [3]. The frequency response depicted in Figure 8-11 was used as a basis for this comparison and was generated using the SFR model with the parameters given in Table 8-2 and a load increase of 0.2 p.u.. The true value of C_{max} and t_{max} were estimated using the online method and 0.2 seconds of this frequency data. The results of this are shown in Table 8-8 and the fit achieved for (8-22) is shown in Figure 8-11.

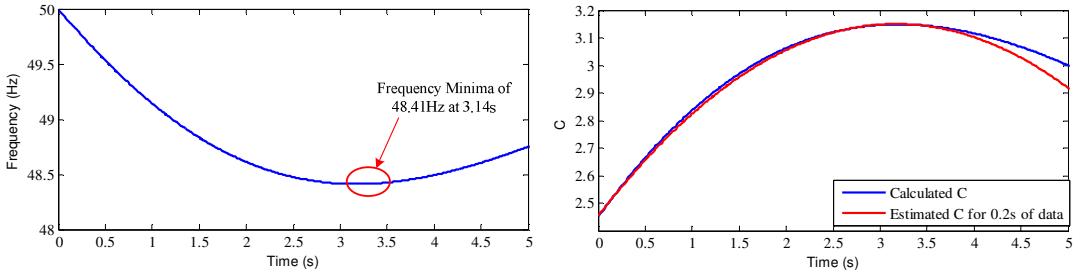

Figure 8-11 – The variation in C(t) for the given frequency trace and the fitting of (8-22) to 0.2 seconds of data

Following the method described in [3] K and T were estimated by fitting the model in Figure 8-9 to the mechanical power output of the SFR model to a step change in load. This estimation was performed using a Newton type algorithm and the estimated K and T values are given in Table 8-8.

The time and magnitude of the maximum frequency deviation was then predicted based on the C_{max} estimation for each method and the results of which are presented in Table 8-8.

Table 8-8 – The Predicted Frequency nadir using the offline and online methods

C_{max} Estimation Method	K (pu)	T (s)	C_{max}	t_{max}(s)	f_{max}(Hz)	t_{error}(s)	f_{error}(Hz)
offline	22.75	9.95	3.23	3.10	48.45	-0.33	0.04
online	-	-	3.14	3.19	48.43	0.05	0.02

The frequency prediction error is slightly smaller for the online method and the time error is significantly smaller and these errors are consistent with those seen in [3]. Therefore, these results indicate that the online estimation method is capable of accurately estimating C_{max}.

8.4.4 Testing the Approximate Model Based Prediction Method using SFR Simulations

The first stage in testing the online C_{max} estimation method proposed in the previous section was performed using the SFR model. This allowed the method to be tested for a wide range of possible system states and disturbance sizes The SFR model parameters used for this test are given in Table 8-9 and 0.2 seconds of frequency data was used for the curve fitting. Each possible combination of these parameter settings

were tested for the disturbances given in Table 8-10. No noise was added to the signals as at this stage it was desirable to test the intrinsic accuracy of the method and not its resilience against noise.

Table 8-9 – Set of SFR parameters used to test the online C_{max} estimation method

D	F_H	H	K_M	R	T_R
1.88	0.06	6.25	1.19	0.06	11.25
1.69	0.06	5.63	1.07	0.06	10.13
1.50	0.05	5.00	0.95	0.05	9.00
1.31	0.04	4.38	0.83	0.04	7.88
1.13	0.04	3.75	0.71	0.04	6.75

Table 8-10 – Set of disturbances used to test the online C_{max} estimation method

ΔP (p.u.)					
-0.20	-0.10	-0.05	0.05	0.10	0.20

The prediction error for each of these cases in terms of both the maximum deviation and time of deviation were calculated. These errors were calculated in terms of the percentage of the true value and histograms of these results for a load increase of 0.2 p.u. are depicted in Figure 8-12. These results show that the online C_{max} estimation method allows consistently accurate predictions of the time and magnitude of the frequency nadir.

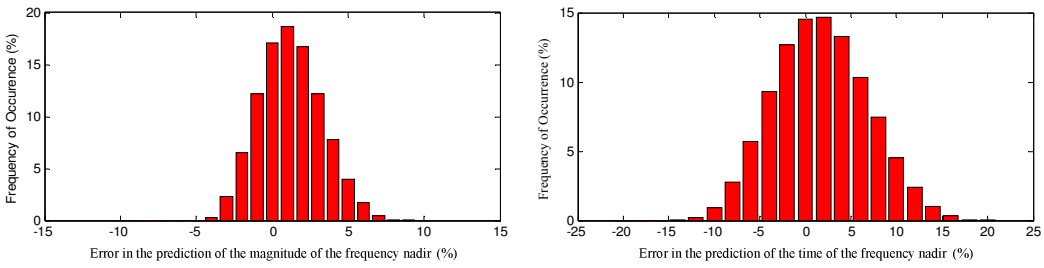

Figure 8-12 – Histograms of prediction errors based on online C_{max} estimation method for a load increase of 0.2 p.u.

However, it also clear that the prediction of the time of the frequency nadir is far less consistent. This is supported by the mean and standard deviation of the prediction results for the other disturbances that are presented in Table 8-11. It should be noted that the symmetry of these results is a function of the symmetry of the SFR model and as such is not indicative of any property of the online C_{max} estimation method beyond the fact that it can be used to predict both positive and negative frequency nadirs.

Table 8-11 – Table of mean and standard deviation of prediction errors for each disturbance size

	Time of the nadir error (%)		Magnitude of the nadir error (%)	
ΔP (p.u.)	mean	σ	mean	σ
0.2	1.67	5.09	1.21	2.05
0.1	1.54	5.10	1.22	2.06
0.05	1.74	5.08	1.21	2.07
-0.05	1.74	5.08	1.21	2.07
-0.1	1.54	5.10	1.22	2.06
-0.2	1.67	5.09	1.21	2.05

Figure 8-13 depicts the relationship between the prediction errors and the true values of C_{max}, the maximum frequency deviation and the time of the maximum frequency deviation for a load increase of 0.2 p.u..

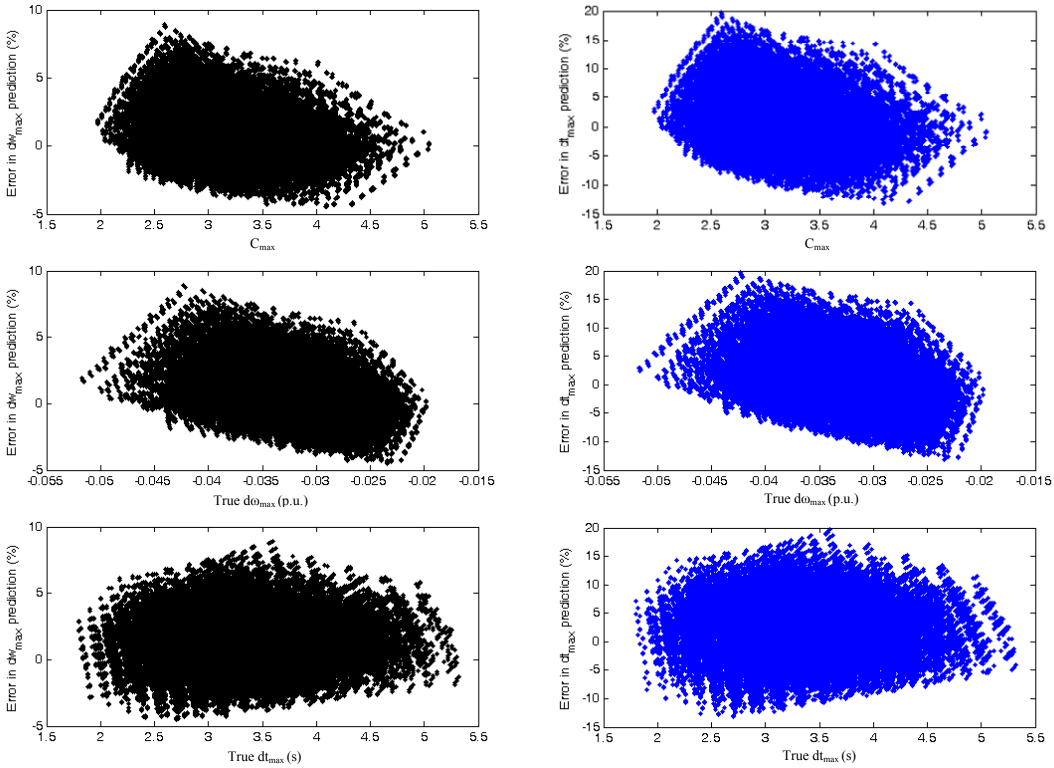

Figure 8-13 – Relationship between prediction errors and the true values of C_{max} and the time and magnitude of the frequency nadir

A comparison of these relationships reveals that the errors in the prediction of the maximum frequency deviation and its time of occurrence follow the same trends. These trends can be described as a shift from overestimation to underestimation as the true value of C_{max} decreases and the maximum frequency deviation increases. These trends exist because of the assumptions on which the prediction method is based. Specifically the assumption described in equations (8-11) and (8-13) that when combined assume that the frequency response of the system can be attributed purely to either the governor or the inertial response. For the combination of a large frequency

deviation and a small governor gain this assumption leads to an overestimation of C_{max}, which results in an under estimation of the time and magnitude of the maximum frequency deviation.

8.5 Adaptive Load Shedding Based on Frequency Prediction

This section describes a novel approach for using predictions of the frequency nadir to design adaptive prediction based emergency frequency control. To demonstrate this potential opportunity, consider the scenario depicted in Figure 8-14.

The SFR model was subjected to two increases in load power, to represent the sequential loss of two generating units. The first disturbance occurred after 1 second and constituted a step increase in load of 0.075 p.u. and the second disturbance occurred after 5 seconds and constituted a step increase in load of 0.225 p.u.. The frequency fell below 48.8 Hz at t=6.2 seconds and automatic deterministic load shedding of 0.05 p.u. was initiated at t=6.3 seconds. A delay of 0.1 seconds and this level of shedding was selected based on the first stage of the National Grid automate load reduction scheme [15].

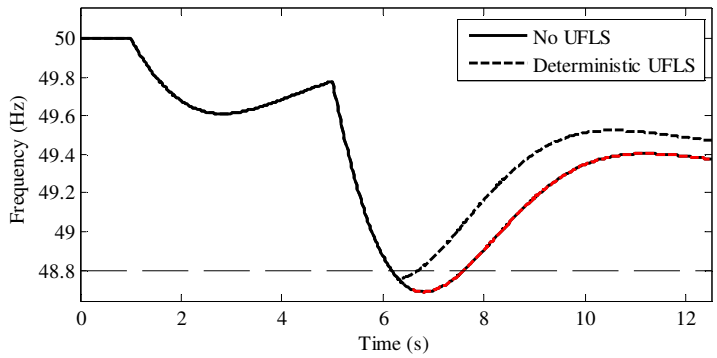

Figure 8-14 – Frequency response for two sequential load increases, the first is after 1 second and is a 0.075 p.u. step increase in load and the second is after 5 seconds and is a 0.225 p.u. step increase in load. The red marking on the No UFLS frequency trace denotes the fact that this response would be unlikely to occur due to the high risk of further contingencies. The load shedding threshold of 48.8 Hz is also marked as a dashed line.

Note that a section of the No UFLS frequency response in Figure 8-14 is marked in red to depict the fact that the recovery of the frequency that is depicted in Figure 8-14 is unlikely to occur due to the high risk of low operating frequency of the system causing secondary contingencies to occur.

The novel online method proposed in this chapter for the prediction of the frequency nadir was applied to this frequency trace using the first 0.2 seconds of frequency data recorded after each disturbance to estimate C_{max} and produced the predictions presented in Table 8-12.

Table 8-12 – Predictions of the frequency nadir for two sequential load increases

Disturbance		True Values		Predicted Values			Errors	
No.	ΔP (p.u.)	Minimum Frequency (Hz)	Time of Minimum (s)	C_{max}	Minimum Frequency (Hz)	Time of Minimum (s)	Minimum Frequency (Hz)	Time of Minimum (s)
1	-0.075	49.61	2.86	5.15	49.64	2.53	0.03	0.33
2	-0.225	48.69	6.78	5.06	48.67	6.56	0.02	0.22

These online predictions could be used to support the frequency control by designing adaptive load shedding actions and the remainder of this section discusses three methods for doing so. For each of these methods the following delays are assumed for the implementation of the prediction algorithm. The round trip communication delays are assumed to be 0.2 seconds, the data processing delays are assumed to be 0.1 seconds and the time period of data required is 0.4 seconds. These delays give a total delay of 0.7 seconds. The 0.4 seconds of data that is included in this delay is longer than the 0.2 seconds used by the C_{max} estimation algorithm. This is to reflect the requirements of any other parameter estimation or disturbance detection algorithms that are necessary, e.g. the novel algorithm proposed in Chapters 6 and 7 for the simultaneous estimation of the time of disturbance and system inertia.

8.5.1 Fixed Predictive Under Frequency Load Shedding

The first strategy for using predictions to support emergency frequency control is to simply deploy the existing deterministic action immediately if the predicted frequency deviation violates the UFLS threshold. This is referred to here as fixed predictive UFLS and based on the algorithm delay of 0.7 seconds that is assumed here the 0.05 p.u. of load shedding could be implemented 0.5 seconds prior to the UFLS threshold being violated.

The result of implementing this fixed predictive UFLS is depicted in Figure 8-15 and from this the improvement in terms of limiting the frequency deviation is clear. This

example demonstrates that one of the key advantages of implementing frequency control based on predictions is that it limits the maximum deviation the system is exposed to and hence it limits the risk of secondary contingencies. In this example, implementing the UFLS 0.5 seconds prior to the UFLS threshold being violated allowed a 0.15 Hz reduction in the size of the maximum frequency deviation, which constitutes a reduction of approximately 15.5 % in the maximum deviation when compared to deterministic UFLS.

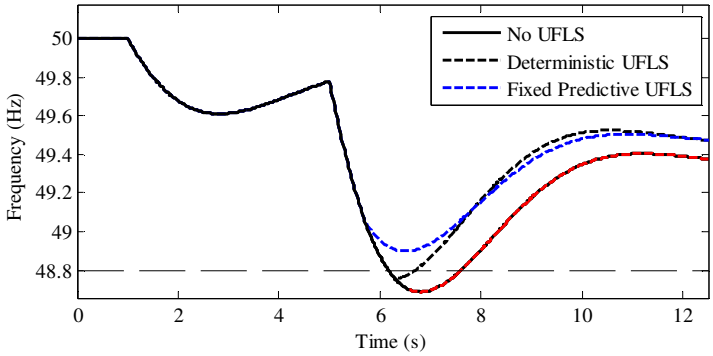

Figure 8-15 – Frequency response for two sequential increases in load when no UFLS, deterministic UFLS and Fixed Predictive UFLS are implemented.

8.5.2 Adaptive Predictive Under Frequency Load Shedding

Another strategy for using predictions to support emergency frequency control is to reduce the amount load shed to the minimum required to limit the maximum frequency deviation to a given target value. This allows the quantity of load shedding deployed, and hence the cost of the control action, to be minimised without compromising stability. However, it will allow a larger frequency deviation to occur than fixed predictive shedding. This is almost a certainty as the quantity of load shed as part of deterministic UFLS is designed to accommodate the worst cases scenario and as such will lead to over shedding in any other scenario.

The minimum level of load shedding that will limit the maximum frequency deviation to the desired value (Δf_{lim}) can be calculated by calculating the load shedding that will create a target frequency deviation (Δf_{tar}) that is defined in the following way.

$$\Delta f_{tar} = \Delta f_{\lim}(1-\xi) - \Delta f_{\max} \quad \text{[p.u.]} \tag{8-26}$$

where Δf_{max} is the predicted maximum frequency and ξ is a security threshold that can be used to guarantee that Δf_{lim} will not be violated.

The necessary level of load shedding (ΔP_S) can then be calculated.

$$\Delta P_S = \frac{2H}{\Delta t}\frac{\Delta f_{tar}}{\left(1 - C\Delta t / 4H\right)} \quad \text{[p.u.]} \tag{8-27}$$

where Δt is the difference between the predicted time of the frequency maxima and the time at which the adaptive predictive load shedding is initiated.

Equations (8-26) and (8-27) were used to calculate the shedding necessary to limit the frequency to a value of 48.8 Hz with a security threshold of 1 %. This value was found to be 0.0302 p.u. and is approximately 40 % less than the deterministic level of load shedding. However, in practice it is likely that this calculated level of adaptive load shedding would represent the theoretical minimum level of shedding and not the actual level of shedding implemented. This is because load shedding is achieved by shedding discrete loads and it is extremely unlikely that any combination of these loads would offer the desired level of shedding so a certain quantity of extra load would also need to be shed. Figure 8-16 gives a comparison of the frequency trajectory for each of the three forms of UFLS discussed to this point.

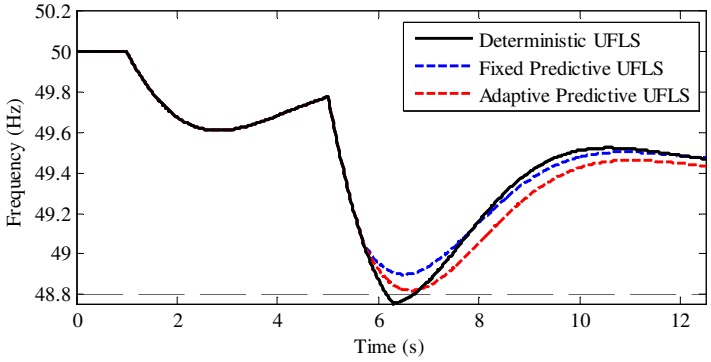

Figure 8-16 – Frequency response for two sequential increases in load when deterministic UFLS, Fixed Predictive UFLS and Adaptive Predictive UFLS are implemented.

Reducing the time necessary to produced a prediction and act upon it will increase the benefit offered by the prediction. Figure 8-17 demonstrates the improved benefit offered by both types of predictive based shedding proposed in this thesis if the

execution time of the prediction method and consequently the shedding delay is reduced. These examples show that the improvement as the shedding delay is reduced is non-linear and that the greatest improvement is made for the initial reduction in the shedding delay, i.e. a reduction from 1.3 seconds to 1.1 seconds offers more benefit than a reduction of 1.1 seconds to 0.9 seconds. In these examples a minimum delay of 0.1 seconds based on the time that is required to physically implement the shedding instruction is assumed. Whilst it is highly unlikely that the smaller shedding delays presented in Figure 8-17 will ever be feasible they were included to demonstrate this variation.

A small the reduction in the improvement in the amount of load shed is seen for shedding delays of below 0.3 seconds in Figure 8-17 B. This occurs because the validity of the assumption that the time of the maximum frequency deviation is unchanged by the shedding begins to break down when the shedding is implemented this quickly.

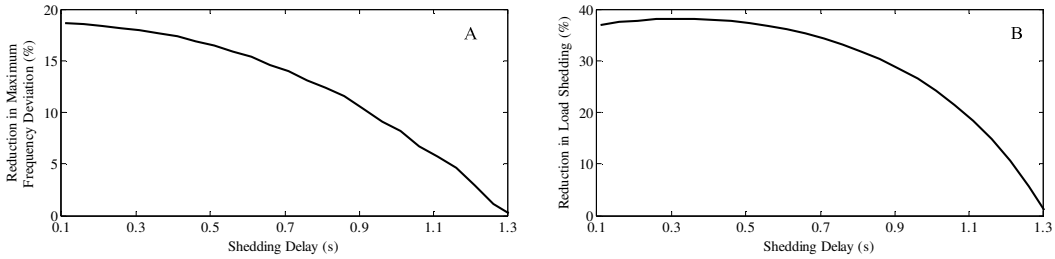

Figure 8-17 – A comparison of the benefit of decreasing the shedding delay in the terms of reducing the size of the maximum deviation for fixed predictive UFLS (A) and reducing the amount of load shed for adaptive predictive UFLS (B). The frequency deviation and load shed by the traditional deterministic UFLS is used as a base line in each respective case.

8.5.2.1 Replacing UFLS with Load Deferral

The introduction of large scale demand response control and energy storage in power systems could allow the opportunity to move away from load shedding as the primary source of emergency under frequency control in a power system. Depicted in Figure 8-18 is the frequency response if the same level of load reduction that was shed based on a prediction in Figure 8-18 were to be simply deferred by one second. Note that whilst this is referred to as load deferral this action could consist of reduced load through demand response control or additional generation from energy storage.

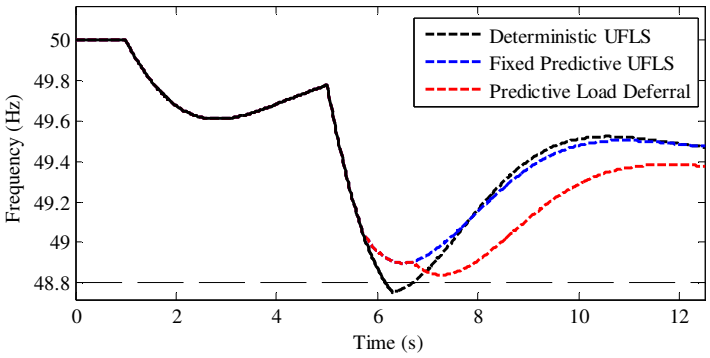

Figure 8-18 – Frequency response for two sequential increases in load when deterministic UFLS, Fixed Predictive UFLS and predictive load deferral are implemented.

Proper implementation of this load deferral would allow frequency stability to be preserved without having to expose the system to load shedding. This is an advantage as whilst load shedding tends to be automatic the restoration of the load tends to be manual so the long term consequences of load shedding are greater than they are for load deferral.

8.5.3 Testing the Approximate Model Based Prediction Method using DIgSILENT™ PowerFactory® Simulations

The next stage of testing the online method for estimating C_{max} involved simulations in DigSILENT™ PowerFactory® [16]. This testing was performed using the IEEE 9 bus test system, depicted in Figure 8-19 and detailed in Appendix D, and demonstrated that the method did not perform as well as it had previously.

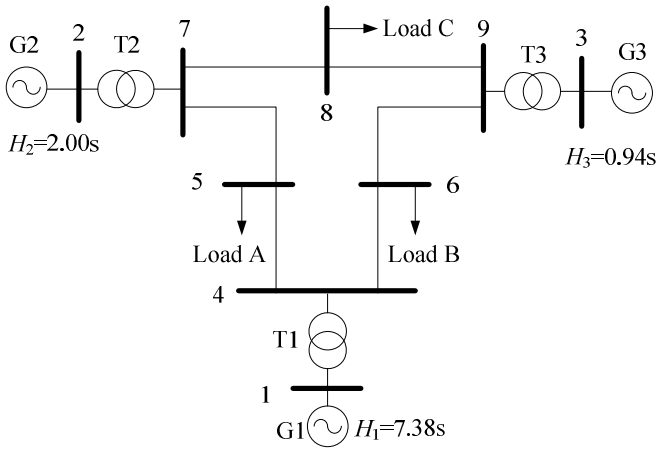

Figure 8-19 – IEEE 9 Bus Test System

A single example is discussed here to describe the problems faced for these simulations. This example consists of recording the frequency and power measurements for G2 and G3 for the disconnection of G1 when it was generating 100 MW. The frequency traces recorded for G2 and G3 were combined into a single frequency trace depicted in Figure 8-20 using the frequency of the inertia centre method, f_H [13].

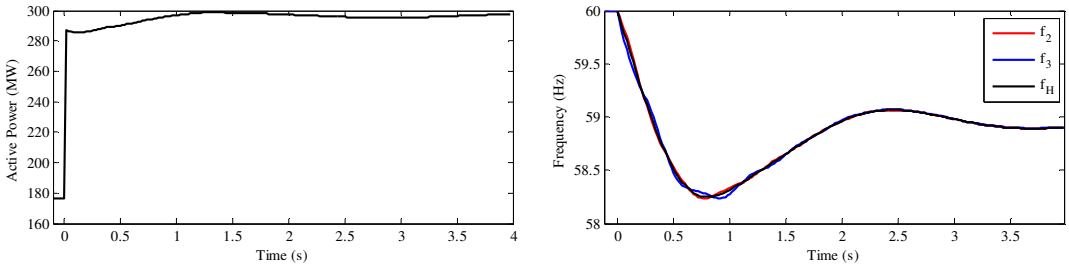

Figure 8-20 – Equivalent frequency and active power for G2 (f_2) and G3 (f_3) of the IEEE 9 bus test system when G1 is disconnected

The online method for estimating C_{max} was applied to this data using a Newton type method to estimate the parameters as before. However, the output of the algorithm for this data differed drastically from that seen for the SFR model. Figure 8-21 and Figure 8-22 can be used to compare this behaviour when the Newton type method was applied for a sliding window with width of ten samples. It is evident that whilst the algorithm is capable of estimating C_{max} and t_{max} when data from approximately 0.5 seconds onwards when compared to the results for the SFR this estimation is far less reliable and also occurs much later, i.e. closer to the time of the frequency nadir.

This behaviour in the C_{max} estimates is due to the corruption of the behaviour of $C(t)$ by the more complex dynamics and particularly oscillations between the two machines. Therefore, if the online C_{max} estimation process is to be applied to more complex power system signals then signal processing techniques must developed to deal with the oscillations and other dynamic behaviour that is compromising the calculation of accurate $C(t)$ values. These additional elements in the frequency response compromise the assumption of no oscillations and uniform system frequency on which the method is based.

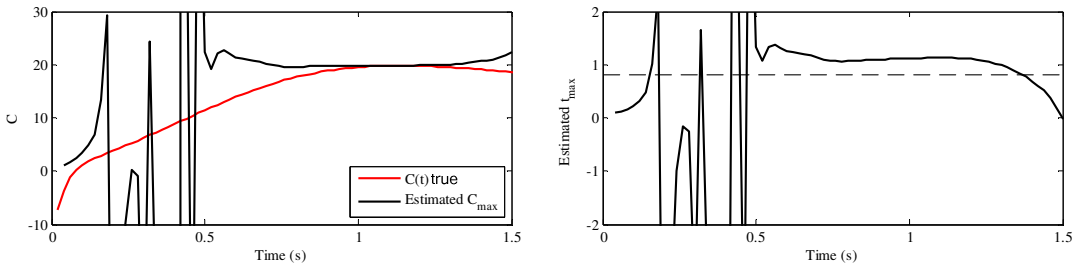

Figure 8-21 – Behaviour of online C_{max} estimation method for IEEE 9 bus test system. The true value of *tmax* is marked with a dashed line and the true value of C_{max} corresponds to the peak of the $C(t)$ true curve.

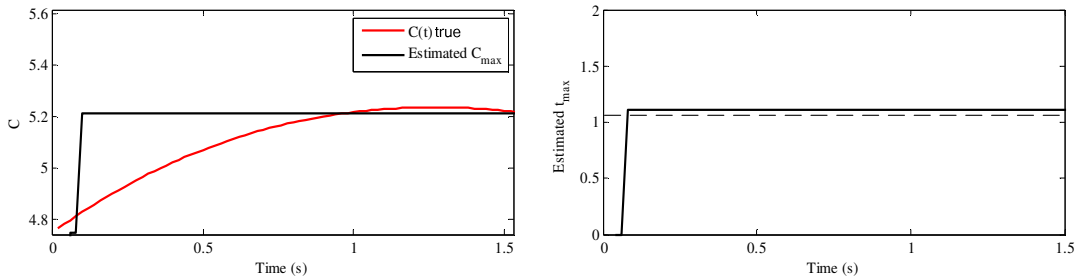

Figure 8-22– Behaviour of online C_{max} estimation method for the SFR model. The true value of *tmax* is marked with a dashed line and the true value of C_{max} corresponds to the peak of the $C(t)$ true curve.

8.6 Chapter Summary

Model based prediction of power system frequency behaviour allows the time and frequency of specific events to be predicted. The research in this chapter dealt with the prediction of the nadir of the frequency response. After an initial assessment of the available models of the system frequency response it became apparent that a highly approximate model would have to be used. The model proposed in [3] was chosen and a novel method was proposed for the online estimation of the governor parameter. This method was tested using the SFR model and found to be accurate. Based on these results several different approaches were proposed for using a prediction of the frequency nadir to improve emergency frequency control. Predictions allow emergency control to be initiated before the traditional thresholds are violated so they can be used to either reduce the size of any deviation or limit the deviation to a target frequency or reduce the amount of load shed. In the example given in Section 8.5 of a sequential loss of generation predictive shedding allowed a reduction of approximately 15.5 % in the size of the deviation, when fixed predictive shedding was used, and

when adaptive predictive shedding was used the quantity of load shedding that was necessary to ensure frequency stability was reduced by approximately 40 %. Furthermore, in the case of both fixed and adaptive predictive shedding the frequency was not allowed to violate the frequency threshold that was used to trigger the traditional deterministic load shedding.

However, the online estimation method proposed here to estimate the parameter values of the approximate model failed to perform with the same level of reliability and accuracy in the case of the more complex power system signals that were simulated in DIgSILENT™ PowerFactory® [16] due to the presence of oscillations in the measured frequency. To address these issues some form of signal processing must be developed that can serve to eliminate the elements that corrupt the estimation process.

A significant challenge when attempting to use approximate models for the online frequency prediction proposed here is defining a model that is sufficiently complex to accurately predict the system response but that is sufficiently simple that the parameter values can be estimated using the data available. This challenge will increase dramatically if power system developments, such as synthetic inertia, were to be included in the system response. Therefore, when developing approximate model based prediction methods in the future it will likely be necessary to tailor the proposed model to specific areas of a system if accurate predictions are to be achieved.

8.7 References

[1] Mirzazad-Barijough, S.; Mashhuri, M.; Ranjbar, A.M.; , "A predictive approach to control frequency instabilities in a wide area system," Power Systems Conference and Exposition, 2009. PSCE '09. IEEE/PES , vol., no., pp.1-6, 15-18 March 2009,

[2] Larsson, M.; Rehtanz, C.; , "Predictive frequency stability control based on wide-area phasor measurements," Power Engineering Society Summer Meeting, 2002 IEEE , vol.1, no., pp.233-238 vol.1, 25-25 July 2002,

[3] Egido, I.; Fernandez-Bernal, F.; Centeno, P.; Rouco, L.; , "Maximum Frequency Deviation Calculation in Small Isolated Power Systems," Power Systems, IEEE Transactions on , vol.24, no.4, pp.1731-1738, Nov. 2009

[4] Anderson, P.M.; Mirheydar, M.; , "A low-order system frequency response model," *Power Systems, IEEE Transactions on* , vol.5, no.3, pp.720-729, Aug 1990

[5] de Mello, F.P.; , "Boiler models for system dynamic performance studies," Power Systems, IEEE Transactions on , vol.6, no.1, pp.66-74, Feb 1991

[6] Inoue, T.; Taniguchi, H.; Ikeguchi, Y.; , "A model of fossil fueled plant with once-through boiler for power system frequency simulation studies," Power Systems, IEEE Transactions on , vol.15, no.4, pp.1322-1328, Nov 2000

[7] Working Group on Prime Mover and Energy Supply, "Dynamic models for combined cycle plants in power system studies ," Power Systems, IEEE Transactions on , vol.9, no.3, pp.1698-1708, Aug 1994

[8] Zhang, Q.; So, P.L.; , "Dynamic modelling of a combined cycle plant for power system stability studies," Power Engineering Society Winter Meeting, 2000. IEEE , vol.2, no., pp.1538-1543 vol.2, 2000

[9] Report, I.C.; , "Dynamic Models for Steam and Hydro Turbines in Power System Studies," Power Apparatus and Systems, IEEE Transactions on , vol.PAS-92, no.6, pp.1904-1915, Nov. 1973

[10] Tapia, A.; Tapia, G.; Ostolaza, J.X.; Saenz, J.R.; , "Modeling and control of a wind turbine driven doubly fed induction generator," Energy Conversion, IEEE Transactions on , vol.18, no.2, pp. 194- 204, June 2003

[11] Kennedy, J.; Eberhart, R.; , "Particle swarm optimization," *Neural Networks, 1995. Proceedings., IEEE International Conference on* , vol.4, no., pp.1942-1948 vol.4, Nov/Dec 1995

[12] R. C. Eberhart, Y. Shi, Particle Swarm Optimization: Developments, Applications and Resources, Evolutionary Computation, 2001. Proceedings of the 2001 Congress on, vol. 1, pp. 81-86, 27-30 May, 2001

[13] I. A. Hiskens, "Nonlinear Dynamic Model Evaluation from Disturbance Measurements", Power Systems, IEEE Transactions on, vol. 16, no. 4, pp. 702-710, 2001

[14] Kundur, P., *Power System Stability and Control* 1994, New York: McGraw-Hill.

[15] Transmission, N.G.E., *The Grid Code*. 2010, National Grid Electricity Transmissions.

[16] DIgSILENT, "DIgSILENT PowerFactory," V 14.0523.1 ed Gomaringen, Germany: DIgSILENT GmbH, 2011.

9 Post-Disturbance Frequency Prediction using the Application of Pattern Classification Theory

This chapter introduces the novel application of pattern classification theory to online frequency prediction in Section 9.1. The concepts behind supervised learning and pattern classification are described in Section 9.2. Section 9.2 also introduces some of the more common pattern classification techniques, namely polynomial regression, multi-layer neural networks and Support Vector Machines (SVMs). Polynomial regression is then applied to the task of classifying the frequency response of a power system in Section 9.3. SVMs are discussed in Section 9.2 but not applied in 9.3. This is because SVMs are one of the most popular and successful pattern classification techniques that are currently available but, for reasons discussed in Section 9.2, could not be applied directly to frequency prediction.

9.1 Chapter Introduction

Pattern Classification theory was considered as a possible method for frequency prediction as it naturally lends itself to the task of prediction [1] [2] [3] [4] [5] and was successfully applied to the task of rotor angle instability prediction in [6] and other non-prediction power system applications such as post-mortem classification of disturbances [7] and power quality events [8] [9].

The concept proposed here for achieving frequency prediction through the use of pattern classification theory consists of using the initial (approximately 0.5 seconds) of the frequency deviation to assign a label that describes the future frequency behaviour of the power system.

Consider the following simple example. After a disturbance occurs in the system observations are made during the initial frequency deviation, depicted in Figure 9-1. These observations are then passed into a pattern classifier that can assign one of the following three labels and define the predicted behaviour:

1. Under Frequency.
2. Over Frequency.
3. Frequency Within Limits.

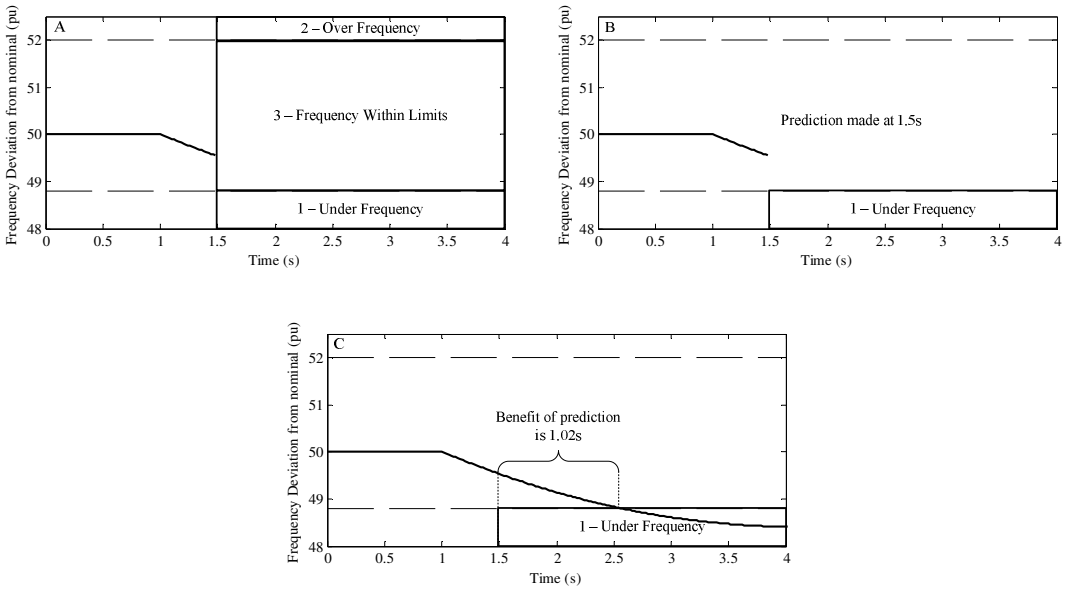

Figure 9-1 – General process for a simple case of frequency prediction based on pattern classification. The measurements made for the initial response (A) are used to classify the future frequency behaviour (B) and this allows frequency control to pre-empt the deviation (C)

The label is assigned to the initial frequency deviation after a delay of t_d, this is assumed to be 0.5 seconds in the example in Figure 9-1 and will be determined by a number of factors such as data processing delays and communication delays. Based on this label actions could be taken by operators or automated control schemes to avert the predicted deviation, instead of waiting for the frequency to violate the threshold.

The application of pattern classification theory involves the use of supervised learning and will be dependent on access to training data in the form of power system simulations and data records from real disturbances. However, this does not mean that it fails to satisfy the requirement that the prediction method operate based on the true system state and not some assumed system state. This is because the classification is based on a process that converts this training data into a set of generalised decision functions that can be applied based on estimates of the true system state.

The difficulty of any pattern classifying task is determined by the degree of similarity between the patterns that belong to different classes. Therefore, the application of pattern classification for power system frequency prediction must overcome the

challenge that the frequency responses and therefore the representative patterns at the class boundaries will be very similar to one another but will have different class memberships.

9.2 Pattern Classification Theory

This section gives a background to the core concepts behind pattern classification, further details can be found in [1][5]. Pattern classification allows symbolic meaning, which is useful to a human or machine based decision making entity, to be extracted from a sub-symbolic pattern source in the form of a class membership. An example, of this extraction would be converting the description of two vertical parallel lines of equal length separated by a shorter perpendicular line into the symbol H. This task comes easily to the human brain but is more challenging for machines.

This class membership is assigned based on the evaluation of a decision function that uses the observations made of the system as an input. The decision function can be viewed as a form of mapping between the input space of the observations and the decision space of the possible classes that allows the classifier to extract the class membership from the observations. To accurately extract the class membership of the observations the decision function must be trained based on existing examples of system behaviour for which the class membership is already known. This training of the decision function is a form of supervised learning that tailors the pattern classifier to be a specific task.

The execution of this process is depicted in Figure 9-2. An additional mapping between the input space and a higher order feature space is usually included in the functional approximation, the result of which is then evaluated using the decision function. This additional mapping is implemented as more features of the input data are visible in this higher order feature space and as such it is easier for the decision function to distinguish between different classes. The decision vector that is returned by this process is compared to a list of target vectors that represent each class.

Each class is represented as a discrete target vector, rather than its symbolic meaning, because this allows mathematical tools to be used to determine which target vector the

decision vector is most similar to and hence which class should be assigned. Target vectors are usually a column of a K by K identity matrix, where K is the number of classes. These target vector assignments are chosen instead of other numerical values, e.g. the class number k, as this assignment guarantees that the Euclidean distance between class vectors will be equal.

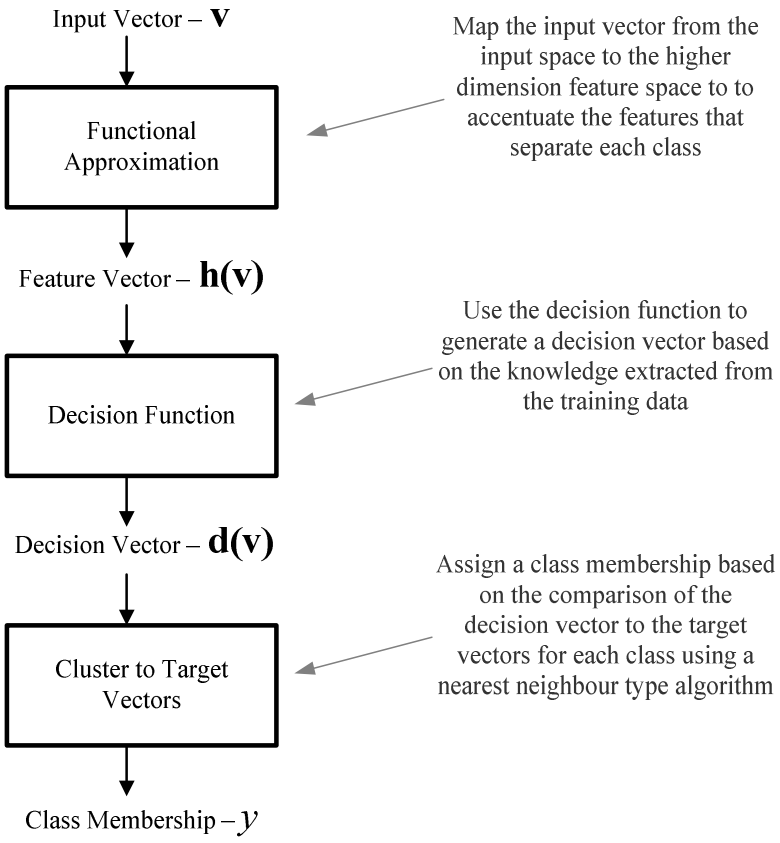

Figure 9-2 – Execution of a generic pattern classifier

The observations can come from any source that is relevant to the system in question but must contain a number of spatially or temporally related observations and not a single isolated observation [1]. For example, in the case of frequency prediction suitable observations would be an estimate of the inertia and a set of post-disturbance frequency and active power measurements.

The K individual classes must be a discrete and finite set, Ω, that collectively represent the entire possible solution space. This is the closed world assumption and is a necessity for the application of pattern classification [1]. This means that the classes must be mutually exclusive and complete, such that any event that may occur can be

classified as belonging to one, and only one, class. In the context of frequency prediction, pattern classification will involve defining a set of classes that represent the full range of possible post-disturbance frequency trajectories.

The functions that map the input space observations into the higher order feature space and the feature vector from the feature space to the decision space tend to be combined into a single decision function that takes the observations as an input and outputs the class membership. The mapping to a higher order space is required in most applications to ensure that the decision function can separate each class using a set of K hyper-planes. This higher dimension space allows easier separation of relationships that may be difficult to distinguish in the input space [1].

A set of observations with a known class membership are used to form a set of training patterns that can be used to train the decision function. This training will entail selecting the parameters of the decision function to satisfy some form of optimization criteria, usually a measure of the error between the target vector of the true class and the decision vector generated by the classifier. The optimization criteria is usually in the form of a least means square optimization as this preserves the non-linearity of the feature space mapping, which is of the up most importance in preserving the generalization offered by the classifier. The general process for training a classifier is presented in Figure 9-3.

This training is necessary as it allows the decision function to be used to classify patterns that lie between the training patterns. This generalisation between the training patterns is a key property of any classifier and is the primary enabler of the application of pattern classification to frequency prediction as it should allow the information contained in a limited set of examples of power system behaviour to be generalized to the entire possible set of power system behaviour.

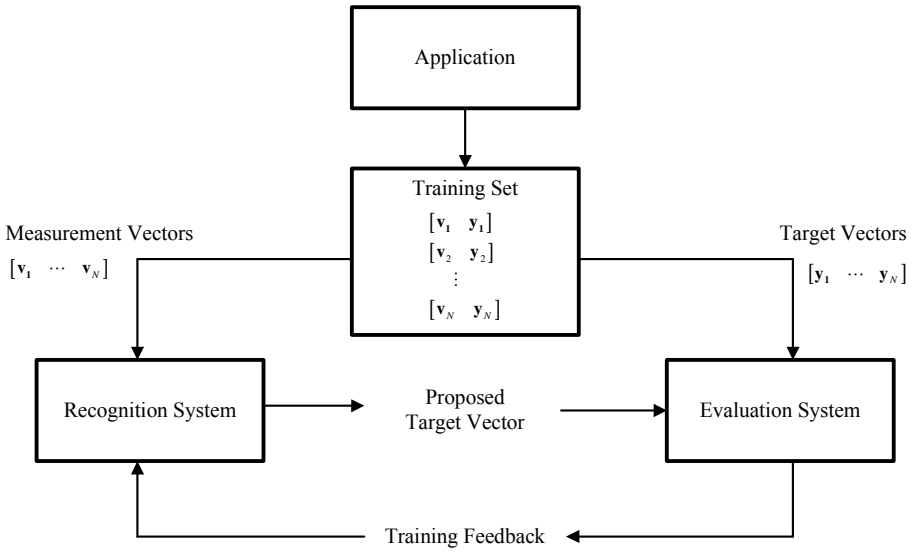

Figure 9-3 – Training process for a generic pattern classifier based on information found in [1].

The set of observation used to train the classifier should encompass the range of possible scenarios that the classifier could face, to ensure proper training. However, it is important that not all of the patterns collected from a system are used to train the classifier. This is because some of these patterns will be needed to test the classifier. Testing a classifier using the data it was trained with, or reclassifying [1], will not test the accuracy of the generalisation offered by the classifier. Therefore, as this generalisation is the key property of a classifier it would not be a worthwhile test. Furthermore, if the design of a specific classifier requires the selection of certain parameter values, e.g. the weights in a neural network, the classifier must be validated before it is tested. This is primarily to ensure that over fitting has not occurred

Over fitting occurs when the hyper planes formed by the decision function are too tightly fitted to the training data [1]. This will usually cause the ability of the hyper plane to accurately generalize between training patterns to be drastically reduced, allowing errors to occur

The training, validation and testing of a pattern classifier can be a time consuming task, particularly when a large number of input observations and training patterns are used. However, this is performed offline and the online execution of the classifier itself will tend to be relatively fast as decision functions will tend to take simple forms such as a linear sum of products.

From this discussion of the basic principles of pattern classification the core requirements for the application of pattern classification are [1] [3]:

1. Sufficient observations of the system or a stochastic pattern source that represents the system to a sufficient degree to form training, validation and testing sets.
2. A finite set of discrete classes that satisfy the closed world assumption.
3. A decision function that converts observation vectors into decision vectors.
4. An optimization criterion that can be used to train the estimations made by the mapping function to come as close as possible to the true class vector.

It is the decision function that links the sub-symbolic and symbolic domains and as such the task of pattern classification primarily consists of the design, training and testing of the mapping function. The supervised nature of this learning process means that any pattern classifier is highly tailored to a specific application. However, general approaches for forming a classifier do exist and three are discussed in this chapter.

9.2.1 Polynomial Regression Classifiers

A polynomial regression classifier uses a decision function that is based on the principle that any reasonable function can be accurately represented by a polynomial of sufficient degree. This is a statistical approach to pattern classifying that assumes the variation between the patterns that map to a single class can be represented using random processes. The polynomial for a scalar decision function $d(\mathbf{v})$, where $\mathbf{v}$ is the N element vector of observations can be defined as follows [1].

$$\begin{aligned} d(\mathbf{v}) = {} & a_0 + a_1 v_1 + a_2 v_2 + \cdots + a_N v_N \\ & + a_{N+1} v_1^2 + a_{N+2} v_1 v_2 + a_{N+3} v_1 v_3 + \cdots \\ & + a \ldots v_1^3 + a \ldots v_1^2 v_2 + a \ldots v_1^2 v_3 + \cdots \end{aligned} \tag{9-1}$$

The first line of this polynomial definition contains the constant term a_0 and the N linear terms, the second line contains the $N(N+1)/2$ quadratic terms whilst the third line contains the cubic terms. This definition can be expanded to an arbitrary polynomial degree G and each of the L terms in the definition represents a basis function of the classifier.

This definition can be represented in the more useful form of a vector product.

$$d(\mathbf{v}) = \mathbf{a}^{\mathbf{T}}\mathbf{x}(\mathbf{v}) \tag{9-2}$$

where

$$\mathbf{x}(\mathbf{v}) = \begin{bmatrix} 1 & v_1 & v_2 & \cdots & v_N & v_1^2 & v_1 v_2 & v_1 v_3 & \cdots & v_1^3 & v_1^2 v_2 & v_1^2 v_3 & \cdots \end{bmatrix}^{\mathbf{T}} \tag{9-3}$$

and

$$\mathbf{a} = \begin{bmatrix} a_0 \\ \vdots \\ a_L \end{bmatrix} \tag{9-4}$$

This allows a vector decision function **d(v)** to be represented as follows

$$\mathbf{d(v)} = \mathbf{A}^{\mathbf{T}}\mathbf{x(v)} \tag{9-5}$$

where *A* is a *K* by *L* matrix of coefficients, where *L* is the length of the polynomial. In a properly trained classifier each element of this vector decision function represents the likelihood of the vector of observations **v** belonging to a specific class.

To determine this class the decision function **d(v)** is then compared to the set of target vectors and a class membership $\tilde{y}$ is assigned based on the target vector that is most similar to the decision vector. This is usually determined using a nearest neighbour type algorithm.

Therefore, when training a polynomial regression classifier for a given set of observations and classes the parameters that must be selected are the degree of the polynomial and the matrix of coefficients.

A suitable classifier for mapping **v** to **d** should be accurate in as many cases as possible; this is achieved by solving a statistical optimization problem that selects the matrix **A** to minimize the probability of any error. However, the probability of error is

unknown in most applications that require the application of pattern classification theory so an equivalent must be determined.

This equivalent is based on Bayes' rule and the minimization of the residual variance of the classification error (S^2) using a least squares objective.

$$S^2 = E\left\{\left|\mathbf{d}(\mathbf{v}) - \mathbf{y}\right|^2\right\} \tag{9-6}$$

From the derivation presented in [1], this optimisation allows the **A** matrix to be selected based on the calculation of the following first order statistical moments.

$$\mathbf{A} = \frac{E\left\{\mathbf{x}\mathbf{y}^T\right\}}{E\left\{\mathbf{x}\mathbf{x}^T\right\}} \tag{9-7}$$

where if the number of training points (M) is sufficiently large these expectations can be approximated as means.

$$\mathbf{A} = \frac{\frac{1}{M}\sum_{i=1}^{M}\mathbf{x}_i{}^T\mathbf{y}_i}{\frac{1}{M}\sum_{i=1}^{M}\mathbf{x}_i{}^T\mathbf{x}_i} \tag{9-8}$$

A useful method for improving the performance of a polynomial regression classifier is confidence mapping [1]. This involves taking the output of a polynomial regression classifier (the first stage classifier) and treating it as the input to another polynomial regression classifier (the second stage classifier). This second stage classifier can then be trained in the same way as the first stage classifier using the true class of each of the original patterns and the decision vector produced by the first stage classifier for each of the original patterns. This process results in a classifier that can be described using $\mathbf{A_1}$ and $\mathbf{A_2}$, the matrix of coefficients for the first and second stage classifiers respectively.

$$\mathbf{d(v)} = \mathbf{A_2^T A_1^T x(v)} \tag{9-9}$$

A polynomial regression classifier is a simple form of classifier that can achieve high levels of accuracy. The decision function is easy to train when calculating approximate statistical moments and offers a direct solution from a linear sum of products. However, this simplicity means that the classifier is particularly susceptible to over fitting.

9.2.2 Artificial Neural Network Classifiers

Pattern classifiers that are based on artificial neural networks attempt to form a functional approximation of a classification problem by synthesizing the neurons found in the human brain and thus mimic the natural solution to the problem of pattern classification [1]. A basic synthetic neuron is depicted in Figure 9-4.

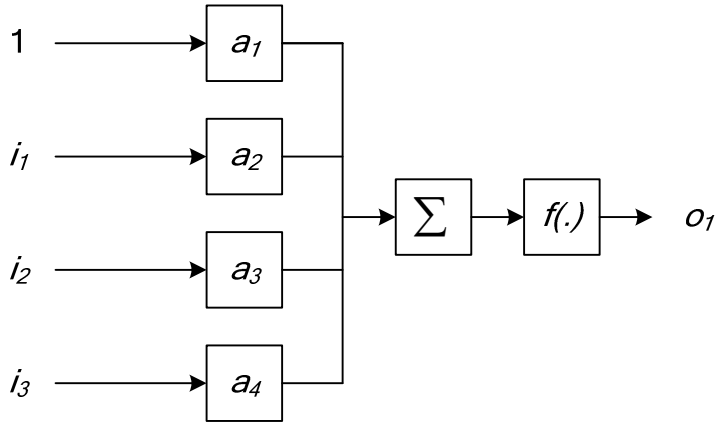

Figure 9-4 – A simple Neuron structure with three inputs, *i*, one output, *o*, and an arbitrary activation function *f*(.)

The neuron inputs can be positive (excitatory) or negative (inhibitory) and with the inclusion of the activation function, *f*(.), this simple structure offers a high degree of flexibility through the weights applied to each input and the non-linear output mapping function. These simple neurons can then be interconnected to form a more complex structure like that depicted in Figure 9-5.

A three layer network can be used to solve a pattern classification problem if the weights and non linear mapping are selected properly. In the case of pattern classification the number of neurons in the input layer is equal to the number of observations in each pattern (*N*) and the number of neurons in the output layer is equal

to the number of possible classes (K). The inputs to each neuron in the input layer are the observations and an integer value, usually 1, to allow a bias or offset for each neuron. Whilst the outputs of the neurons in the output layer are used to form the decision vector, so each output neuron corresponds to a single class.

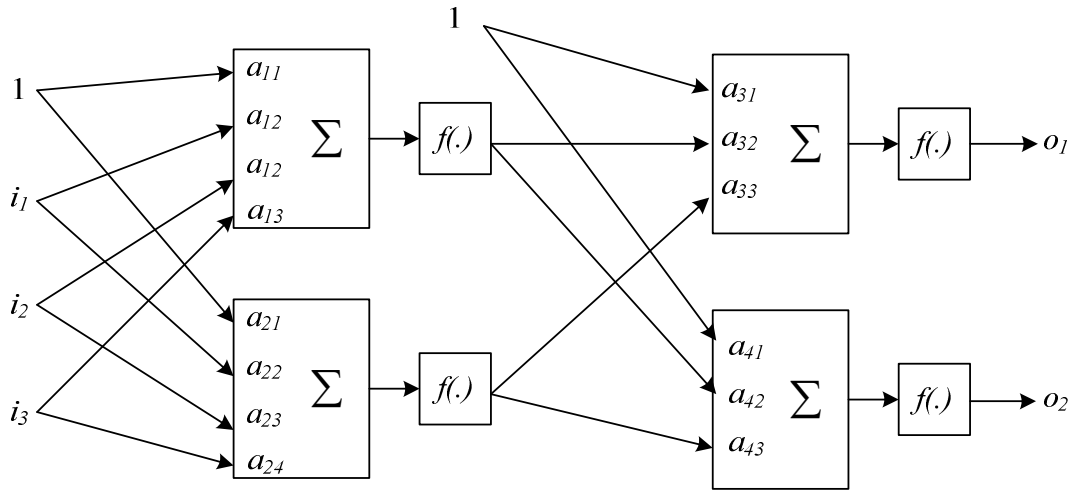

Figure 9-5 – A more complex structure for a multi-layer neural network

The optimal neuron weights can be determined by solving an optimization problem that optimizes the fitting of the decision vector to the true target vectors for the training data. The optimization function used here is a least means square.

$$S^2 = \frac{1}{M}\sum \left|\mathbf{z}_o(\mathbf{v}_i) - \mathbf{y}_i\right|^2 \tag{9-10}$$

where M is the number of learning patterns used and $\mathbf{z}_o$ is the output of the output layer of the network.

The nonlinear mapping function, or activation function, is a vital part of this classifier as it prevents the neural network from collapsing into a simple linear combination. Many activation functions exist, including linear ramps and discrete step functions but a sigmoid is used here as it offers a high degree of customization for only two parameters.

$$s(x) = \frac{1}{1+\exp\left(-\left(x-B\right)/T\right)} \tag{9-11}$$

The parameter T controls the slope of the sigmoid and the parameter B controls the midpoint of the slope. Gradient descent methods are commonly used to train neural network based classifiers due to their ease of implementation and convergence to a single solution although they do incur high computational costs [1][2].

Pattern classifiers based on neural networks are particularly susceptible to over fitting due to the large number of local minima that exist in the solution space of the neuron weights. This weakness can be mitigated by including a validation stage. This validation involves the weights being optimised for the training set provided that this optimization does not degrade performance for the validation set. This make the training process take longer but this is acceptable given the improvement it offers in the generalization of the classifier as the process is performed offline. However, one problem with validation is that it will require more data be used for the training process and thus less will be available for testing.

9.2.3 Support Vector Machines

The task of training a pattern classifier can be summarized as the task of finding a directed hyper plane that separates each class of data from the others [5]. When training the pattern classifier a set of training data points, each of which represents a single set of observations, is used to determine the properties of this hyper plane. Clearly, the training data points that are closest to the hyper plane will be the most important and these are the Support Vectors (SVs) that lend their name to the Support Vector Machine (SVM) pattern classifier.

SVMs assign a class to a previously unknown vector of observations ($\mathbf{x}$) by evaluating a function of the SVs for a specific problem. This function is the decision function, and for a two class problem, where the true class label (y_i) for class 1 is 1 and for class 2 it is -1, can be formulated as follows:

$$d(\mathbf{x}) = \sum_{i \in S} \alpha_i y_i \, \mathrm{H}(\mathbf{x}_i, \mathbf{x}) + b \tag{9-12}$$

where S is the set of SVs and the importance of the i^{th} SV is defined by α_i.

The class assigned to the unknown vector of observations (**x**) is based on the sign of the decision function. Specifically, if $d(\mathbf{x}) > 0$ then it is assigned to class 1 and if $d(\mathbf{x}) < 0$ it is assigned to class 2.

The set *S* of SVs and the bias *b* can be determined in a number of ways. Presented in (9-13) is the objective function for a L_1 soft margin, polynomial kernel, SVM. The derivation of the following equations from (9-12) and further discussion of them can be found in [4] and [5]. This function is optimised by maximising Q with respect to α_i and subject to (9-14) and (9-15) as well as the complimentary Karush-Kuhn-Tucker (KKT) conditions (9-16), (9-17), (9-18) and (9-19). This will return a set of *M* α_i values, each of which corresponds to one of the *M* training data points. If α_i is non-zero then the corresponding training data point is a SV and the importance of this SV is proportional to α_i. Only the training data that represents an SV is used in the classifier. This concave quadratic programming problem can be solved with a global optimum if the classification problem is linearly separable. The problem consists of maximizing:

$$\mathrm{Q}(\boldsymbol{\alpha}) = \sum_{i=1}^{M} \alpha_i - \frac{1}{2} \sum_{i=1}^{M} \alpha_i \alpha_j y_i y_j \, \mathrm{H}(\mathbf{x}_i, \mathbf{x}_j) = \max_{\boldsymbol{\alpha}} \tag{9-13}$$

subject to:

$$\sum_{i=1}^{M} y_i \alpha_i = 0 \qquad \text{for } i = 1, \cdots, M \tag{9-14}$$

and

$$0 \le \alpha_i \le C \qquad \text{for } i = 1, \cdots, M \tag{9-15}$$

as well as the complimentary KKT conditions:

$$\alpha_i \left(y_i \left(\sum_{j=1}^{M} y_j \alpha_j \, \mathrm{H}(\mathbf{x}_i, \mathbf{x}_j) \right) - 1 + \xi_i \right) = 0 \qquad \text{for } i = 1, \cdots, M \tag{9-16}$$

$$(C - \alpha_i)\xi_i = 0 \qquad \text{for } i = 1, \cdots, M \tag{9-17}$$

$$\alpha_i \geq 0 \qquad \text{for } i = 1, \cdots, M \qquad (9\text{-}18)$$

$$\xi_i \geq 0 \qquad \text{for } i = 1, \cdots, M \qquad (9\text{-}19)$$

where ξ_i is one of the M relaxation parameters that allow the incorporation of the soft margin parameter C into the formulation.

The parameter C is used in this formulation to allow the SVM to use soft margins instead of the hard margins used in the previous examples of pattern classifiers. Using soft margins introduces a slack variable that allows a sub optimal hyper plane to be determined for linearly inseparable cases. This is achieved by allowing some of the training data to be misclassified if this offers a sufficient improvement in the generalization abilities of the classifier, where sufficient is determined by the parameter C, and a larger C reduces the tolerance of the SVM for such misclassification. L_2 soft margin SVMs determine the tolerable error differently and this renders a more complex set of equations that are described in [5]. Soft margins are particularly advantageous if the training data contains observation errors or mislabelling errors, i.e. the wrong class label is assigned to the data, as such errors can prevent a hard margin classifier from being properly trained.

The introduction of soft margins separates the SVs into two groups: bounded SVs (BSVs) where the corresponding α_i is equal to C and unbounded SVs (USVs) where the corresponding α_i is less than C but still greater than zero. These are separated in the calculation of b so as to ensure an unbiased estimate.

The function H is a kernel that allows the input vector of observations to be mapped to a higher dimension space in which it is easier to separate the classes; in some cases it may in fact not be even possible to separate the classes in lower order spaces. This kernel function could be of any form, including linear, polynomial or a radial basis function, provided that it has a defined inner product. However, regardless of the form of kernel used it should be normalized so that the value of the kernel is not dependent on its length.

The results presented in this chapter do not include the application of SVMs to the task of frequency prediction. This is because the complexity of a power system and the multitude of low probability events that must be considered as part of the training set, if the observation space is to be properly represented, meant that their were a very large number of training candidates that had to be considered. As the Wolfe dual is used the degree of this quadratic optimization is the number training data points and this meant that the size of the optimization problem that had to be solved to determine the support vectors became so large that it could not be solved in a reasonable period of time.

Another challenge of implementing SVMs for frequency prediction occurs because the direct decision functions used by SVMs are intended for the separation of two distinct classes. Therefore, if SVMs are to be used to solve the problem of frequency prediction they must be extended to solve a multi-class problem. Several methods for achieving this extension have been proposed including one against all, pair wise and all at once [5]. Therefore, it is likely that this issue could be overcome if a method were found for training the individual SVMs in a reasonable amount of time.

9.3 Applying Pattern Classification to the SFR Model

The results presented in this section demonstrate the application of pattern classification theory for predicting the post-disturbance frequency behaviour of a power system. The observations used for the input vector are the inertia, the size of disturbance and measurements of frequency recorded for the first 0.5 seconds of the frequency response. Much of the information contained in adjacent samples of the frequency is redundant so to reduce the size of the input vector only every fifth sample was used, and the reporting frequency of the measurements is 50 Hz.

A set of patterns of this nature were created for each combination of the SFR parameters in Table 9-1 and for each disturbance size in Table 9-2.

Table 9-1 – Range of SFR parameters used to generate patterns

D	F_H	H	K_M	R	T_R
1.88	0.06	6.25	1.19	0.06	11.25
1.69	0.06	5.63	1.07	0.06	10.13
1.50	0.05	5.00	0.95	0.05	9.00
1.31	0.04	4.38	0.83	0.04	7.88
1.13	0.04	3.75	0.71	0.04	6.75

Table 9-2 – Range of disturbances used to generate patterns

ΔP (p.u.)					
-0.20	-0.10	-0.05	0.05	0.10	0.20

Training, validation and testing sets were then selected from this larger set of patterns to investigate the behaviour of the classifier when solving a classification problem for which class membership is assigned based on the class in which the maximum frequency deviation (f_{max}) lies. This classification problem has five classes as defined in Figure 9-6 and Table 9-3.

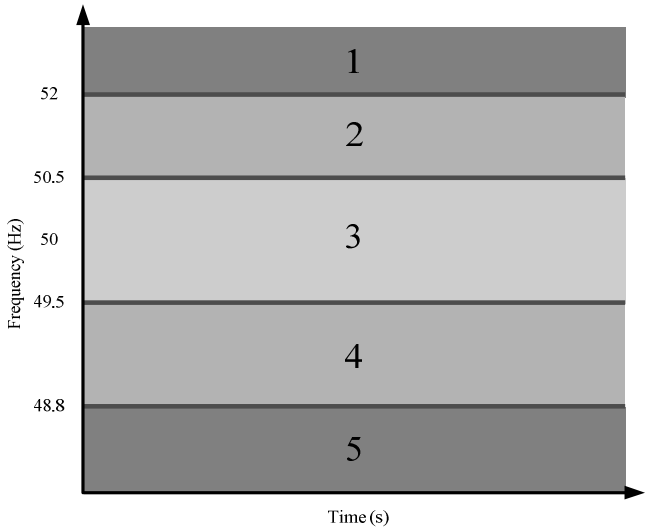

Figure 9-6 – The boundaries that separate the range of the frequency response into five classes

Table 9-3 – Inequalities that define the class boundaries

Class Label	Condition
$y = 1$	$f_{\max} \geq 52.0\text{Hz}$
$y = 2$	$50.5\text{Hz} < f_{max} < 52.0\text{Hz}$
$y = 3$	$49.5\text{Hz} \leq f_{max} \leq 50.5\text{Hz}$
$y = 4$	$48.8\text{Hz} < f_{max} < 49.5\text{Hz}$
$y = 5$	$48.8\text{Hz} \geq f_{max}$

9.3.1 Five Class Polynomial Regression Pattern Classifier

This demonstration of the application of a polynomial regression pattern classifier to the five class problem described in Figure 9-6 and Table 9-3 will begin by addressing the variation in the performance of the classifier for different polynomial degrees and training set sizes.

One measure of the performance of a classifier is the percentage of the testing patterns that it classifies correctly. The variation in this measure with the learning set size is depicted in Figure 9-7 A for a range of polynomial degrees. Furthermore, in Figure 9-7 B the results of applying confidence mapping, a second stage of classification based on the output of the original classifier, is depicted for the same range of polynomial degrees and learning set sizes.

For these results 100 classifiers were trained for each combination of polynomial degree and learning set size and it is the mean of these results that is presented in Figure 9-7. Each classifier was trained using a randomly selected set of training patterns that represented each class and in all of these cases the classifiers were tested using the same testing set.

Initially the increase in the quantity of training data improves the performance of the classifier dramatically. This improvement occurs because the probability of the randomly selected training set representing the entire observation space increases with each additional training example. However, the improvement in performance for each additional training example declines rapidly as the probability tends toward 1 for larger training sets.

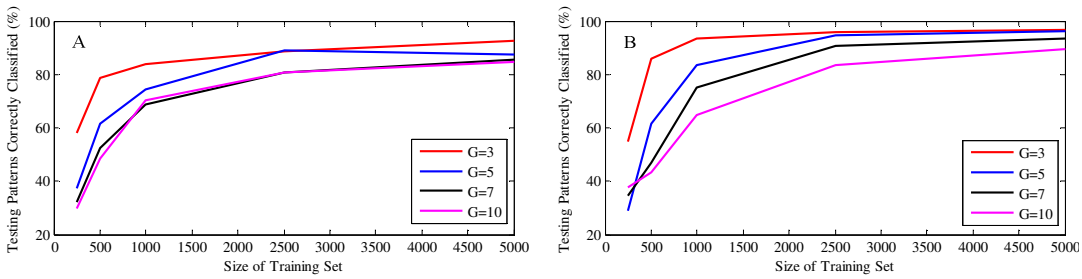

Figure 9-7 – Variation in the percentage of correctly classified testing pattern for a range of polynomial degrees and learning set sizes both without confidence mapping (A) and with confidence mapping (B).

The fall in performance seen in Figure 9-7 as the polynomial degree is increased occurs because of over fitting. Over fitting occurs when the decision function defined during the training process is fitted too tightly to the training data which compromises the generalization power of the classifier. This fall in performance is more significant when confidence mapping is used because this second stage of classification increases the risk of over fitting.

The risk of over fitting is particularly significant for a polynomial regression classifier because it is trained to maximise the classification success for the training set and does not seek to maximise the generalisation power of the classifier, as SVMs and other soft margin classifiers can be. Therefore, the selection of the polynomial degree must balance the risk of over fitting against the improved accuracy offered by mapping to a higher dimension space.

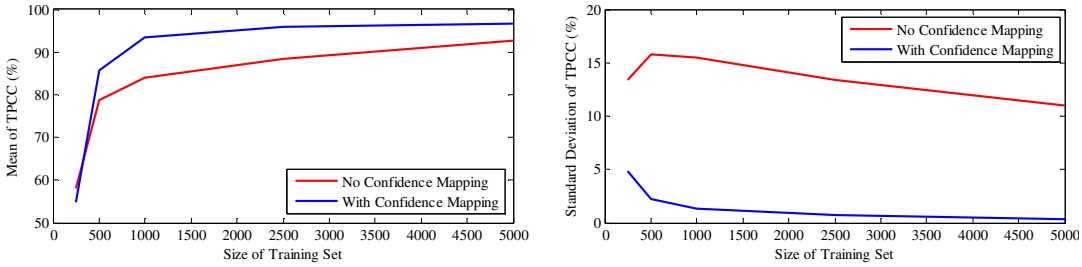

Figure 9-8 – Comparison of the mean and standard deviation of the percentage of correctly classified testing patterns for a polynomial degree of 3 with and without confidence mapping.

In Figure 9-8 the effect of including confidence mapping is shown to be a small improvement in the mean and a significant improvement in the standard deviation. However, the percentage of correctly classified testing points is not a complete measure of the performance of a classifier.

Other measures of performance will now be described for a single example in which the polynomial degree was 3 and 5000 training patterns were used. This classifier was then tested for 10,000 testing patterns and the percentage of correctly classified testing patterns was 95.9 % without the confidence mapping and 96.6 % with the confidence mapping, so as in Figure 9-8 the confidence mapping offered only a limited improvement.

The percentage of correct classifications indicates that when no confidence mapping was used 4.1 % of testing patterns were incorrectly classified and this fell to 3.2 % with the use of confidence mapping. However, this measure does not represent the severity of the misclassification, where severity can be defined as the number of class boundaries that separate the erroneously assigned label from the true label. A simple way to capture this information is to compare the true class label to the class label assigned by the classifier. Table 9-4 and Table 9-5 contain this comparison of the assigned class label and the true class label for the case with no confidence mapping is and for the case with confidence mapping respectively. This comparison is arranged in such a way that the diagonal elements of Table 9-4 and Table 9-5 represent correctly classified testing cases whilst the off-diagonal elements represent incorrectly classified testing cases.

This comparison shows that whilst the use of confidence mapping offers only a limited improvement in the percentage of correctly classified testing patterns it eliminates the severe misclassifications that occur in the case of no confidence mapping that are marked in red in Table 9-4.

Table 9-4 – Comparison of true and assigned class without confidence mapping

		Assigned Class				
		1	2	3	4	5
True Class	1	19130	890	0	0	0
	2	1170	18560	300	0	0
	3	0	0	20000	0	0
	4	0	10	800	19060	170
	5	0	0	0	50	19970

Table 9-5 – Comparison of true and assigned class with confidence mapping

		Assigned Class				
		1	2	3	4	5
True Class	1	19120	880	0	0	0
	2	1160	18550	290	0	0
	3	0	0	19990	10	0
	4	0	0	790	19050	160
	5	0	0	0	40	19960

This assessment of the severity of any misclassification can be supported by using the statistical behaviour of each element of the decision vector for the case where it is supposed to be activated (equal to 1) and deactivated (equal to zero). This behaviour allows the probabilities of misclassification to be assessed and Figure 9-9 and compares the probability density of each element of the decision vector for the testing

patterns for each class with and without the confidence mapping. The ideal case for the plots in Figure 9-9 for the decision vector **d** of an L class problem is a single Dirac delta centred at 1 for **d**(y), where y is the true class membership, and L-1 Dirac deltas centred at 0 for all other elements of **d**.

It can be seen in Figure 9-9 that the probability density for the decision vector elements that should be deactivated in each case are more tightly concentrated around zero. This means that the confidence mapping affords a significant increase in the generalization power of the classifier, as demonstrated by the elimination of the extreme misclassification cases when comparing Table 9-4 and Table 9-5. With this improvement the only decision vector elements that threaten to be erroneously activated are the neighbours of the true class decision vectors e.g. **d**(2) and **d**(4) for y=3.

This occurs because of the arbitrary nature of the class boundaries that were selected based on frequency security limits. In this context these class boundaries are arbitrary in nature because at the boundary they do not separate frequency trajectories with remarkably different characteristics. Consider the fact that despite the similarity between two frequency trajectories that have a minimum frequency of 48.79 Hz and 48.81 Hz, respectively, they are assigned to different classes.

This challenge could be overcome by using a more advanced classifier that combines the class label with an index that represents the degree of certainty. Furthermore, increasing the number of classes has the potential to alleviate the consequences of this problem. If the number of classes were to be increased then the range of frequency covered by each class would be reduced so the severity of any misclassification would be reduced. For example, consider the case in which the class label of 4 is assigned to a pattern with a true class of 5. This will mean that a dangerous under frequency will be treated as a frequency that is outside of the statutory limits. However, if class 4 were to be separated into two classes then the neighbour of class 5 would represent a large deviation below the statutory limit and the severity of the error in the meaning of the classification would be reduced. Whilst this would decrease the severity of the error in the meaning of the classification it would increase the percentage of incorrect classifications, due to the increased number of boundaries, and increase the complexity of the classifier training process.

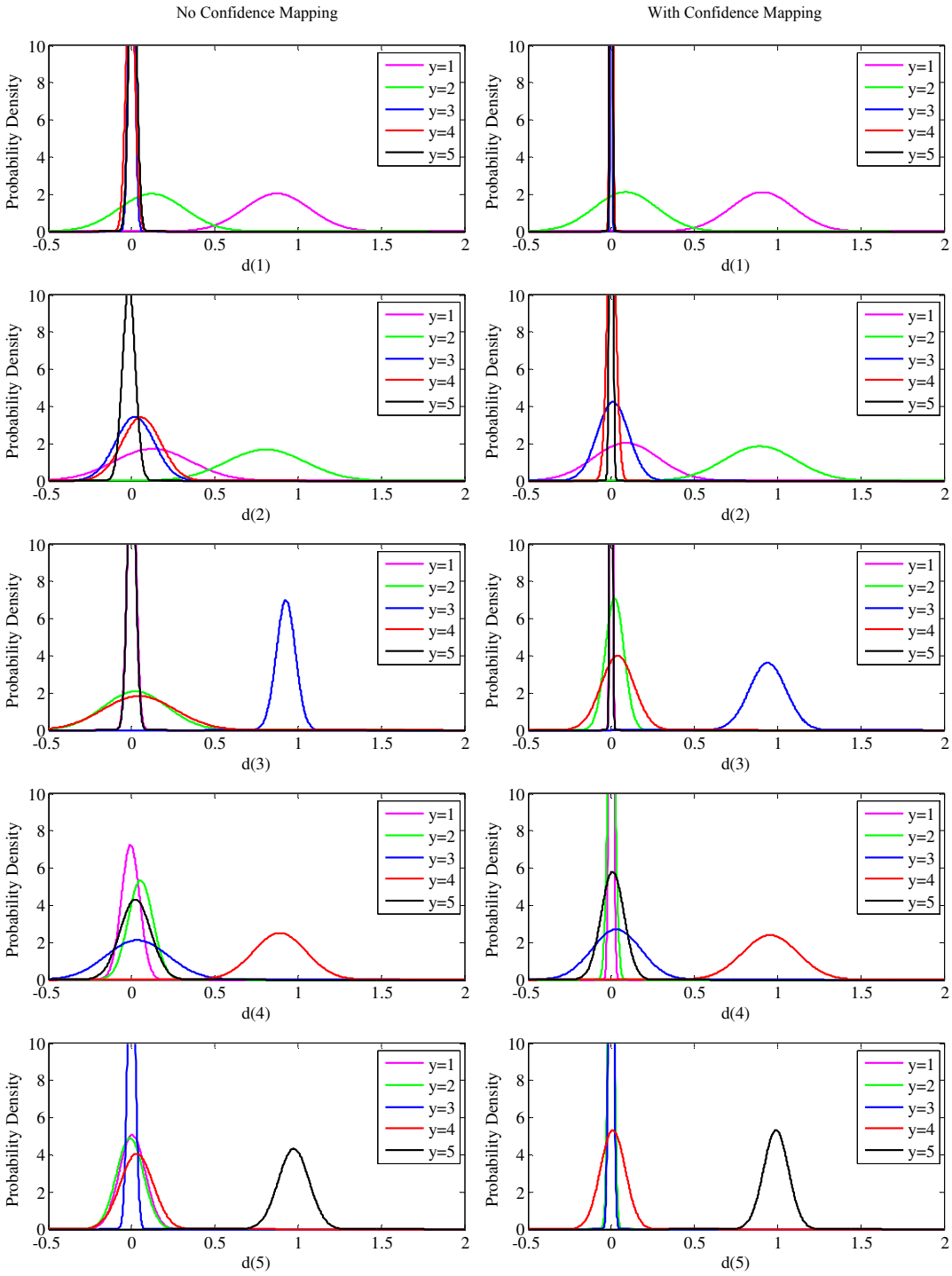

Figure 9-9 – The probability density for each element of the decision vector d when responding to patterns that belong to each of the five class, both with and without confidence mapping. The supporting data for these normal distributions is in Appendix C.

9.4 Chapter Summary

The results presented in this chapter have demonstrated that it is possible to accurately predict the frequency behaviour of a power system using pattern classification theory. A classifier can be used to predict the thresholds that the frequency trajectory will violate and not specific frequency values. Therefore, the support offered by these predictions would be of the form of activating the existing deterministic actions prior to their traditional activation thresholds actually being violated. This form of support was shown to be quite effective in the results presented in Section 8.5.1 for fixed predictive shedding.

A significant advantage of performing frequency prediction using pattern classification instead of approximate models is that the variations in the state of a power system are included into the construction of the classifier during the training process. However, performing this training process for a practical power system will pose several challenges. The first of these is that the complexity of a power system means that there is a vast range of possible system configurations and contingencies that the training set must represent and as such the training set is likely to be very large. Furthermore, the training data for large frequency deviations will likely need to be constructed primarily based on simulated data due the rarity of large frequency deviations in contemporary power systems.

Further work that should be considered based on this research is the investigation of methods for applying a SVM, or other fuzzy classifier, to this multi-class pattern classification problem. These classification techniques are more robust against over classification and should offer improved performance in general and they would likely offer a particular improvement as the nature of fuzzy classifiers could help overcome the challenge posed by an increase in erroneous classifications at the class boundaries.

9.5 References

[1] Schurmann, J. “Pattern Classification: A Unified View of Statistical and Neural Approaches.”, Wiley and Sons, 1996

[2] Michie, D., Spegelhalter, D.J., Taylor, C.C., “Machine Learning, Neural and Statistical Classification.”, Ellis Horwood, 1994

[3] James, M. “Classification Algorithms”, Collins, 1985

[4] Campbell, C., Yin, Y., “Learning with Support Vector Machines”, Morgan and Claypool, 2011

[5] Shigeo, A. “Support Vector Machines for Pattern Classification”, Springer, 2005

[6] Rajapakse, A.; Gomez, F.; Nanayakkara, K.; Crossley, P.; Terzija, V.; , "Rotor angle instability prediction using post-disturbance voltage trajectories," Power and Energy Society General Meeting, 2010 IEEE , vol., no., pp.1, 25-29 July 2010

[7] Gaouda, A.M.; Kanoun, S.H.; Salama, M.M.A.; Chikhani, A.Y.; , "Pattern recognition applications for power system disturbance classification," *Power Delivery, IEEE Transactions on* , vol.17, no.3, pp. 677- 683, Jul 2002

[8] Jiansheng Huang; Negnevitsky, M.; Nguyen, D.T.; , "A neural-fuzzy classifier for recognition of power quality disturbances," *Power Delivery, IEEE Transactions on* , vol.17, no.2, pp.609-616, Apr 2002

[9] Chilukuri, M.V.; Dash, P.K.; , "Multiresolution S-transform-based fuzzy recognition system for power quality events," *Power Delivery, IEEE Transactions on* , vol.19, no.1, pp. 323- 330, Jan. 2004

10 Thesis Summary

This chapter summarises the intent of this research (Section 10.1) as well as providing some conclusions on the success of this research, relative to its original goals, (Section 10.2). Finally, the contributions made by this research are discussed in Section 10.3 and some recommendations for future developments of this research are made in Section 10.4.

10.1 Introduction

The research presented in this thesis dealt with the creation of new methods for predicting the post disturbance frequency behaviour of a power system. These predictions of the post-disturbance frequency behaviour can be used to design adaptive frequency control actions that can improve the performance of occasional ancillary frequency control services. The primary advantage of using predictions to initiate and design frequency control actions, rather than passive pre-determined thresholds, is that it allows the system to respond before the traditional deterministic frequency control thresholds are violated and design adaptive actions based on the actual system conditons. This reduces the quantity of control actions that must be taken as well as the threat of a large frequency deviation triggering secondary contingencies or even a cascade of failures. These occasional frequency control services are responsible for limiting the frequency excursion after a large disturbance to the power balance and as such play a key role in ensuring frequency stability and reducing the risks of blackouts.

Research into these methods for frequency prediction was particularly relevant at this time due to the threats posed to the provision of frequency control by many of the developments that will occur in the nature of power systems in the coming decades. Furthermore, the advent of synchronised measurement technology (SMT) was a key enabler for this research as this technology, combined with the necessary wide area monitoring, protection and control (WAMPAC) infrastructure, provides unprecedented access to the measurements of system frequency and active power on which these frequency prediction methods depend.

10.2 Thesis Conclusions

The first goal of this research was to investigate the operating environment in which any frequency prediction method would need to operate. This investigation dealt with three main areas in detail. These were:

1. The existing frequency control practices in power systems.
2. The power system developments that have the potential to compromise the success of frequency control.
3. The SMT and WAMPAC resources that will be available to support a frequency prediction method.

This investigation revealed that the primary advantage offered by using frequency prediction to support frequency control was that it would allow frequency control to respond before the frequency deviation developed. Therefore, using frequency predictions would allow frequency stability to be preserved using less drastic control measures as faster frequency control actions are more efficient frequency control actions. More importantly, using frequency predictions would allow system operators to limit the size of any frequency deviation by initiating control actions based on what will happen and not what has happened. Limiting the size of any deviation would limit the risk of a deviation triggering secondary contingencies or even a cascade of failures.

This investigation of the operating environment also allowed the requirements that an online frequency prediction method would need to satisfy to be defined. The review of existing frequency control in Chapter 2 revealed that failing to ensure satisfactory frequency control could leave systems vulnerable to cascading generator outages and blackouts. Therefore, a frequency prediction algorithm must be both secure and dependable and as such a high degree of accuracy should be expected from any prediction algorithm. Furthermore, the high speed of operation demanded of frequency control means that any prediction algorithm must itself operate quickly if it is to be useful.

The discussion of power system developments in Chapter 3 highlighted that the frequency behaviour and configuration of future power systems will be increasingly uncertain due to features such as a high penetration of intermittent generation and a

responsive demand side. Therefore, prediction algorithms should be capable of performing the online estimation of any system parameters which they require and that this estimation must be performed quickly and with only limited system measurements due to the high speed of operation of frequency control.

The review of SMT and WAMPAC in Chapter 4 revealed that whilst these technologies offer unprecedented real time access to system measurements it would be unrealistic to expect complete observability of the system and instant access to these measurements. Therefore, the prediction algorithms created during this research must consider the communication, data processing and other delays that will be inherent to a WAMPAC system and seek to limit the scope of the data required by the algorithm to minimise these delays.

When defining the concept of online prediction of the post-disturbance frequency behaviour of a power system in Chapter 5 it became clear that the prediction method used determined the form of the prediction that could be made and that a wide variety of possible forms of prediction exist. Furthermore, it was determined that, regardless of the form of prediction desired or the prediction method used, parameter estimation would play a key role in the creation of a suitable frequency prediction method and that the most important parameter that must be estimated was the inertia.

Successful model parameter estimation requires an accurate representation of the physical process that is being modelled. This was a focus of the research presented in Chapter 8. To ensure that the predictions based on the results of this parameter estimation are accurate it is necessary to ensure that the parameter estimation methods are accurate, robust. These parameter estimation methods must also execute quickly. This is necessary so as to minimise the execution time of the prediction algorithm and consequently maximise the benefit offered by the prediction. Furthermore, the short time frame in which frequency prediction must operate, if it is to support frequency control, meant that these estimation methods would have access to only a limited quantity of system measurements that would represent only the initial period of the post-disturbance frequency deviation. This limitation posed a challenge to parameter estimation due to the observabilty of system parameters during this period; this is discussed in detail in Chapter 8.

The importance of inertia in determining the initial post-disturbance frequency behaviour of a power system meant that creating an accurate and reliable method for the estimation of inertia, defined using the *H* constant, was the next goal of this research. A review of the existing literature that dealt with *H* estimation revealed that the common approach was the post-mortem application of the swing equation based on frequency measurements and a known size and time of disturbance. The method created as part of this research applied a modified swing equation using a sliding window approach to generate accurate online estimates of *H* based on frequency and active power measurements and a known time of disturbance; this method is described in Chapter 6. The dependence of the window based method on a known time of disturbance was a significant flaw. Therefore, the next goal of the research was to eliminate this dependency and Chapter 7 describes the algorithm that was created to achieve this goal. This algorithm is designed to operate continuously and is capable of detecting when a disturbance occurs in the system and then simultaneously performing the online estimation of both *H* and the time of disturbance. Estimating the time of disturbance in this way not only eliminated the weakness of the *H* estimation method but also generated a valuable input for any other necessary parameter estimation methods.

Having created a novel method for the estimation of *H* and the time of disturbance the next goal of this research was to begin investigating possible methods for achieving frequency prediction. The first form of prediction considered was based on approximate models like those proposed in previous research into frequency prediction. The approximate model that could be used was found to be heavily dependent on the parameters that could be estimated in the time available. This limitation resulted in only a simple two parameter model being considered. The first parameter was *H* and the second was an approximate governor ramp determined by the parameter *C*. In previous work the value of *C* was calculated based on an offline calculation that depended on the gain parameter *K* and the time constant *T* of every generator in the system; *K* and *T* were estimated based on data gathered during mechanical testing of the generators.

Eliminating the dependence of this method on the offline testing of every generator and allowing this prediction method to satisfy the requirements defined earlier became the next goal of this research. To achieve this goal a novel non-linear Newton type

parameter estimation method was created that allowed *C* to be estimated online based on measurements of frequency and active power, this is described in Chapter 8. This *C* based prediction method was tested for a variety of simulations based on the simplified frequency response model proposed in and was found to be very accurate. Furthermore, demonstrations were performed of an adaptive form of load shedding based on these predictions and it was found that the necessary shedding could be reduced by approximately 40 % without compromising frequency stability. Unfortunately, the necessary simplicity of the model, to facilitate parameter estimation, meant that this work on approximate models encountered issues when the frequency response became more complex, e.g. when oscillations were present in the system.

In addition to the work on achieving frequency predictions by using approximate models a second method of achieving frequency prediction was also investigated as part of this research. This entailed the creation of frequency prediction methods that used pattern classification theory, a form of supervised machine learning, and the details of which are discussed in Chapter 9. Pattern classification was investigated as a possible avenue for achieving frequency prediction in an attempt to overcome the complexity of defining approximate models of the frequency response the accuracy of which were adequate but that were of sufficient simplicity so that the parameters could be estimated online. The offline training process for a pattern classifier is performed only once and creates a decision function that inherently represents this complexity and the possible variation in the power system state by using previous examples of power system behaviour, which could be either simulated or recorded from the power system. The output of the decision function determines the class of the frequency response and is based on a range of possible inputs that are estimated online for the system state during the disturbance. Therefore, the use of offline data to train the classifier does not violate the requirements imposed on the prediction methods created during this research.

10.3 Contributions

The research presented in this thesis was focused on the creation of online post-disturbance frequency prediction methods that could serve to support occasional and

emergency frequency control actions. The main contributions of this research can be separated into four parts:

1. Definition of generic requirements.
2. Creation of an on-line method of identifying the time of a disturbance and predicting the system inertia at that time.
3. Creation of an on-line means of predicting the nadir of the post-disturbance frequency response.
4. Creation of a frequency prediction method using pattern classifier techniques

These are described as follows.

1. A definition of the generic requirements of a method for predicting the post-disturbance frequency behaviour of a power system (Chapter 5) that was based on a review of the existing frequency control and the anticipated developments in power systems and synchronised measurement technology. The key elements of this definition are that a prediction method is required to:
   - Operate quickly, in a matter of seconds, if it is to support the fast actions demanded from occasional and emergency frequency control.
   - Be both secure and dependable as any failure in frequency control will compromise frequency stability and consequently the stability of the power system.
   - Be capable of performing the online estimation of any model parameter values that are required by the prediction method to overcome the increased level of uncertainty that is anticipated in future power systems.
   - Seek to minimise the time taken to create a prediction as the primary benefit of frequency prediction is that it allows control actions to be implemented before the predicted deviation occurs, so any delay in the performing the prediction will reduce the benefit offered by the prediction.

2. Creation of an online method for the simultaneous detection of the time at which a disturbance occurred in a power system, or area of a power system, and the estimation of the inertia of that system, or area (Chapters 6 and 7). This

method uses the swing equation and a comparison of the residue between a set of sliding filter windows; the key benefits of this online method are:

- The exploitation of the availability of synchronised measurements will allow it to replace the traditional offline and post-mortem methods for estimating system inertia.
- The inertia is a key parameter in determining the initial system frequency response to a disturbance and as such its online estimation is a necessity if the potential benefits of post-disturbance frequency prediction are to be realised.
- Simultaneously estimating the inertia and the time of disturbance means that the method is not dependent on any outside applications for a time of disturbance estimate and this estimate can also be used to support other applications; e.g. the estimation of any other parameters required by a prediction method.

3. An online method that uses measurements of the initial (0.5 seconds) frequency and active power response to determine the parameter values of an approximate model of the frequency response and thereby predict the nadir of the post-disturbance frequency response. This is achieved by solving this model for the condition of a zero first derivative with respect to time (Chapter 8). This research was based on an existing prediction method and the improvements made during the course of this research are:
   - An online parameter estimation method that eliminates the dependence of the original method on the offline testing of every generator in the system.
   - The proposal of two alternate methods for using these predictions to design adaptive load shedding strategies.
     i. The first method initiated fixed load shedding based on a prediction and in the example case allowed a 15.5 % reduction in the minimum frequency.
     ii. The second method determined the minimum amount of load shedding that would ensure frequency stability and in the example case allowed a reduction of approximately 40 % in the amount of load shed.

4. Creation of a frequency prediction method using pattern classifier techniques (Chapter 9). This method defined the future frequency behaviour of the system in terms of five class labels (extreme under frequency, below statutory limit, within statutory limits, above statutory limit and extreme over frequency) using the initial post-disturbance frequency and active power behaviour and a polynomial regression classifier. The primary benefit of this approach to frequency prediction is that the supervised learning process that is used to train the classifier will implicitly represent the variation in the system; reducing the need for online parameter estimation when compared to an approximate model based approach.

10.4 Future Developments

The research presented in this thesis has successfully delivered on the majority of its goals and it has made several contributions. A number of possible developments of this work exist in terms of both improving the novel methods created during this research and extending research into the field of frequency prediction.

The inertia estimation method presented in Chapters 6 and 7 could be improved by introducing a control loop that automatically adjusts the algorithm parameters (most likely the dynamic threshold ratio, tr) as the noise conditions in the system change. It could also be possible to use the duration of the convergence (the time for which $flag_D$ is high) as a measure of the certainty that a disturbance has occurred. Further research could also include testing the algorithm by applying it to long periods of data that does not contain a disturbance to properly verify the likelihood of false detections. This is because any uncertainty regarding the accuracy of the detections made will severely compromise the usefulness of the application due to the potential consequences of applying unnecessary control actions to the power system.

A model based method for predicting the post-disturbance frequency nadir is proposed in Chapter 8. Further research into this method should focus on improving its performance when applied to power system signals that contain a higher level of oscillations. Furthermore, an investigation of the variation in the value of the

approximate parameter C for different system conditions and generation portfolios would be of interest. The prediction supported adaptive load shedding scheme proposed in Chapter 8 demonstrated the potential to reduce the level of load shedding necessary without compromising frequency stability. However, further research will be necessary to determine the level of benefit offered and the potential for incorporating demand response control into this scheme.

The research presented in Chapter 9 demonstrated that it is possible to predict the future behaviour of the power system frequency using pattern classification theory. This research could be developed further by investigating methods for applying these techniques to a more complete power system model, particularly in terms of generating a suitable learning set for a system that is as complex as a large transmission system.

A consideration for the long term development of any of the methods proposed in this thesis would be a methodology that allows them to be satisfactorily tested in a practical situation. This is a concern as all of the proposed methods deal with large disturbances that are a low probability event in contemporary power systems and as such limited testing data and opportunities will exist for validating the performance of the methods.

Appendices

Appendix A – Deriving the Swing Equation in terms of electrical frequency and active power

The following is the derivation of the modified swing equation that is used in this thesis.

Take the following equation (A-1) that defines the speed changes of a rotating shaft with a moment of inertia of $J\ kgm^2$ and negligible mechanical damping when exposed to an imbalance between the mechanical driving torque (T_m) and electrical load torque (T_e).

$$J\frac{d\omega_m}{dt} = T_m - T_e \quad [N.m] \tag{A-1}$$

The mechanical speed of the shaft ω_m can be decomposed into a fixed speed, i.e. the synchronous speed ω_{sm} and some fixed offset α, and a deviation from this fixed speed $\Delta\omega_m$. This allows the change in speed induced by the imbalanced torque to be expressed separately from the fixed rotating speed, or reference frame.

$$\omega_m t = \left(\omega_{sm} t + \alpha\right) + \Delta\omega_m \quad [rad] \tag{A-2}$$

The second derivative of (A-2) is given in (A-3).

$$\frac{d\omega_m}{dt} = \frac{d\Delta\omega_m}{dt} \quad [rad/s] \tag{A-3}$$

This indicates that only the change in speed should be considered when applying the swing equation. Therefore, substituting (A-3) into (A-1) gives:

$$J\frac{d\Delta\omega_m}{dt} = T_m - T_e \quad [N.m] \tag{A-4}$$

The power applied to the shaft is equal to the product of the torque and the speed. Therefore, substituting this relationship into (A-4) and multiplying both sides of the equation by ω_{sm}, and assuming that in the period immediately after the disturbance $\omega_{sm} \approx \omega_m$ gives the following expression:

$$J\omega_{sm}\frac{d\Delta\omega_m}{dt} = P_m - P_e \quad [W] \tag{A-5}$$

where, P_m and P_e are the mechanical driving and electrical load power applied to the shaft, respectively.

Given the following definition of the inertia constant *H* in terms of a power base of S_B

$$H = \frac{1/2\, J\omega_{sm}^{\,2}}{S_B} \quad [s] \tag{A-6}$$

Substitution (A-6) into (A-5) gives the swing equation in terms of H as follows.

$$2H\frac{S_B}{\omega_{sm}}\frac{d\Delta\omega_m}{dt} = P_m - P_e \quad [W] \tag{A-7}$$

This expression of the swing equation is in terms of power and mechanical speed. The relationship between mechanical and electrical speed is governed by the number of poles (*p*) the generator has.

$$\omega_m = \frac{\omega_e}{p/2} \quad [rad/s] \tag{A-8}$$

When substituting (A-8) into (A-7) for the synchronous speed and speed change the $p/2$ terms cancel and leave the following per unit equation when it is recognised that ω_{sm} and S_B are the base values of the speed and power respectively.

$$2H\frac{d\Delta\omega_e}{dt} = P_m - P_e \quad \text{[p.u.]} \tag{A-9}$$

Finally, this can be expressed in terms of electrical frequency as speed and frequency are equivalent in a per unit system.

$$2H\frac{d\Delta f}{dt} = P_m - P_e \quad \text{[p.u.]} \tag{A-10}$$

Appendix B – Overview of the Improved Particle Swarm Algorithm (IPSO)

This appendix contains a description of the execution of the IPSO used in this thesis. The IPSO algorithm uses a swarm of particles to iteratively search the solution space for the solution to an optimisation problem. Each particle has a position and velocity. The position is a vector of the parameters being estimated and the velocity is the change in this position that will be made for the next iteration. The algorithm terminates when a given number of iterations have been executed, or when a given fitness is reached. Fitness is a measure of the quality of the position of a particle. A flowchart of the basic execution of the IPSO algorithm is shown in Fig. A-1.

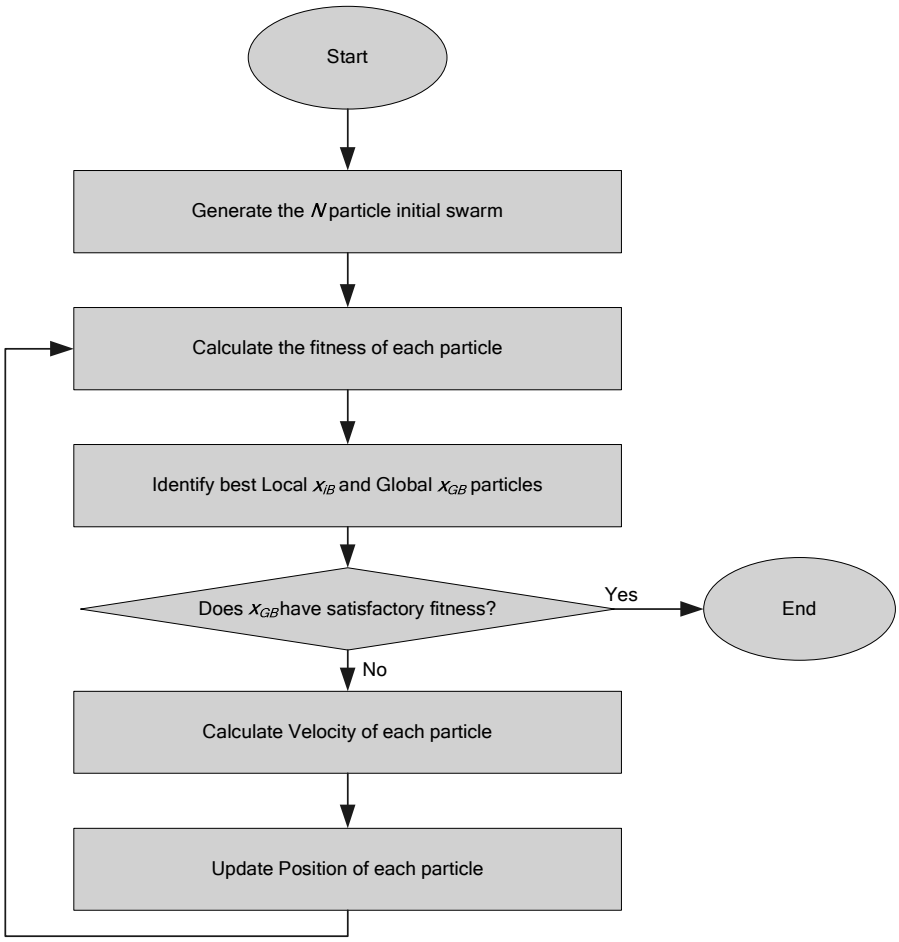

Figure A-1 – Improved particle swarm optimisation (IPSO) uses a swarm of particles to search for the solution to a optimisation problem. The multiple initial guesses offered by the swarm concept overcomes the issue of unknown initial states and the flexible structure should allow the algorithm to be adjusted to find a local minima of the true *H* and *D* values.

Each particle position, x, consists of a vector of the model parameters, so the i^{th} particle in the j^{th} iteration is defined as follows:

$$x_{ij} = \lfloor H_{ij} \quad D_{ij} \rfloor \tag{A-11}$$

Each particle is initialised with a random initial state. These initial states are bounded so the issue of an unknown system state can be overcome by defining a set of bounds that will most probably contain the true parameter values.

$$\begin{aligned} 0 < H_{i0} < H_{\max} \\ 0 < D_{i0} < D_{\max} \end{aligned} \tag{A-12}$$

Each of these particles represents a possible solution to the optimisation problem. The problem of fitting the mass load response to measured frequency data can be converted into the following optimisation problem for the i^{th} particle:

$$\begin{aligned} &\min(\sum_{k=1}^{N}(S_k - ML_{ik})weig_k) \\ &weig_k = \exp(1-(k/N)) \end{aligned} \tag{A-13}$$

where, for the N measurements, S_k is the k^{th} measurement of the frequency, ML_k is the k^{th} element of the mass load response and $weig_k$ is a weighting function.

The fitness of each particle is the inverse of the result of A.3. For each particle the position with highest fitness that has ever been held by that particle is recorded as x_{iB}, and used to determine the future velocity of the particle. In addition, the particle with the highest fitness, from the N x_{iB} particles, is recorded as x_{GB}. Therefore, x_{GB} represents the best solution that has been found by any particle in any iteration that has been completed at that stage of algorithm. This particle is used to determine the future velocity, v, of all particles. The influence these best particles have on the velocity calculation is controlled by the parameters c_1 and c_2. These are the cognitive and swarm sensitivities of the velocity.

$$v_{i(j+1)} = \omega v_{ij} + c_1 r_1 (x_{ij} - x_{iB}) + c_2 r_2 (x_{ij} - x_{GB}) \tag{A-14}$$

Where, r_1 and r_2 are random numbers and ω is the inertia weight. The inertia weight is used to determine how much the past velocity influences the future velocity. The position of a particle is then updated using the velocity.

$$x_{i(j+1)} = x_{ij} + v_{i(j+1)} \tag{A-15}$$

The flexibility of the equations used to define fitness and velocity allow the algorithm to successfully solve a wide variety of optimization problems. One drawback of the IPSO algorithm is that the use of random numbers in the velocity calculation means that the solution found is not the only solution to the problem, i.e. if the same IPSO algorithm is executed twice it will most likely return different solutions.

Appendix C – Supporting Information for Polynomial Regression Figures

This appendix contains the data used to form the probability density plots for each element of the polynomial regression classifiers decision vector in Chapter 9. Table A-1 and A-2 contain the mean and standard deviation of the normal distributions of the decision vector elements, the probability density of which were plotted in the main body. Figure A-1 contains the original histograms that these distributions were fitted to.

Table A-1 – The mean and standard deviation of the decision vector elements for each class of patterns without confidence mapping

	d(1)		**d**(2)		**d**(3)		**d**(4)		**d**(5)	
	mu	σ	*mu*	σ	*mu*	σ	*mu*	σ	*mu*	σ
y=1	0.8765	0.1959	0.1287	0.2321	0.0006	0.0257	-0.0063	0.0551	0.0044	0.0788
y=2	0.1235	0.1973	0.8086	0.2371	0.0250	0.1914	0.0542	0.0745	-0.0096	0.0811
y=3	-0.0003	0.0175	0.0201	0.1159	0.9275	0.0570	0.0359	0.1876	-0.0009	0.0217
y=4	-0.0068	0.0261	0.0586	0.1169	0.0473	0.2172	0.8930	0.1585	0.0312	0.0981
y=5	0.0072	0.0230	-0.0161	0.0380	-0.0003	0.0240	0.0232	0.0923	0.9749	0.0921

Table A-2 – The mean and standard deviation of the decision vector elements for each class of patterns with confidence mapping

	d(1)		**d**(2)		**d**(3)		**d**(4)		**d**(5)	
	mu	σ	*mu*	σ	*mu*	σ	*mu*	σ	*mu*	σ
y=1	0.9108	0.1890	0.0908	0.1962	0.0003	0.0068	0.0001	0.0117	0.0000	0.0151
y=2	0.0890	0.1884	0.8960	0.2145	0.0205	0.0561	0.0016	0.0218	-0.0001	0.0164
y=3	-0.0002	0.0037	0.0110	0.0940	0.9407	0.1101	0.0320	0.1474	-0.0007	0.0129
y=4	0.0008	0.0072	0.0022	0.0267	0.0386	0.0995	0.9578	0.1663	0.0101	0.0748
y=5	-0.0003	0.0058	0.0000	0.0088	-0.0002	0.0061	0.0085	0.0686	0.9907	0.0748

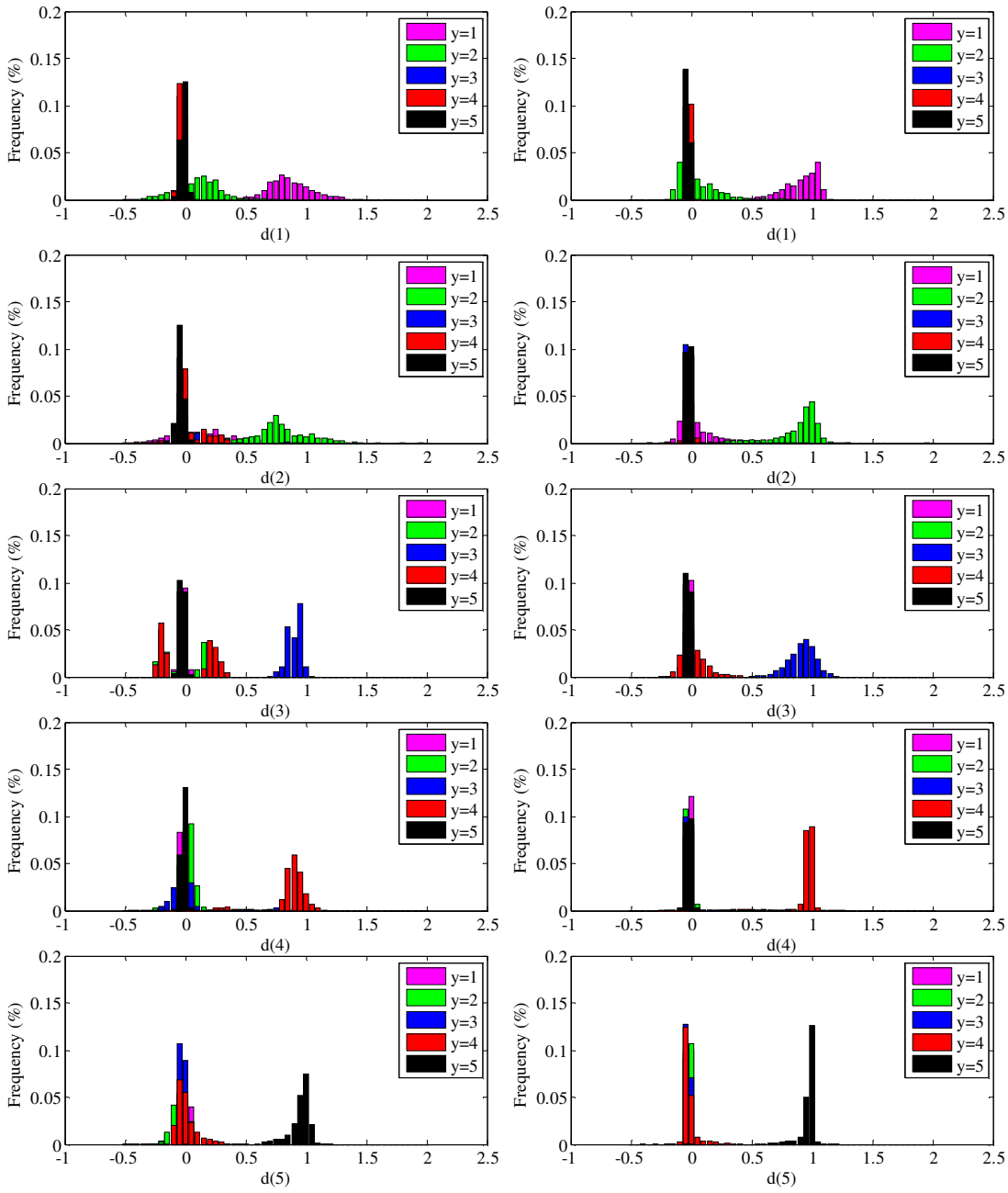

Figure A-2 – Histograms of decision vector elements

Appendix D – Simulated Test System Parameters

This appendix contains the parameters for the IEEE 39 Bus and 9 Bus test systems that were used to perform simulations for this research.

Table A-3 – Generator Data for 9 Bus test system

Generator	Bus	Rating (MVA)	H (s)	Ra	Xl	Xd	Xq	Xd′	Xq′	Td0′	Tq0′	Td0″	Tq0″
1	1	247.5	9.544	0.00	0.034	0.15	0.10	0.06	0.10	8.96	0.00	0.01	0.01
2	2	192	3.333	0.00	0.052	0.90	0.86	0.12	0.20	6.00	0.54	0.06	0.04
3	3	128	2.352	0.00	0.074	1.31	1.26	0.18	0.25	5.89	0.60	0.04	0.03

Table A-4 – Transmission line Data for 9 Bus test system

Bus		Impedance (Ω)		
From	To	R	X	B(μS)
4	5	5.29	44.97	333
4	6	8.99	48.67	299
5	7	16.93	85.17	578

Bus		Impedance (Ω)		
From	To	R	X	B (μS)
6	9	20.63	89.93	677
7	8	4.50	38.09	282
8	9	6.30	53.32	395

Table A-5 – Transformer Data for 9 Bus test system

Bus			
From	To	Short Circuit Voltage uk (%)	Copper Losses (kW)
4	1	5.76	0
7	2	6.25	0
9	3	5.86	0

Table A-6 – Bus injection Data for 9 Bus test system

Bus Information			Load		Generation	
Bus No.	Bus Type	Voltage (p.u.)	P (MW)	Q (MVAr)	P (MW)	Q (MVAr)
1	PV	1.04	0	0	80	–
2	SL	–	0	0	–	–
3	PV	1.025	0	0	100	–
4	PQ	–	0	0	0	–
5	PQ	–	125	50	0	–
6	PQ	–	90	30	0	–
7	PQ	–	0	0	0	–
8	PQ	–	0	0	0	–
9	PQ	–	100	35	0	–

Table A-7 – Generator Data for 39 Bus test system

Generator	Bus	Rating (MVA)	H (s)	Ra	Xl	Xd	Xq	Xd′	Xq′	Td0′	Tq0′	Td0″	Tq0″
1	39	1400	50.00	0.00	0.00	0.20	0.19	0.06	0.08	7.00	0.70	0.01	0.01
2	31	1000	1.50	0.00	0.35	2.95	2.82	0.70	1.70	6.56	1.50	0.09	0.21
3	32	1000	1.75	0.00	0.30	2.50	2.37	0.53	0.88	5.70	1.50	0.07	0.11
4	33	1000	1.40	0.00	0.30	2.62	2.58	0.44	1.66	5.69	1.50	0.05	0.21
5	34	1000	1.30	0.00	0.54	6.70	6.20	1.32	1.66	5.40	0.44	0.17	0.21
6	35	1000	1.60	0.00	0.22	2.54	2.41	0.50	0.81	7.30	0.40	0.06	0.10
7	36	1000	1.30	0.00	0.32	2.95	2.92	0.49	1.86	5.66	1.50	0.06	0.23
8	37	1000	1.20	0.00	0.30	2.90	2.80	0.57	0.91	6.70	0.41	0.07	0.11
9	38	1200	1.60	0.00	0.13	2.11	2.05	0.31	0.59	4.79	1.96	0.04	0.07
10	30	1000	2.10	0.00	0.13	1.00	0.69	0.31	0.31	10.20	0.10	0.04	0.01

Table A-8 – Transmission line Data for 39 Bus test system

Bus		Impedance (Ω)		
From	To	R	X	B(μS)
1	2	1.8515	21.7419	1321
1	39	0.5290	13.2250	1715
10	11	0.2116	2.2747	138
10	13	0.2116	2.2747	138
13	14	0.4761	5.3429	326
14	15	0.9522	11.4793	692
15	16	0.4761	4.9726	323
16	17	0.3703	4.7081	254
16	19	0.8464	10.3155	575
16	21	0.4232	7.1415	482
16	24	0.1587	3.1211	129
17	18	0.3707	4.3378	249
17	27	0.6877	9.1517	608
2	25	3.7030	4.5494	276
2	3	0.6877	7.9879	486
21	22	0.4232	7.4060	485
22	23	0.3174	5.0784	349

Bus		Impedance (Ω)		
From	To	R	X	B (μS)
23	24	1.1638	18.5150	682
25	26	1.6928	17.0867	970
26	27	0.7406	7.7763	453
26	28	2.2747	25.0746	1475
26	29	3.0153	33.0625	1945
28	29	0.7406	7.9879	471
3	18	0.5819	7.0357	404
3	4	0.6877	11.2677	419
4	14	0.4232	6.8241	261
4	5	0.4232	6.7712	254
5	6	0.1058	1.3754	82
5	8	0.4232	5.9248	279
6	11	0.3703	4.3378	263
6	7	0.3174	4.8668	214
7	8	0.2116	2.4334	147
8	9	1.2167	19.2027	719
9	39	0.5290	13.2250	2268

Table A-9 – Transformer Data for 39 Bus test system

Bus			
From	To	Short Circuit Voltage uk (%)	Copper Losses (kW)
10	32	2.0000	0
11	12	4.3529	160
12	13	4.3529	160
19	20	1.3818	70
19	33	1.4217	70
2	30	1.8100	0
20	34	1.8022	90
22	35	1.4300	0
23	36	2.7204	50
25	37	2.3208	60
29	38	1.5620	80
6	31	2.5000	0

Table A-10 – Bus injection Data for 39 Bus test system

			Load		Generation	
Bus No.	Bus Type	Voltage (p.u.)	P (MW)	Q (MVAr)	P (MW)	Q (MVAr)
1	PQ	–	0	0	0	0
2	PQ	–	0	0	0	0
3	PQ	–	322	2.4	0	0
4	PQ	–	500	184	0	0
5	PQ	–	0	0	0	0
6	PQ	–	0	0	0	0
7	PQ	–	233.8	84	0	0
8	PQ	–	522	176	0	0
9	PQ	–	0	0	0	0
10	PQ	–	0	0	0	0
11	PQ	–	0	0	0	0
12	PQ	–	7.5	88	0	0
13	PQ	–	0	0	0	0
14	PQ	–	0	0	0	0
15	PQ	–	320	153	0	0
16	PQ	–	329	32.3	0	0
17	PQ	–	0	0	0	0
18	PQ	–	158	30	0	0
19	PQ	–	0	0	0	0
20	PQ	–	0	0	0	0
21	PQ	–	274	115	0	0
22	PQ	–	0	0	0	0
23	PQ	–	247.5	84.6	0	0
24	PQ	–	308.6	-92.2	0	0
25	PQ	–	224	47.2	0	0
26	PQ	–	139	17	0	0
27	PQ	–	281	75.5	0	0
28	PQ	–	206	27.6	0	0
29	PQ	–	283.5	26.9	0	0
30	PV	1.0475	0	0	250	–
31	SL	0.982	9.2	4.6	–	–
32	PV	0.9831	0	0	650	–
33	PV	0.9972	0	0	632	–
34	PV	1.0123	0	0	508	–
35	PV	1.0493	0	0	650	–
36	PV	1.0635	0	0	560	–
37	PV	1.0278	0	0	540	–
38	PV	1.0265	0	0	830	–
39	PV	1.03	628	103	1000	–

Appendix E – List of Publications

Journal Publications

1. Gonzalez-Longatt, F.M.; Wall, P.; Regulski, P.; Terzija, V.; , "Optimal Electric Network Design for a Large Offshore Wind Farm Based on a Modified Genetic Algorithm Approach," *Systems Journal, IEEE* , vol.6, no.1, pp.164-172, March 2012
2. Lei Ding; Gonzalez-Longatt, F.M.; Wall, P.; Terzija, V.; , "Two-Step Spectral Clustering Controlled Islanding Algorithm," *Power Systems, IEEE Transactions on* , vol.28, no.1, pp.75-84, Feb. 2013
3. Wall, P.; Gonzalez-Longatt, F.M.; Terzija, V.; , " On-Line Power System Inertia Calculation using Wide Area Measurements," (Submitted)
4. Wall, P.; Terzija, V.; , " Simultaneous Estimation of the Time of Disturbance and Inertia Available in a Power System," (Submitted)

Conference Publications

1. Wall, P.; González-Longatt, F.; Terzija, V.; , "Demonstration of an inertia constant estimation method through simulation," *Universities Power Engineering Conference (UPEC), 2010 45th International* , vol., no., pp.1-6, Aug. 31 2010-Sept. 3 2010
2. Gonzalez-Longatt, F.M.; Wall, P.; Terzija, V.; , "A simplified model for dynamic behavior of permanent magnet synchronous generator for direct drive wind turbines," *PowerTech, 2011 IEEE Trondheim* , vol., no., pp.1-7, 19-23 June 2011
3. Regulski, P.; Gonzalez-Longatt, F.; Wall, P.; Terzija, V.; , "Induction generator model parameter estimation using improved particle swarm optimization and on-line response to a change in frequency," *Power and Energy Society General Meeting, 2011 IEEE* , vol., no., pp.1-6, 24-29 July 2011
4. Gonzalez-Longatt, F.; Regulski, P.; Wall, P.; Terzija, W.; , "Fixed speed wind generator model parameter estimation using improved particle swarm optimization and system frequency disturbances," *Renewable Power Generation (RPG 2011), IET Conference on* , vol., no., pp.1-5, 6-8 Sept. 2011

5. Lei Ding; Wall, P.; Terzija, V.; , "A novel controlled islanding algorithm based on constrained spectral clustering," *Advanced Power System Automation and Protection (APAP), 2011 International Conference on* , vol.2, no., pp.951-956, 16-20 Oct. 2011
6. Gonzalez-Longatt, F.; Regulski, P.; Wall, P.; Terzija, V.; , "Procedure for estimation of equivalent model parameters for a wind farm using post-disturbance on-line measurement data," *Innovative Smart Grid Technologies (ISGT Europe), 2011 2nd IEEE PES International Conference and Exhibition on* , vol., no., pp.1-7, 5-7 Dec. 2011
7. Wall, P.; Gonzalez-Longatt, F.; Terzija, V.; , "Estimation of generator inertia available during a disturbance," *Power and Energy Society General Meeting, 2012 IEEE* , vol., no., pp.1-8, 22-26 July 2012